ISBN 978-82-326-6013-1 (printed ver.)
ISBN 978-82-326-5832-9 (electronic ver.)
ISSN 1503-8181 (printed ver.)
ISSN 2703-8084 (electronic ver.)

NTNU
Norwegian University of
Science and Technology

Doctoral thesis
Emil Hjelseth Thyri

Doctoral theses at NTNU, 2022:318

Emil Hjelseth Thyri

COLREGs-aware Trajectory Planning and Collision Avoidance for Autonomous Surface Vessels

Doctoral theses at NTNU, 2022:318

NTNU
Norwegian University of
Science and Technology
Thesis for the degree of
Philosophiae Doctor
Faculty of Information Technology
and Electrical Engineering
Department of Engineering Cybernetics

NTNU
Norwegian University of
Science and Technology

Emil Hjelseth Thyri

COLREGs-aware Trajectory Planning and Collision Avoidance for Autonomous Surface Vessels

Thesis for the degree of Philosophiae Doctor

Trondheim, October 2022

Norwegian University of Science and Technology
Faculty of Information Technology
and Electrical Engineering
Department of Engineering Cybernetics

NTNU
Norwegian University of Science and Technology

Thesis for the degree of Philosophiae Doctor

Faculty of Information Technology
and Electrical Engineering
Department of Engineering Cybernetics

ISBN 978-82-326-6013-1 (printed ver.)
ISBN 978-82-326-5832-9 (electronic ver.)
ISSN 1503-8181 (printed ver.)
ISSN 2703-8084 (electronic ver.)

Doctoral theses at NTNU, 2022:318

Printed by Skipnes Kommunikasjon AS

Abstract

This thesis considers trajectory planning and collision avoidance for autonomous surface vessels (ASVs) operating in complex domains in the presence of other vessels. In particular, the task of maneuvering in compliance with the International Regulations for Preventing Collisions at Sea (COLREGs), which are the rules of the road on water, is considered. The contributions are directed towards COLREGs-aware trajectory planning and collision avoidance, where COLREGs rules 8 and 13-17 are addressed. These rules consider the conduct of vessels in encounters where risk of collision is present. The rules address how the maneuvering obligations are assigned to the involved vessels as a function of the encounter geometry and relative velocity. Rules 13-15 are encounter-type specific and consider overtaking encounters, head-on encounters, and crossing encounters, respectively. Rules 8, 16, and 17 address in more general terms how vessels that have either give-way or stand-on obligations are to maneuver to reduce the risk of collision. The main motivation behind the work is to enable electric autonomous passenger ferries as an efficient and environmentally friendly means of transporting pedestrians in urban environments. Still, the concepts and methods are applicable to most surface vessel operations.

The first step in maneuvering in compliance with the COLREGs is to determine which rules that apply to the ASV. In this work, a COLREGs classification algorithm has been developed, to determine the encounter type and hence the maneuvering obligations of the ASV in a vessel-to-vessel encounter between the ASV and each so called target ship, which is another vessel that the ASV must avoid collision with.

Determining the obligations of the ASV is, however, the easy part, whereas maneuvering in compliance with the obligations is a more challenging one. The COLREGs are written by humans and for humans, and its formulation is in some parts qualitative, to allow for humans to assess the situation based on experience and skills. This poses a challenge when it comes to evaluating and acting on these rules through machine code, where quantitative statements are preferred. This thesis presents a novel mechanism for enforcing maneuvering in compliance with the COLREGs.

It comprises a target ship domain with broad consideration to the regulations, where the encounter type, encounter geometry, relative velocity and available space to maneuver are considered. The domain is designed such that if the ASV maneuvers as to not violate the domain, the ASV is consequently maneuvering in compliance with the encounter-type specific COLREGs rules 13-15 and 17. By enforcing the target ship domains as strict constraints in the trajectory planning and collision avoidance algorithms, the proposed domain robustly enforces COLREGs compliance independently of other objectives such as trajectory tracking, energy efficiency and passenger comfort.

Several reactive collision avoidance methods are also proposed for ensuring safe operation of ASVs in dynamic and unstructured areas with other vessels and restricted space to maneuver. The methods include capacity for COLREGs-aware maneuvering when avoiding collision with target ships, and also collision avoidance with static obstacles with complex geometries. The methods have a varying degree of coupling with the ASV's guidance, navigation, and control (GNC) system, which makes the proposed mechanisms for COLREGs-aware and collision-free maneuvering easy to integrate in an arbitrary GNC architecture.

A trajectory planner for path following and collision avoidance with static and dynamic obstacles is also proposed. The trajectory planner is formulated as an optimal control problem, minimizing the tracking error to the path and the induced accelerations. In addition to the COLREGs rules considered by enforcing the novel target ship domain, the trajectory planner includes consideration to rules 8 and 16, regarding making maneuvers that are readily apparent and performed in ample time to stay well clear of target ships which the ASV has give-way obligations to. This is achieved by assigning windows of reduced cost for the tracking error and the induced accelerations in the control horizon. These windows facilitate any maneuver to avoid collision to be performed within them. The windows are parameterized by a small set of intuitive parameters, and enable, if circumstances of the case admit, maneuvers to avoid collision to be conducted in ample time, in accordance with Rule 8 and Rule 16.

The work in this thesis has both a theoretical and practical focus, to develop and also test new methods. The proposed navigation algorithms have been tested through an extensive set of simulations in relevant operational domains, where it is demonstrated that the proposed target ship domain robustly enforces compliance with COLREGs rules 13-15 and 17, and that the windows of reduced cost increase compliance with rules 8 and 16. Furthermore, some algorithms have been tested in full-scale experiments with an electric prototype autonomous passenger ferry. In the experiments, a radar- and lidar-based target tracking system has been applied to close the autonomy loop, demonstrating that the proposed methods are suitable

for real-time operation, and are robust to a realistic level of noise and uncertainties in the tracking data.

Preface

This thesis is submitted in partial fulfillment of the requirements for the degree of philosophiae doctor (PhD) at the Norwegian University of Science and Technology (NTNU). The work has been carried out at the Department of Engineering Cybernetics (ITK).

Associate Professor Morten Breivik has been the main supervisor of this work, and Associate Professor Anastasios Lekkas and Professor Roger Skjetne have co-supervised the work. The work has been funded through the NTNU Digital Transformation project Autoferry, and has simultaneously been affiliated with the Centre for Autonomous Marine Operations and Systems (NTNU AMOS).

Acknowledgements

I am very grateful for the support of my supervisors throughout the work on this PhD. Specifically, I would like to thank Morten Breivik for your early encouragement and motivational speech on the bright future of maritime autonomy, and for giving me the opportunity to pursue a PhD in this field. You have been supportive and helpful, and our regular meetings have helped keep this project on track and moving forward. I also want to thank Anastasios Lekkas for helping me establish a plan for my research and for your guidance along the way, and Roger Skjetne for your precise input on topics in guidance and control.

Throughout this work, I have had the pleasure of collaborating with a bunch of great people. I would particularly like to thank my office mate Glenn Bitar, for showing me the ropes when I first started, for good discussions, and for your assistance in experiments. You made an excellent rubber duck. It helped me a lot. Conducting full scale experiments with an autonomous vessel is not a one-man show. In this regard, I want to thank Erik Wilthil, Bjørn-Olav H. Eriksen and Andreas L. Flåten for your assistance in this. I admire your courage to get onboard the autonomous vessel and the boats on its collision course. Thank you Erlend A. Basso for

your input and discussions on theoretical concepts, it put me on a path towards my proudest contributions in this field.

A period of pandemic-related home office enhanced my appreciation for the social work environment. I would therefore like to thank all my colleagues at ITK for the great work environment, and specifically the people at Nyhavna, for all the non-work related discussions in the Exit room.

To my parents, Andres and Eva Kristin, thank you for everything you have done for me. With your support, pursuing my interests has always felt both safe and easy. It has enabled me to get to where I am today, and for that I am truly grateful.

And finally, Rebecca, thank you for your patience while I made these boats not crash. Your appreciation for what this work means to me has been invaluable, and your continuous support kept me going when going was tough.

July 2022, Trondheim
Emil H. Thyri

Contents

Acronyms

AIS automatic identification system

APF artificial potential field

ARPA automatic radar plotting aid

ASV autonomous surface vessel

AUV autonomous underwater vehicle

CBF control barrier function

COLAV collision avoidance

COLREGs International Regulations for Preventing Collisions at Sea

CPA closest point of approach

DCPA distance at closest point of approach

DOF degrees of freedom

DP dynamic positioning

DW dynamic window

ENC electronic nautical chart

GNC guidance, navigation, and control

IMO International Maritime Organization

LOS line of sight

MPC model predictive control

OCP optimal control problem

OOW officer on watch

TCPA time to closest point of approach

USV unmanned surface vehicle

VO velocity obstacle

Chapter 1

Introduction

This chapter gives a motivation for the work in this thesis, a brief summary of the contributions, and an outline for the remainder of the thesis.

1.1 Motivation

The technological development is moving forward at an unprecedented rate. The fourth industrial revolution is well underway, where inter-connectivity and digitalization enable an even larger part of traditionally manual tasks to be automated. The development of cyber-physical systems with advanced means of sensing and interacting has enabled tasks of a higher complexity to be automated. Furthermore, through algorithms for comprehension and planning, systems can reach high-level mission objectives autonomously, and hence remove the need for humans to take an active part in the control loop. Today, this development is most apparent in the automotive domains, where autonomous cars can navigate in complex traffic situations and transport goods and people without human intervention [1].

Some of the first efforts towards autonomous vehicles originated from humans wanting to deploy vehicles into domains where remote control was a challenge, like the *Stanford Cart*, a four-wheeled vessel initially developed for testing how the lunar surface could be traversed by a remotely operated vehicle [2]. By giving the vehicle the ability to comprehend, reason, and act on its own, it can operate for longer periods without human intervention. For the same reasons, autonomy is applied for underwater vehicles, like the *Hugin* autonomous underwater vehicle (AUV) by Kongsberg Maritime, having capacity for several days of autonomous subsea survey operations [3]. Another early application for ocean-based autonomy is in the defense sector [4, 5], where autonomy can reduce risk to personnel. In 2016, the *Sea Hunter*, a high-speed submarine hunter autonomous surface vessel (ASV) depicted in Figure 1.1a [6], performed its first sea trials.

(a) (b)

Figure 1.1: Some examples of early maritime autonomous vessels. (a) The DARPA prototype vessel *Sea Hunter*, developed for unmanned and autonomous anti-submarine operations [7]. (b) The world's first autonomous car ferry *Falco*. Photo is from [8].

In addition to being an enabler for entering new domains and operations, autonomy can increase the safety of traditional operations. A report from the European Maritime Safety Agency analyzing reported marine accidents in the period 2011-2018, stated that more than 54% of all casualties with ships were due to navigational errors. Out of a total of 4104 reviewed accidents, 65.8% were attributed to erroneous human actions [9]. By deploying autonomous systems for situational awareness, comprehension, planning, and maneuvering, erroneous human actions can hopefully be mitigated.

In recent years, perhaps the largest push towards autonomy in the maritime domain has been in the shipping and transport sector. In 2018, Rolls-Royce demonstrated the world's first autonomous ferry transit with the *Falco* car ferry[1][8], shown in Figure 1.1b. In January 2022, the Mitsui group demonstrated the world's first autonomous navigation and berthing for the container vessel *Mikage* [10]. In April 2022, China announced the deployment of the world's first autonomous container vessel into commercial service [11].

Several ongoing initiatives propose to use autonomous electric cargo vessels for short-sea shipping, to replace fossil-fueled road vehicles, and thereby reduce both emissions and the strain on the road networks. In April 2022, the electric container ship Yara Birkeland had its maiden voyage transporting fertilizer from Herøya to Brevik, where it is set to replace more than 40 000 truck journeys a year. The vessel is currently manually operated, but it is planned to gradually move to remote and autonomous operation over the next years. Similarly, the grocery-logistics company ASKO has an ongoing project to replace 2 million kilometers of truck transport by electric ASVs, saving 5000 tonnes of CO2 every year

[1]Video from world's first autonomous ferry demonstration, by Rolls Royce: `https://www.youtube.com/watch?v=JW57ZMjL_fc&ab_channel=Rolls-Royce` (accessed June 17, 2022).

(a) (b)

Figure 1.2: Urban autonomous ferry concepts. (a) Concept by the maritime autonomy company Zeabuz. © 2020 Zeabuz, (b) Small passenger ferry by RoBoat. Photo by Reuters.

[12].

This technology development has also enabled new thinking when it comes to urban infrastructure. Since the first industrial revolution, the urbanization has skyrocketed, and it is predicted that 68% of the world's population will live in urban areas by 2050 [13]. This development poses challenges with infrastructure, pollution, and congestion as the urban growth continues. A large portion of the world's urban areas are located near waterways, where the waterways for centuries were the main transportation veins until the car became a commodity and transitioned transportation from water to land. Now, many urban areas are struggling with road congestion, while the waterways are underutilized. Autonomous technology lays down a foundation for new solutions to these old problems by enabling a revitalization of the use of the waterways [14, 15].

In 2017, the Norwegian University of Science and Technology (NTNU) started developing the *milliAmpere*, the world's first autonomous passenger ferry prototype. The initial intention for the ferry was to demonstrate that small autonomous passenger ferries are a viable alternative to building permanent infrastructure like bridges [16]. The ferry has demonstrated fully autonomous transit operation on several occasions. Its successor, *milliAmpere 2*, is set for pilot operation in Trondheim in 2022. Furthermore, Zeabuz, a spinoff from NTNU, is aiming to deliver flexible solutions for maritime mobility in several segments including urban passenger transport [17]. Another similar initiative named RoBoat is proposing to use ASVs for passenger transport, garbage collection, and package delivery [18]. Concept vessels from Zeabuz and RoBoat are shown in Figure 1.2.

An ASV must have the capability to comprehend, plan, and act with due regard to its surroundings and mission objectives to achieve an efficient operation while ensuring the safety of itself, its passengers or cargo, and other agents. An integral component of this is the capacity for maneuvering

in compliance with the International Regulations for Preventing Collisions at Sea (COLREGs), which are the rules of the road on water and which applies to all vessel traveling upon the high seas. ASVs must adhere to these rules to ensure a frictionless interaction with manned vessels. The focus of this thesis is therefore within the field of autonomous maneuvering in the maritime domain, where its main contributions are methods and algorithms for safe, efficient, and protocol-compliant maneuvering of ASVs.

This type of technology will enable the realization of ASVs as a sustainable and flexible solution to the problems we are facing today with regard to transportation of people and cargo, reducing the strain on current infrastructure and reducing the environmental impact of current operations. The technology can increase both efficiency and safety of existing operations, and it will expand the toolbox of maritime vessels and, hence, extend the boundaries for what is achievable by means of maritime vessels, with respect to economical consideration and environmental conditions.

Furthermore, working within this field has been immensely fun. In my opinion, there are not many technologies that are as exciting as autonomy. While the contributions add to decades of prior research and development, it now seems that the plane that is maritime autonomy is speeding down the runway, soon to take off. And that is a plane I want to be on.

1.2 The Autoferry project

During my PhD, I have been part of the Autoferry project, which is one out of nine so-called Digital transformation projects at NTNU. The full project name explains what it is about: "Autonomous all-electric passenger ferries for urban water transport", see also [19]. The main hypothesis of the project is that autonomous passenger ferries can operate safely alongside other vessels in confined and congested environments such as urban water channels. Verifying this requires a broad multi-disciplinary approach, where the research methods combine theory, simulations, and experimental testing and validation. Hence, the main project goal is to develop groundbreaking new concepts and methods to enable the development of autonomous passenger ferries for environmentally-friendly and flexible transport of people in urban water channels.

To achieve the main goal, the project has been divided into six main research areas with corresponding goals:

1. Automation and autonomy: Achieving a safe and precise crossing of the city canal in Trondheim using an integrated automation and autonomy system.

2. Multi-sensor tracking via shore- and ferry-based sensors: Achieving a

Figure 1.3: The unique equipment that the Autoferry project has contributed to establish and has access to. The *milliAmpere* is a prototype electric autonomous passenger ferry. It is named after the world's first all electric car ferry *Ampere* [20]. The *milliAmpere2* is a full-scale electric autonomous passenger ferry that is planned for trial operation in Trondheim in 2022. The Shore Control Lab is an advanced infrastructure for research and development in remote monitoring and control of autonomous maritime systems, and human-machine interaction.

multi-sensor target tracking system which provides reliable situational awareness, consisting of both on-shore and on-board sensors.

3. All-electric power and propulsion: Achieving a digitized all-electric power and propulsion system with rapid charging.

4. Human factors, remote monitoring and control: Achieving a safe and efficient human-machine interaction between the autonomous ferry and its environment, including remote operators, passengers and other vessels.

5. Communications and cyber security: Achieving a secure and reliable communication and navigation system.

6. Risk management: Achieving a novel risk management framework tailored to autonomous passenger ferries.

To work on these areas, the project comprises nine PhD candidates and seven key scientists. My research has focused on the first research area on automation and autonomy, where I have worked on developing methods for autonomous maneuvering of ASVs in urban areas. In particular, the main focus has been toward trajectory planning and collision avoidance in partial compliance with the COLREGs. As such, the project has access to two electric passenger ferry prototypes, which shorten the distance from theoretical research to experiments, and several of the contributions described in this thesis have therefore been tested in full-scale experiments.

Figure 1.3 illustrates some of the unique equipment that the project has contributed to establish and has access to.

Finally, it should be mentioned that the Autoferry project activities and results interact with other projects in an ecosystem around Autoferry, which constitutes a strategic portfolio that contributes toward realizing the main project goal, which is very ambitious and not possible to realize through one single project, and which can result in the world's first autonomous urban passenger ferry and contribute to creating new high-tech jobs. This ecosystem has been established through strategic collaboration between the NTNU departments and researchers involved in the Autoferry project, see more detailed descriptions in [21] and [22].

1.3 Contributions at a glance

The main contributions of the work presented in this thesis are focused towards autonomous maneuvering of ASVs operating in confined areas and in the presence of other vessels. The work is largely focused on collision avoidance with both static and dynamic obstacles, with COLREGs-compliant maneuvering in the presence of other vessels. As such, situation-specific features such as the confinedness and available space have been considered when planning maneuvers to avoid collision. Efforts have been made on improving methods for classifying vessel-to-vessel encounters with respect to the COLREGs rules regarding vessels in sight of each other, to determine the encounter type and hence which rules that apply. Furthermore, efforts have been made on automating the process of evaluating the performance of autonomous maneuvering algorithms to facilitate large-scale simulation-based assurance of maritime autonomous systems. Also, efforts have been made regarding vessel motion control, including low-level actuator control. Finally, significant work has been put into testing and evaluating the performance of these algorithms on the prototype vessel *milliAmpere*.

The contributions of the work can be summarized as follows, with references to the papers listed in Section 1.4:

- Development of a trajectory planning algorithm for short transit operations for ASVs, e.g., canal, river, or harbour crossings, where the crossing is to follow a predefined path. The method handles collision avoidance (COLAV) with dynamic obstacles by assigning a polygonal safety domain to each target ship, and representing that domain in a path-time space, where the safety domain's occupation of the path in time is represented as a polygon. A velocity profile for the predefined path is then calculated by traversing the path-time space with Dijkstra's algorithm. The computational complexity of this

trajectory planner is low, making it suitable for real-time operation. The work is presented in Paper A.

- Improvement of an existing algorithm for encounter classification, to correctly determine the maneuvering responsibility of the ownship in a vessel-to-vessel encounter based on the geometry and relative velocity of the encounter. The method determines the encounter type, and hence which of the encounter-type specific rules of the COLREGs that the ownship should abide by. The work is presented in Paper D.

- Development of a novel domain for dynamic obstacles where the domain is formulated such that if the ASV maneuvers as to not violate the domain, the ASV also maneuvers in compliance with the encounter-type specific rules from the COLREGs, namely rule 13-15 and 17. The COLREGs are considered by first classifying each vessel-to-vessel encounter to determine which rules apply, and subsequently by assigning a domain to the dynamic obstacle as a function of the geometry and relative velocity of the encounter, as well as some encounter-type specific parameters. Furthermore, the size of the domain is adjusted based on the available space to maneuver. The work is presented in Paper D.

- Development of a reactive maneuvering algorithm for ASVs that considers collision avoidance with both static and dynamic obstacles through the use of control barrier functions (CBFs). The method considers the ownship vessel dynamics by including a three degrees of freedom (DOF) vessel model of the ASV when formulating the CBFs. The output of the algorithm is either a generalized 3-DOF force or actuator setpoint that ensures collision-free maneuvering of the ASV. The work is presented in Paper B and Paper D.

- Experimental verification of a complete autonomous maneuvering system in confined space operation. The system comprises a radar- and lidar-based tracking system for estimating the position and velocity of other vessels, the aforementioned reactive maneuvering algorithm, and a CBF-based COLAV system for static obstacles, with input from both electronic nautical charts (encs) and lidar. The work is presented in Paper D.

- Development of a novel COLREGs-specific velocity obstacle, applicable to the popular velocity obstacle (VO) algorithm for COLAV. The novel velocity obstacle ensures that the ASV maneuvers in compliance with the COLREGs rules 13-15 and 17 when in presence of other vessels. The work is presented in Paper E.

- Development of a trajectory planning algorithm for ASVs operating in confined areas with traffic. The method considers both static and dynamic obstacles by formulating an optimal control problem (OCP) for the ASV, where static and dynamic obstacles are represented as constraints to the ASV states in the control horizon. In addition to the rules 13-15 and 17, the method includes compliance with rules 8 and 16 by controlling the timing and duration of avoidance maneuvers through dynamic cost-gain profiles for the gains in the OCP objective function. The work is presented in Paper F.

- Development of a path-following controller for an electric double-ended ferry. In the motion controller design, several inherent challenging physical properties of the vessel is considered. Specifically, the lack of directional stability combined with slow thruster dynamics. The controller is formulated through a backstepping approach, where the dynamics of the vessel's overactuated thruster system is included by first formulating a novel thrust allocation law on closed form. The work is presented in Paper C.

An in-depth discussion of these contributions is provided in Chapter 3.

1.4 Publications

This thesis is based on five peer-reviewed papers, and one paper submitted for review. The papers are enumerated as Paper A through Paper F in chronological order of publication. The contributions of the research papers can be illustrated in a simplified architecture of the situational awareness, planning, and control modules for an autonomous vessel as seen in Figure 1.4.

Publications included in this thesis

Paper A [23]

E. H. Thyri, M. Breivik, and A. M. Lekkas. "A path-velocity decomposition approach to collision avoidance for autonomous passenger ferries in confined waters". In: *Proceedings of the 20th IFAC World Congress*. Berlin, Germany, 2020, pp. 14628–14635. DOI: `https://doi.org/10.1016/j.ifacol.2020.12.1472`.

Paper B [24]

E. H. Thyri, E. A. Basso, M. Breivik, K. Y. Pettersen, R. Skjetne, and A. M. Lekkas. "Reactive collision avoidance for ASVs based on control barrier functions". In: *Proceedings of the 2020 4th IEEE Conference on Control Technology and Applications (CCTA)*. Montreal, QC,

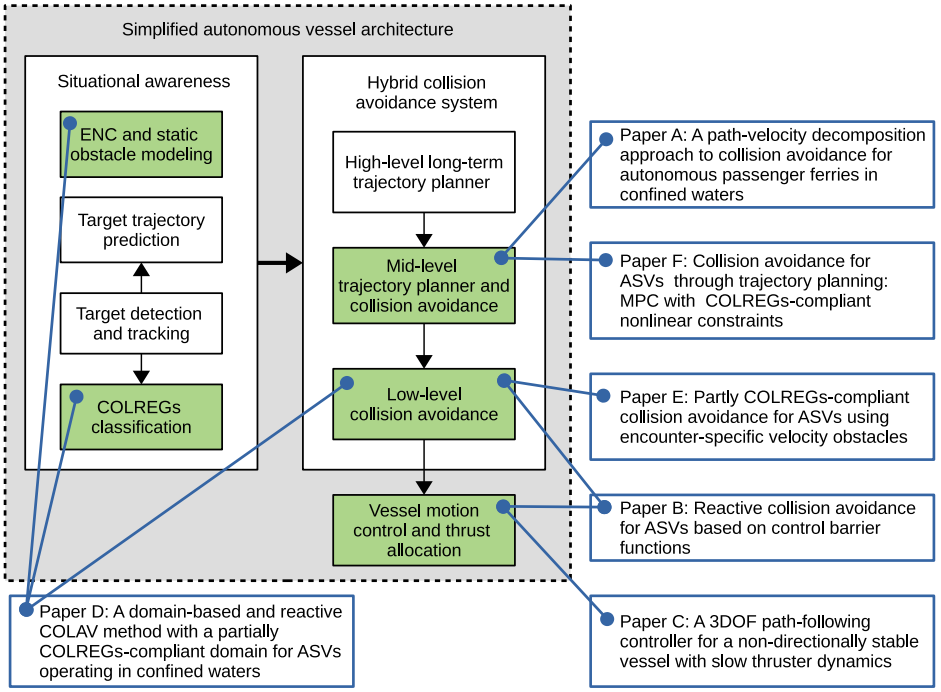

Figure 1.4: The contributions of this thesis in the scope of a simplified architecture of the situational awareness, planning, and control modules for an autonomous vessel.

Canada, 2020, pp. 380–387. ISBN: 978-1-7281-7140-1. DOI: https://doi.org/10.1109/CCTA41146.2020.9206340.

Paper C [25]

E. H. Thyri, G. Bitar, and M. Breivik. "A 3DOF path-following controller for a non-directionally stable vessel with slow thruster dynamics". In: *IFAC-PapersOnLine* 54.16 (2021). 13th IFAC Conference on Control Applications in Marine Systems, Robotics, and Vehicles (CAMS) 2021, pp. 288–294. ISSN: 2405-8963. DOI: https://doi.org/10.1016/j.ifacol.2021.10.106.

Paper D [26]

E. H. Thyri and M. Breivik. "A domain-based and reactive COLAV method with a partially COLREGs-compliant domain for ASVs operating in confined waters". In: *Field Robotics* 2 (2022), pp. 632–677. DOI: https://doi.org/10.55417/fr.2022022.

Paper E [27]

E. H. Thyri and M. Breivik. "Partly COLREGs-compliant collision avoidance for ASVs using encounter-specific velocity obstacles". In: *Proceedings of the 14th IFAC Conference on Control Applications in*

Marine Systems, Robotics, and Vehicles (CAMS) 2022. Copenhagen, Denmark, 2022.

Paper F [28]
E. H. Thyri and M. Breivik. "Collision avoidance for ASVs through trajectory planning: MPC with COLREGs-compliant nonlinear constraints". In: *Modeling, Identification and Control* 43.2 (2022), pp. 55–77. DOI: https://doi.org/10.4173/mic.2022.2.2.

Other publications

- E. A. Basso, E. H. Thyri, K. Y. Pettersen, M. Breivik, and R. Skjetne. "Safety-critical control of autonomous surface vehicles in the presence of ocean currents". In: *Proceedings of the 2020 4th IEEE Conference on Control Technology and Applications (CCTA)*. Montreal, Canada, 2020, pp. 396–403. DOI: https://doi.org/10.1109/CCTA41146.2020.9206276 [29].

- J. Matouš, E. A. Basso, E. H. Thyri, and K. Y. Pettersen. "Unifying reactive collision avoidance and control allocation for multi-vehicle systems". In: *Proceedings of the 2021 5th IEEE Conference on Control Technology and Applications (CCTA)*. 2021, pp. 76–81. DOI: 10.1109/CCTA48906.2021.9658918 [30].

- E. F. Brekke, E. Eide, B.-O. H. Eriksen, E. F. Wilthil, M. Breivik, E. Skjellaug, Ø. K. Helgesen, A. Lekkas, A. B. Martinsen, E. H. Thyri, T. Torben, E. Veitch, O. A. Alsos, and T. A. Johansen. "milliAmpere: An autonomous ferry prototype". In: *Journal of Physics: Conference Series* 2311.1 (2022), p. 012029. DOI: https://doi.org/10.1088/1742-6596/2311/1/012029 [21].

Master theses co-supervised

During the work on this thesis, I have contributed to the supervision of five Master's students. The topics of the theses are all in the field of maritime collision avoidance, where three students have developed methods for trajectory planning and collision avoidance based on optimal control, artificial potential fields and visibility graph-based path planning, and one student has combined a local and a global trajectory planning method in a hybrid structure for open sea and confined-space collision avoidance. The final student focused on simulation-based testing of collision avoidance algorithms, and developed a fuzzy logic-based system for evaluating the performance of autonomous maneuvering algorithms with respect to COLREGs-compliance, safety and passenger comfort.

Working with these students has been a rewarding experience, where discussing challenges related to the problem they considered exposed me to their ideas and solutions, which most certainly has made a positive impact on my own research.

- A. Yttisrud. "Hybrid collision avoidance for autonomous passenger ferries". MA thesis. Norwegian University of Science and Technology (NTNU), Trondheim, Norway, 2020. URL: https://hdl.handle.net/11250/2656722 [31].
- H. Berget. "An area-time trajectory planning approach to collision avoidance for confined-water vessels". MA thesis. Norwegian University of Science and Technology (NTNU), Trondheim, Norway, 2021. URL: https://hdl.handle.net/11250/2781076 [32].
- O. J. O. Kirkerud. "COLREGs-aware collision avoidance for autonomous surface vehicles using encounter-specific artificial potential fields". MA thesis. Norwegian University of Science and Technology (NTNU), Trondheim, Norway, 2022. URL: https://ntnuopen.ntnu.no/ntnu-xmlui/ [33].
- E. Hestvik. "COLREGs-aware and MPC-based trajectory planning and collision avoidance for autonomous surface vessels". MA thesis. Norwegian University of Science and Technology (NTNU), Trondheim, Norway, 2022. URL: https://ntnuopen.ntnu.no/ntnu-xmlui/ [34].
- E. Løvoll. "Evaluating collision avoidance algorithms in urban and semi-restricted waters using fuzzy logic". MA thesis. Norwegian University of Science and Technology (NTNU), Trondheim, Norway, 2022. URL: https://ntnuopen.ntnu.no/ntnu-xmlui/ [35].

1.5 Outline

The rest of this thesis is structured as follows: Background material on the COLREGs, previous work on collision avoidance at sea, vessel safety domains and validation of autonomous systems is presented in Chapter 2. A more in-depth presentation of the thesis' contributions is provided in Chapter 3. Chapter 4 gives concluding remarks and recommendations for further work. Finally, the publications written as part of the PhD work are reprinted in Chapter 5.

Chapter 2

Background

2.1 The traffic rules at sea

For millennia, the sea has been an important fairway for people and merchandise across the globe. While the ocean is large, the risk of collision between vessels is small, but never zero. And over the past decades, with the introduction of the steam engine, the number of vessels has skyrocketed. To mitigate the risk of collision, vessels are today subject to a set of traffic rules for the maritime road.

These rules were developed over several centuries, where a signals book issued by Admiral Lord Richard Howe in 1776 contained a rule saying that a vessel with another vessel on her starboard side shall give way by a starboard maneuver [36]. It was first in 1846 that a set of rules were given a statutory force, when the English Parliament enacted a set of rules drawn up by the London Trinity House, a charity dedicated to safeguarding shipping and seafarers [37]. The rules described actions to be taken by steam vessels meeting in narrow channels or in crossing encounters with other steam-driven vessels, and how sailing vessels were to maneuver to avoid collision with other sailing vessels.

The regulations have since been revised in several rounds, to include rules for lights and lanterns, sound signals, traffic separation schemes, and new technology like radar. The rules received their last major revision at an international conference in London in 1972 held by the International Maritime Organization (IMO), and are today called The International Regulations for Preventing Collisions at Sea (COLREGs).

The regulations have four main parts:

- **Part A**: General Rules 1-3
- **Part B**: Steering and sailing rules Rules 4-19
- **Part C**: Light and shapes Rules 20-31

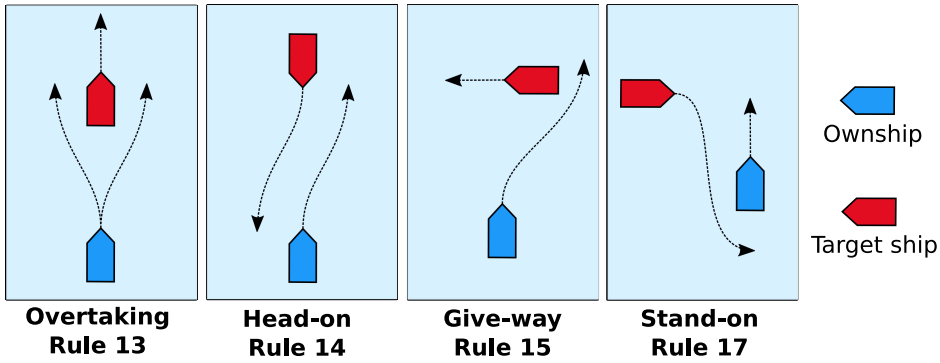

Figure 2.1: Illustration of situations where COLREGs rules 13-15 and 17 applies to the blue ownship vessel, in an encounter with the red target ship vessel.

- **Part D**: Sound and light signals Rules 32-37

The COLREGs apply to all vessels upon the high seas and in all waters connected to the high seas by waterways navigable by seagoing vessels. Hence, for autonomous vessels to maneuver upon the high seas, they must maneuver in accordance with these regulations. In this thesis, the task of COLREGs compliance for maneuvering is considered. While the autonomous vessels must comply with all the rules, this work is limited to consider only a subset of the rules, namely the rules regarding motor-driven vessels in sight of one another. Specifically, Rule 8 and rules 13-17 are considered. In the following, the most relevant parts of the rules are given, more or less as they are written in [37]. Figure 2.1 illustrates encounters between two vessels, where rules 13-15 and 17 apply.

Rule 8: Action to avoid collision

Any action taken to avoid collision should be positive, made in ample time and with due regard to the observance of good seamanship. Any alternation of course and speed to avoid collision shall if circumstances of the case admit be large enough to be readily observable for other vessels. A succession of small alternations should be avoided. If there is sufficient sea room, alternation of course alone is the preferred action, provided that it does not result in another collision.

Rule 13: Overtaking

Any vessel overtaking another vessel shall keep out of the way of the vessel being overtaken. A vessel is deemed to be overtaking another when approaching her from more than 22.5° abaft her beam. When a vessel is in doubt as to whether she is overtaking another, she shall assume that she is, and act accordingly. Any subsequent alternation of bearing between the two vessels shall not relieve the overtaking vessel of her duty to give way until she is finally past and clear.

Rule 14: Head on

When two power-driven vessels are meeting on a reciprocal or nearly reciprocal course so as to involve risk of collision, each shall alter her course to starboard and pass each other port to port.

Rule 15: Crossing

When two power-driven vessels are crossing so as to involve risk of collision, the vessel which has the other on her own starboard side shall keep out of the way, and if the circumstances of the case admit, avoid crossing ahead of the other vessel.

Rule 16: Action by the give-way vessel

A vessel that is obliged to keep out of the way of another vessel, shall as far as possible take early and substantial action to keep well clear.

Rule 17: Action by the stand-on vessel

When two vessels are meeting as to one is obliged to give way, the other vessel is the stand-on vessel and is obliged to keep her course and speed. The stand-on vessel may however take action to avoid collision when it is apparent that the give-way vessel is not taking appropriate action to give way, but in doing so, should avoid making a port maneuver for a vessel on her port side.

These regulations are written by humans for human interpretation, and since the rules can not explicitly consider all possible situations or encounters between vessels at sea, they are written intentionally vague. This both allows for, and requires, that the seamen maneuvering these encounters apply their knowledge, experience, and skills to fully appreciate the situation and to maneuver *with due regard to the observance of good seamanship*.

This vagueness does, however, complicate the task of enforcing the rules through autonomous algorithms, since *ample time* and *due regard* is not yet a Python or C++ module. Furthermore, there are regulatory boundaries that are not yet adapted to account for autonomous technology. In particular when the responsibility for comprehension and decision making is moved from human to machine. Specific challenges related to this is further discussed by Ringbom [38].

2.2 Collision avoidance at sea

Despite having a set of regulations for avoiding collisions at sea, collisions do still happen. The causes for this are several, but a large portion of the collisions come as a result of wrongful decisions by the humans controlling the vessels [9]. Great efforts have therefore been put into reducing the

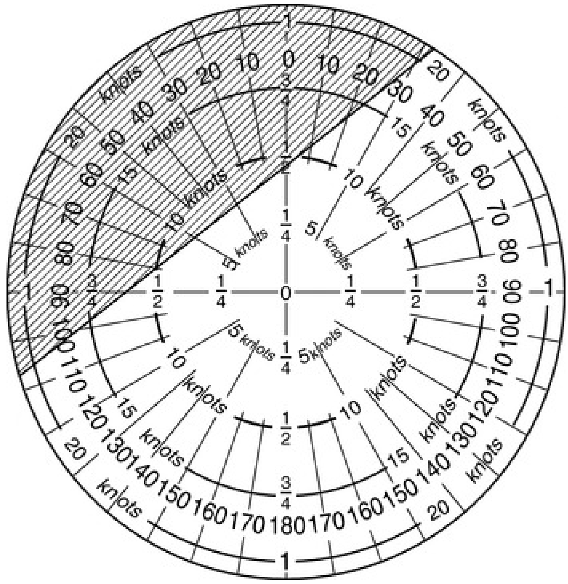

Figure 2.2: The anti collision indicator from 1968. The disc represents the course and speed combinations for a vessel, and the shaded region marks the combinations that will lead to collision or conflict with another vessel. The OOW can select course and speed combinations from the non-shaded regions to mitigate the collision risk. Figure from [39].

risk of collision, by developing aids for humans to evaluate a situation and determine the right cause of action. Already in 1968, Mitrofanov [39] proposed the anti-collision indicator, an analogue computer calculating a set of course and speed combinations that will result in collision with another vessel, based on measurements of the relative bearing and relative velocity to other vessels. The relative bearing and velocity measurements were obtained manually by the use of radar. The anti collision indicator is shown in Figure 2.2, where the shaded regions indicate course and speed combinations that are in conflict with an opposing vessel, and the non-shaded regions are collision-free speed and course combinations.

Around the same time, automatic radar plotting aid (ARPA) was developed [36], where the first commercially available system was the Norcontrol DataBridge, developed by the Norwegian company Norcontrol [40] with capacity for tracking up to eight vessels, and plotting position, speed and course estimates by the use of radar [41]. The ARPA systems also included estimates of distance at closest point of approach (DCPA) and time to closest point of approach (TCPA) between the ownship and target ships, providing the officer on watch (OOW) with enhanced situational awareness to make decisions on when and how to maneuver [42]. However, these decision support aids did not provide the OOW with maneuvering

instructions, and ultimately, it came down to the watch officers to determine the correct choice of action.

In 1970, systems for calculating a safe maneuver based on information from the ARPA emerged. The Sperry collision avoidance system, developed by Sperry Marine Systems, predicted the future trajectory of other vessels, and determined areas of danger in the velocity space of the ownship [43]. The system also proposed course change maneuvers that would result in passing either fore or astern of target ships. Still, these systems required the human operator to control the vessel, but in 1968, Dove et al. [44] proposed to couple a system for collision avoidance maneuver detection with the vessel's actuators to directly control the vessel, and hence remove the human from the control loop. A vessel equipped with such a system, and ARPA for situational awareness can to some degree be considered an autonomous vessel.

Over the following decades, along with the improvements of computers, great efforts were put into developing methods and algorithms for automatic or autonomous control of vessels, with the objective of efficient and safe maneuvering. The reader is advised to see the works of Tam, Bucknall and Grieg [45], for a comprehensive review of collision avoidance and path planning methods for ships in close range encounters in the period from 1955 to 2008. The authors highlight several limitations with the methods developed up to that time, relating to the lack of consideration to the full complexity of safe and efficient maneuvering of a vessel. In particular, the lack of consideration to external conditions like weather in the path planning methods, and the lack of consideration for the planned path when calculating collision avoidance maneuvers. More than pointing out limitations, this highlights the task complexity, and the difficulty of solving it by a single monolithic method. This led to the emergence of hybrid structures for autonomous maneuvering, where the planning and maneuvering objectives are distributed over several layers.

In the works of Larson, Bruch, and Ebken [4] and Larson, Bruch, Halterman, Rogers, and Webster [46], a hybrid structure for autonomous maneuvering of an ASV was presented. The method comprises a deliberate planner for early handling of encounters by the use of ARPA, automatic identification system (AIS) and ENC, and a component for reactive maneuvering in the short-time horizon based on radar data and cameras. The benefits of such hybrid structures have been further pursued by Loe [47], where he demonstrated how a global path planning method in combination with a reactive maneuvering algorithm can ensure safe collision-free maneuvering and convergence to a desired destination in complex and non-convex environments. Casalino et al. [48] proposed a 3-layered architecture for a surveillance unmanned surface vehicle (USV) operating in harbour area. In the architecture, the top layer comprised a graph-based path planner that

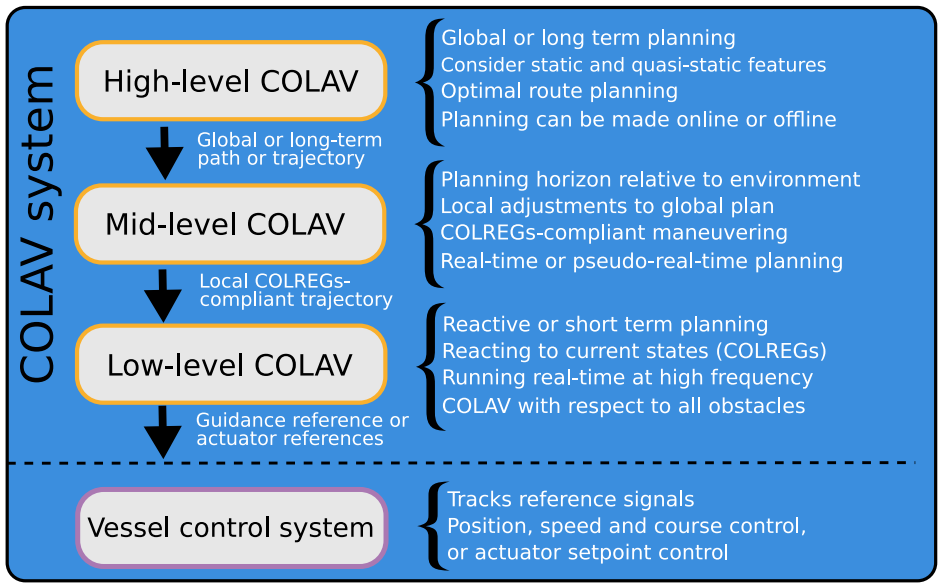

Figure 2.3: A 3-layered hybrid collision avoidance structure, where the objectives related to multi-objective collision-free maneuvering is distributed over several algorithms at different layers with different requirements to response times. Figure from Paper F.

considered static obstacles by the use of ENC, the mid-level considered unmapped static and dynamic obstacles, and the lowest level considered reactive maneuvering and collision avoidance with all obstacles to ensure the baseline safety of the ASV operation. Other works applying hybrid systems for maneuvering of ASVs includes Švec et al. [49], Serigstad et al. [50], Bitar et al. [51], and Eriksen et al. [52].

Figure 2.3 shows a generic 3-layered hybrid COLAV system similar to the one in [48] and [52]. In this system, the high level COLAV handles long-term or global path or trajectory planning, and considers static and quasi-static features like obstacles from ENC, and weather and current data, to calculate a more or less optimal transit route for the vessel. For ASV operations with variations in destination, such as a surveillance vessel, this planning must be done online. However, for location-specific operations like ferry transits, this planning can be done offline.

The mid-level COLAV considers both static and dynamic obstacles. The planning horizon of this level should match the dynamics of the features in the operational domain. For deep-sea shipping operations, a relevant horizon could be tens of minutes, or even hours, while for small ASVs in unstructured domains like harbours, a horizon of several minutes might be suitable. The mid-level COLAV makes local adjustments to the long-term path or trajectory, and in avoiding dynamic obstacles, should show compliance with the maneuver specific rules from the COLREGs

introduced in Section 2.1.

The low-level COLAV is a reactive layer that ensures the baseline safety of the vessel by reactively avoiding both static and dynamic obstacles that pose an immediate collision risk to the ASV, either from unmapped static obstacles, late detection of target ships, or unpredictable target ship behaviour not accounted for in the higher levels.

In the following, a review of existing algorithms suited for the bottom two layers in the hybrid COLAV system is given. The review is not exhaustive, and the reader is advised to see [53] for a survey of path planning and collision avoidance algorithms, and [54] for a comparative study of the algorithms reviewed in [53]. For trajectory planning methods suitable for the top-level COLAV, the reader should see the work of Bitar [55].

The VO algorithm is a reactive collision-avoidance method based on similar principles as the anti-collision indicator by Mitrofanov from 1968. In 1993, the VO algorithm was reinvented by Fiorini and Shiller [56],[57]. The method is based on representing dynamic obstacles as velocity obstacles in the velocity space of the vessel, where velocities within the VOs will result in a collision, given that all vessels maintain their velocity. When all relevant obstacles are represented in the velocity space, the task of collision avoidance comes down to selecting a velocity from the unobstructed parts of the velocity space. The simplicity and intuitive nature of the method has made it popular for collision avoidance in several fields, and it has frequently been applied for ASV collision avoidance [58–60]. In 2014, Kuwata, Wolf, Zarzhitsky, and Huntsberger [61] augmented the method to consider parts of the COLREGs. They propose to first evaluate the risk of collision with other vessels by using DCPA and TCPA estimates. If risk of collision is deemed to exist, an additional velocity obstacle is assigned to the vessels, where this VO blocks all velocities that result in passing the opposing vessel on the starboard side. They also demonstrated the method on an ASV in full-scale experiments with a radar- and camera-based tracking system, where the ASV resolved head-on and give-way crossing encounters in compliance with Rule 14 and Rule 15.

The additional VO from [61] is adopted by several others, like Kufoalor et al. [62], where an assessment of the level of cooperative behaviour between encountering vessels is considered to adjust the size of the VOs, and Zhao et al. [63], where the method for evaluating the risk of collision is based on evidential reasoning, and Huang et al. [64] and Shaobo et al. [65], where the dynamic constraints of the vessel is considered by use of generalized VOs. Furthermore, in [65] the risk of collision is evaluated by a fuzzy-logic system, and they also propose a finite state machine (FSM) to monitor interactive actions by other vessels during a maneuver, enabling re-evaluations if the maneuver is not effective. The same VO is also applied

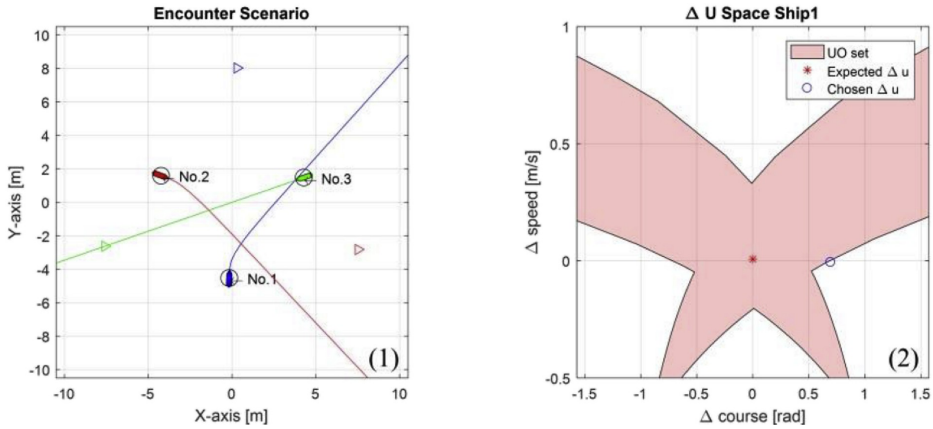

Figure 2.4: Left side shows an encounter between three vessels. The right side is the velocity space of Ship 1, where the resulting generalized VOs from the opposing vessels are shown in red. Figure is from [64].

by Cho et al. [66], where it is enforced as a soft constraint by penalizing velocity candidates within that VO in the cost function. In Figure 2.4, the velocity space of a vessel in an encounter with two other ships is shown. The resulting VOs from the opposing vessels are shown in red.

The dynamic window (DW) is another collision avoidance algorithm, proposed by Fox et al. [67], for maneuvering of indoor ground robots. The method consists of constructing a discrete finite set of possible velocities for the vessel, and subsequently removing all velocities that either are not reachable (outside of the dynamic window), or result in a collision within a given time. A maneuver from the remaining set of velocities can then be chosen based on objectives such as how well the velocity coincides with the desired direction of travel. The velocity space and dynamic window of a land-based robot is shown in Figure 2.5. In [68], the DW algorithm is applied for ASV collision avoidance with a radar-based target tracker. In [69], COLREGs consideration is included by first evaluating the collision risk in a vessel-to-vessel encounter based on estimated DCPA and TCPA, and if risk of collision is deemed to exist, all velocity candidates that correspond to a port maneuver are removed, hence forcing any maneuver to avoid collision to be a starboard maneuver.

Another popular method for reactive maneuvering is the artificial potential field (APF) method, also called virtual force field. The method consists of assigning a virtual attractive and repulsive force to the goal position and obstacles, respectively, and then calculating a velocity reference from the orientation and magnitude of the resulting potential field at the position of the vessel, as illustrated in Figure 2.6a. In [70], APF is applied for ASV path following and collision avoidance. A fuzzy-logic based rule

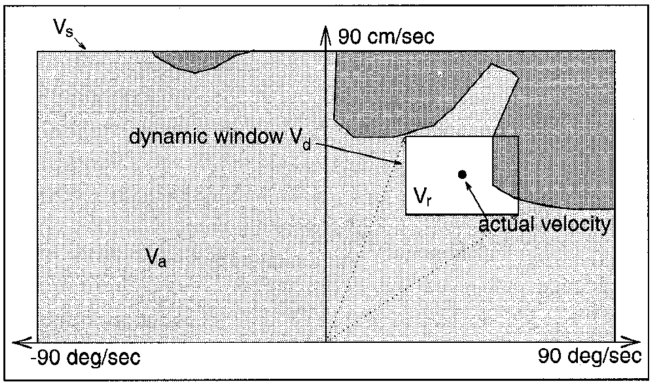

Figure 2.5: The velocity space for a mobile land-based robot capable of moving forward at 0.9 m/s and yawing at 90 °/s. The dynamic window is the set of velocities that are reachable within a given time, and the dark grey regions are inadmissable velocities that result in collision within a given time. Collision avoidance comes down to selecting an admissable velocity from the dynamic window. Figure from [67].

system is proposed for determining the need for evasive maneuvers with respect to dynamic obstacles. The fuzzy system scales the weight of the path following and collision avoidance objectives accordingly. Compliance with the COLREGs is enforced by only enabling starboard manuevers. Another approach to consider COLREGs in the APF method was proposed by Lee et al. [71], where they augmented the APF with vortex fields of counter-clockwise direction. The vortex fields were centered on the position of the target ships, as shown in Figure 2.6b. The vortex fields altered the direction of the APF close to the target ships, giving a bias towards starboard maneuvers for collision avoidance.

The VO and DW can both apply a discretized set of maneuvers. Hence, searching the maneuver space is fast. This makes them ideal for reactive collision avoidance, as they can be run at a high frequency, and give immediate reaction to new sensor input or tracking data. The output of both algorithms is a velocity vector that can be directly realized by the vessel's control system, making them suitable for the low-level COLAV in the hybrid structure in Figure 2.3. However, the reactive nature of the methods makes them unsuitable for handling the more vague parts of the COLREGs, like rules 8 and 16. Furthermore, they are prone to producing locally optimal maneuvers with respect to global path-following objectives. To improve compliance with these parts, trajectory planning methods must be applied. By planning a trajectory for a future horizon, and by making predictions of the future states of other vessels within that horizon, maneuvers can be conducted in ample time, and a more qualified choice of maneuver can be made.

A popular approach to trajectory planning is model predictive control

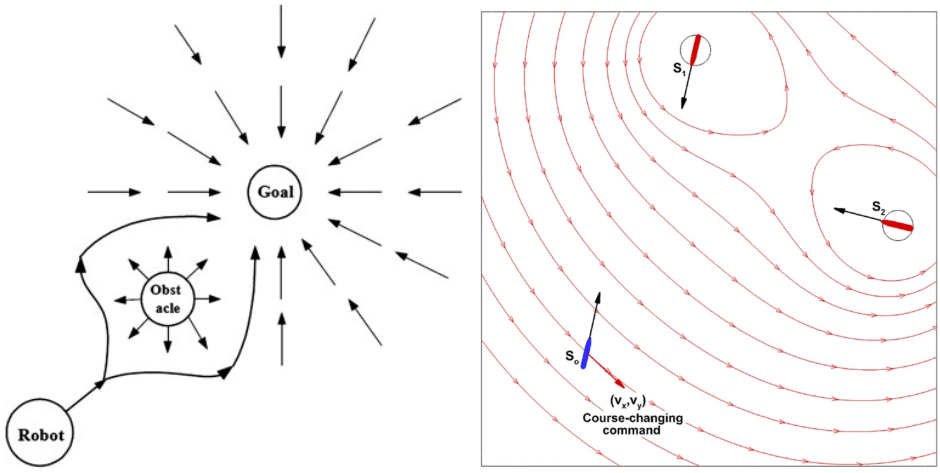

(a) (b)

Figure 2.6: Artificial potential field method. (a) Repulsive forces from obstacles and attractive forces from goals are superimposed. The resultant force at the position of the robot gives the direction of the velocity vector. Figure from [70]. (b) Vortex-like fields with counter clockwise direction at the position of target ships motivate starboard maneuvers when avoiding collision. Figure from [71].

(MPC)-based optimal control methods, where the trajectory planning problem is formulated as an OCP subject to a set of constraints. The format of the optimal control problems is ideal for handling both mission and safety objectives, e.g., trajectory planning and collision avoidance, since mission objectives can be motivated through the objective function, while safety objectives can be enforced through constraints. This can ensure that the safety objectives are not compromised on behalf of other objectives.

Such MPC-based trajectory planners for ASVs are proposed by Eriksen and Breivik [72], Xue et al. [73], and Abdelaal and Hahn [74], where an OCP is formulated based on a nonlinear vessel model. Collision avoidance with static and dynamic obstacles is enforced by assigning circular domains to the obstacles and formulating constraints in the configuration space of the trajectory with respect to the circle boundaries. In [72], Rule 8 is considered by a cost function that favours course change maneuvers of a certain magnitude. However, no consideration to rules 13-17 is made. In [73] and [74], a higher cost on port maneuvers in the objective function is proposed to facilitate compliance with Rule 14 and Rule 15. All three methods are demonstrated through simulations, but the robustness in terms of COLREGs compliance is questionable, since a bias towards starboard maneuvers shows only a limited appreciation of the principles of the maneuvering regulations. Furthermore, by enforcing starboard maneuvers

in the cost function, port maneuvers are still admissable if it results in sufficient reduction in cost, with respect to other objectives. The risk involved in making port maneuvers to avoid close quarters can not be overstated. Furthermore, modeling static obstacles as circles, does not scale well to cluttered and confined space areas with complex geometries. This can however be handled by constructing convex sets that are free of static obstacles along the transit path, as proposed by Brito et al. [75], for maneuvering a robot in an unstructured indoor environment, and Martinsen et al. [76] for docking and berthing of ASVs.

A challenge with nonlinear optimal control-based methods formulated in a continuous configuration space is that such problems require advanced solvers. The runtime for the solver can also be fluctuating, depending on the conditions of the problem. Typically, the time for finding an optimal solution is not upper bounded. Furthermore, efficient off-the-shelf solvers like IPOPT [77] and SNOPT [78] are local solvers, with no guarantees of finding the global minimum. Typical constraints for collision avoidance, like e.g. circular constraints, result in a non-convex configuration space with local minima passing on either side of each obstacle. Hence, the solvers are prone to converge to locally optimal solutions.

A simulation-based MPC approach to local trajectory planning is proposed by Tan et al. [79], which mitigates these challenges by discretizing the configuration space of the trajectory planner. This gives a predictable runtime, and guarantees a global solution, albeit for a reduced configuration space. The method is a two-step process. First, a set of short-term trajectory candidates is constructed by simulating a vessel model performing a finite set of course and speed change maneuvers. Thereafter, each trajectory is evaluated based on criteria for arrival time, cross track error and safety, and the best scoring trajectory candidate is chosen. The safety is evaluated based on the candidate trajectory's intersection with a target ship domain. They propose an encounter-specific target ship domain for head-on, give-way crossing, and stand-on crossing encounters, which comprises a circular domain centered at the position of the target ship, and an additional geometry that extends the domain to the side of the target ship that the vessel should avoid passing on, according to the COLREGs.

A similar method is proposed by Eriksen et al. [80]. They consider collision avoidance for a high-speed ASV with nonlinear dynamics. A set of trajectory candidates is constructed by simulating a vessel model performing three consecutive maneuvers of a fixed duration, where the maneuvers are sampled from a finite set of surge speeds and yaw rates. A cost function is applied to evaluate each candidate trajectory based on its tracking error to a reference trajectory, and its intersection with a target ship domain. The authors propose a target ship domain, shown in Figure 2.7b, which is constructed from quarter ellipses with increased

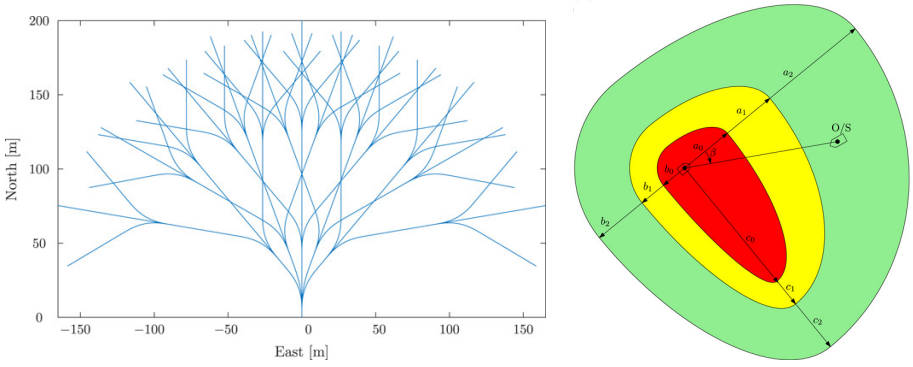

(a) (b)

Figure 2.7: The branching course model predictive control algorithm for collision avoidance for high-speed ASV. (a) A set of trajectory candidates constructed by simulating three consecutive maneuvers. (b) A target ship domain with the target ship in the red areas, and an ownship in the green area. Figure from [80].

extension to the fore and starboard of the target ship. This gives a higher cost for trajectories passing close in front, or on the starboard side of the target ship, and hence facilitates passing behind or port to port in compliance with Rule 14 and Rule 15. The method is demonstrated in full-scale experiments with a target ship in open waters, where it demonstrates partial compliance with COLREGs Rule 14 and Rule 15.

Another simulation-based method for ASV collision avoidance is proposed by Johansen et al. [81], where a finite set of maneuvers are applied for simulating trajectory candidates for the ownship. Each trajectory candidate is evaluated by their tracking error from a nominal trajectory, and a risk metric as a function of collision risk and grounding risk. Furthermore, an asymmetric cost favouring starboard maneuvers over port maneuvers is proposed for compliance with COLREGs rules 14 and 15. The method is tested in full-scale experiments with up to several target ships in [82, 83]. It is further augmented by Tengesdal et al. [84, 85] by improving the collision risk evaluation in vessel-to-vessel encounters, and in [86] by using an intent model to predict the behaviour and future trajectory of target ships to improve the risk-evaluation for each trajectory candidate. The method demonstrates partial COLREGs compliance through simulations and experiments. However, it is also prone to non-compliant behaviour, which is due to the multi objective evaluation of each trajectory, considering tracking error, collision safety, maneuver compliance, and grounding risk, as is demonstrated in [81].

While the use of a discrete set of trajectories in [80] and [81] improves consistency with respect to runtime, it considerably reduces the available configuration space of the trajectory. This is not a problem in itself,

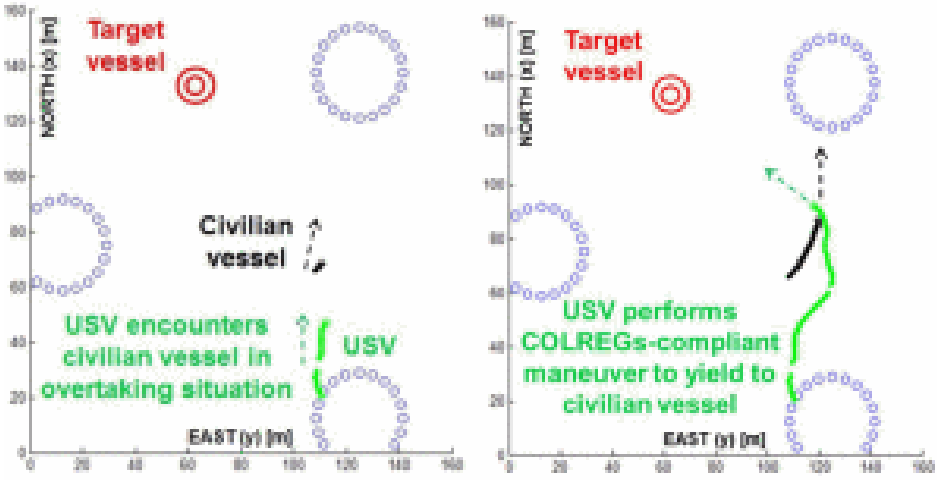

Figure 2.8: Scenario from experimental results in [87, 88]. The USV overtakes by a starboard maneuver, and crosses in front of the civilian vessel, instead of overtaking on the port side, which is a better choice given the goal position denoted "Target vessel". This happens because COLREGs compliance is enforced by only allowing starboard maneuvers. Figure from [88].

however, it adds domain dependency to the method, that is, the magnitude and duration of maneuvers required in open sea encounters is different than for confined areas like fjords, harbours, or canals. If the ASV from [80] was to navigate a canal, of 100 m width, a large set of the trajectory candidates in Figure 2.7a would lead to collision with the canal banks.

A hybrid collision avoidance system for confined space maneuvering is proposed by Shah et al. [87], comprising a graph-based trajectory planner and VO for reactive collision avoidance. The trajectory planner is a lattice-based A* search-method, where collision risk and the availability of contingency maneuvers with respect to dynamic vessels is considered. Furthermore, they apply a prediction model for the future trajectory of other vessels based on historic behaviour and a priori knowledge of the vessels' goals. In the prediction model, they apply the VO algorithm for modeling COLREGs-compliant behaviour. In the trajectory planner, COLREGs considerations are included by evaluating a set of control actions from each position in the lattice structure, and removing control actions that result in port maneuvers if risk of collision is deemed to exist [88]. The method is demonstrated through experiments where it shows some degree of COLREGs compliance. However, the lack of appreciation to the maneuvering principles of COLREGs by simply avoiding port maneuvers is clear from the experimental data. In the scenario shown in Figure 2.8, the ASV overtakes a target ship on the starboard side, and proceeds to cross in front of it, instead of overtaking on the port side, which is a better

choice given its goal, denoted "Target vessel" in the figure.

Over the years, several promising methods have been developed for collision avoidance for maritime vessels. All of the reviewed methods are demonstrated to give more or less collision-free maneuvering. However, when maneuvering to avoid collision with other vessels, the ASV must adhere to the COLREGs. This is paramount to ensure the safety of the ASV and other vessels, as the main purpose of these regulations is to prevent collisions at sea, and other vessels will expect the ASV to manuever in compliance with them. In this regard, two recurring shortcomings in the reviewed work have been identified: (1) The mechanisms for avoiding collisions do not show full appreciation for the maneuver-specific parts of the COLREGs, and (2) The COLREGs considerations are not enforced by strict constraints, which allows for non-compliant maneuvering if it increases performance with respect to other objectives. The main contributions of this thesis are towards improving these shortcomings.

2.3 Ship safety domains

As seen in the previous section, when evaluating maneuvers to avoid close quarters with other vessels, and in particular when considering the the safe passing distance, a domain is often applied to the target ships. The domain is designed so that if the target ship's domain is not violated, the risk of collision is at an acceptable level. Such domains have for a long time been a tool for human operators to evaluate the efficiency of avoidance maneuvers. The simplest version of such a domain is a circle with its center at the position of the target ship, which effectively is the same as the DCPA estimates available in the early ARPA systems.

The ship domains as a concept was introduced by Fujii and Tanaka [89]. The domain they proposed was formulated based on studies of marine traffic in congested areas in Japan. It takes the form of an ellipse with its major axis aligned with the heading of the vessel, as shown in Figure 2.9a. This domain effectively demands a larger range to other vessels in front and aft of the ownship, than on the side. Another early ship domain is proposed by Goodwin [90], where the domain is derived from a statistical study of the passing distances between vessels in historical ship encounters. The domain is shown in Figure 2.9b, and it comprises three sectors with varying radial extension around the position of the vessel. The sector extension gives the minimum preferable passing distance to another vessel in give-way, stand-on and overtaking encounters. They also discuss how the range in each sector is affected by factors like vessel speed, size, traffic intensity and operational domain. A more comprehensive review of ship domains and their application is given in [45].

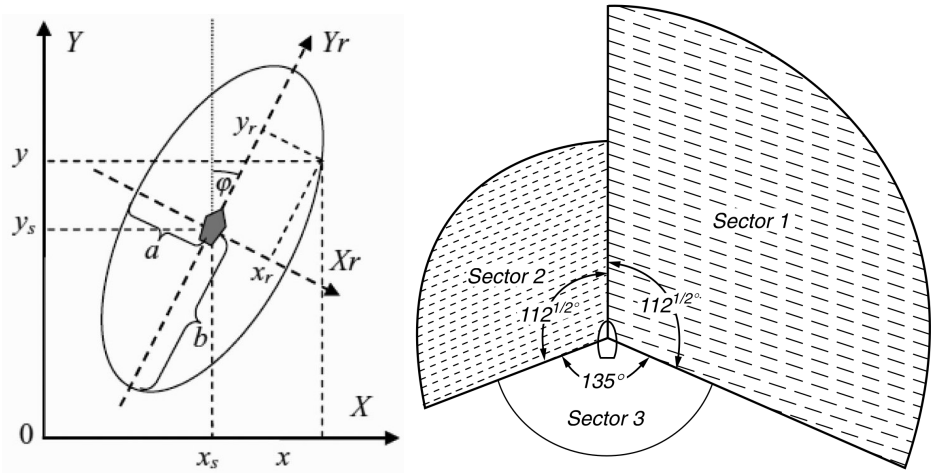

(a) (b)

Figure 2.9: Ship safety domain. (a) Elliptical domain with extended safe distance to the fore and aft of the vessel [89]. (b) Domain constructed from sectors with varying extension in the relevant areas for overtaking, give-way crossing, and stand-on crossing [90].

The concept of a ship safety domain is useful for both human and machine navigators when evaluating the risk of collision or the need for a maneuver to avoid close quarters. However, ship domains like the ones by Fujii and Tanaka [89] and Goodwin [90] do not in themselves suggest a maneuver to resolve a potential conflict. For human navigators, this decision is made based on experience and knowledge. For autonomous maneuvering systems, this must be derived by other means. From Section 2.2, it was highlighted that enforcing COLREGs-compliant maneuvers by means of a pure cost contribution to a multi-objective optimization problem gives little robustness, and that non-compliant maneuvers should rather be restricted by hard constraints. However, it was also shown that primitive constraints, like removing the option of port maneuvers, show limited appreciation of the maneuvering principles of the COLREGs.

Applying spatial ship safety domains, often called target ship domains, and enforcing them as strict constraints, is a common approach, as in [61, 72–74] where circular domains are applied. Some propose to take COLREGs into account by extending the domain on the side opposite to the compliant side, such as the domains by Chiang and Tapia [91] and Tan et al. [79], shown in Figure 2.10b and Figure 2.10a, respectively. The domains from [91] and [79] with suitable trajectory planners are demonstrated in numerical simulations in head-on encounters with two vessels approaching dead-on on parallel paths, and in dead-on crossing encounters on perpendicular paths, where compliant maneuvering is shown.

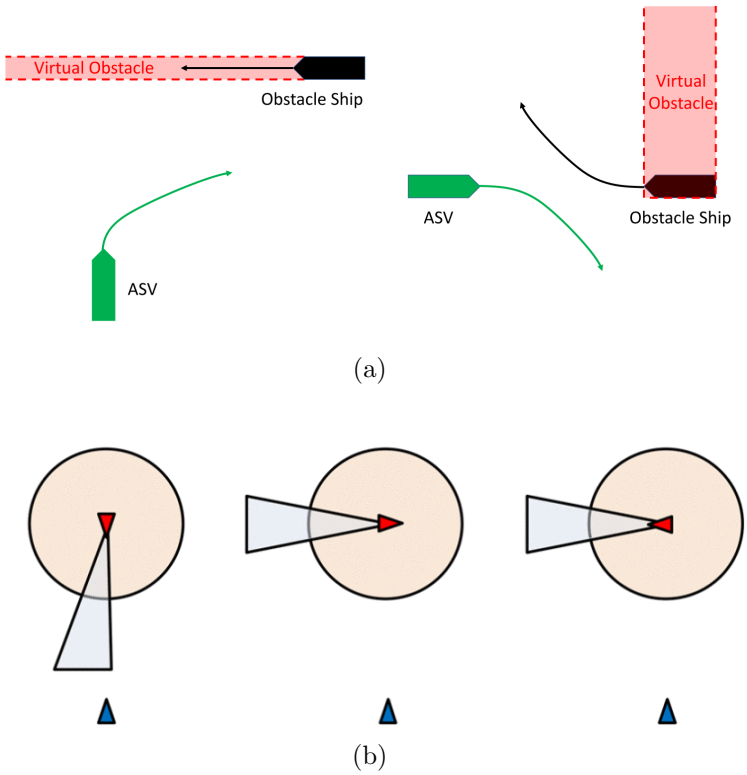

Figure 2.10: COLREGs-specific target ship domains extending further towards the non-compliant side, to motivate passing on the rules-compliant side. (a) Figure from [91]. (b) Figure from [79].

However, the robustness of the domains is questionable, where it is fair to assume that, for example with some separation of the paths in head-on encounters, would result in a port maneuver to pass starboard to starboard, which the COLREGs specifically advices against.

If the ship domain in itself is the mechanism for enforcing COLREGs-compliant maneuvering, the domain must be designed in such a way that it restricts non-compliant maneuvers in all encounter geometries. Target ship domains that only span the spatial dimensions might not be sufficient, since also the relative velocity, i.e., the maneuvering of the vessels prior to the closest point of approach (CPA), is an important feature in the regulations. Some of the main contributions in this thesis are therefore towards a target ship domain that is spanning both the spatial and velocity dimensions, to cover all non-compliant maneuvering options, and hence give robust compliance in multi-objective operations.

2.4 Vessel model

The methods for collision avoidance reviewed in Section 2.2 apply assumptions about the behaviour of the ownship through what is often called a vessel model. The vessel model is a conceptual or mathematical description of the ownship that can be used to make predictions of the future behaviour of the vessel. A comprehensive overview of vessels models commonly used in maritime applications is given in [92].

In the collision avoidance literature, a vessel model is often applied for two purposes: One is to predict the future states of the vessel as a function of the vessel's control input, to enable optimization of the control input with respect to the planning objectives. The other purpose is to model the dynamic constraints of the vessel to ensure dynamic feasibility of the position, velocity, and acceleration references from the collision avoidance system.

In a hybrid collision avoidance structure, introduced in Section 2.2, the requirements for the vessel model can vary between the separate layers. The choice of vessel model can be dependent on the runtime requirements for each layer and the considerations that are made in that layer. A high-precision model can result in increased runtime, but also enables a more precise optimization with respect to the vessel states that are considered in the planning objectives. The choice of vessel model is therefore mostly dependent on the objectives of the trajectory planning or collision avoidance method. The vessel model must be fit for its purposes, and describe with sufficient precision the future states of the ownship that are relevant for the planning objectives. E.g., in [48] and [93], two methods for global trajectory planning and collision avoidance with static obstacles are considered, but the vessel models applied in each planner differ considerably since in [93], an additional objective of energy optimization is considered. In [48], a graph-based path planner with a model without velocity or acceleration dynamics is applied, while [93] applies, a high-fidelity 3-DOF vessel model including the vessel's velocity and acceleration to estimate how the environmental forces and the friction from the water affect the ownship's energy usage.

The vessel type of the ownship also affects the choice of vessel model, e.g., for the mid-level trajectory planners in [23] and [72]. In [23], only the velocity dynamics of the ownship are considered. The planner gives trajectories with discontinuous speed profiles and thereby infinite acceleration. However, the trajectory planner is designed for an ownship that is fully actuated and moving at a low speed, and hence the tracking error resulting from the steps in velocity is acceptable. While in [72], trajectory planning and collision avoidance for an underactuated high-speed ASV is considered. In the trajectory planner, a 3-DOF vessel model must be applied to consider the non-holonomic constraints of the vessel and hence

ensure a trajectory that can be tracked with acceptable tracking error by the ASV.

When considering safety-critical objectives such as collision avoidance, a large tracking error can affect the safety of the ownship and target ships if it is not properly considered. If an upper bound on this tracking error can be determined either analytically or empirically, the tracking error can be compensated for by, e.g., extending the boundary of the ship safety domain correspondingly. However, if quantifying the tracking error or compensating for it is infeasible, the shortcomings of the vessel model must be handled at a lower level in the hybrid structure. This is discussed in [24], where a reactive collision avoidance method considering a 3-DOF vessel model including velocity, acceleration and the vessel actuators is proposed to ensure the bottom-line safety of a hybrid collision avoidance system, independent of the performance of higher COLAV levels.

In the collision avoidance methods proposed in this thesis, a variety of vessel models are applied. In the cases where the applied model differs considerably from the actual ownship vessel, the effects of these model errors are discussed. Furthermore, the modelling errors are compensated for in the low-level control by the use of a reference model to ensure continuous velocity and acceleration reference signals in the vessel's motion control system.

Chapter 3

Contributions

This chapter contains a detailed description of the contributions in this thesis.

3.1 Trajectory planning and collision avoidance for canal crossings

At the start of this PhD work, the *milliAmpere* had only recently been commissioned with thrusters, a thrust allocation algorithm, dynamic positioning (DP) capacities, and a navigation system based on GPS. At this point, the vessel did not have any capacity for autonomous maneuvering. One of the goals of the Autoferry project is to to demonstrate the potential for autonomous passenger ferries as a viable alternative to building bridges for pedestrians in urban areas. Therefore, the first use case that we considered was a short ferry crossing of about 100 m between Ravnkloa and Vestre Kanalkai in the center of Trondheim. The transit area is depicted in Figure 3.1.

The objective was to develop a method for maneuvering the vessel from its current position to a desired docking location on either side of the canal. Furthermore, the maneuvering method should have capacity for avoiding collision with other vessels moving in the canal. The short transit length and the restricted maneuver space required a maneuvering method that did not deviate far from a nominal transit path between the docking locations, as this would result in an unnecessary lengthening of the transit route, and also risk conflict with static obstacles.

Therefore, a method based on the principles of path-velocity decomposition was developed. This principle was first introduced by Kant and Zucker [94], where they proposed to separate the trajectory planning problem into a dual problem of path planning and velocity planning by first generating a path that is free of collision with static obstacles, and then generating

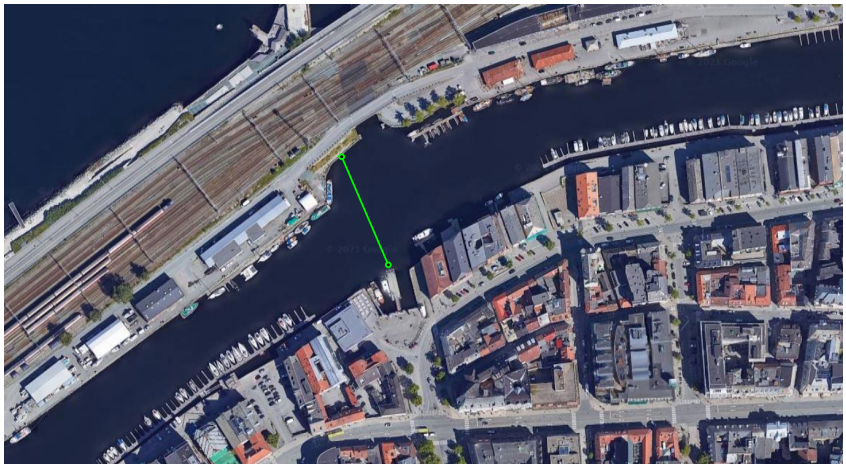

Figure 3.1: Short crossing between Ravnkloa and Vestre Kanalkai in the canal in Trondheim. The transit path of about 100 m and the two docking locations are indicated by the green line. Courtesy of Google Maps.

a velocity profile for that path, where the resulting trajectory is free of collision with both static and dynamic obstacles. By applying a predefined path connecting the two docking locations, we could ensure that the ferry would not deviate from the transit area due to excessive maneuvering when avoiding other vessels. The proposed trajectory planning method is described in Paper A.

This trajectory planning method was first tested on the *milliAmpere* in the summer of 2019, in a large harbour basin in *Brattøra* in Trondheim. At this point, the ferry did not have a situational awareness system capable of detecting other vessels, so the experiments were run with simulated obstacle vessels. The results of these experiments are included in Paper A.

After the ferry was fitted with exteroceptive sensors, and a target tracking system, this trajectory planning method has been used to demonstrate fully autonomous ferry operation on several occasions, such as a 3-hour continuous dock-to-dock crossing operation between Ravnkloa and Vestre Kanalkai with traffic in the canal in December 2020, and in a demonstration for the French navigation authority visiting on behalf of the Paris Olympics organization during an event in Trondheim on the 7th of April 2022 [95]. A still frame from a video[1] from the 3-hour test conducted in December 2020 is shown in Figure 3.2. In the bottom left corner, the target ship domain of two tracked vessels are shown. One of them is the track of the

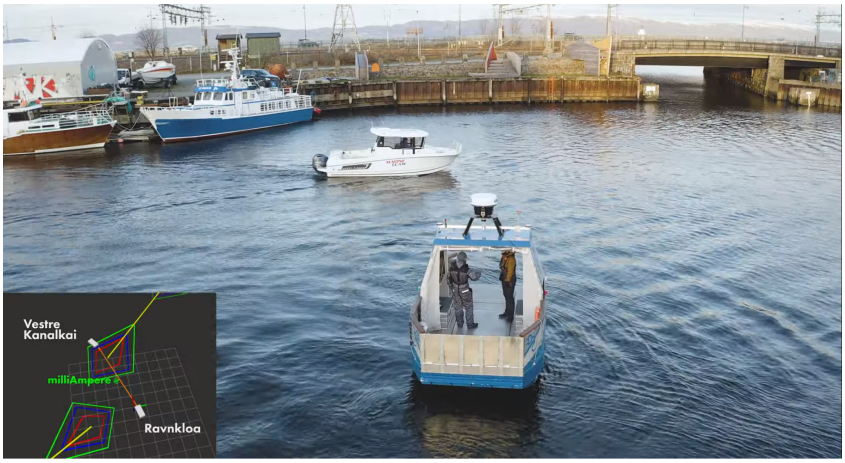

Figure 3.2: Still-frame from a video of a 3-hour test of continuous autonomous ferry crossing with the *milliAmpere* between Ravnkloa and Vestre Kanalkai. The *milliAmpere* is in the center in the foreground. The bottom left corner shows the obstacle representation of two tracked vessels in proximity to the transit path[1].

white leisure vessel passing in front of the *milliAmpere*.

3.2 Encounter classification

For an autonomous vessel to maneuver in compliance with the COLREGs, the ASV's maneuvering obligations with respect to other vessels must first be determined. In Paper D, a method for classifying a vessel-to-vessel encounter with respect to the COLREGs is presented. The proposed method classifies the ASV to be in one of the following encounter types, where the corresponding encounter-type specific rule from the COLREGs applies:

- Overtaking on starboard side (OT_s): **Rule 13**.
- Overtaking on port side (OT_p): **Rule 13**.
- Head-on (HO): **Rule 14**.
- Give-way crossing (GW): **Rule 15**.
- Stand-on crossing(SO): **Rule 17**.
- Safe (SF): No rules apply.

[1]Video from the 3-hour test of autonomous crossing with *milliAmpere* in the canal in Trondheim, `https://www.youtube.com/watch?v=Ry3-yxVaDuE&list=PLc2vvxBHfBcoHvfcIRsFROmJzXhbJCvb5&index=2&ab_channel=NTNUCybernetics`(accessed June 15, 2022).

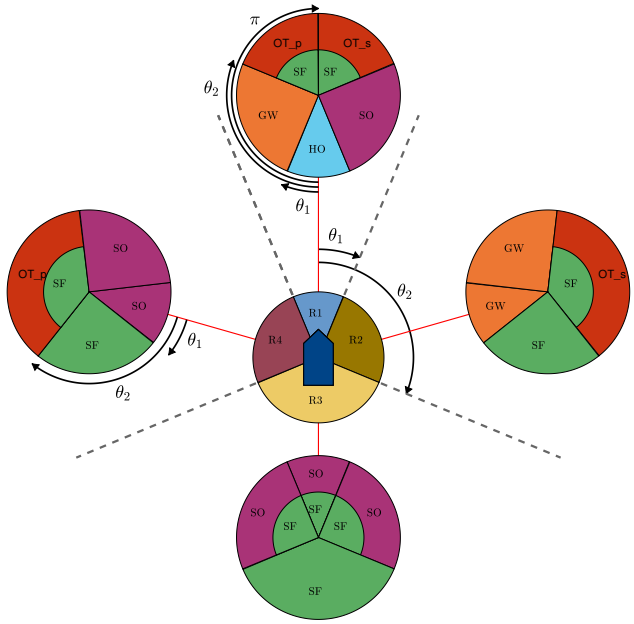

(a)

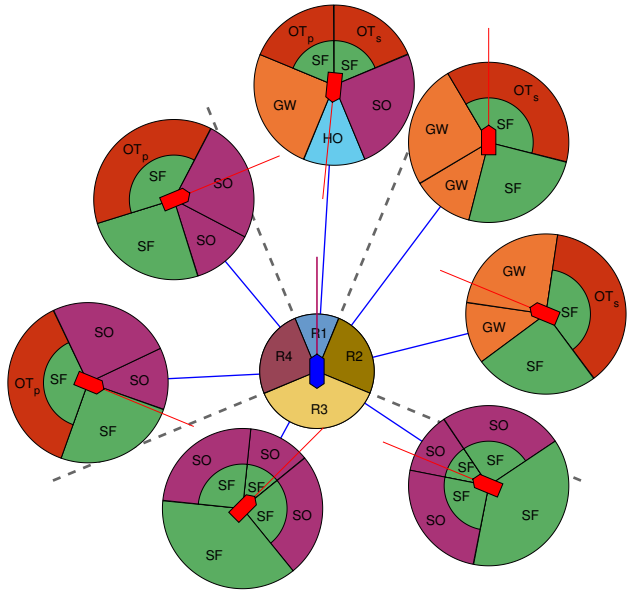

(b)

Figure 3.3: COLREGs encounter classification. (a) Graphical representation of the method. Ownship is at the center, with surrounding sectors with individual sector circles. (b) Classification examples. The sector circle is placed on the position of the target ship, and the sector that the heading of the target ship resides in gives the encounter type. In the sectors with multiple options, the safe (SF) encounter type is chosen if the range between the vessels is increasing. Figures are from Paper D.

The proposed method is based on previous work by Tam and Bucknall [96]. Through extended use of their method, some shortcomings were identified, where it produced wrongful encounter classifications for encounter geometries that were close to the thresholds between head-on and crossing, and overtaking and crossing. The method proposed here improves upon these shortcomings by a more precise mapping of the encounter geometry to the principles of encounter classification described in the COLREGs.

In addition to improving the precision of the classification method, an additional distinction on overtaking encounters has been introduced. Where the original method considered overtaking encounters as one single category, we propose to distinguish between overtaking on the starboard side of the vessel and overtaking on the port side of the vessel. This is very relevant when applying encounter-type specific domains to the target ship as a mechanism for COLREGs-compliant maneuvering, since the two overtaking options require distinct domains to enforce the correct maneuver. The distinction in the classification method was made based on the relative heading between the vessels, where selecting the correct overtaking side ensures that the give-way vessel does not cross in front of the overtaken vessel immediately after overtaking it.

The classification method is based on a graphical interpretation of the encounter, shown in Figure 3.3a, along with examples of classification of several target ships with varying relative position and orientation to the ownship at the center of the figure. Classification is done in two steps; first, the relative bearing of the target ship from the ownship is used to assign the target ship to one of the four sectors around the ownship in Figure 3.3a, then the corresponding circle is placed at the position of the target ship, and the encounter type is determined to be the one in the sector of the circle that the heading of the target ship resides in. In sectors with two encounter types, the SF encounter type is chosen if the range between the vessels is increasing, as proposed by Eriksen et al. [52].

The proposed classification method also includes the functionality introduced in [52], with a state machine that holds any classification other than SF until the encounter is resolved. This ensures that the classification, and hence the maneuver obligation of the ASV, does not change due to the avoidance maneuver of the ASV, e.g., in an overtaking encounter, the overtaking vessel has a continued obligation to give-way and stay clear of the overtaken vessel also after the overtaking vessel has passed the overtaken vessel.

In addition to the collision avoidance method in Paper D, this classification method is also applied in the reactive collision avoidance algorithms in Paper E and the trajectory planner in Paper F, and in the Master's theses [33] and [35].

3.3 Target ship domain

As discussed in Section 2.3, a common way of handling the task of collision avoidance is to assign a safety domain to the target ship, and then formulate a maneuvering law or trajectory planner that maneuvers so as to not violate that domain. However, when the safety domain is applied as the mechanism for COLREGs-compliant maneuvering, the target ship domain must be designed so that it enforces the maneuvering behaviour that the encounter type calls for.

Paper B presents a domain that is assigned to the target ship which considers the specific COLREGs rules that apply. The domains are designed so that if the ownship maneuvers to not violate the domain, it is also maneuvering in compliance with COLREGs rules 13-15 and 17. This is done by first classifying the encounter type, and then formulating the domain as a function of encounter type-specific parameters. The domain is designed as a straight line intersecting the line of sight between the ownship and the target ship, where a deflection angle is applied to orient the line so that the ownship is deflected to the rules-compliant side when approaching the domain.

This domain is further developed in Paper D, where two improvements are included. First, consideration to the operational domain and the available space to maneuver is included. This is relevant for ASVs operating in areas with varying degree of space to maneuver in, e.g., transit operations traversing both confined harbour or canal areas as well as more open sea areas. In confined areas, passing another vessel with a DCPA of 20 m can be considered as acceptable conduct, but doing the same in more open waters would be considered unsafe behaviour. Therefore, to reduce domain-dependency of the system parameters, the available maneuver space should be considered in the target ship domain. We propose to handle this by introducing an estimate of the available space to maneuver at the side of the target ship that the ownship should pass, which is calculated from an ENC. This estimate is then used to scale the size of the target ship domain, that is, the minimum distance from the position of the target ship to the domain boundary.

The second addition to the domain is included to address the challenge of compliant maneuvering when the ownship with give-way obligations is approaching the target ship with such a geometry that the side at which the ownship should pass the target ship is not clear. For example, when the two vessels are approaching each other at near reciprocal course so that they are likely to pass starboard to starboard at a close distance. If the encounter is such that a maneuver is required, it should be resolved by a comprehensive course-change maneuver to starboard to pass the target ship port to port. If instead, a small course change to port is applied

by the ownship to increase the margins of the passing distance, this can put the ownship in direct conflict with the target ship if it performs a rules-compliant starboard maneuver. The importance of not performing such conflicting maneuvers is highlighted by Cockroft and Lameijer [37], where they also back up this claim by examples from maritime law. In [97], the author points out the lack of appreciation for the non-compliance of such port maneuvers in the maritime collision avoidance literature.

In Paper D, we propose to mitigate this possibility of non-compliance by introducing a mechanism specifically for determining the most fitting side at which to pass the target ship. The distinction is made based on the bearing of the target ship from the ownship, relative to the angle of the relative velocity vector between the two vessels. Furthermore, a bias term is added to the angle of the relative velocity vector, so that the threshold for the distinction is shifted in favour of passing on the rules-compliant side. Distinct deflection angles are used to orient the target ship domain based on the preferred side to pass on, to restrict the ownship from maneuvering to the opposite non-preferred side. The efficiency of this mechanism is demonstrated in Figure 3.4, showing a batch of ownship trajectories from vessel-to-vessel encounters with a target ship that follows the same trajectory for every encounter in each plot. The ownship applies the proposed target ship domain as means to achieve COLREGs-compliant maneuvering. The effect of this mechanism is clearly demonstrated, where the ownship either performs a starboard maneuver to give way, or maintains its course and speed to pass at a safe distance.

Since this distinction on what side to pass the target ship on is made based on the orientation of the relative velocity vector, consideration of maneuvers performed by the target ship during the encounter is inherent to the method. E.g., if the target ship in Figure 3.4a was to perform a starboard maneuver at an early stage, some of the constant velocity trajectories that pass starboard to starboard would instead result in a starboard maneuver to pass port to port.

The principles of this target ship domain is applied to the collision avoidance methods in Paper B, Paper D, Paper E, and Paper F, where it is demonstrated through simulations to enforce maneuvers that are compliant with the encounter-type specific COLREGs rules 13-15 and 17. In Paper D, a collision avoidance system using this domain is also demonstrated in full-scale experiments with a target ship that is tracked by radar and lidar [28].

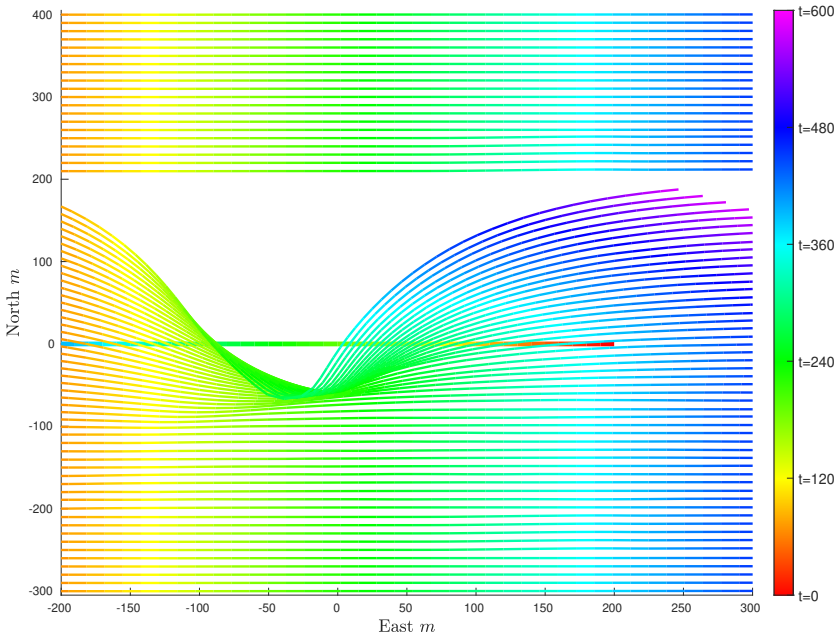

(a) Head-on encounters

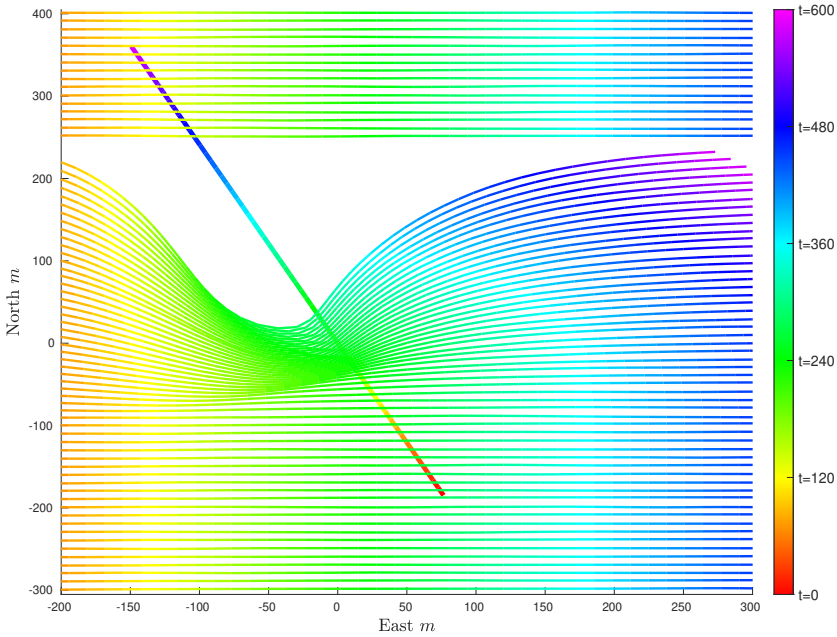

(b) Give-way crossing encounters

Figure 3.4: Batch simulations demonstrating the effects of the method for determining which side the ownship should pass the target ship on. In the figure, a batch of ownship trajectories are moving west to east. The target ship follows the same trajectory in each simulation, moving east to west in (a), and diagonally in (b). Figures are from Paper D.

3.4 Reactive collision avoidance

Several of the papers included in this thesis describe reactive maneuvering methods that handle both path or trajectory tracking and collision avoidance.

Paper B presents a trajectory tracking and collision avoidance method for ASVs. In the method, a version of the target ship domain as discussed in the previous section is applied, where the domain boundary is enforced by control barrier functions (CBFs). The CBFs are formulated with respect to a 3-DOF model of the *milliAmpere* vessel, including a linearized model of the vessel's thruster dynamics. The trajectory tracking and collision avoidance objectives are formulated as a quadratic problem minimizing the tracking error to a reference trajectory by optimizing the actuator setpoints for the vessel's azimuth thrusters, subject to the constraints from the CBFs and actuator rate constraints. The method is suitable for the bottom layer of a hybrid structure as shown in Figure 2.3. By unifying the collision avoidance objectives with the thrust allocation method, the baseline safety of a complex collision avoidance system comprising several layers of planning can be ensured, by directly restricting the actuator setpoints from unsafe configurations. The method is demonstrated in simulations and shows compliance with COLREGs rules 13-15 and 17.

A downside with the method in Paper B arises from the guidance method that is applied, where it attempts to strictly follow a time-parameterized reference trajectory. Avoidance maneuvers make the ownship deviate from the reference trajectory, and as a consequence, the velocity must be increased to catch up with the reference. This affects the performance in terms of passenger comfort, perceived safety, and predictable behaviour. In Paper D, a new guidance method based on line of sight (LOS) is proposed, which allows the vessel to deviate from the reference path while at the same time gives a smooth velocity profile and good tracking of the reference speed.

Furthermore in Paper D, the collision avoidance method is augmented with functions for handling static obstacles. The paper proposes a method for constructing a convex set around the position of the ownship that is free of static obstacles based on ENC. The boundary of the convex free set is enforced by CBFs in a similar way as for the target ship domain. The proposed method for constructing the convex set is designed to be applied to both ENC and lidar data. Through full-scale experiments in a canal area, it is demonstrate how the lidar can be used to effectively compensate for static obstacles that are not mapped in the ENC, such as floating docks, docked vessels, and sea-markings. This is demonstrated in Figure 3.5, where an overview of a scenario from the experiments is shown. In the figure, the ownship is the blue vessel, the obstacles from

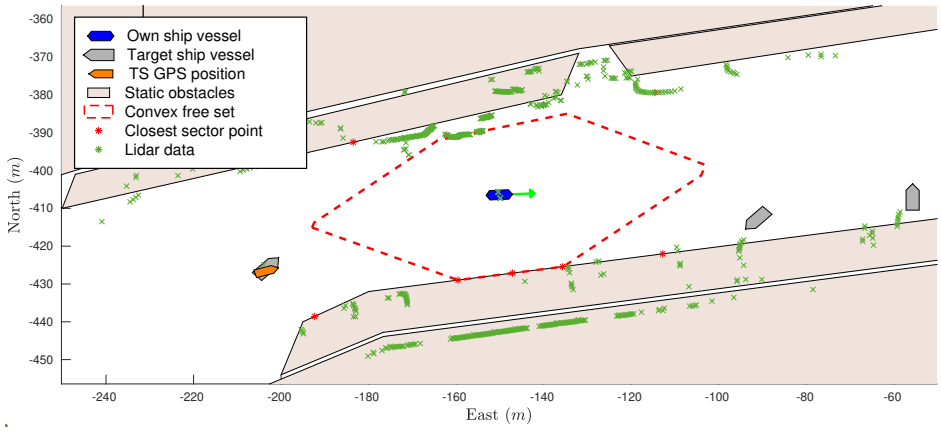

Figure 3.5: A convex set that is free from obstacles, constructed from lidar data and ENC. The lidar data compensates for unmapped features like docked vessels, as can be seen from the lidar measurements of the the hulls of several vessels to the north of the ownship.

the ENC are sand colored, and the lidar measurements are shown as green crosses. Above the position of the ownship in the figure, the boundary of the convex set, indicated by the red polygon, is restricted by the lidar measurements. Here, the lidar detects the hull of a docked vessel along the quay, which is not in the ENC.

Paper D describes a complete system for path following and collision avoidance for ASVs operating in the presence of static obstacles and other vessels. The system is suitable for the low-level COLAV layer in the hybrid system in Figure 2.3. The system inputs a set of waypoints with corresponding speed references, navigation data from a GPS, lidar data, and tracking data for other vessels, and it outputs a generalized force to the vessel's thrust allocation system. The system is demonstrated through experiments with closed-loop autonomy, where a radar- and lidar-based tracker is used for tracking target ships. The system has capacity for autonomous maneuvering in compliance with COLREGs rules 13-15 and 17.

In Paper E, the mechanisms for collision avoidance from Paper D are adapted to the popular velocity obstacle collision avoidance algorithm. Instead of applying CBFs as means of enforcing the boundaries of the target ship domains and the obstacle-free convex set, the domains are encoded as velocity obstacles. The proposed collision avoidance system is not dependent on a particular vessel guidance and control system, and can hence easily be applied to an arbitrary ASV guidance, navigation, and control (GNC) system to achieve collision-free maneuvering with respect to both static obstacles and other traffic.

3.5 Trajectory planning and collision avoidance

The methods presented in Section 3.4 are all reactive, in the sense that the mechanisms for avoiding collision with other vessels are based on the current estimates of the ownship and target ship states, and the current speed and course references of the ownship. The methods do not apply any predictions of the future states of the other vessels, nor do they make any considerations to the future reference trajectory in calculating the maneuvers. This makes it challenging to consider the more vague parts of the COLREGs. Specifically, rules 8 and 16 regarding making maneuvers in ample time, *with due regard to good seamanship*, and making maneuvers that are *readily apparent to another vessel*.

To achieve an improved compliance with these rules, comprehension of how an encounter between two vessels will evolve is needed. In particular, the ability to estimate if a risk of collision between the vessels exists, and if so, to estimate time and place of a critical point in the encounter, e.g., the critical distance and time to critical distance. When a sufficient understanding of the situation is established, the timing and magnitude of maneuvers to ensure safe passage can be determined to be *with due regard to good seamanship*.

Paper F describes a trajectory planning method for ASVs based on a receding horizon MPC approach. The method has capacity to plan trajectories that are dynamically feasible and collision-free with both static and dynamic obstacles. The trajectory planning problem is formulated as an optimal control problem (OCP) for a 2-DOF model of the vessel's position, velocity, and acceleration. The collision avoidance objectives are encoded as constraints to the OCP. The optimization objectives are to minimize tracking error to a reference trajectory and the induced acceleration.

Dynamic obstacles are considered by applying the classification method described in Section 3.2 and the target ship domain discussed in Section 3.3. Constraints for the OCP are formulated with respect to target ship domains at the predicted position of the target ships throughout the control horizon. The future trajectory of target ships can be estimated by an arbitrary method. However, in Paper F, a constant velocity model is applied. Specific consideration to COLREGs Rule 17, regarding stand-on obligations, is included by introducing a vessel priority list, where constraints are formulated only for the vessels in the list. The stand-on requirements are considered by excluding target ships to which the ownship has a stand-on obligation from the list, until it is eventually clear that the target ship is not abiding its give-way duty.

Consideration of rules 8 and 16 is handled through the introduction of windows of reduced cost on acceleration and tracking error in the planning

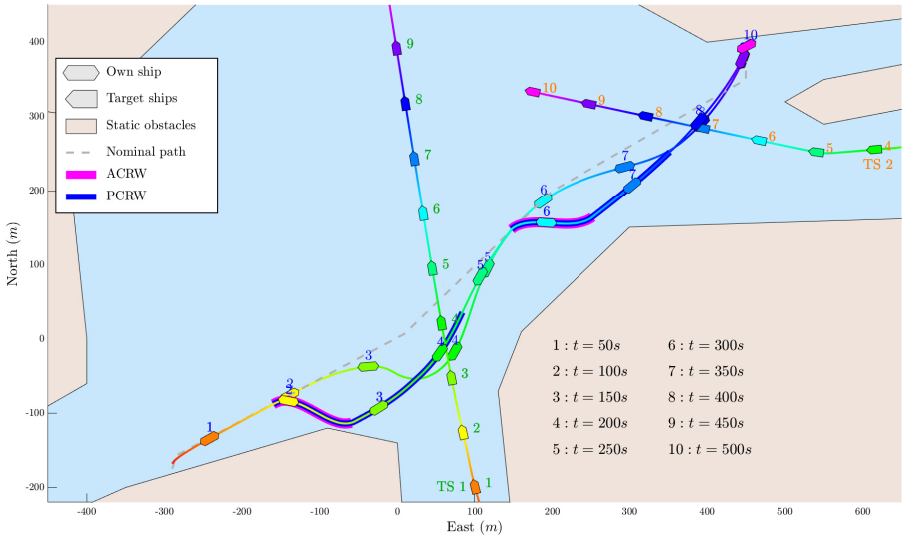

Figure 3.6: Comparison of the ownship trajectory with and without the use of windows of reduced cost for controlling the timing and magnitude of the maneuver. The windows of reduced acceleration cost and tracking error cost are superimposed on the ownship trajectory in purple and blue, respectively, denoted ACRW and PCRW in the legend. The figure is from Paper F.

horizon. The windows of reduced acceleration cost facilitates a maneuver to avoid close quarter to be performed within that window, while the window of reduced tracking error cost allows the trajectory to deviate from the reference trajectory for the duration of the avoidance maneuver. These windows of reduced cost are parameterized by a small set of intuitive parameters, and their timing and duration are calculated based on the estimated time to a critical distance to the target ships in the priority list. This concept is demonstrated in Figure 3.6, where the trajectory from an ownship maneuvering with and without these windows in encounters with two target ships is shown. In the figure, the ownship trajectories are moving from bottom left to top right. The two other trajectories are the target ships. For the ownship where windows of reduced cost are applied, the acceleration and tracking error windows are indicated by a thick purple and blue line, respectively, superimposed on the trajectory. The benefit of this contribution is apparent, where it allows the ownship to make an earlier and more apparent avoidance maneuver.

When optimizing with respect to multiple objectives, the objectives can be contradictory, and prioritization can be a challenge. This is the case when considering objectives such as trajectory tracking, minimum acceleration, and collision avoidance, as was pointed out in Section 3.4. In particular, maneuvers to maintain a safe distance to target ships result in

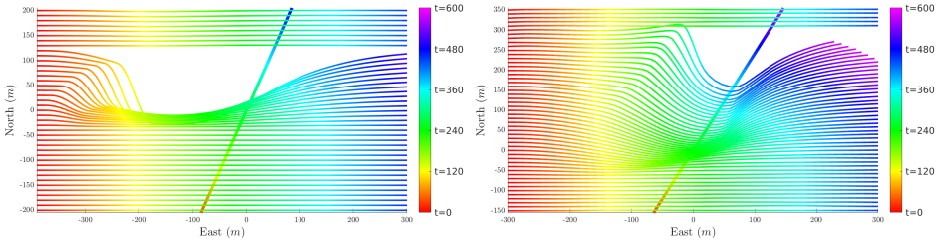

Figure 3.7: Batch simulations demonstrating the benefits of long term planning (a) over reactive maneuvering (b). By predicting the future risk of collision at an early stage, maneuvers can be initiated in ample time and with due regard to good seamanship. Figures are from Paper F.

deviation from the reference trajectory and, hence, a large tracking error. Furthermore, when the tracking error increases, the relative cost of high acceleration is reduced. This can lead to unwanted high acceleration in the start and end of an avoidance maneuver in order to keep the tracking error low. In Paper F, this is mitigated by calculating the reference trajectory for the OCP as a weighted average between a trajectory calculated by a LOS guidance approach, which converges to the reference path, and the optimal trajectory from the previous solution of the OCP. This shifts the reference trajectory closer to the optimal trajectory, which reduces the tracking error of the optimal trajectory, and thereby reducing the effect of the tracking error cost dominating the acceleration usage cost in the objective function. The rationale behind this solution is that safety has precedence, and hence maneuvering in a predictable manner and in compliance with the COLREGs is the top priority. The weighted average applied when calculating the reference trajectory ensures that the reference converges back to the reference path if the risk of collision ceases to exist.

The trajectory planning method is demonstrated through a large set of simulations of vessel-to-vessel encounters in open sea, as well as simulations in urban areas with a varying degree of confined space, where it shows compliance with COLREGs rules 8 and 13-17. The benefit of a long-term trajectory planning method over a short-term reactive method is illustrated in Figure 3.7. Here, Figure 3.7a shows trajectories for the ownship when applying the trajectory planning method from Paper F, while in Figure 3.7b the reactive method from Paper D is applied. By predicting the future states of events, the risk of collision can be detected at an early stage, and maneuvers to avoid collision can be conducted in ample time and with due regard to good seamanship.

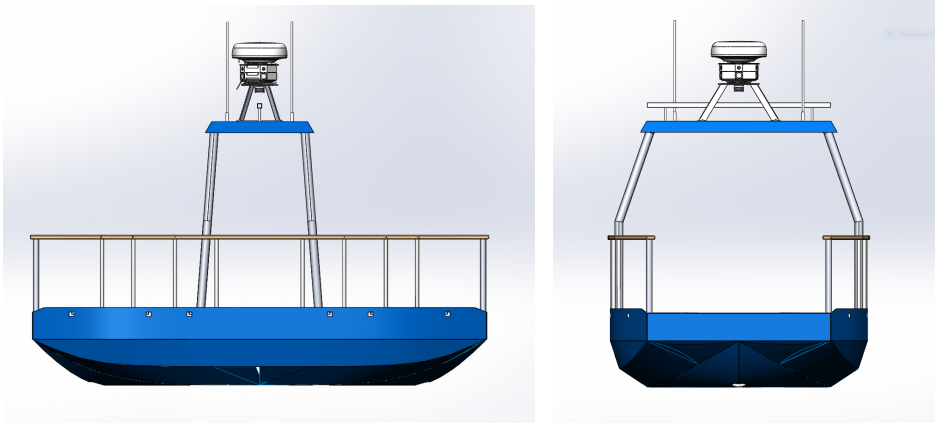

(a) (b)

Figure 3.8: Side and front view of the *milliAmpere*. The hull has a shallow draft, no keel, and a small length to beam ratio, which gives it little directional stability and passive damping. Courtesy of NTNU by Glenn Angell.

3.6 Path-following controller

The *milliAmpere* vessel, which is a half-scale prototype of an autonomous passenger ferry, is designed for canal and river crossings. To minimize the effect of drag from water currents running perpendicular to the transit route, as is often the case when crossing a river, the vessel has a shallow draft and a flat-bottomed hull, as can be seen from Figure 3.8. This is great for energy efficiency, but the lack of a keel gives the vessel very little passive damping in the sway mode. Furthermore, the vessel is bi-directional, and the hull is symmetric in both the longitudinal and lateral axes. Hence, the vessel has an inherent instability in yaw. The destabilizing forces are increasing for increasing surge velocities, and becomes a problem when exceeding about 1 m/s.

In addition, the two azimuth thrusters of the vessel have slow dynamics. So, despite being geometrically fully actuated, realizing a thrust command can take a relatively long time, where the dynamics of the azimuth angles have similar time constants to the dynamics of the vessel yaw angle, much due to the lack of passive damping. In combination with the yaw instabilities, this makes the vessel challenging to control at velocities exceeding 1 m/s.

To mitigate this, a 3-DOF path-following controller has been developed for the vessel. The control law is formulated through a 3-step backstepping process, where the thruster dynamics are included in the final step of the backstepping by first formulating a novel thrust allocation law, allowing the fully actuated thrust allocation problem to be formulated on closed

form. By including the thruster dynamics in the control law, the effects of the slow azimuth rotation can be mitigated, and by actively controlling the sway velocity to zero, the destabilizing effects on the hull are reduced. The proposed controller improves the performance of the vessel's motion control system compared to previous control methods for the vessel, and is able to maintain a stable heading at velocities close to the maximum velocity of the vessel. This work is reported in Paper C.

Chapter 4

Conclusions and further work

This thesis is focused on the tasks of trajectory planning and collision avoidance for autonomous surface vessels (ASVs) in the presence of other vessels in both open and restricted waters.

A trajectory planning algorithm has been developed specifically for short transit operations where the maneuvering space of the vessel is limited to a small set of predefined paths. This enables the reduction of the trajectory planning problem to a velocity planning problem, which enables the problem to be solved by a low-complexity algorithm with a limited runtime. Furthermore, it reduces the need for considering static obstacles in the planning, and gives predictability in the maneuvering of the ferry, by ensuring that the vessel position is confined to the predefined paths, or the space between them. The method is demonstrated through simulations and several short- and long-duration full-scale experiments.

The International Regulations for Preventing Collisions at Sea (COLREGs) is a set of regulations that applies to all vessels, and includes a set of rules for how vessels are to maneuver in the presence of each other to reduce the risk of collision. The first step in maneuvering in compliance with these rules is to determine which rules applies for each encounter. Hence, a COLREGs classification algorithm that determines the maneuvering obligations of the ownship vessel with respect to other vessels has been developed. The algorithm improves upon an existing method with a more precise consideration of the geometry in each vessel-to-vessel encounter. The classification algorithm determines which of the encounter-type specific COLREGs rules 13-17 apply, and it includes a state machine for maintaining the correct classification as the encounter evolves.

Determining the obligations of the ASV is, however, the easy part, whereas maneuvering in compliance with the obligations is a more challeng-

ing one. In particular, it is challenging when multiple competing objectives are at play, such as trajectory planning, passenger comfort, and collision avoidance. This thesis presents a mechanism for enforcing COLREGs-aware behaviour in the vessel's trajectory planning or reactive maneuvering algorithms. It comprises a target ship domain with broad consideration to the COLREGs, where the encounter type, encounter geometry, relative velocity, and available space to maneuver are considered. By enforcing the target ship domains as strict constraints in the maneuvering algorithm, the proposed domain robustly enforces COLREGs compliance independently of other objectives. The target ship domain is applied to three different maneuvering algorithms, where it demonstrates robust compliance with COLREGs rules 13-17.

Several reactive collision avoidance methods for ensuring safe operation of ASVs in dynamic and unstructured areas with other traffic, and limited space to maneuver, have been developed in this PhD project. The methods include capacity for COLREGs-aware maneuvering, as well as collision avoidance with static obstacles with complex geometries. The methods have varying degree of coupling with the vessel's guidance, navigation, and control (GNC) system, ranging from a collision avoidance method fully integrated with the trajectory tracking and thruster controls as in Paper B, to a collision avoidance method decoupled from the vessel's motion controllers as in Paper E and Paper F. This makes the proposed mechanisms for COLREGs-aware collision-free maneuvering with respect to both static and dynamic obstacles easy to integrate in an arbitrary GNC architecture.

A trajectory planner for path following and collision avoidance with static and dynamic obstacles has also been developed. The trajectory planner is formulated as an optimal control problem, minimizing the tracking error to the path and the induced accelerations. In addition to COLREGs rules 13-15 and 17, the planner includes consideration to rules 8 and 16, regarding the making of readily apparent maneuvers in ample time to stay well clear of vessels which the ownship has give-way obligations to. This quality is achieved by assigning windows of reduced cost for tracking errors and accelerations in the control horizon, which facilitate a potential maneuver to avoid collision to be performed within the windows. The cost reduction windows are parameterized by an intuitive set of parameters that set the timing and duration of the maneuver. By calculating these parameters based on the predicted closest point of approach (CPA) for the target ships, the maneuvers to reduce risk of collision can be made in ample time, to ensure good compliance with the expected social conduct of the COLREGs.

The methods developed in this thesis have been verified through extensive simulations. Two types of simulation scenarios have been considered.

The first is an extensive set of vessel-to-vessel encounters in so called batch simulations in open waters to verify the COLREGs-compliance of the method. This set of scenarios is constructed by a distributed sampling from two parameters, one being the relative heading between the two vessels, and the other being the lateral offset of the ownship's trajectory from a trajectory where the vessels collide dead-on. Through these simulations, it is demonstrated that the proposed target ship domain robustly enforces compliance with COLREGs rules 13-15 and 17, and the windows of reduced cost increases compliance with rules 8 and 16. The other type is more complex simulations in a relevant operational domain with static obstacles, varying degree of space to maneuver in, and multiple other vessels with different behaviours. In these simulations, the autonomous maneuvering methods are demonstrated to handle multiple objectives like path- or trajectory-following, collision avoidance, and COLREGs-compliance. In particular, the following is demonstrated:

- The capacity to maneuver away from the reference path or trajectory when an avoidance maneuver is needed, and to converge back to the path or trajectory when risk of collision has been mitigated.
- The ability to maintain an acceptable distance to target ships in both very confined areas and in more open waters.
- The capacity to handle multi-vessel encounters where the opposing vessels are on either constant velocity trajectories or maneuvering.
- That COLREGs compliance is strictly enforced in all encounters despite competing objectives.
- The runtimes of the proposed methods are feasible for real-time operation.

The control barrier function (CBF)-based collision avoidance method from Paper D has been deployed to the *milliAmpere* and tested in full-scale experiments in a canal in Trondheim. In the experiments, closed-loop autonomy was achieved with a radar- and lidar-based tracking system for detection of target ships and estimating their position and velocity. Through the experiments, it was demonstrated that:

- The trajectory tracking and collision avoidance system is capable of tracking the reference path with sufficient precision in a canal with unmodeled current and wind disturbances.
- The collision avoidance mechanisms are robust to the level of noise and uncertainties in the target tracking data. This indicates that the method is suitable to work with state-of-the art tracking systems.

- In confined area operation with a short separation to static and dynamic obstacles, lidar data can effectively be used to compensate for unmapped features in the electronic nautical chart (ENC) and vessels not detected by the target tracker.
- With a target tracker based on exteroceptive sensors that track target ships' position and velocity relative to the ownship, and a lidar that measures the range and bearing to static obstacles, the collision avoidance capacities are robust to uncertainties in, and even loss of, navigation data. It is, however, still prone to grounding and obstacles not detectable by lidar.
- The method is suitable for real-time applications.

During the experiments, the experience from the persons onboard both the *milliAmpere* and the controlled target vessel was that the autonomous vessel maneuvered in a predictable manner, with smooth but yet readily apparent maneuvers, and that it maintained a safe distance to both the target vessel and static obstacles, even in confined areas where the separation between the vessels was less than 15 m.

Further work

While we are getting closer to autonomous maritime operations, there is still a lot of work to be done within several related topics. During the work on the contributions described in this thesis, the following topics were identified to be relevant for further advancement in the field of ASVs:

COLREGs-compliant maneuvering: While this thesis proposes methods for autonomous COLREGs-compliant maneuvering, it only attempts to address a subset of the rules and regulations that applies. Other rules that are most relevant for urban area operation, and that should be considered in future work are:

- Rule 6, regarding proceeding at safe speed. When encountering traffic in confined areas, the speed should be adjusted accordingly, and in very confined areas, the speed should be adjusted to avoid overtaking when the space to do so is limited.
- Rule 7, regarding evaluating the risk of collision. Evaluating the collision risk is preliminary to reducing risk of collision. Improved methods for evaluating the risk of collision in confined areas with multiple maneuvering vessels should be pursued.
- Rule 9, regarding maneuvering in narrow channels. This is relevant for ASVs maneuvering in canals and areas where vessels are restricted

to a dredged traffic lane. In such domains, the stand-on obligations in overtaking encounters are particularly important to not impede an overtaking vessel. Furthermore, in such scenarios, cooperative behaviour to reduce collision risk for all vessels is a relevant objective.

- Rule 18, regarding responsibility between vessels types. Consideration to the specific obligations for sailing vessels, fishing vessels, and vessels restricted in their ability to maneuver should be made in the autonomous maneuvering. Work on detection and classification of these vessels must then also be pursued.
- COLREGs Part D, regarding signs and signals. The sounds and signals of other vessels should be interpreted and considered when predicting the future behaviour of other vessels. The ownship should also have the capacity to sound the correct signals to indicate its own intentions.

Intent inference: The performance of trajectory planning algorithms are very much dependent on the estimate of the future trajectory of other vessels. The common assumption of constant velocity behaviour holds well for vessels maneuvering on the open sea or for short time intervals relative to the vessel speeds, but not so much in confined areas where the presence of static obstacles and other vessels requires active maneuvering. Therefore, methods for predicting the future trajectory of other vessels based on historic traffic patterns, vessel types, destination prediction, and vessel-to-vessel interactions would greatly increase the precision of such planners.

Adapting regulations: At this point, rules and regulations are not formulated with autonomous vessels in mind. The COLREGs and other regulations that apply to maritime vessels have formulations that are not unifiable with unmanned and autonomous vessels. Early efforts should be made to start adjusting these regulations for the new and emerging technology, to avoid posing a hindrance to the development while at the same time ensuring the safety of existing maritime vessels and operations.

Simulation-based testing: To build trust in the capabilities of autonomous systems, an assurance case for such systems must be built based on rigorous methods. Simulation-based testing in high-fidelity simulators will play a major role for this purpose, since achieving a sufficient test coverage in relevant scenarios through physical testing is both infeasible and unsafe.

In addition to precise simulators, two other components must be in place for simulation-based verification to be efficient: (1) A system for sampling the simulator input space, i.e., determining the scenarios that the system is tested in, and (2) metrics for automatically evaluating

the performance of the system from the tests. In particular, developing metrics for evaluating the ASVs performance w.r.t. COLREGs is a task of similar complexity to that of developing the methods for maneuvering in compliance with the COLREGs. However, it is a prerequisite for efficiently verifying autonomous maneuvering algorithm, and hence also for deploying ASVs into operational domains other than the most simple cases. It should therefore be given more attention than today in the field of maritime collision avoidance.

Chapter 5

Publications

This chapter contains reprints of the publications that are a part of this thesis.

Paper A A path-velocity decomposition approach to collision avoidance for autonomous passenger ferries in confined waters

Published paper by E. H. Thyri, M. Breivik, and A. M. Lekkas. "A path-velocity decomposition approach to collision avoidance for autonomous passenger ferries in confined waters". In: *Proceedings of the 20th IFAC World Congress*. Berlin, Germany, 2020, pp. 14628–14635. DOI: https://doi.org/10.1016/j.ifacol.2020.12.1472.

Bibliography entry [23].

A Path-Velocity Decomposition Approach to Collision Avoidance for Autonomous Passenger Ferries in Confined Waters

Emil H. Thyri * **Morten Breivik** * **Anastasios M. Lekkas** *

* *Centre for Autonomous Marine Operations and Systems (AMOS), Department of Engineering Cybernetics, Norwegian University of Science and Technology (NTNU). NO-7491 Trondheim, Norway.*

Abstract: A deliberate collision avoidance approach for autonomous surface vehicles operating in confined waters with high traffic is presented. The approach focuses on dynamic obstacles, by assuming a predefined set of paths that are collision-free with respect to static obstacles. Hence, the collision avoidance problem is reduced to a velocity planning problem, which is solved by first transforming all dynamic obstacles to a path-time space and subsequently constructing a conditioned visibility graph and traversing it with Dijkstra's algorithm. The performance of this approach is demonstrated through both simulations and full-scale experiments in Trondheim harbor, using the NTNU milliAmpere ferry platform and virtual dynamic obstacles.

Keywords: Autonomous surface vehicle, collision avoidance, path-velocity decomposition

1. INTRODUCTION

Zero-emission autonomous passenger ferries have received increasing attention in recent years. Such ferries can provide a much needed option for reducing the stress on existing urban infrastructure by utilizing the waterways. Moreover, their acquisition and operation are expected to cost less than pedestrian and bicycle bridges, while at the same time enabling bridge-free waters for leisure boats and sailboats. In addition, electric autonomous transport can reduce operator cost by automation, and air pollution by replacing fossil-fuel alternatives. The task repetitiveness and small area of operation restrict the complexity of autonomous navigation for urban waterways, and make it a fine case for bridging the interaction between autonomous systems and humans.

There are two major tasks that must be solved for autonomous systems to become a reality:

(1) Situational awareness, which is sensing and describing all aspects of the situation that are relevant for the execution of the mission. For autonomous surface vehicles (ASVs) this includes navigation and obstacle tracking.
(2) Automated planning in accordance with the understanding of the situation in a way that solves the mission in a satisfactory manner. For ASVs, this consists of planning trajectories from the current position to a desired destination which gives a predictable behaviour and avoids collision.

In the remainder of this paper, we will focus on the task of collision avoidance (COLAV) through deliberate trajectory planning. We assume that data on position, heading, velocity and extent of all relevant moving obstacles is available.

Previous work considering COLAV in the maritime domain includes development of reactive short-term and deliberate long-term methods, as well as combinations of such methods in hybrid structures. The hybrid structures can reap the benefit of both the long-term or global planning that often comes at a high computational cost, as well as the short-term responsiveness of reactive algorithms which typically have low computational cost. Figure 1 illustrates such a hybrid COLAV architecture with a long-term path and trajectory planner in combination with a reactive short-term COLAV algorithm. The work done by Bitar et al. (2019) describes a long-term trajectory planner that uses an optimization-based path planner to determine a path that is collision-free with static obstacles, in combination with an MPC approach to plan a local trajectory that is collision-free with regard to dynamic obstacles. In (Kuwata et al., 2014), a version of the reactive velocity obstacle (VO) algorithm with COLREGs features is implemented and validated through full-scale experiments. The VO algorithm selects a velocity pair from a finite set of admissible velocities that ensure no collision, at the cost of potentially deviating from the initial trajectory. Another reactive algorithm is the branching-course model predictive control (BC-MPC) algorithm developed by Eriksen et al. (2019). The algorithm simulates a finite set of maneuvers for a short time-horizon and chooses the best combination of maneuvers according to some cost function. Both the VO and BC-MPC algorithms receive a path or trajectory which they track while adapting to dynamic obstacles by generating adjustments to the heading and velocity references. However, such adjustments can cause large deviations from the nominal path and might not be feasible for confined waters.

In this paper, we propose a trajectory planning method with COLAV functionality for the specific case of autonomous passenger ferries operating in confined waters

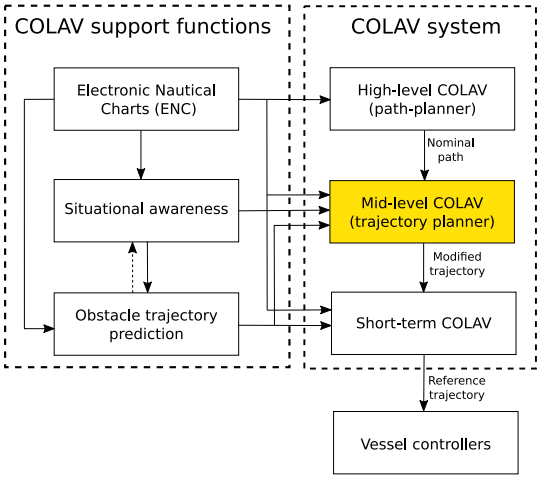

Fig. 1. A hybrid COLAV architecture as suggested in (Eriksen, 2019), with support functions such as ENC and situational awareness.

with high traffic. The approach is based on the principle of path-velocity decomposition, where the paths are predetermined and collision-free with regard to any static obstacles. The paths can be computed either offline or in a higher level in the COLAV architecture as in Fig. 1. The proposed method is suitable as a mid-level COLAV system in a hybrid system as the one depicted. In addition to the trajectory planning capabilities of the method, it is augmented with functionality for validation of the current trajectory according to updated obstacle data, where a failed validation triggers a replanning. This augmentation provides reactive features that make the method robust to changes in obstacle course and velocity.

The method of path-velocity decomposition was first suggested in (Kant and Zucker, 1986), where the moving obstacles are transformed onto the path-time space, based on the assumptions of constant obstacle behaviour, which in our case correspond to constant course over ground (COG) and speed over ground (SOG). A conditioned visibility-graph (Vgraph) is constructed in path-time space, and then traversed with Dijkstra's algorithm to find a collision-free velocity profile. This approach has been suggested for land-based robotics in (Fraichard and Laugier, 1993), and a similar approach is also applied to maritime COLAV with regard to static obstacles as a path-planner in (Casalino et al., 2009), but has to our best knowledge not been applied to COLAV for dynamic obstacles in the maritime domain.

We use a three degree-of-freedom (3-DOF) notation where $\boldsymbol{\eta}_v = [N_v, E_v, \psi_v]^\mathsf{T}$ is the ownship vessel pose in an Earth-fixed North-East-Down (NED) reference frame denoted $\{n\}$, and $\boldsymbol{\eta}_k = [N_k, E_k, \psi_k]^\mathsf{T}$ is the pose of obstacle k in $\{n\}$.

The remainder of this article is structured as follows: In Section 2, the velocity planning algorithm is described in detail along with its reactive features. Section 3 presents the simulation environment and results, while Section 4 presents the full-scale experimental results. Finally, Section 5 provides concluding remarks and future work.

2. COLLISION AVOIDANCE APPROACH

The suggested COLAV approach can be separated into two algorithms:

- **Algorithm 1** is the deliberate part of the COLAV system, which calculates a velocity profile for a path, and outputs a trajectory.
- **Algorithm 2** is the reactive part, which validates the current trajectory against most recent obstacle data. Algorithm 2 is used to trigger a replanning in Algorithm 1, see pseudocode below.

Algorithm 1 *VELOCITY_PLANNER()*

```
Input: Paths, Obstacle Tracking Data,Waypoints
atDestination = false
while atDestination == false do
    isValid = VALIDATE_CURRENT_WAYPOINTS();
    if isValid == false then
        calculate_obstacle_representations();
        transform_obstacles_to_path_time();
        construct_Vgraph();
        traverse_Vgraph();
        calculate_trajectory_from_waypoints();
    end
    atDestination = check_if_at_destination();
end
```

Algorithm 2 *VALIDATE_CURRENT_WAYPOINTS()*

```
Input: Waypoints, Obstacle Tracking Data
Output: boolean isValid
isValid = true;
if Current Waypoints is Empty then
    isValid = false;
    return isValid;
else
    calculate_obstacle_representations();
    for Every subpath in Waypoints do
        transform_obstacles_to_path_time();
        Intersection=test_for_intersection(subpath);
        if Intersection then
            isValid = false;
            return isValid;
        end
    end
    return isValid;
end
```

2.1 Predefined Paths

A set of five nominal paths is used. The paths are numbered 1 to 5, from port to starboard relative to the transit direction. Each nominal path is defined by n indexed waypoints, with $n-1$ subpaths connecting the waypoints. The subpaths are assumed to be straight lines between two consecutive waypoints. However, a path can be made up from an arbitrary number of waypoints to approximate a curved path. All nominal paths end up in the same point, the destination of the transit, but do not have the same starting point. Since the position of the ferry might not

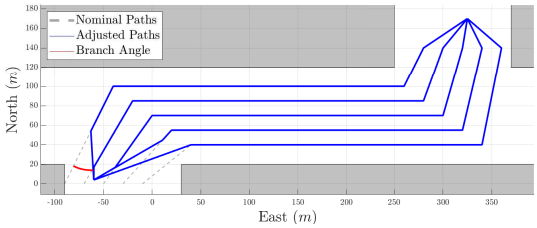

Fig. 2. Nominal paths and adjusted paths for a vessel at $[N_v, E_v] = [4, -60]$. The branch angle of 30° is illustrated in red for the first nominal path.

be on any of the nominal paths, a set of five adjusted paths are constructed. The first waypoint of all adjusted paths, wp_1, is the position of the ferry. For each of the five adjusted paths, the position of the second waypoint wp_2 is found by identifying the subpath i in the corresponding nominal path that is closest to the ferry, and subsequently calculating the position of wp_2 on the subpath such that the line from wp_1 to wp_2 makes a 30° angle to subpath i. We call this angle the branch angle. If the coordinates of wp_2 exceed the length of the subpath, wp_2 is set to the position of waypoint $i+1$. Lastly, the nominal waypoints from index $i+1$ to n are added to the adjusted paths. Fig. 2 shows the nominal paths through an east-west oriented canal, and the adjusted paths for a vessel located in $[N_v, E_v] = [4, -60]$. The branch angle is illustrated in red. In the choice of branch angle, factors such as passenger comfort, vessel maneuverability, transit length and COLREGs should be considered. As a compromise between readily apparent maneuvers and excessive maneuvering, we have used a branch angle of 30°.

2.2 Obstacle Representation

For robustness and ease of computation, we suggest a simplified obstacle representation that captures the relevant features of a dynamic obstacle. A diamond shaped region of collision (ROC) is placed around the obstacle in a way that fully encapsulates its estimated extension, in addition to the extension of ownship (OS), which is a designation used for the ferry. By doing this, the OS can be considered as a point without extension when constructing the Vgraph in the path-time space. A method for calculating the extent of the ROC is described by Lozano-Perez (1983). In addition to the ROC, we introduce two more regions: The high penalty region (HPR) and the low penalty region (LPR). A simplified obstacle representation is shown in Fig. 3. Each of the ROC, HPR and LPR for obstacle k are calculated according to

$$c_f = [N_k + l_f cos(\psi_k), E_k + l_f sin(\psi_k)], \quad (1)$$

$$c_a = [N_k + l_a cos(\psi_k + \pi), E_k + l_a sin(\psi_k + \pi)], \quad (2)$$

$$c_s = [N_k + l_s cos(\psi_k + \pi/2), E_k + l_s sin(\psi_k + \pi/2)], \quad (3)$$

$$c_p = [N_k + l_p cos(\psi_k - \pi/2), E_k + l_p sin(\psi_k - \pi/2)], \quad (4)$$

where c_f, c_a, c_s and c_p are the coordinates of the vertices in $\{n\}$ for the fore, aft, starboard and port direction respectively, and l_f, l_a, l_s and l_p denote the corresponding lengths of extension from the center of the obstacle. An appropriate length needs to be assigned to comply with the dimensions of the OS and the obstacle, including

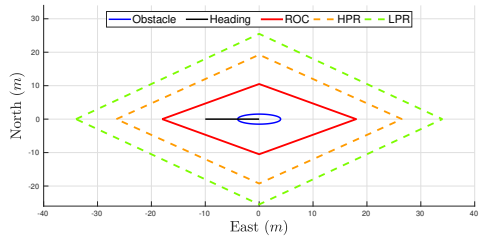

Fig. 3. Simplified obstacle representation for an 8 m long and 4 m wide obstacle traveling west.

any desired safety factor and perimeter size. Here, a symmetrical extension has been used, with

$$l_f = l_a = (l_k + l_{os} + l_{fa\_region}) \quad (5)$$

$$l_s = l_p = (w_k + l_{os} + l_{sp\_region}) \quad (6)$$

where l_k and w_k are the length and width of obstacle k, and l_{os} is the length of OS. The variables l_{fa_region} and l_{sp_region} are the additional region sizes and are set to $l_{sp\_LPR} > l_{sp\_HPR} > l_{sp\_ROC} > 0$ and $l_{fa\_LPR} > l_{fa\_HPR} > l_{fa\_ROC} > 0$ for the ROC, HPR and LPR, respectively.

2.3 Transformation to Path-Time Space

To construct the Vgraph, the obstacle representation in $\{n\}$ is transformed to the path-time space. The transformation gives surfaces in path-time space that correspond to the obstacle representations occupation of the path in time. Since the obstacle representation consists of line segments moving in $\{n\}$, the problem consists of finding the intersection between each line segment with each subpath as a function of time. The assumption of constant obstacle behaviour ensures that the intersection is a line segment, and can be defined by its end-points $I_1 = [p_1, t_1]$ and $I_2 = [p_2, t_2]$ in path-time space, where the intersection line can be parameterized as

$$I = \frac{p - p_1}{p_2 - p_1} = \frac{t - t_1}{t_2 - t_1}, \quad I \in [0, 1], \quad (7)$$

where $[p, t]$ is a point on the line I. A general method for finding the intersection in $\mathbb{R}^3$ is given in (Kant and Zucker, 1986). We use the following method for finding I_1 and I_2 in $\mathbb{R}^2$:

The subpath P_j is subpath no. j in an adjusted path. In particular, P_j starts in $wp_s = [N_s, E_s]$, ends in $wp_e = [N_e, E_e]$ and has length $d_j = \sqrt{(N_e - N_s)^2 + (E_e - E_s)^2}$. The subpath is parameterized by

$$P_j = \frac{N - N_s}{a} d_j + d_{j-1} = \frac{E - E_s}{b} d_j + d_{j-1}, \quad (8)$$

where the point $[N, E]$ is located on the subpath for $P_j \in [d_{j-1}, d_j]$, with $a = N_e - N_s$ and $b = E_e - E_s$ where

$$d_{j-1} = \sum_{m=1}^{j-1} d_m \quad (9)$$

is the accumulated length for all prior subpaths. This gives the path the intuitive unit [m]. Further, assume an obstacle representation line segment L from $l_1 = [N_1, E_1]$ to $l_2 = [N_2, E_2]$ at time $t = t_0$, moving with a linear velocity $v = [v_N, v_E]$. The line is parameterized as

$$L = \frac{N - N_1 - v_N(t - t_0)}{c} = \frac{E - E_1 - v_E(t - t_0)}{d}, \quad (10)$$

where the point $[N, E]$ is located on the line segment for $L \in [0, 1]$ with $c = N_2 - N_1$ and $d = E_2 - E_1$, giving the four equations

$$\frac{P_j - d_{j-1}}{d_j} a + N_s = N, \tag{11}$$

$$\frac{P_j - d_{j-1}}{d_j} b + E_s = E, \tag{12}$$

$$Lc + N_1 + v_N(t - t_0) = N, \tag{13}$$

$$Ld + E_1 + v_E(t - t_0) = E. \tag{14}$$

By combining (11) and (13), and (12) and (14), N and E is eliminated, and the set of equations is reduced to

$$Lc + N_1 + v_N(t - t_0) = \frac{P_j - d_{j-1}}{d_j} a + N_s, \tag{15}$$

$$Ld + E_1 + v_E(t - t_0) = \frac{P_j - d_{j-1}}{d_j} b + E_s. \tag{16}$$

Equations (15)-(16) contain three unknown variables, $P_j \in [d_{j-1}, d_j]$, $L \in [0, 1]$ and $t \in (-\infty, \infty)$.

There are three possibilities for the intersection: I) the full length of L passes through P_j, II) L does not pass through P_j, or III) part of L passes through P_j. Start by assuming the first case, and solve (15)-(16) for $L = 0$ and $L = 1$ to get I_1 and I_2 respectively. If this gives $p_1, p_2 \in [d_{j-1}, d_j]$ this corresponds to I. If either $p_1, p_2 < d_{j-1}$ or $p_1, p_2 > d_j$, this is II and $I_1, I_2 = \emptyset$. Any other combination, where p_1 and p_2 is either on each side of the set $[d_{j-1}, d_j]$, or one is within the set and one is outside the set, corresponds to III. In this case, for each $p_i \notin [d_{j-1}, d_j], i \in [1, 2]$, set $P_j = d_{j-1}$ or $P_j = d_j$, corresponding to the boundary p_i is violating, and solve (15)-(16) to find t_i. The path-time coordinates of the ends of the intersection are $I_i = [p_i, t_i]$.

The I_1 and I_2 coordinates are calculated for all line segments in all obstacle representations, for each subpath to construct one path-time space representation for each of the five adjusted paths. Figure 4(a) shows the transformed obstacle representation of four moving obstacles onto a 104 m long straight-line path. In the transformation, three sets are constructed for each adjusted path; $\boldsymbol{N}$ is the node set, containing all intersection-points I_1 and I_2 from the transformation of all HPR and LPR, also including the node $I_{OS} = [0, t]$ at the start of the path, where t is the current time. $\boldsymbol{R}$ and $\boldsymbol{H}$ are the set of intersection line segments I from the transformation of all ROC and HPR, respectively.

2.4 Constructing the Vgraph

A traditional Vgraph is constructed from all edges connecting two nodes that do not intersect any edges in $\boldsymbol{R}$. Since the Vgraph is in the path-time space, it requires a few additional conditions, the second and third condition were formulated in (Kant and Zucker, 1986). First, time along an edge must be monotonically increasing. Furthermore, the velocity of an edge must be limited to the maximum velocity of the ferry, V_{max}. In addition, since the OS is located at $I_{OS} = [0, t]$, edges that are not reachable from the current coordinates are also omitted. For the Vgraph to span from I_{OS} to the end of the path, a set of end-nodes $\bar{\boldsymbol{N}}$ are calculated, one for each node in $\boldsymbol{N}$. For all end-nodes $\bar{n}_s$, $p_s = d_{n-1}$ according to (9), and

$$t_s = t_k + \frac{p_s - p_k}{V_{des}} \tag{17}$$

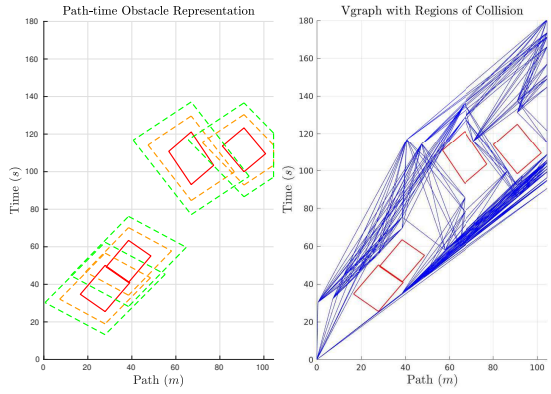

(a) (b)

Fig. 4. Path-time space. (a) Four obstacle representations transformed to path-time space. (b) Constructed Vgraph with ROC from four obstacles.

where p_k and t_k are the path and time coordinates of the corresponding node in $\boldsymbol{N}$, and V_{des} is the desired transit velocity. The edge set $\boldsymbol{E}$, for the Vgraph, is determined by including all combinations of node pairs (n_i, n_j) from $\boldsymbol{N} \cup \bar{\boldsymbol{N}}$ that hold the conditions

C_1: $\overline{n_i, n_j} \cap \boldsymbol{R} = \emptyset$,
C_2: $|\frac{p_j - p_i}{t_j - t_i}| \leq V_{max}$,
C_3: $t_i < t_j$,
C_4: $|\frac{p_i}{t_i - t}| \leq V_{max}$ and
C_5: $t_i > t$.

For each edge in $\boldsymbol{E}$, a cost is calculated as

$$c_{ij} = c_t + c_v + c_l + c_n + c_{HPR}, \tag{18}$$

where c_t, c_v and c_l is the cost on time, velocity and length,

$$c_t = (t_j - t_i)k_t, \tag{19}$$

$$c_v = \left| \frac{(p_j - p_i)}{(t_j - t_i)} - V_{des} \right| k_v, \tag{20}$$

$$c_l = |p_j - p_i| k_l, \tag{21}$$

where $k_t > 0$, $k_v > 0$ and $k_l > 0$ are tuning parameters, c_n is the cost related to the node n_j and is either $k_{HPR} > 0$ or $k_{LPR} > 0$ depending on whether the node originates from the HPR or LPR. Lastly, c_{HPR} is set to k_{HPR} if $\overline{n_i, n_j} \cap \boldsymbol{H} \neq \emptyset$ and 0 if $\overline{n_i, n_j} \cap \boldsymbol{H} = \emptyset$ to penalize edges that pass through high penalty regions.

Figure 4(b) shows a Vgraph in path-time space with the four obstacles from Fig. 4(a). Joseph Kirk's Matlab implementation of Dijkstra's algorithm is used to traverse the graph (Kirk, 2015).

2.5 Trajectory from Waypoints

Dijkstra's algorithm outputs a set of path-time waypoints that make up the minimum-cost path. Furthermore, (11)-(12) are used to find the corresponding NED waypoints of the path-time waypoints. From the NED waypoints, along with time-coordinates of the path-time waypoints, we calculate a time-parameterized reference trajectory by using a third-order reference model (Fossen, 2011).

Fig. 5. The milliAmpere moving in Trondheim harbour.

2.6 Validation and Replanning

Algorithm 2 introduces the reactive features to the COLAV approach by periodically validating the current trajectory. The validation is performed by first constructing the set $\boldsymbol{R}$ like in Subsection 2.3, by transforming the ROC of all obstacles onto the path spanned by the current NED waypoints. Then, the algorithm constructs the set $\boldsymbol{S}$ of line segments from all subpaths connecting two consecutive waypoints in the current path-time waypoints, and lastly, checks for any intersections between the two sets. The current trajectory is valid if $\boldsymbol{S} \cap \boldsymbol{R} = \emptyset$, and not valid if $\boldsymbol{S} \cap \boldsymbol{R} \neq \emptyset$. If the test renders the current trajectory not valid, a replanning is performed in Algorithm 1, while the other case triggers no actions. In the simulations and experiments, the validation is performed with a time period of $T = 4\,\text{s}$. The validation period should reflect the situational awareness system's ability to detect changes in obstacle speed and course. Another approach could be to trigger the validation when a change in course or heading for one or more of the obstacles is detected. In that case, only the ROCs of the obstacles with changed behaviour need to be transformed onto the path-time space.

3. SIMULATION RESULTS

Three simulations are implemented in Simulink with a 3-DOF model of the experimental ferry prototype milliAmpere shown in Fig. 5. A system overview of the simulator and guidance, navigation and control (GNC) system is given in Fig. 6. The vessel model and thruster model parameters are taken from the work of Pedersen (2019), where the vessel and thruster parameters used are listed in tables 3.4 and 3.9 respectively. The control system is the model reference adaptive controller described in (Sæther, 2019).

In the simulations, obstacle data without noise is available at all times. The data is provided by an obstacle simulator that can simulate different obstacle behaviours. In the presented results, three obstacle behaviours have been used; constant behaviour, "pass in front" and "slow down". The "pass in front" behaviour for obstacle k is active when it has a relative bearing to the ferry $b_{rel} \in (\pi/4, 3\pi/4)$ or $b_{rel} \in (-3\pi/4, -\pi/4)$, while having closing speed $v_{close} > 0$ and $l < l_{trig}$, where $l = \sqrt{(N_v - N_k)^2 + (E_v - E_k)^2}$ is the distance from the obstacle to the ferry and $l_{trig} > 0$ is a trigger distance. When the "pass in front" behaviour is triggered, the obstacle course is adjusted to aim for a point 20 m straight in front of the ferry. The "slow down" behaviour scales the obstacle velocity according to

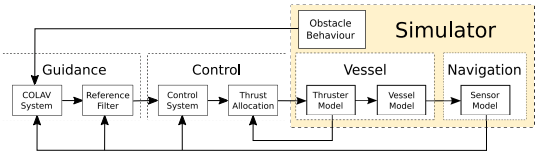

Fig. 6. Simulator and GNC system overview. The orange box contains the modeled vessel and sensor systems. The guidance and control systems are the same for both the simulations and experiments.

Table 1. Parameters

Name	Value	Unit	Name	Value	Unit
V_{des}	1.0	$\text{m} \cdot \text{s}^{-1}$	k_{HPR}	20	1
V_{max}	1.2	$\text{m} \cdot \text{s}^{-1}$	k_{LPR}	0	1
k_t	10	s^{-1}	l_{fa_ROC}	5.0	m
k_v	2	$\text{s} \cdot \text{m}^{-1}$	l_{sp_ROC}	2.5	m
k_l	1	m^{-1}	l_{fa_HPR}	12.5	m
l_{trig}	40	m	l_{sp_HPR}	11.2	m
r_1	40	m	l_{fa_LPR}	20.0	m
r_2	10	m	l_{sp_LPR}	17.5	m

$$\bar{v_k} = v_k f(l) \tag{22}$$

where $\bar{v_k}$ and v_k are the scaled and nominal velocity of obstacle i respectively, and

$$f(l) = \begin{cases} 1, & \text{if } l > r_1 \\ \frac{l - r_2}{r_1 - r_2}, & \text{if } r_1 \geq l \geq r_2 \\ 0, & \text{otherwise,} \end{cases} \tag{23}$$

where $r_1 > r_2 > 0$ are the limits for the scaling. The parameter values for simulations and experiments are given in Table 1.

The COLAV approach is tested in two environments:

- Environment 1 is a crossing over a narrow canal with traffic traveling close to perpendicular to the nominal paths.
- Environment 2 is a canal-crossing with a majority of the transit along the canal and hence parallel to the traffic.

3.1 Simulation 1

Simulation 1 is in Environment 1, with four obstacles traveling along the canal, two approaching from each side. The obstacles have constant behaviour. The ferry starts with initial condition $\boldsymbol{\eta_{v_0}} = [0, 0, 0.2915]^\intercal$. Fig. 7 gives situation overviews at different times of the transit. In the situation overviews, the ferry with course and track history is blue, and the obstacles with course and track history are red. The obstacle representations are included. The grey dashed lines give the nominal paths, and the solid grey areas indicate the canal-banks. The along path velocity and velocity reference are shown in Fig. 8, where the green dashed line denotes the time of velocity-planning.

From the figures, one can see that the ferry starts off with a close to zero velocity to let the two obstacles approaching from the port side pass, while moving from $path3$ to $path4$. Subsequently it accelerates to near transit velocity for the remainder of the transit. The change of path allows the

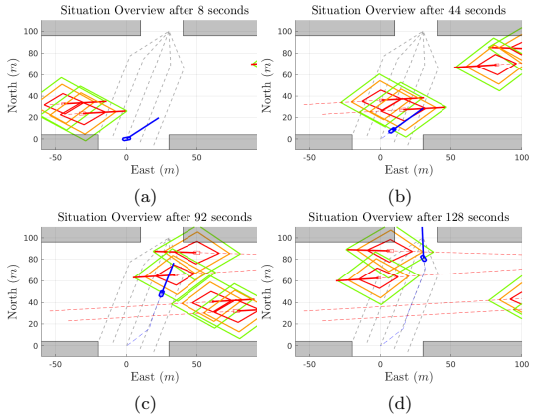

Fig. 7. Simulation 1: Situation overview of the transit. Obstacles have constant behaviour.

ferry to keep transit velocity and still pass behind the two obstacles approaching from starboard. From Fig. 8 one can see that only the initial planning was necessary. This is due to the obstacle behaviour complying with the assumptions made in the transformation to the path-time space.

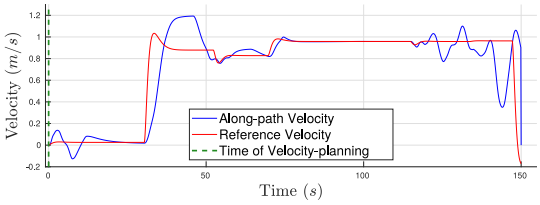

Fig. 8. Simulation 1: Along-path velocity and reference. Only the initial velocity-planning was necessary.

3.2 Simulation 2

Simulation 2 is also in Environment 1, with four dynamic obstacles traveling along the canal, two approaching from each side. The obstacles maneuver to pass in front of the ferry if they enter the enabling sector. The ferry has initial condition $\boldsymbol{\eta}_{\boldsymbol{v_0}} = [0, 0, 0.2915]^\mathsf{T}$. Fig. 9 shows snapshots from the transit and Fig. 10 shows the along-path velocity and velocity reference.

From the velocity profile, we can see that the ferry starts off at transit velocity, and performs a replanning at $t = 8\,\mathrm{s}$, which is triggered by one of the obstacles from the port side adjusting its heading as it enters the enabling sector. The replanning makes the ferry stop and wait for the obstacles to pass, as can be seen from Fig. 10. At $t = 36\,\mathrm{s}$, the ferry proceeds at transit velocity. At $t = 84\,\mathrm{s}$, a second replanning is triggered by the second obstacle approaching from the starboard side as it alters its course. This gives a re-planned trajectory that changes to $path5$ and follows this path at transit velocity to the destination. This simulation shows the reactive qualities of the COLAV system that are introduced by Algorithm 2.

3.3 Simulation 3

Simulation 3 is in Environment 2 with ten dynamic obstacles traveling along the canal, five approaching from each

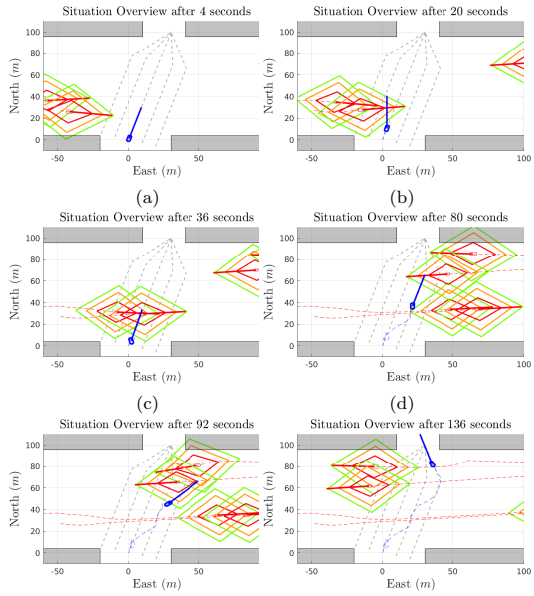

Fig. 9. Simulation 2: Situation overview of the transit. Obstacles have the "pass in front" behaviour. The ferry changes path at each replanning.

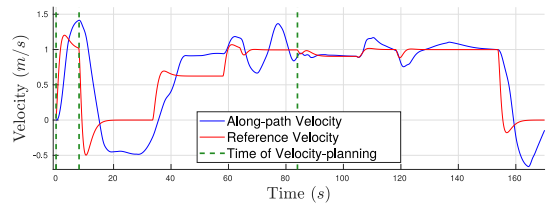

Fig. 10. Simulation 2: Along-path velocity and reference. Two replans are triggered in addition to the initial velocity-planning.

side. The obstacles have constant behaviour. The ferry starts with initial condition $\boldsymbol{\eta}_{\boldsymbol{v_0}} = [0, -50, 0]^\mathsf{T}$. Fig. 11 shows snapshots from the transit, and Fig. 12 shows the along-path velocity and reference. This simulation demonstrates two interesting aspects of the COLAV method. One is the ability to handle high traffic, where the OS merges in-between five moving obstacles, and is unaffected by the five moving obstacles passing in the other direction within a short distance to the OS. An optimization-based algorithm like the one in (Hagen et al., 2018) might handle the same situation by altering course and/or heading to minimize some risk function. The other aspect is its ability to trail behind (or in front of) another obstacle at matching velocity in a lane-keeping manner, which is an intuitive and safe way of maneuvering in such confined waters.

4. EXPERIMENTAL RESULTS

The experiment is conducted with milliAmpere depicted in Fig. 5. The experimental test platform is a 5 m by 2.8 m prototyping platform developed by NTNU that is used for developing and testing sensor systems, situational aware-

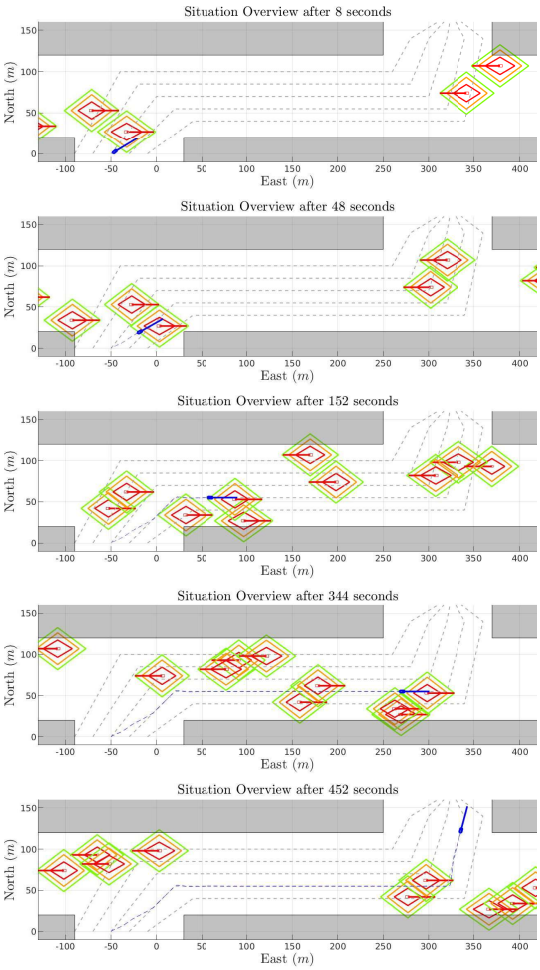

Fig. 11. Simulation 3: Situation overview of the transit. Obstacles have constant behaviour.

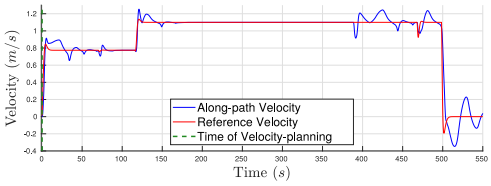

Fig. 12. Simulation 3: Along-path velocity and reference. Only the initial velocity-planning is necessary due to constant obstacle behaviour.

ness algorithms, human machine interaction and COLAV systems. The experiment is conducted in a shielded part of Trondheim harbour with little traffic. The guidance and control system is the same as for the simulations. The code is generated from Simulink to run in ROS [1] , and runs on an Axiomtek eBOX670-883-FL with an Intel Core I7 processor and Ubuntu OS. The sensor model is replaced by

[1] Robot operating system, `https://www.ros.org/about-ros/`

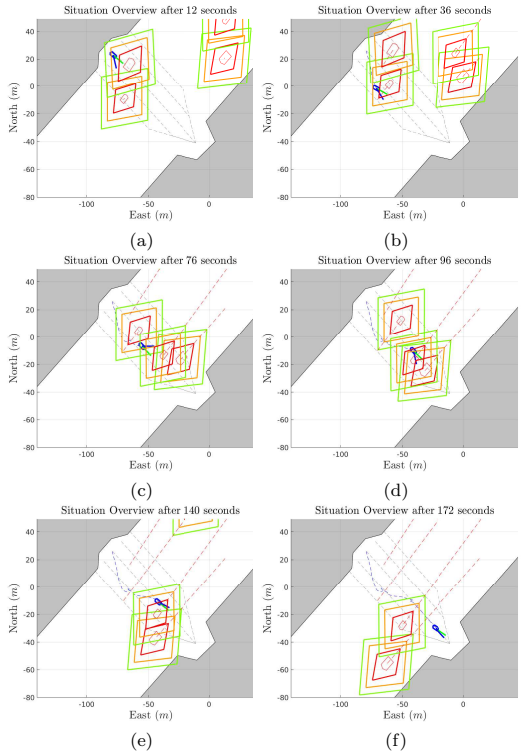

Fig. 13. Experiment: Situation overview of the transit. Obstacles act according to the "slow-down" behaviour.

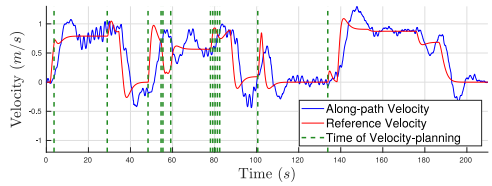

Fig. 14. Experiment: Along-path velocity and reference. Several replans are triggered due to the unpredictable obstacle behaviours.

a navigation system consisting of a Vector™ VS330 GNSS Receiver with Real Time Kinematic (RTK) capacity, and an Xsens MTi-20 IMU, providing a position accuracy of 10 mm in the horizontal plane and 0.05° in heading. The experiment is run with virtual obstacles in the same obstacle simulator as for the simulations. The reference filter, control system, thrust allocation and obstacle simulator all run with a period of 0.1 s to ensure sufficient trajectory tracking. As mentioned, the COLAV algorithms run the validation with eventual replanning at a period of 4 s. In a scenario with 4 moving obstacles and 5 nominal paths, each made from 3 subpaths, Algorithm 2 and Algorithm 1 in sequence are able to finish calculations in about 0.2 s without any effort to optimize the code for runtime.

The presented experiment is chosen from the set of experiments in (Thyri, 2019). In the experiment the obstacles

act according to the "slow-down" behaviour. Figure 13 gives a situation overview of the transit and Fig. 14 gives the planned and actual velocity profile for the transit. The ferry starts off along $path5$ at about 0.8 m/s to pass behind the two obstacles heading north-east. As the obstacles slow down, a replan is triggered that brings the ferry to a stop for about 15 s awaiting the obstacles to pass. Subsequently, the ferry moves back to $path3$ to pass behind the two obstacles traveling south-east. As the obstacles slow down, the current plan is rendered infeasible, and a series of replans are triggered around 80 s into the transit. The ferry is eventually halted for about 50 s to wait for the obstacles to proceed before the transit is completed without further replans. This scenario shows how the reactive features of the COLAV approach makes it able to adapt to deviations from the assumptions on constant obstacle behaviour that are made in the transformation to path-time space. Another remark is that the velocity planner causes the ferry to stop at two occasions which is because the 30° branch angle used in calculating the adjusted paths and the short distance to the closest obstacle makes all five adjusted paths pass through the ROC of that obstacle. A solution to this could be to have a dynamic construction of the adjusted paths, e.g. in a higher level of the COLAV architecture. Another solution could be to pair the velocity planner with a more reactive COLAV algorithm that would allow deviations from the adjusted paths. A third thing to note about the stop-and-go behaviour is that it puts demands on the vessel actuation system. For the algorithm to work in the presence of environmental disturbances from wind and current, the vessel needs to be fully actuated in order to maintain tracking for both position and heading when stationary. This is particularly important for passenger transport to ensure passenger comfort and safety. For underactuated ASVs, a solution can be to introduce a $V_{min} > 0$ condition on the edges when constructing the Vgraph.

5. CONCLUSION

A simple and robust deliberate COLAV approach for autonomous passenger ferries is presented in this paper. The method can run in real time and produces predictable and intuitive trajectories in confined waters with high-traffic. It can also adapt to unforeseen changes without deviating from the predefined transit paths, ensuring safe maneuvering in confined waters.

Future work includes improving COLREGs compliance by augmenting the obstacle representation, analyzing the completeness of the method, pairing the velocity planner with a reactive COLAV algorithm, improving the trajectory tracking and control system, and testing the COLAV approach together with real object tracking data from exteroceptive sensors to see how it handles noise and uncertainty.

ACKNOWLEDGEMENTS

This work was supported by the NTNU Digital transformation project Autoferry and the Research Council of Norway through the Centres of Excellence funding scheme with project number 223254.

REFERENCES

Bitar, G., Eriksen, B.O.H., Lekkas, A.M., and Breivik, M. (2019). Energy-optimized hybrid collision avoidance for ASVs. In *Proc. 18th European Control Conference (ECC)*, 2522–2529. Naples, Italy. doi:10.23919/ECC.2019.8795645.

Casalino, G., Turetta, A., and Simetti, E. (2009). A three-layered architecture for real time path planning and obstacle avoidance for surveillance USVs operating in harbour fields. In *Proc. OCEANS 2009-EUROPE*, 1–8. Bremen, Germany. doi:10.1109/OCEANSE.2009.5278104.

Eriksen, B.O.H., Breivik, M., Wilthil, E.F., Flåten, A.L., and Brekke, E.F. (2019). The branching-course model predictive control algorithm for maritime collision avoidance. *Journal of Field Robotics*. doi:10.1002/rob.21900.

Eriksen, B.O.H. (2019). *Collision Avoidance and Motion Control for Autonomous Surface Vehicles*. Ph.D. thesis, Norwegian University of Science and Technology (NTNU), Trondheim, Norway.

Fossen, T.I. (2011). *Handbook of Marine Craft Hydrodynamics and Motion Control*. John Wiley & Sons.

Fraichard, T. and Laugier, C. (1993). Path-velocity decomposition revisited and applied to dynamic trajectory planning. In *Proc. IEEE International Conference on Robotics and Automation (ICRA)*, volume 2, 40–45. Atlanta, USA.

Hagen, I.B., Kufoalor, D.K.M., Brekke, E.F., and Johansen, T.A. (2018). MPC-based collision avoidance strategy for existing marine vessel guidance systems. In *Proc. IEEE International Conference on Robotics and Automation (ICRA)*, 7618–7623. Brisbane, Australia. doi:10.1109/ICRA.2018.8463182.

Kant, K. and Zucker, S.W. (1986). Toward efficient trajectory planning: The path-velocity decomposition. *The International Journal of Robotics Research*, 5, 72–89.

Kirk, J. (2015). Dijkstra's minimum cost path algorithm. URL `https://se.mathworks.com/matlabcentral/fileexchange/20025-dijkstra-s-minimum-cost-path-algorithm`.

Kuwata, Y., Wolf, M.T., Zarzhitsky, D., and Huntsberger, T.L. (2014). Safe maritime autonomous navigation with COLREGs, using velocity obstacles. *IEEE Journal of Oceanic Engineering*, 39(1), 110–119. doi:10.1109/JOE.2013.2254214.

Lozano-Perez (1983). Spatial planning: A configuration space approach. *IEEE Transactions on Computers*, C-32(2), 108–120. doi:10.1109/TC.1983.1676196.

Pedersen, A.A. (2019). *Optimization Based System Identification for the milliAmpere Ferry*. Master's thesis, Norwegian University of Science and Technology (NTNU), Trondheim, Norway.

Sæther, B. (2019). *Development and Testing of Navigation and Motion Control Systems for milliAmpere*. Master's thesis, Norwegian University of Science and Technology (NTNU), Trondheim, Norway.

Thyri, E.H. (2019). *A Path-Velocity Decomposition Approach to Collision Avoidance for Autonomous Passenger Ferries*. Master's thesis, Norwegian University of Science and Technology (NTNU), Trondheim, Norway.

Paper B Reactive collision avoidance for ASVs based on control barrier functions

Published paper by E. H. Thyri, E. A. Basso, M. Breivik, K. Y. Pettersen, R. Skjetne, and A. M. Lekkas. "Reactive collision avoidance for ASVs based on control barrier functions". In: *Proceedings of the 2020 4th IEEE Conference on Control Technology and Applications (CCTA)*. Montreal, QC, Canada, 2020, pp. 380–387. ISBN: 978-1-7281-7140-1. DOI: https://doi.org/10.1109/CCTA41146.2020.9206340.

Bibliography entry [24].

Reactive collision avoidance for ASVs based on control barrier functions

Emil H. Thyri, Erlend A. Basso, Morten Breivik, Kristin Y. Pettersen, Roger Skjetne, Anastasios M. Lekkas

***Abstract*— A reactive collision avoidance method for autonomous surface vehicles based on control barrier functions (CBFs) is proposed. An encounter between the ownship (the vessel that we control) and a target ship is classified, in accordance with the International Regulations for Preventing Collisions at Sea (COLREGs), to be either a head-on, overtake, give-way, stand-on or a safe situation with respect to the ownship. Subsequently, a spatial region is assigned to the target ship based on the classification, and this region is used to define a collision-free set. Based on this, a CBF is formulated to ensure forward invariance of the collision-free set. This CBF can then be applied as an inequality constraint to any guidance, navigation and control system with an optimization-based trajectory tracking or thrust allocation system. The method is verified through simulations and is seen to handle head-on, overtaking and crossing situations with both give-way and stand-on duty in compliance with COLREGs rules 13-15 and 17.**

I. Introduction

Autonomous surface vehicles (ASVs) today constitute a large category of vessels with some degree of autonomy, that are used in the research, commercial and defence sectors. Over the past decade, a large effort has been focused towards increasing the level of autonomy of such vessels, with a goal of improved safety, improved efficiency, improved precision of operations, reduced operational cost or extended mission capability.

If fully autonomous commercial ASVs are going to be a reality, the safety of the operation must be ensured. For ASVs operating in proximity to other vessels, the task of collision-free maneuvering, is arguably of highest importance. The International Regulations for Preventing Collisions at Sea (COLREGs) constitute a ruleset that dictates, among other things, the duties of a vessel in vessel-to-vessel encounters. The COLREGs have been developed over several decades by humans for human operators [1]. This human-centered approach makes them open to interpretations, with qualitative formulations like ”in ample time” and ”if circumstances admit” as criteria for executing maneuvers [2]. Several classification and evaluation schemes have been developed for risk assessment with regards to COLREGs. The authors of [3] have taken a step towards quantifying the values of parameters related to COLREGs interpretation, to make a uniform framework for evaluating the collision avoidance (COLAV) performance of ASVs. [4] describes a method for assessing the collision risk and classifying, with regard to COLREGs, the situation of surface ships in close encounters. The COLREGs must at some point be adjusted to take into account the co-existence between human-piloted and autonomous vessels [5], but until then, ASVs must act ”with due regard to the observance of good seamanship”.

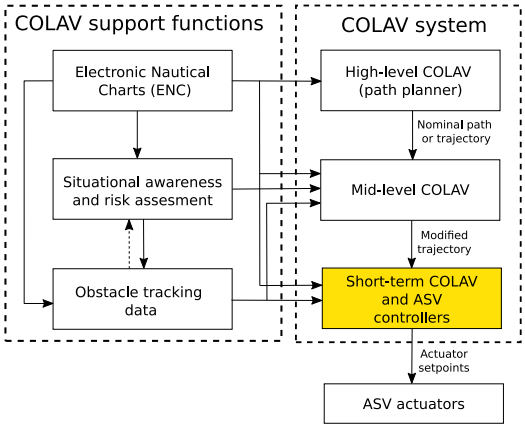

Fig. 1. A slightly modified version of the hybrid COLAV structure suggested in [6]. The contribution of this paper is in the yellow area, where we have merged a short-term reactive COLAV with the vessel controllers.

Once a correct interpretation of the situation is made, the COLREGs dictate the duty of the vessels involved in the encounter. This duty might involve either altering or keeping a constant course and/or speed. Several algorithms in the literature have been developed for the purpose of acting in accordance with the rules to a greater or lesser extent, and go by the name COLAV algorithms. The complexity of the task of COLREGs-compliant maneuvering makes it hard to solve by one algorithm alone. Therefore, hybrid architectures like the one illustrated in Fig. 1 are used to combine the benefits from two or more algorithms complementing each other [7], [8]. The complexity of the COLAV systems makes it difficult to assess the space of possible outcomes from all situations, and proving safety, which is essential for ASVs to operate for even short periods of time without supervision, becomes hard.

In recent years, control barrier functions (CBFs) have emerged as the safety equivalent to what control Lyapunov functions (CLFs) are for stability [9]. The main feature of CBFs for COLAV is that they can ensure forward invariance to any set that can then be designed to be a safe operating

This work was supported by the NTNU Digital transformation project Autoferry and the Research Council of Norway through the Centres of Excellence funding scheme, project no. 223254

The authors are with the Centre for Autonomous Marine Operations and Systems (AMOS), Department of Engineering Cybernetics, Norwegian University of Science and Technology (NTNU), NO-7491, Trondheim, Norway {emil.h.thyri, erlend.a.basso, kristin.y.pettersen, roger.skjetne, anastasios.lekkas}@ntnu.no, morten.breivik@ieee.org

set regarding the task, i.e. a set free of collision. CBFs have been used to ensure safety in a robot [10] and a swarm of robots [11], for lane keeping and adaptive cruise control in automotive systems [12], and for COLAV with static obstacles for underwater snake robots [13] and ASVs [14]. To the best of our knowledge, however, CBFs have not been applied to maritime COLAV in vessel-to-vessel encounters for ASVs before.

The contribution of this paper is a CBF-based reactive COLAV method for ASVs that is suitable as a short-term COLAV module in the structure in Fig. 1. The method is reactive in the way that only the current states are used to determine a control action, as opposed to trying to optimize some objective over a (short) time horizon in a deliberate manner. The approach can be made minimally intrusive to potential higher level COLAV modules by designing the safe operating set of the reactive COLAV method so that the safe sets of higher level COLAV modules are contained within that set, and by that ensuring that the reactive algorithm only comes into play when the safe set of higher level COLAV modules are violated. The method also complements the COLREGs considerations of higher levels by handling the obligations regarding emergency maneuvers. The approach is versatile and can be applied to any guidance, navigation and control (GNC) system with an optimization-based trajectory tracking or thrust allocation system.

The remainder of this paper is organized as follows: Section II provides some background theory on control barrier functions. Section III explains the COLREGs considerations that are made. In Section IV, we propose the control barrier function for the suggested COLAV approach. Simulation results are presented and discussed in Section V, before Section VI concludes the paper.

II. Control Barrier Functions

This section introduces background theory on CBFs. In this paper, we consider nonlinear control affine systems on the form

$$\dot{\boldsymbol{x}} = \boldsymbol{f}(\boldsymbol{x}) + \boldsymbol{g}(\boldsymbol{x})\boldsymbol{u}, \quad \boldsymbol{x}(0) = \boldsymbol{x}_0, \tag{1}$$

where $\boldsymbol{f} : \mathbb{R}^n \to \mathbb{R}^n$ and $\boldsymbol{g} : \mathbb{R}^n \to \mathbb{R}^m$ are locally Lipschitz, $\boldsymbol{x} \in D \in \mathbb{R}^n$ contains the states of the system and $\boldsymbol{u} \in U \in \mathbb{R}^m$ is the control input. Such systems describe a variety of field robotic systems in air, on land and at sea. Further, we assume a set $\mathcal{C}$, that is safe regarding the system task. This set is said to be forward invariant with respect to (1) if for a given a solution to (1), $\boldsymbol{x} : [0, t_1] \to \mathbb{R}^n$,

$$\boldsymbol{x}(0) \in \mathcal{C} \implies \boldsymbol{x}(t) \in \mathcal{C}, \quad \forall t \in [0, t_1]. \tag{2}$$

A barrier function is a continuously differentiable function $h\colon \mathbb{R}^n \to \mathbb{R}$, where the safe set $\mathcal{C}$ is defined as a super-zero level set to $h(\boldsymbol{x})$, that is,

$$\begin{aligned} \mathcal{C} &= \{\boldsymbol{x} \in \mathbb{R}^n : h(\boldsymbol{x}) \geq 0\}, \\ \partial\mathcal{C} &= \{\boldsymbol{x} \in \mathbb{R}^n : h(\boldsymbol{x}) = 0\}, \\ \mathrm{Int}(\mathcal{C}) &= \{\boldsymbol{x} \in \mathbb{R}^n : h(\boldsymbol{x}) > 0\}, \end{aligned} \tag{3}$$

where $\mathrm{Int}(\mathcal{C})$ is the interior of $\mathcal{C}$. Ensuring invariance of $\mathcal{C}$ implies that $h(\boldsymbol{x}) \geq 0$ along the trajectories of (1). Positivity of $h(\boldsymbol{x})$ can be shown if

$$\dot{h}(\boldsymbol{x}(t)) = \frac{\partial h}{\partial x}\left(f(\boldsymbol{x}) + g(\boldsymbol{x})\boldsymbol{u}(\boldsymbol{x})\right) \geq -\alpha\left(h(\boldsymbol{x}(t))\right), \tag{4}$$

for some extended class-κ function $\alpha : \mathbb{R} \to \mathbb{R}$. If there exists a continuous function $\boldsymbol{u} : \mathbb{R}^n \to \mathbb{R}^m$ such that (4) is satisfied, then $h(\boldsymbol{x})$ is a valid control barrier function for (1) [12].

CBFs can be applied to optimization-based control allocation as an inequality constraint [9],

$$\boldsymbol{u}^* = \underset{\boldsymbol{u}}{\arg\min} \quad \frac{1}{2}\|\boldsymbol{u} - \boldsymbol{k}(\boldsymbol{x})\|^2, \tag{5}$$

subject to (4). Here, $\boldsymbol{k}(\boldsymbol{x})$ is a nominal control law that can be provided by an arbitrary controller that is suitable for the control objective.

A. Notation

We use the following notation for vessel states; $\boldsymbol{p} = [N, E]^\mathsf{T} \in \mathbb{R}^2$ are the North-East coordinates and $\psi \in [-\pi, \pi]$ is the heading of our controlled ownship (OS) in a local NED frame, $\chi \in [-\pi, \pi]$ is the course of the OS and $\boldsymbol{\nu} = [v_u, v_v, v_r]^\mathsf{T} \in \mathbb{R}^3$ are the surge, sway and yaw velocities in a body-fixed reference frame. The target ship (TS), the opposing ship in an encounter, has the same states, but with subscript TS. For the TS, we assume $\psi_{TS} = \chi_{TS}$.

III. Situation Classification and Target Ship Domain

This section introduces the COLREGs considerations that are made. Based on these, we propose a TS vessel domain that we later, in Section IV, use to define the safe set $\mathcal{C}$ that is collision free and COLREGs-compliant regarding the rules presented in this section.

Acting in accordance with COLREGs is a two-step process. First, the rules that apply for the situation must be determined. Subsequently, the appropriate action must be taken. For a reactive COLAV system, a subset of the rules in section II of the COLREGs, regarding conduct of vessels in sight of one another, are relevant. Here follows a description of the set of COLREGs that we consider [2]:

- **Rule 13** *Any vessel overtaking another vessel shall keep out of the way of the vessel being overtaken. A vessel approaching another vessel from a direction of more than* $22.5\,\mathrm{deg}$ *abaft her beam is an overtaking vessel. Any subsequent alternation of bearing between the two vessel shall not relieve the overtaking vessel of the duty of keeping clear of the overtaken vessel until she is finally past and clear.*
- **Rule 14** *When two power-driven vessels are meeting on reciprocal or nearly reciprocal courses so as to involve risk of collision each shall alter her course to starboard so that each shall pass on the port side of the other.*
- **Rule 15** *When two power-driven vessels are crossing so as to involve risk of collision, the vessel which has the other on her own starboard side shall keep out of the*

way and shall, if the circumstances of the case admit, avoid crossing ahead of the other vessel.

- **Rule 17** *Where one of two vessels is to keep out of the way, the other shall keep her course and speed. The latter vessel may take action to prevent collision if it is apparent that the vessel required to keep out of the way is not taking appropriate action.*

A. Classification

Classification is in this case the process of determining which situation the OS is in with respect to COLREGs, and thereby what rules the OS should abide by. The authors of [4] have developed a framework for geometric COLREGs interpretation based on the relative bearing of the TS to the OS, using

$$\varphi = \text{atan2}((E_{TS} - E), (N_{TS} - N)) - \chi, \tag{6}$$

as well as the course of the TS relative to the course of the OS, namely $\chi_{rel} = \chi_{TS} - \chi$. The classification deems OS one of the following situations, where the corresponding rules apply.

- Overtaking (OT): **Rule 13**.
- Head-on (HO): **Rule 14**.
- Give-way (GW): **Rule 15**.
- Stand-on (SO): **Rule 17**.
- Safe (SF): No rules apply.

In [6], an augmented version of the classification algorithm is presented, where some of the OT, GW and SO situations from the first paper, are deemed safe if the relative velocity between the OS and the TS is positive, that is, if the distance between them is increasing. The latter paper also includes a state machine that holds any classification other than SF until it is again classified as SF. The state machine ensures the latter part of **Rule 13**, which states that the overtaking vessel needs to be past and clear to be relieved of the give-way obligation from the overtaking.

In this paper, we use the geometrical classification method from [6], with a small addition. We have included distinction in the classification, regarding whether an overtaking situation should result in passing the TS on the starboard or port side. We denote these two situations by OT_s and OT_p, respectively. The distinction is based on χ_{rel}, choosing OT_p for $\chi_{rel} \geq 0$ and OT_s for $\chi_{rel} < 0$. This addition ensures that OS crosses behind TS in a close-quarter overtaking situation.

Figure 2 shows the geometrical interpretation. In the figure, OS is in the center. The angles $[\theta_1, \theta_2, \theta_3]^\mathsf{T} = [22.5°, 90°, 112.5°]^\mathsf{T}$ divide the surrounding into symmetrical relative bearing sectors. The circles represent target ships inside each of the relative bearing sectors. When classifying which COLREGs situation the OS is in with respect to a TS, (6) is used to determine which relative bearing sector the TS is in, and the course of the TS relative to the OS is then used to classify the situation.

Potential maneuvers by TS are not considered in the classification, and throughout the whole paper, the following assumption is made:

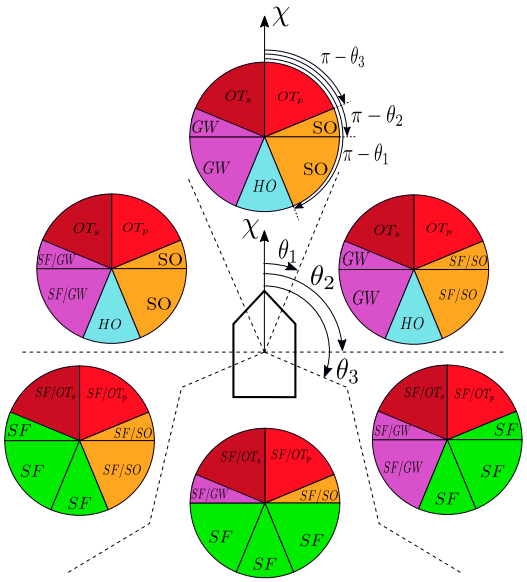

Fig. 2. Illustration of geometric COLREGs interpretation based on [4] and [6]. The OS is in the center, with course χ. The circles correspond to target-ships in each of the relative bearing sectors around the OS. The relative bearing of TS to OS is used to determine the correct relative bearing sector, and the course of TS relative to OS is used to classify the COLREGs situation within that sector. In circle segments with two possible classifications, the former is used if the relative velocity between the OS and TS is negative, and the latter is used if it is greater than, or equal to, zero.

Assumption 1. *During the encounter, all target ships keep a constant course and speed.*

This is a fair assumption in overtaking and give-way situations, as COLREGs then deem the TS to satisfy stand-on obligations, i.e., to keep a constant course and speed. When the TS is in a head-on or a give-way situation, with respect to the OS, on the other hand, this assumption will generally not hold, since the TS is obligated to perform a change of course and/or speed. However, if both the OS and TS act in accordance with rules 13-15 and 17, the maneuvers of the TS will only aid the resolving of the situation. Therefore, the assumption that TS keeps a constant course and speed is a (mild) worst-case assumption.

B. Target Ship Domain

Once a classification of the situation is made, and the COLREGs rules that apply are given accordingly, compliant actions must be taken. A common approach is to define a TS domain around the target ship and adjust the OS course and/or speed in a way that prevents the OS from entering the TS domain. To comply with COLREGs, the domain is often extended to the front and/or starboard of the TS to facilitate passing port to port in head-on situations and behind in crossing situations [4], [15]. A phenomenon that can occur with such domain-based approaches is contouring, i.e. that the OS follows the contour of the TS domain if the nominal trajectory of the OS crosses into the TS domain [16]. If the

COLAV method facilitates contouring, the domain should be designed in such a way that the contouring behaviour mimics the desired behaviour. In particular, COLREGs Rule 8 should be considered, which states that any alteration of course and/or speed to avoid collision shall be large enough to be readily apparent, and that a succession of small alteration of course and/or speed should be avoided.

We propose a domain defined by a straight line dividing the North-East plane into two half planes with the OS and the TS in separate halves. Figure 3 illustrates the domain of the red TS and the OS in blue. The line is intersecting the point $\boldsymbol{p}_D$ at a right angle to the line from $\boldsymbol{p}_D$ to the center of the TS at $\boldsymbol{p}_{TS}$. The point $\boldsymbol{p}_D$ is positioned at a distance $l > 0$ from $\boldsymbol{p}_{TS}$, and its position is given by

$$\boldsymbol{p}_D = \boldsymbol{p}_{TS} + \begin{bmatrix} \cos(\alpha) \\ \sin(\alpha) \end{bmatrix} l, \tag{7}$$

with

$$\alpha = \chi_{TS} + \varphi_{TS} + \alpha_d. \tag{8}$$

The angle φ_{TS} is the relative bearing from the OS to the TS

$$\varphi_{TS} = \text{atan2}(\bar{E}, \bar{N}) - \chi_{TS}, \tag{9}$$

with $\bar{N} = (N - N_{TS})$ and $\bar{E} = (E - E_{TS})$. The angle $\alpha_d \in (-\pi, \pi)$ is a design parameter that can be used to alter the behaviour of the system. In particular, we use it to avoid stagnation and alter the direction of deflection of the OS on the TS domain. If $\alpha_d = 0$ and the OS is approaching the TS at relative bearing $\varphi = 0$, it will approach the TS domain at a right angle and stagnation will occur, where the OS slows down and subsequently deflects to either side depending on multiple factors such as tracking error, actuator orientation, etc. We therefore use α_d to facilitate deflecting to one or the other side along the TS domain in accordance with COLREGs by determining an appropriate α_d for each of the situations {SO, OT$_s$, OT$_p$, HO, GW}. A good choice of α_d will also ensure that when contouring, the avoidance maneuver is a positive, readily apparent course-change maneuver. The parameter $l > 0$ is a tuning parameter that gives a lower bound on the shortest allowable distance between the TS and the OS. To ensure that no collision occurs, independent of the orientation of the TS and OS, the parameter l should be chosen such that $l > 1/2(l_{OS} + l_{TS})$, where l_{OS} and l_{TS} are the lengths of the OS and TS, respectively.

IV. Control Barrier Function Design

In this section, we propose a control barrier function that ensures that the OS does not violate the TS domain defined in the previous section. The CBF is formulated with respect to the TS domain, where we include both the Euclidean distance to the domain, as well as the relative velocity towards the domain. First, we define the point

$$\boldsymbol{p}_B = \boldsymbol{p}_D + (\boldsymbol{p} - \boldsymbol{p}_D)^\mathsf{T} \boldsymbol{n}_{p_D} \boldsymbol{n}_{p_D}, \tag{10}$$

as the point on the TS domain closest to the OS, where

$$\boldsymbol{n}_{p_D} = \boldsymbol{R}_2(\phi) \boldsymbol{n}_x, \tag{11}$$

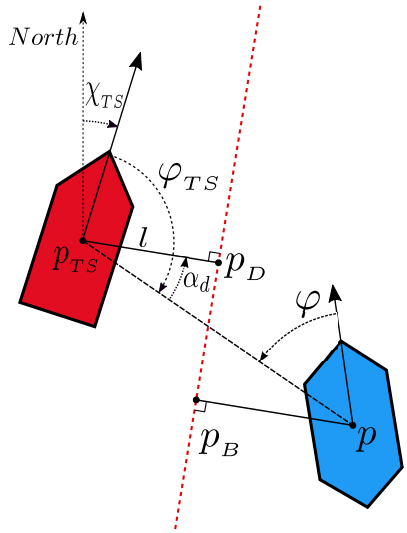

Fig. 3. Target ship in red, is located at $\boldsymbol{p}_{TS}$ with course χ_{TS}, relative bearing to the OS φ_{TS} and angle of deflection α_d. The TS domain is given by the red dashed line passing through $\boldsymbol{p}_D$ at a distance $l > 0$ from the center of the TS. The OS is located at $\boldsymbol{p}$ with $\boldsymbol{p}_B$ as the closest point on the TS domain. All angles are positive in the clockwise direction.

is the tangent unit vector to the TS domain with $\phi = \alpha - \pi/2$, and where $\boldsymbol{n}_x$ is a unit vector pointing North, and

$$\boldsymbol{R}_2(\phi) = \begin{bmatrix} \cos(\phi) & -\sin(\phi) \\ \sin(\phi) & \cos(\phi) \end{bmatrix} \tag{12}$$

is the two-dimensional rotation matrix. The point $\boldsymbol{p}_B$ is shown in Fig. 3.

Based on this, we define the CBF by

$$h(\boldsymbol{x}) = \boldsymbol{n}_{\tilde{p}}^\mathsf{T} \tilde{\boldsymbol{p}} + c \boldsymbol{n}_{\tilde{p}}^\mathsf{T} \dot{\tilde{\boldsymbol{p}}}, \tag{13}$$

where $\boldsymbol{x} = [\boldsymbol{p}^\mathsf{T}, \dot{\boldsymbol{p}}^\mathsf{T}, \boldsymbol{p}_{TS}^\mathsf{T}, \dot{\boldsymbol{p}}_{TS}^\mathsf{T}, \chi_{TS}]^\mathsf{T}$, $\tilde{\boldsymbol{p}} = \boldsymbol{p}_B - \boldsymbol{p}$ and $\boldsymbol{n}_{\tilde{p}}$ is the unit vector of $\tilde{\boldsymbol{p}}$. The first term of $h(\boldsymbol{x})$ is the Euclidean distance from the OS to the TS domain, and the second term is the relative velocity between the OS and the TS domain, weighted by $c > 0$. The parameter c mitigates between the distance to the TS domain and the velocity by which the OS is allowed to approach the domain with. The weight should reflect the stopping distance and/or turning radius of the OS. The time derivative of $h(\boldsymbol{x})$ becomes

$$\dot{h}(\boldsymbol{x}) = \dot{\boldsymbol{n}}_{\tilde{p}}^\mathsf{T} \tilde{\boldsymbol{p}} + \boldsymbol{n}_{\tilde{p}}^\mathsf{T} \dot{\tilde{\boldsymbol{p}}} + c(\dot{\boldsymbol{n}}_{\tilde{p}}^\mathsf{T} \dot{\tilde{\boldsymbol{p}}} + \boldsymbol{n}_{\tilde{p}}{}^\mathsf{T} \ddot{\tilde{\boldsymbol{p}}}), \tag{14}$$

with $\dot{\tilde{\boldsymbol{p}}} = \dot{\boldsymbol{p}}_B - \dot{\boldsymbol{p}}$, where $\dot{\boldsymbol{p}} = [\dot{N}, \dot{E}]^\mathsf{T}$ is the North-East velocity of the OS. The time derivative of the unit vector $\boldsymbol{n}_{\tilde{p}}$ is

$$\dot{\boldsymbol{n}}_{\tilde{p}} = \frac{\dot{\tilde{\boldsymbol{p}}}}{\sqrt{\tilde{\boldsymbol{p}}^\mathsf{T} \tilde{\boldsymbol{p}}}} - \frac{\tilde{\boldsymbol{p}} \tilde{\boldsymbol{p}}^\mathsf{T} \tilde{\boldsymbol{p}}}{(\tilde{\boldsymbol{p}}^\mathsf{T} \tilde{\boldsymbol{p}})^{3/2}}. \tag{15}$$

Further, the time derivative of $\boldsymbol{p}_B$ is

$$\begin{aligned} \dot{\boldsymbol{p}}_B =& \dot{\boldsymbol{p}}_D + (\dot{\boldsymbol{p}} - \dot{\boldsymbol{p}}_D)^\mathsf{T} \boldsymbol{n}_{p_D} \boldsymbol{n}_{p_D} + (\boldsymbol{p} - \boldsymbol{p}_D)^\mathsf{T} \dot{\boldsymbol{n}}_{p_D} \boldsymbol{n}_{p_D} \\ &+ (\boldsymbol{p} - \boldsymbol{p}_D)^\mathsf{T} \boldsymbol{n}_{p_D} \dot{\boldsymbol{n}}_{p_D}, \end{aligned} \tag{16}$$

where $\dot{\boldsymbol{p}}_D$ is the derivative of (7)

$$\dot{\boldsymbol{p}}_D = \dot{\boldsymbol{p}}_{TS} + \begin{bmatrix} -\sin(\alpha) \\ \cos(\alpha) \end{bmatrix} l\dot{\alpha}, \tag{17}$$

and the TS domain tangent unit vector derivative is

$$\dot{\boldsymbol{n}}_{p_D} = \frac{\partial \boldsymbol{R}_2(\phi)}{\partial \phi}\dot{\phi}\boldsymbol{n}_x. \tag{18}$$

From Assumption 1, χ_{TS} is assumed constant. We get

$$\dot{\phi} = \dot{\alpha} = \dot{\varphi}_{TS} = \nabla \operatorname{atan2}(\bar{E}, \bar{N})^{\mathsf{T}}\dot{\tilde{\boldsymbol{p}}}, \tag{19}$$

where $\dot{\tilde{\boldsymbol{p}}} = \dot{\boldsymbol{p}} - \dot{\boldsymbol{p}}_{TS}$ denotes the relative velocity between the two vessels. Lastly, from (14), the double time derivative of $\tilde{\boldsymbol{p}}$ is

$$\begin{aligned} \ddot{\tilde{\boldsymbol{p}}} =& \ddot{\boldsymbol{p}}_D - \ddot{\boldsymbol{p}} + (\ddot{\boldsymbol{p}} - \ddot{\boldsymbol{p}}_D)^{\mathsf{T}}\boldsymbol{n}_{p_D}\boldsymbol{n}_{p_D} + 4(\dot{\boldsymbol{p}} - \dot{\boldsymbol{p}}_D)^{\mathsf{T}}\dot{\boldsymbol{n}}_{p_D}\boldsymbol{n}_{p_D} \\ &+ 2(\boldsymbol{p} - \boldsymbol{p}_D)^{\mathsf{T}}(\ddot{\boldsymbol{n}}_{p_D}\boldsymbol{n}_{p_D} + \dot{\boldsymbol{n}}_{p_D}\dot{\boldsymbol{n}}_{p_D}), \end{aligned} \tag{20}$$

with

$$\ddot{\boldsymbol{n}}_B = \left(\frac{\partial^2 \boldsymbol{R}_2(\phi)}{\partial \phi^2}\dot{\alpha} + \frac{\partial \boldsymbol{R}_2(\phi)}{\partial \phi}\ddot{\alpha} \right) \boldsymbol{n}_x, \tag{21}$$

and

$$\ddot{\boldsymbol{p}}_D = \begin{bmatrix} -\cos(\alpha) \\ -\sin(\alpha) \end{bmatrix} l\dot{\alpha} + \begin{bmatrix} -\sin(\alpha) \\ \cos(\alpha) \end{bmatrix} l\ddot{\alpha}, \tag{22}$$

where

$$\ddot{\alpha} = \nabla^2 \operatorname{atan2}(\bar{E}, \bar{N})\dot{\tilde{\boldsymbol{p}}} + \nabla \operatorname{atan2}(\bar{E}, \bar{N})\ddot{\tilde{\boldsymbol{p}}}. \tag{23}$$

Again, from Assumption 1, $\ddot{\boldsymbol{p}}_{TS} = \boldsymbol{0}$ and, therefore, $\ddot{\tilde{\boldsymbol{p}}} = \ddot{\boldsymbol{p}}$.

To utilize the proposed CBF in a reactive COLAV scheme, we consider the 3-DOF model of an ASV on the form

$$\dot{\boldsymbol{p}} = \boldsymbol{R}_{2,3}(\psi)\boldsymbol{\nu}, \tag{24}$$

$$\dot{\boldsymbol{\nu}} = \boldsymbol{M}^{-1}(\boldsymbol{C}(\boldsymbol{\nu}) + \boldsymbol{D}(\boldsymbol{\nu}))\boldsymbol{\nu} + \boldsymbol{M}^{-1}\boldsymbol{B}\boldsymbol{u}, \tag{25}$$

where $\boldsymbol{M}$ is the inertia matrix including hydrodynamic added mass, $\boldsymbol{C}(\boldsymbol{\nu})$ is the Coriolis-centripetal matrix including hydrodynamic added mass, $\boldsymbol{D}(\boldsymbol{\nu})$ is the damping matrix, $\boldsymbol{B}$ is the thruster configuration matrix [17], $\boldsymbol{u}$ is the control input and

$$\boldsymbol{R}_{2,3}(\psi) = \begin{bmatrix} \cos(\psi) & -\sin(\psi) & 0 \\ \sin(\psi) & \cos(\psi) & 0 \end{bmatrix}. \tag{26}$$

The time derivative of (24) is then

$$\ddot{\boldsymbol{p}} = \dot{\boldsymbol{R}}_{2,3}(\psi)\boldsymbol{\nu} + \boldsymbol{R}_{2,3}(\psi)\dot{\boldsymbol{\nu}}, \tag{27}$$

which is the acceleration of the position of OS in the North-East-Down frame.

By inserting (25) into (27), and then substituting for $\ddot{\boldsymbol{p}}$ in (23) and (20), the time derivatives from (15), (16) and (20) can be substituted in (14) to get $\dot{h}(\boldsymbol{x})$ on the form

$$\dot{h}(\boldsymbol{x}) = F(\boldsymbol{x}) + G(\boldsymbol{x})\boldsymbol{u}, \tag{28}$$

which is affine in the control input $\boldsymbol{u}$. From this, we see that (28) matches the form of the inequality constraint in (5), with $\frac{\partial h}{\partial x}f(\boldsymbol{x}) = F(\boldsymbol{x})$ and $\frac{\partial h}{\partial \boldsymbol{x}}g(\boldsymbol{x}) = G(\boldsymbol{x})$. Hence, the CBF in (13) ensures forward invariance of a set that is both collision-free and COLREGs-compliant with the rules presented in Section III.

The class-κ function $\alpha(\cdot)$ in (5) ensures forward invariance of the set $\mathcal{C}$ without restricting any sublevel set of $\mathcal{C}$ to be forward invariant, by allowing $\dot{h}(\boldsymbol{x})$ to be increasingly negative as the value of $h(\boldsymbol{x})$ increases. The minimal intrusive feature of this approach is provided by selecting an appropriate $\alpha(\cdot)$ so that when $h(\boldsymbol{x})$ is sufficiently large, the control input $\boldsymbol{u}$ is restricted only by the capacity of the thruster system, and not by the inequality constraint in (5). This, in turn, ensures that the trajectory tracking objectives from any higher level in a hybrid COLAV structure will be performed without intrusion from the reactive COLAV method that we propose in this paper.

We propose the use of the linear function $\alpha(h(\boldsymbol{x})) = \gamma h(\boldsymbol{x})$ for some $\gamma > 0$ sufficiently small to ensure a region $0 < h(\boldsymbol{x}) < h_{lim}$ where the restrictions on $\boldsymbol{u}$ from the inequality constraints in (5) increase with a rate that complies with the rate saturations of the vessel actuators. This is especially important to ensure feasibility of the quadratic optimization problem if the actuator rate constraints are additional inequality constraints in (5). The gain γ is found through trial and error. An analytic approach to finding an upper bound on γ for a particular vessel is left for future work.

V. Simulations

This section presents simulation results from four scenarios:

1) **Head-on:** The OS and the TS are on near reciprocal courses. In accordance with COLREGs, both vessels should alter their course to starboard.
2) **Overtaking:** The OS is overtaking the TS, and should keep out of the way of the TS.
3) **Give-way crossing:** The OS and the TS are on crossing courses. The OS is the give-way vessel, and shall keep out of the way of the TS and avoid crossing ahead of the TS.
4) **Stand-on crossing:** The OS and the TS are on crossing courses. The OS is the stand-on vessel, and shall keep a constant course and speed until it is apparent that the give-way vessel, the TS, is not taking appropriate action.

All simulations have one target ship that keeps a constant heading aligned with the course, and a constant speed throughout the simulation in accordance with Assumption 1. The simulations are run in Simulink with a 3-DOF model of the *milliAmpere* vessel depicted in Fig. 4, which is a 3×5 meter prototyping platform for fully electric autonomous passenger ferries. The vessel is equipped with two azimuth thrusters positioned along the fore-aft centerline, symmetrically about the beam. The model parameters and how they are estimated are described in [18]. The ferry is designed for operation in urban waterways where vessel speed is restricted by law, and recreational vessels make up most of the traffic. We therefore consider low-speed trajectories with target ships of size 6×3 meters.

In the simulations, the guidance system provides the reference trajectory. In a hybrid architecture like the one

Fig. 4. The milliAmpere experimental platform in Trondheim harbour.

presented in Section I, the trajectory would be calculated by the mid-level COLAV system, and would ideally be collision-free. To achieve the desired simulation scenarios, we use a guidance system that outputs a straight line, constant velocity trajectory reference from $[N_s, E_s] = [0, 0]$ to $[N_e, E_e] = [200, 60]$. The motion controller is the quadratic program CLF-based controller proposed in [14] that handles trajectory tracking and thrust allocation in a unified controller by solving a quadratic optimization problem. The controller considers the rate constraints and saturation effects in the actuators by applying appropriate inequality constraints. The navigation system delivers the navigation data $\boldsymbol{p}$, $\dot{\boldsymbol{p}}$ and $\boldsymbol{\nu}$ without noise. The TS states $\boldsymbol{p}_{TS}$ and $\dot{\boldsymbol{p}}_{TS}$ are also assumed available without noise.

The parameters that are used in the simulations are given in Table I.

TABLE I
TS DOMAIN PARAMETERS

Parameter	Value	Parameter	Value
α_d (SO)	$0\,\text{rad}$	α_d (GW)	$-\pi/8\,\text{rad}$
α_d (OT_s)	$-\pi/10\,\text{rad}$	l	$10\,\text{m}$
α_d (OT_p)	$\pi/10\,\text{rad}$	c	$15\,\text{s}$
α_d (HO)	$-\pi/5\,\text{rad}$	γ	$0.1\,/\text{s}$

Two figures are included for each simulation. One showing a situation overview at seven timestamps with $16s$ intervals. The other showing the course of the OS and course of the reference trajectory, along with a graph that indicates when the classification deems a situation other than the safe situation, and with vertical grey dashed lines at the times of the timestamps used for the situation overviews.

A. Scenario 1 Head-on

In this simulation, the TS is traveling south with $\chi_{TS} = \pi\,\text{rad}$ and speed of $1\,\text{m/s}$. At timestamp 2, the OS starts a starboard course change maneuver to avoid entering the TS domain. The maneuver endures until about timestamp 4, as can be seen from Fig. 6, where the situation is deemed safe, and the OS adjusts course to get back on the reference trajectory. The OS avoids collision by passing port to port in accordance with **Rule 14**. An appropriate reaction from the TS would be a starboard maneuver, which would increase the

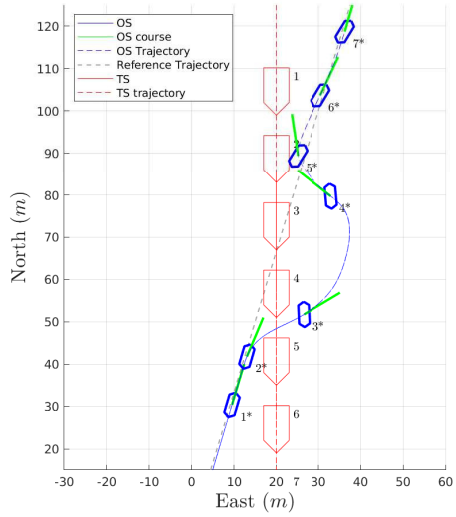

Fig. 5. **Scenario 1 Head-on:** The OS is approaching the TS in a head-on situation. The OS avoids collision by adjusting course to starboard in accordance with **Rule 14**.

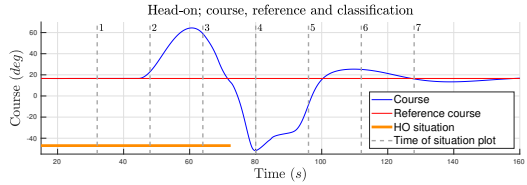

Fig. 6. **Scenario 1 Head-on:** The situation is correctly classified as a head-on situation. The OS performs a hard-starboard maneuver to avoid entering the TS domain.

margin between the vessels. From Fig. 5, it is apparent that the OS has varying velocity during the evasive maneuver. This is due to the inequality in (5) initially restricting the control options, causing the vessel to slow down and deviate to starboard. This, in turn, causes the OS to lag behind the constant velocity trajectory reference. After some time, when the situation is classified as safe, the OS can again utilize the full capacity of the thruster system and accelerates to catch up with the trajectory reference. Similar behavior is present in all four simulations.

B. Scenario 2 Overtaking

In this simulation, the TS is traveling north with $\chi_{TS} = 0\,\text{rad}$ and a speed of $0.2\,\text{m/s}$. From Fig. 8, it can be seen that the situation is correctly classified as OT_s, and the OS adjusts course to starboard as it approaches the TS to avoid entering the TS domain. The starboard maneuver lasts for about $45s$ before the OS has passed the TS, and the situation is deemed safe. From Fig. 7, it can be seen that the OS passes behind the TS and overtakes on the starboard side. The OS keeps clear of the TS in accordance with **Rule 13**.

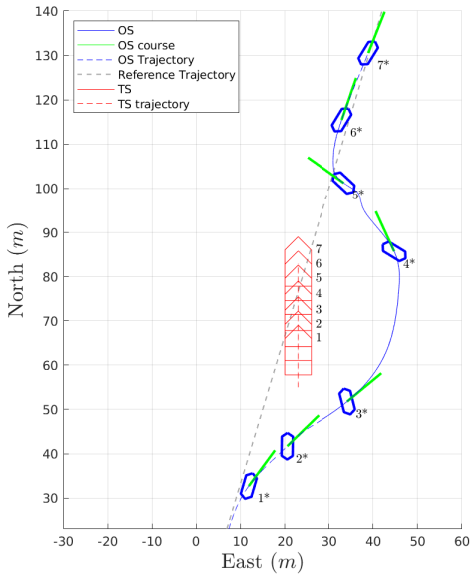

Fig. 7. **Scenario 2 Overtaking:** The OS is approaching the TS in an overtaking situation. The OS avoids collision by adjusting course to starboard and passes behind the TS in accordance with **Rule 13**.

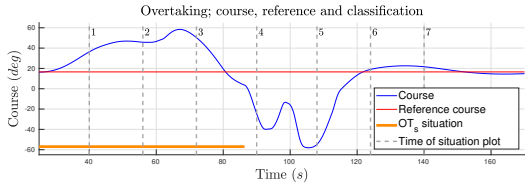

Fig. 8. **Scenario 2 Overtaking:** The χ_{rel} deem it an OT$_s$ situation, and the OS performs a starboard course change to avoid entering the TS domain. When the OS is clear, the situation changes to SF.

C. Scenario 3 Give-way crossing

In this simulation, the TS is traveling west with $\chi_{TS} = -\pi/2\,\mathrm{rad}$ and speed of $1\,\mathrm{m/s}$. The two vessels are at crossing courses, and the OS has the give-way duty. From Fig. 10, it can be seen that the situation is correctly classified as a give-way situation, and that the OS adjusts course to starboard. The choice of α_d ensures that when contouring, the avoidance maneuver is a positive, readily apparent course-change maneuver. Between timestamps 3 and 4, the OS is abaft of the TS, with such a relative velocity to TS that the situation is deemed safe, and the OS maneuvers towards the reference trajectory, as can be seen in Fig. 9. The OS gives way to the TS and avoids crossing ahead of it, in accordance with **Rule 15**.

D. Scenario 4 Stand-on crossing

In this simulation, the TS is traveling east with $\chi_{TS} = \pi/2\,\mathrm{rad}$ and speed of $1\,\mathrm{m/s}$. Fig. 12 shows that the situation is classified as SO. The OS should therefore keep a constant

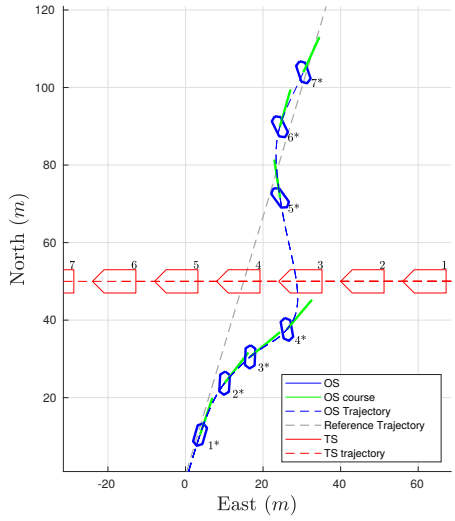

Fig. 9. **Scenario 3 Give-way crossing:** The OS is approaching the TS in a give-way situation. The OS avoids collision by adjusting course to starboard in accordance with **Rule 15**.

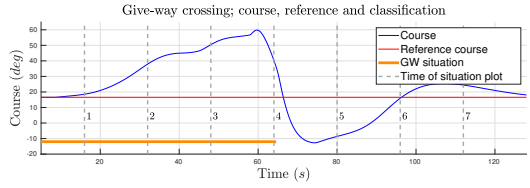

Fig. 10. **Scenario 3 Give-way crossing:** The situation is correctly classified as a give-way situation. The OS performs a hard starboard maneuver to avoid collision.

course and speed unless it is apparent that the TS is not abiding its give-way duty. Just before timestamp 1, the OS starts a hard starboard maneuver to avoid violating the TS domain. Since the TS is not abiding, the OS starts deviating from the reference trajectory. After some time, the OS loops back around and passes behind the TS, due to the angle α increasing as the TS moves alongside the OS. The OS avoids collision, and acts in accordance with **Rule 17**. The looping maneuver is arguably not a very efficient one, and in some situations, the deviation can be much greater if the OS gets ”caught” by the TS domain. In confined waters, where the surroundings can be cluttered with static obstacles and sea-markings, such deviations can produce serious consequences. If the OS was instead to handle the situation by initially altering the course to port, it would violate **Rule 17** and put itself in harms way if the TS was to suddenly abide its duty and alter its course to starboard. The last option would be to reduce the speed and/or stop. This would also worsen the situation if the TS was to abide, but would prevent the deviation from the reference trajectory and at the same time increase the time window for the TS to react. Since the presented COLAV method is merged with the

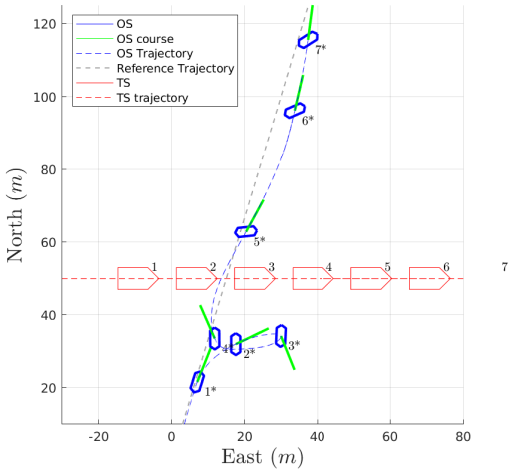

Fig. 11. **Scenario 4 Stand-on crossing:** The OS starts a hard starboard maneuver at timestamp 1, but as the TS moves alongside the OS, the relative bearing φ_{TS} changes so that the direction of deflection changes, and the OS loops around to pass behind the TS.

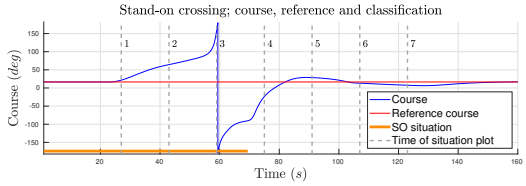

Fig. 12. **Scenario 4 Stand-on crossing:** The OS has the right of way, and starts a hard starboard maneuver at timestamp 1 to avoid collision. The OS gets caught by the TS domain, and ends up deviating from the trajectory.

trajectory tracking control system, it does not comply well with stopping unless the trajectory reference also stops. An approach to this would be to instead track a time-shifted trajectory reference, but such an augmentation is left for future work.

VI. Conclusion and Future Work

In this paper, we have proposed a reactive collision avoidance method for ASVs based on control barrier functions (CBFs). We have shown how a vessel-to-vessel encounter can be classified with respect to COLREGs, in order to assign a relevant domain to the target ship (TS) based on the classified situation. We have used simple domains, defined by a single straight line dividing the North-East plane in two parts, to assure predictable and effective maneuvers. We have then proposed a CBF to ensure that the TS domains are not violated. The proposed approach can be made both minimally intrusive and compliant with rate-constraints in the actuators by selecting an appropriate class-κ function. The method is illustrated through simulations of head-on and overtaking, as well as stand-on and give-way crossing situations, where it demonstrates to be compliant with COLREGs rules 13-15 and 17.

Future work includes designing the TS domain in a way that gives optimal evasive maneuvers regarding safety and passenger comfort, and validation via full-scale experiments. This includes to find a lower limit on the gain γ and to determine which maneuvers are the most effective for a given actuator configuration.

References

[1] P. Belcher, "A sociological interpretation of the COLREGS," *Journal of Navigation*, vol. 55, no. 2, pp. 213–224, 2002.

[2] COLREGs. (1995, November) International regulations for preventing collisions at sea. [Online]. Available: http://inoa.net/zeilen/colreg.html

[3] K. Woerner, M. Benjamin, M. Novitzky, and J. Leonard, "Quantifying protocol evaluation for autonomous collision avoidance: Toward establishing COLREGs compliance metrics," *Autonomous Robots*, vol. 43, May 2018.

[4] C. Tam and R. Bucknall, "Collision risk assessment for ships," *Journal of Marine Science and Technology*, vol. 15, pp. 257–270, Sep. 2010.

[5] T. Porathe, "Is COLREG enough? Interaction between manned and unmanned ships," in *Proc. International Conference on Marine Navigation and Safety of Sea Transportation*, June 2017, pp. 191–194.

[6] B.-O. H. Eriksen, G. Bitar, M. Breivik, and A. M. Lekkas, "Hybrid collision avoidance for ASVs compliant with COLREGs rules 8 and 13–17," *Frontiers in Robotics and AI*, p. 11, 2020.

[7] Ø. A. G. Loe, "Collision avoidance for unmanned surface vehicles," Master's thesis, Norwegian University of Science and Technology (NTNU), Trondheim, Norway, 2008.

[8] G. Bitar, B.-O. H. Eriksen, A. M. Lekkas, and M. Breivik, "Energy-optimized hybrid collision avoidance for ASVs," in *Proc. 18th European Control Conference (ECC)*, Naples, Italy, June 2019, pp. 2522–2529.

[9] A. D. Ames, S. Coogan, M. Egerstedt, G. Notomista, K. Sreenath, and P. Tabuada, "Control barrier functions: Theory and applications," in *Proc. European Control Conference (ECC)*, Naples, Italy, June 2019, pp. 3420–3431.

[10] P. Glotfelter, I. Buckley, and M. Egerstedt, "Hybrid nonsmooth barrier functions with applications to provably safe and composable collision avoidance for robotic systems," *IEEE Robotics and Automation Letters*, vol. 4, no. 2, pp. 1303–1310, April 2019.

[11] D. Panagou, D. M. Stipanovi, and P. G. Voulgaris, "Distributed coordination control for multi-robot networks using Lyapunov-like barrier functions," *IEEE Transactions on Automatic Control*, vol. 61, no. 3, pp. 617–632, March 2016.

[12] A. D. Ames, X. Xu, J. W. Grizzle, and P. Tabuada, "Control barrier function based quadratic programs for safety critical systems," *IEEE Transactions on Automatic Control*, vol. 62, no. 8, pp. 3861–3876, Aug 2017.

[13] E. A. Basso and K. Y. Pettersen, "Task-priority control of redundant robotic systems using control Lyapunov and control barrier function based quadratic programs," in *Proc. 21st IFAC World Congress*, Berlin, Germany, Jul 2020.

[14] E. A. Basso, E. H. Thyri, K. Y. Pettersen, M. Breivik, and R. Skjetne, "Safety-critical control of autonomous surface vehicles in the presence of ocean currents," in *Proc. 4th IEEE Conference On Control Technology and Applications*, Montreal, Canada, Aug. 2020.

[15] B.-O. H. Eriksen, M. Breivik, E. F. Wilthil, A. L. Flåten, and E. F. Brekke, "The branching-course model predictive control algorithm for maritime collision avoidance," *Journal of Field Robotics*, vol. 36, no. 7, pp. 1222–1249, Aug. 2019.

[16] S. Moe and K. Y. Pettersen, "Set-based line-of-sight (LOS) path following with collision avoidance for underactuated unmanned surface vessel," in *Proc. Mediterranean Conference on Control and Automation (MED)*, Athens, Greece, June 2016, pp. 402–409.

[17] T. I. Fossen, *Handbook of Marine Craft Hydrodynamics and Motion Control*. John Wiley & Sons, 2011.

[18] A. A. Pedersen, "Optimization based system identification for the milliAmpere ferry," Master's thesis, Norwegian University of Science and Technology (NTNU), Trondheim, Norway, 2019.

Paper C A 3DOF path-following controller for a non-directionally stable vessel with slow thruster dynamics

Published paper by E. H. Thyri, G. Bitar, and M. Breivik. "A 3DOF path-following controller for a non-directionally stable vessel with slow thruster dynamics". In: *IFAC-PapersOnLine* 54.16 (2021). 13th IFAC Conference on Control Applications in Marine Systems, Robotics, and Vehicles (CAMS) 2021, pp. 288–294. ISSN: 2405-8963. DOI: https://doi.org/10.1016/j.ifacol.2021.10.106.

Bibliography entry [25].

A 3DOF Path-Following Controller for a Non-Directionally Stable Vessel with Slow Thruster Dynamics

Emil H. Thyri * **Glenn Bitar** * **Morten Breivik** *

* *Centre for Autonomous Marine Operations and Systems (AMOS), Department of Engineering Cybernetics, Norwegian University of Science and Technology (NTNU). NO-7491 Trondheim, Norway. (e-mail: emil.h.thyri@ntnu.no,glennbitar@outlook.com, morten.breivik@ieee.org)*

Abstract: In this paper, a 3DOF path-following controller for an electric double-ended passenger ferry prototype is presented. The controller is formulated through a 3-step backstepping approach, taking into consideration several challenging physical properties of the vessel, such as a lack of passive damping in the vessel hull, lack of directional stability, and slow thruster dynamics compared to the vessel dynamics. The controller design also features a new thrust allocation approach that allows the thrust allocation of the over-actuated thruster system to be formulated on closed form, which enables us to include the thruster dynamics in the control law. The performance of the suggested 3DOF controller is demonstrated and compared to two other controllers through simulations with a model of the electric passenger ferry.

Keywords: 3DOF path-following control, non-directionally stable vessel, slow thruster dynamics, vectorial backstepping, thrust allocation.

1. INTRODUCTION

The motivation for the work presented in this paper is to develop a controller for the transit stage of a dock-to-dock operation for the milliAmpere vessel, which is an experimental platform for developing and testing technology for autonomous surface vessels. Three challenges with the physical properties of the vessel have been identified:

- The hull geometry of the milliAmpere vessel, which can be seen in Fig. 1, has a shallow draft and small length-to-beam ratio, makes it lack passive damping. This is particularly an issue in the sway and yaw mode. This manifests itself both in the lack of directional stability and in high sway velocity and thereby high sideslip angle when yawing.
- Inherent instability in yaw of the vessel's hull when the surge velocity exceeds about 1 m/s, where the forces on the hull act to turn the hull's broad-side towards the direction of travel. The mathematical interpretation of this is that when surging, the sideslip angle β has an unstable equilibrium at $\beta = 0$, and stable equilibriums at $\beta \sim \pm\pi/2$. The destabilizing yaw moment is increasing for increasing magnitude of β.
- The slow thruster dynamics of the vessel's two azimuth thrusters make it time-constrained fully actuated, despite being geometrically fully actuated. The dynamics of the azimuth angles have similar time constants to the dynamics of the vessel yaw angle, much due to the lack of passive damping. In combination with the yaw-instabilities, this makes the vessel heading hard to control at velocities exceeding 1 m/s.

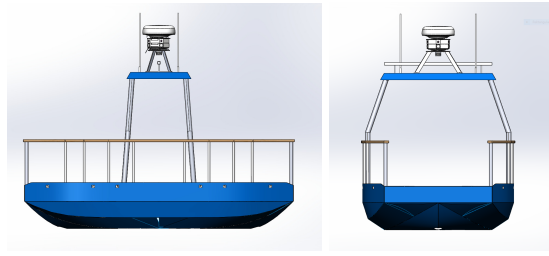

Fig. 1. Front and side view of the milliAmpere hull. The hull has a beam of 3 m and a length of 5 m. Due to the small length-to-beam ratio, the shallow draft and the flat bottom, the vessel lacks directional stability and passive damping. This makes it highly maneuverable, but at the same time requires fast thruster dynamics for precise vessel control. Courtesy of Glenn Angell.

In the controller presented in this paper, we therefore consider the listed problems in the controller design in an attempt to improve the performance. In addition to the controller design, a novel thrust allocation method is formulated, where a new set of control inputs puts the thrust allocation problem on closed form, in the sense that it is no longer underdetermined, and can be solved explicitly without optimization-based methods. The control law for the thruster setpoints are formulated through a backstepping method based on the one presented in (Khalil, 2013) and (Fossen, 2011). The proposed thrust

allocation allows us to include the thruster dynamics in the controller design.

Traditionally, 2 degrees of freedom (DOF) controllers have been used instead of 3DOF controllers when designing controllers for transit operations, both because most vessels are underactuated (at transit speed), and because fully actuated vessels have limited actuation effect in sway at high surge velocities. Extensive work has been done on this topic for sway-underactuated surface vessels, see (Pinkster and Nienhuis, 1986), (Lefeber et al., 2003), (Fossen et al., 2003), (Fossen, 2011) and (Eriksen and Breivik, 2017) and the references therein. A 2DOF approach, however, requires a hull with sufficient sway-yaw damping to control the vessel course through the heading. Additionally, a majority of the work does not consider the vessel actuators beyond the degree of actuation. They only consider the actuator geometry, i.e. geometrical placement, and typically not how long it takes for an actuator to obtain its desired force by rotating and/or changing RPM. For systems where the thruster dynamics is much faster than the vessel dynamics, neglecting the actuator dynamics is an acceptable simplification. For systems where this is not the case, neglecting the thruster dynamics can result in high allocation errors, poor tracking and instability. For such systems, the actuator dynamics should therefore be considered in the controller design.

The remainder of this paper is structured as follows: In Section 2, we introduce the vessel model. Section 3 describes the new thrust allocation approach. In Section 4, we present the controller design. Section 5 contains simulation results. Finally, Section 6 concludes the paper.

2. VESSEL MODELING

In the controller design, a 3DOF vessel model is applied, describing the vessel pose and velocity in the plane in a local NED frame (Fossen, 2011). The vessel states are given by the vectors $\boldsymbol{\eta} = [x, y, \psi]^T \in \Re^2 \times S$, which is the north and east position, and vessel heading, and $\boldsymbol{\nu} = [u, v, r]^T$, which is the body-fixed velocity in surge and sway, and yaw rate, respectively. In addition, the vessel has two azimuth thrusters positioned along the fore-aft centerline. The actuator states are the azimuth angles $\boldsymbol{\alpha} = [\alpha_f, \alpha_a]^\mathsf{T} \in S^2$ and the propeller RPMs $\boldsymbol{\omega} = [\omega_f, \omega_a]^\mathsf{T} \in \Re^2$, where subscripts f and a refer to the fore and aft thruster, respectively.

The ship's dynamics from Fossen (2011) are given by

$$\dot{\boldsymbol{\eta}} = \mathbf{R}(\psi)\boldsymbol{\nu}, \tag{1}$$

$$\mathbf{M}\dot{\boldsymbol{\nu}} + \mathbf{C}(\boldsymbol{\nu})\boldsymbol{\nu} + \mathbf{D}(\boldsymbol{\nu})\boldsymbol{\nu} = \boldsymbol{\tau}(\boldsymbol{\alpha}, \boldsymbol{\omega}), \tag{2}$$

where $\mathbf{R}(\psi)$ represents the principal rotation around the z-axis

$$\mathbf{R}(\psi) = \begin{bmatrix} \cos\psi & -\sin\psi & 0 \\ \sin\psi & \cos\psi & 0 \\ 0 & 0 & 1 \end{bmatrix}, \tag{3}$$

$\mathbf{M}$ is the inertia matrix including hydrodynamically added mass

$$\mathbf{M} = \begin{bmatrix} m_{11} & 0 & 0 \\ 0 & m_{22} & m_{23} \\ 0 & m_{32} & m_{33} \end{bmatrix}, \tag{4}$$

$\mathbf{C}(\boldsymbol{\nu})$ is the Coriolis-centripetal matrix

$$\mathbf{C}(\boldsymbol{\nu}) = \begin{bmatrix} 0 & 0 & c_{13}(v,r) \\ 0 & 0 & c_{23}(u) \\ -c_{13}(v,r) & -c_{23}(u) & 0 \end{bmatrix}, \tag{5}$$

and $\mathbf{D}(\boldsymbol{\nu})$ is the damping matrix

$$\mathbf{D}(\boldsymbol{\nu}) = \begin{bmatrix} d_{11}(u) & 0 & 0 \\ 0 & d_{22}(v,r) & d_{23}(u,v,r) \\ 0 & d_{32}(u,v,r) & d_{33}(u,v,r) \end{bmatrix}, \tag{6}$$

The generalized force produced by the thrusters is given by

$$\boldsymbol{\tau}(\boldsymbol{\alpha}, \boldsymbol{\omega}) = \begin{bmatrix} \Phi(\omega_f)\cos\alpha_f + \Phi(\omega_a)\cos\alpha_a \\ \Phi(\omega_f)\sin\alpha_f + \Phi(\omega_a)\sin\alpha_a \\ l_f\Phi(\omega_f)\sin\alpha_f + l_a\Phi(\omega_a)\sin\alpha_a \end{bmatrix}, \tag{7}$$

where the function $\Phi(\omega_i)$ is fitted to bollard-pull data, and maps the propeller rotational velocity to a force, and l_f and l_a are lengths from the ship's body origin to the fore and aft thruster respectively. Since milliAmpere is fore-aft symmetric, $l_f = -l_a$.

The model for the thruster azimuth angle and propeller dynamics are

$$\dot{\alpha}_i = \frac{K_{i,\alpha}(\alpha_{i,d} - \alpha_i)}{\sqrt{(\alpha_{i,d} - \alpha_i)^2 + \epsilon_i^2}}, \tag{8}$$

$$\dot{\omega}_i = K_{i,\omega}(\omega_{i,d} - \omega_i), \tag{9}$$

where $K_{i,\alpha} > 0$, $\epsilon_i > 0$ and $K_{i,\omega} > 0$ for $i \in \{f, a\}$. All model parameters are determined through the work done by Pedersen (2019), where an optimization-based approach to system identification from experimental data is applied. Conversion of units for $K_{i,\alpha}$ and ϵ_i is necessary since they were estimated in degrees, and we use radians. That is, $K_{i,\alpha} = \frac{\pi}{180^\circ} K^*_{i,\alpha}$ and $\epsilon_i = \frac{\pi}{180^\circ}\epsilon^*_i$, where the starred variables are the numerical values given in (Pedersen, 2019).

3. THRUST ALLOCATION

Since the vessel has four control inputs and is overactuated, the thrust allocation is not trivial. The authors of (Johansen and Fossen, 2013) give a thorough survey of existing methods for thrust allocation for over-actuated systems by means of optimization-based algorithms, where a generalized force can be realized by an arbitrary number of actuators. The actuator setpoints are optimized with respect to objectives such as minimal wear and tear or energy consumption. Such methods are suitable when the dynamics of the thrusters relative to the system are fast enough that they can be omitted in the controller design. If this is not the case, and the thruster and vessel dynamics have comparable time constants, the thruster dynamics must be considered in the controller design.

As mentioned, this is the case for the milliAmpere, which we demonstrate through the introduction of the time-to-actuation (TTA) metric. We define this as the time it takes from thruster setpoints are set and until the normalized allocation errors

$$\tilde{X} = \frac{X - X_d}{X_d}, \tag{10}$$

$$\tilde{Y} = \frac{Y - Y_d}{Y_d}, \tag{11}$$

$$\tilde{N} = \frac{N - N_d}{N_d}, \tag{12}$$

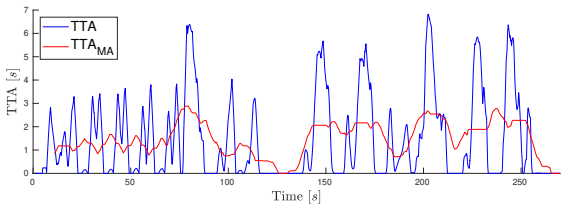

Fig. 2. Simulated TTA and moving average over 20 s, TTA_{MA}.

are less than 15%, where X_d and Y_d are the desired surge and sway forces respectively, and N_d is the desired sway moment corresponding to the thruster setpoints. The TTA is determined by simulating the thruster states from the configuration they are in when the setpoints are set. The TTA is shown in Fig. 2 for a simulated transit. The figure shows the TTA and a moving average of the TTA over a 20 s interval, denoted TTA_{MA}. From the graph, we can see that it takes the thrusters on average more than two seconds to realize $\boldsymbol{\tau}_d$ for parts of the transit. In an equal amount of time the milliAmpere can yaw close to 90° by a yaw moment from its thrusters, or around 45° by a sudden gust of wind. This advocates considering the thruster dynamics when formulating a control law for this vessel.

To do this, we propose a method where first the thrust allocation is simplified and formulated on closed form, and subsequently the thruster dynamics are included as part of the controller design. The input space is thus reduced from $\Re^2 \times S^2$ to $\Re \times S^2$ by the introduction of a new desired state vector

$$\boldsymbol{\rho}_d := [F_d, \alpha_d, \gamma_d]^\mathsf{T} \tag{13}$$

with a corresponding state vector

$$\boldsymbol{\rho} := [F, \alpha, \gamma]^\mathsf{T}. \tag{14}$$

This mapping is physically intuitive, where F is the total force produced by the thrusters, and the angles α and γ actuate the yaw moment and sway force respectively. The relationship between the new thruster states and the original thruster states is illustrated in Fig. 3.

The mapping from the new reduced set of thruster states $\boldsymbol{\rho}$ to the thruster states $\boldsymbol{\omega} = [\omega_f, \omega_a]^\mathsf{T}$ and $\boldsymbol{\alpha} = [\alpha_f, \alpha_a]^\mathsf{T}$ is given by

$$\begin{bmatrix} \omega_f \\ \omega_a \\ \alpha_f \\ \alpha_a \end{bmatrix} = \begin{bmatrix} \Omega(\frac{F}{2}) \\ \Omega(\frac{F}{2}) \\ \alpha + \gamma \\ -\alpha + \gamma \end{bmatrix}, \tag{15}$$

where the force F is split equally between the fore and aft thrusters. The function $\Omega(F)$ is the inverse of $\Phi(\omega)$, and maps a force to the corresponding rotational velocity of the propeller. The mapping from $\boldsymbol{\rho}$ to the generalized force is then

$$\boldsymbol{\tau} = \begin{bmatrix} F\cos\alpha\cos\gamma \\ F\cos\alpha\sin\gamma \\ lF\sin\alpha\cos\gamma \end{bmatrix}. \tag{16}$$

This new input space reduces the number of control input variables in the thrusters from 4 to 3 by assigning equal thrust to both thrusters. This restricts the theoretical performance of the thruster system, however, it allows us to formulate the thrust allocation problem on closed form,

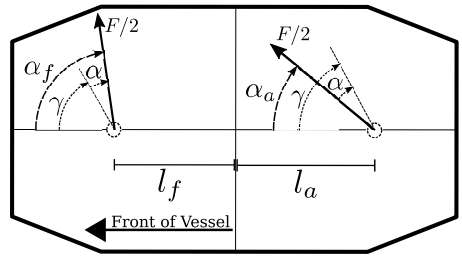

Fig. 3. Thruster configuration of the milliAmpere. Relationship between the new thruster states α and γ, and α_f and α_a are indicated.

which enables us to consider the thruster dynamics in the controller design.

From a desired force vector $\boldsymbol{\tau}_d = [X_d, Y_d, N_d]^\mathsf{T}$, the mapping to the control variables $\boldsymbol{\rho}_d$ is

$$\boldsymbol{\rho}_d = \begin{bmatrix} {}^1\!/_{(lX_d)}\sqrt{X_d^4 l^2 + X_d^2 Y_d^2 l^2 + X_d^2 N_d^2 + Y_d^2 N_d^2} \\ \text{atan2}(N_d, lX_d) \\ \text{atan2}(Y_d, X_d) \end{bmatrix}. \tag{17}$$

In the mapping (17), the following assumptions are applied:

Assumption 1. X_d is always positive.

Assumption 2. The force X_d is large enough in relation to both Y_d and N_d such that the sum of the absolute value of the angles α_d and γ_d are always less than $\pi/2$.

Since the controller is intended for transit, where the major component of the velocity will be in the surge direction, the first assumption is ensured. The proposed controller is hence not suitable for station-keeping operations, and the controller will have to be paired with one suitable for low-speed, station-keeping and docking operations for a full dock-to-dock operation. The second assumption is more restrictive since it puts limitations on the reference signals in sway and yaw, in addition to limiting the magnitude of environmental forces the vessel can handle for a given surge velocity. Yet, at transit velocities, the X component should be sufficiently large to ensure the assumption holds for reasonable yaw rates and environmental disturbances.

3.1 New thruster state dynamics

To include the thruster dynamics in the controller design, a dynamic model for the new thruster states that is affine in the control input $\boldsymbol{\rho}_d$ is needed. There is no trivial way to formulate the dynamics of F, α and γ on an affine form in terms of the dynamics of (8) and (9), since $\Omega(.)$ is a nonlinear lookup-table based on bollard-pull data, and the dynamics of the azimuth angle is a nonlinear function in both α and γ. We therefore chose to model the new thruster states as first-order systems with suitable time constants, with

$$\dot{F} = \frac{1}{T_F}(F_d - F), \tag{18}$$

where the time constant is chosen to be the same as for the propeller dynamics, namely $T_F = 1/K_{i,\alpha}$, and

$$\dot{\alpha} = \frac{1}{T_\alpha}(\alpha_d - \alpha), \tag{19}$$

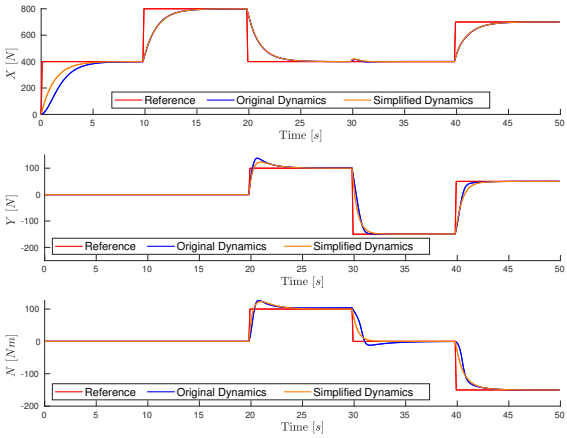

Fig. 4. Comparison of the original thruster dynamics in (8) and (9), and the proposed simplified thruster dynamics in (21).

$$\dot{\gamma} = \frac{1}{T_\gamma}(\gamma_d - \gamma), \tag{20}$$

where the choice of time constants need to consider the slow dynamics of the azimuth angle.

This puts the new thruster state dynamics on the form,

$$\dot{\boldsymbol{\rho}} = \boldsymbol{K}_T(\boldsymbol{\rho}_d - \boldsymbol{\rho}), \tag{21}$$

where $\boldsymbol{K}_T = diag(1/T_F, 1/T_\alpha, 1/T_\gamma)$ and $\boldsymbol{K}_T > 0$.

In Fig. 4, the simplified thruster dynamics and the original thruster dynamics are compared. For the dynamics (8) and (9), the setpoints are found by the thrust allocation method from (Torben et al., 2019). For the dynamics in (21), the setpoints are found by (17). The deviation in X for low magnitudes arise because the thrusters have a deadband at low propeller RPM which is considered in $\Phi(.)$ but not in (18).

4. CONTROLLER DESIGN

In this section, the 3DOF path-following controller is formulated through a 3-step backstepping approach, where the final step includes the dynamics of the newly introduced thruster states in the closed-form thrust allocation. The controller design is made based on the following state-space system where $\boldsymbol{x}$ is the integral of the velocity, and $\boldsymbol{\rho}_d$ is the control input,

$$\dot{\boldsymbol{x}} = \boldsymbol{\nu}, \tag{22}$$

$$\boldsymbol{M}\dot{\boldsymbol{\nu}} + \boldsymbol{C}(\boldsymbol{\nu})\boldsymbol{\nu} + \boldsymbol{D}(\boldsymbol{\nu})\boldsymbol{\nu} = \boldsymbol{\tau}(\boldsymbol{\rho}, \boldsymbol{\rho}_d), \tag{23}$$

$$\dot{\boldsymbol{\tau}}(\boldsymbol{\rho}, \boldsymbol{\rho}_d) = \boldsymbol{B}(\boldsymbol{\rho})\boldsymbol{K}_T(\boldsymbol{\rho}_d - \boldsymbol{\rho}), \tag{24}$$

with

$$\boldsymbol{B}(\boldsymbol{\rho}) = \begin{bmatrix} c(\alpha)c(\gamma) & -Fs(\alpha)c(\gamma) & -Fc(\alpha)s(\gamma) \\ s(\gamma)c(\alpha) & -Fs(\gamma)c(\alpha) & Fc(\gamma)c(\alpha) \\ ls(\alpha)c(\gamma) & Flc(\alpha)c(\gamma) & -Fls(\alpha)s(\gamma) \end{bmatrix}, \tag{25}$$

where $\boldsymbol{B}(\boldsymbol{\rho})$ is the time derivative of (16) with respect to $\boldsymbol{\rho}$, and $s(.)$ and $c(.)$ are the sine and cosine function respectively.

4.1 Backstepping

Step 1 First, we consider the dynamics of $\tilde{\boldsymbol{x}}$, which is the integral of the velocity error $\tilde{\boldsymbol{\nu}} = \boldsymbol{\nu} - \boldsymbol{\nu}_d$, where $\boldsymbol{\nu}_d \in \Re^3$ is the desired body-fixed velocity vector. Hence, $\tilde{\boldsymbol{x}}$ holds the integral error of the surge and sway velocity, and the heading error. By including integral effects, steady-state disturbances can be compensated for. For $\tilde{\boldsymbol{x}}$, we consider $\boldsymbol{\nu}$ as the control input. Then, let

$$\boldsymbol{\nu} = \boldsymbol{z}_1 + \boldsymbol{\alpha}_1, \tag{26}$$

where $\boldsymbol{\alpha}_1$ is a stabilizing vector that will be defined shortly, and $\boldsymbol{z}_1 = \boldsymbol{\nu} - \boldsymbol{\alpha}_1$ is a new state variable. The dynamics of $\tilde{\boldsymbol{x}}$ can then be written as

$$\begin{aligned} \dot{\tilde{\boldsymbol{x}}} &= \boldsymbol{\nu} - \boldsymbol{\nu}_d \\ &= \boldsymbol{z}_1 + \boldsymbol{\alpha}_1 - \boldsymbol{\nu}_d. \end{aligned} \tag{27}$$

A control Lyapunov function (CLF) is formulated as

$$V_1 = \frac{1}{2}\tilde{\boldsymbol{x}}^\mathsf{T}\tilde{\boldsymbol{x}}, \tag{28}$$

with the time derivative

$$\dot{V}_1 = \tilde{\boldsymbol{x}}^\mathsf{T}(\boldsymbol{z}_1 + \boldsymbol{\alpha}_1 - \boldsymbol{\nu}_d). \tag{29}$$

The vector field $\boldsymbol{\alpha}_1$ can then be designed to stabilize the dynamics of $\tilde{\boldsymbol{x}}$. We define it as

$$\boldsymbol{\alpha}_1 := \boldsymbol{\nu}_d - \boldsymbol{K}_p\tilde{\boldsymbol{x}}, \tag{30}$$

with $\boldsymbol{K}_p = \boldsymbol{K}_p^\mathsf{T} > 0$. This gives the state dynamics

$$\dot{\tilde{\boldsymbol{x}}} = -\boldsymbol{K}_p\tilde{\boldsymbol{x}} + \boldsymbol{z}_1, \tag{31}$$

and the CLF derivative

$$\begin{aligned} \dot{V}_1 &= \tilde{\boldsymbol{x}}^\mathsf{T}(-\boldsymbol{K}_p\tilde{\boldsymbol{x}} + \boldsymbol{z}_1) \\ &= -\tilde{\boldsymbol{x}}^\mathsf{T}\boldsymbol{K}_p\tilde{\boldsymbol{x}} + \boldsymbol{z}_1^\mathsf{T}\tilde{\boldsymbol{x}}. \end{aligned} \tag{32}$$

Here, $\dot{V}_1 < 0\ \forall \tilde{\boldsymbol{x}} \in \Re^3 \notin \{\boldsymbol{0}\}$ if $\boldsymbol{z}_1 = \boldsymbol{0}$, hence the $\tilde{\boldsymbol{x}} = \boldsymbol{0}$ is UGAS if $\boldsymbol{z}_1 = \boldsymbol{0}$.

Step 2 We now address the new state $\boldsymbol{z}_1$. An augmented CLF with the pseudo-kinetic energy of the system is formulated as

$$V_2 = \frac{1}{2}\boldsymbol{z}_1\boldsymbol{M}\boldsymbol{z}_1 + V_1, \tag{33}$$

where $\boldsymbol{M} > 0$ is the inertia matrix.

The CLF time derivative is

$$\begin{aligned} \dot{V}_2 &= \boldsymbol{z}_1\boldsymbol{M}\dot{\boldsymbol{z}}_1 + \dot{V}_1 \\ &= \boldsymbol{z}_1[\boldsymbol{\tau}(\boldsymbol{\rho}, \boldsymbol{\rho}_d) - \boldsymbol{M}\dot{\boldsymbol{\alpha}}_1 - (\boldsymbol{C}(\boldsymbol{\nu}) + \boldsymbol{D}(\boldsymbol{\nu}))\boldsymbol{\alpha}_1 \\ &\quad - (\boldsymbol{C}(\boldsymbol{\nu}) + \boldsymbol{D}(\boldsymbol{\nu}))\boldsymbol{z}_1] - \tilde{\boldsymbol{x}}^\mathsf{T}\boldsymbol{K}_p\tilde{\boldsymbol{x}} + \boldsymbol{z}_1^\mathsf{T}\tilde{\boldsymbol{x}} \\ &= \boldsymbol{z}_1[\boldsymbol{\tau}(\boldsymbol{\rho}, \boldsymbol{\rho}_d) - \boldsymbol{M}\dot{\boldsymbol{\alpha}}_1 - (\boldsymbol{C}(\boldsymbol{\nu}) + \boldsymbol{D}(\boldsymbol{\nu}))\boldsymbol{\alpha}_1) \\ &\quad - (\boldsymbol{C}(\boldsymbol{\nu}) + \boldsymbol{D}(\boldsymbol{\nu}))\boldsymbol{z}_1 + \tilde{\boldsymbol{x}}] - \tilde{\boldsymbol{x}}^\mathsf{T}\boldsymbol{K}_p\tilde{\boldsymbol{x}}. \end{aligned} \tag{34}$$

The generalized force $\boldsymbol{\tau}(\boldsymbol{\rho}, \boldsymbol{\rho}_d)$ can now be considered as the control input, and

$$\boldsymbol{\tau}(\boldsymbol{\rho}, \boldsymbol{\rho}_d) = \boldsymbol{z}_2 + \boldsymbol{\alpha}_2, \tag{35}$$

where $\boldsymbol{z}_2$ is a new state variable and $\boldsymbol{\alpha}_2$ is a stabilizing vector that can be designed to stabilize $\boldsymbol{z}_1$, that we define as

$$\boldsymbol{\alpha}_2 := \boldsymbol{M}\dot{\boldsymbol{\alpha}}_1 + (\boldsymbol{C}(\boldsymbol{\nu}) + \boldsymbol{D}(\boldsymbol{\nu}))\boldsymbol{\alpha}_1 - \tilde{\boldsymbol{x}} - \boldsymbol{K}_d\boldsymbol{z}_1 \tag{36}$$

with $\mathbf{K}_d = \mathbf{K}_d^\mathsf{T} > 0$. By appropriate selection of the entries in $\mathbf{K}_d$, the low passive damping in sway and yaw can be compensated for. The choice of $\boldsymbol{\alpha}_2$ gives the new state dynamics

$$\dot{\boldsymbol{z}}_1 = -(\boldsymbol{C}(\boldsymbol{\nu}) + \boldsymbol{D}(\boldsymbol{\nu}) + \boldsymbol{K}_d)\boldsymbol{z}_1 - \tilde{\boldsymbol{x}} + \boldsymbol{z}_2, \tag{37}$$

and the CLF derivative

$$\dot{V}_2 = \boldsymbol{z}_1^\top \boldsymbol{z}_2 - \boldsymbol{z}_1(\boldsymbol{C}(\boldsymbol{\nu}) + \boldsymbol{D}(\boldsymbol{\nu}) + \boldsymbol{K}_d)\boldsymbol{z}_1 - \tilde{\boldsymbol{x}}^\top \boldsymbol{K}_p \tilde{\boldsymbol{x}}, \quad (38)$$

which is negative definite and hence UGAS in $\tilde{\boldsymbol{x}} = \boldsymbol{0}$ and $\boldsymbol{z}_1 = \boldsymbol{0}$ if $\boldsymbol{z}_2 = \boldsymbol{0}$.

Step 3 Finally, the new state $\boldsymbol{z}_2$ is addressed. A further augmented CLF is defined as

$$V_3 := \frac{1}{2}\boldsymbol{z}_2^\top \boldsymbol{z}_2 + V_2 \quad (39)$$

with the time derivative

$$\begin{aligned} \dot{V}_3 &= \boldsymbol{z}_2^\top \dot{\boldsymbol{z}}_2 + \dot{V}_2, \\ &= \boldsymbol{z}_2^\top (\dot{\boldsymbol{\tau}}(\boldsymbol{\rho}, \boldsymbol{\rho}_d) - \dot{\boldsymbol{\alpha}}_2) + \boldsymbol{z}_1^\top \boldsymbol{z}_2 \\ &\quad - \boldsymbol{z}_1(\boldsymbol{C}(\boldsymbol{\nu}) + \boldsymbol{D}(\boldsymbol{\nu}) + \boldsymbol{K}_d)\boldsymbol{z}_1 - \tilde{\boldsymbol{x}}^\top \boldsymbol{K}_p \tilde{\boldsymbol{x}}, \\ &= \boldsymbol{z}_2^\top (\boldsymbol{B}(\boldsymbol{\rho})\boldsymbol{K}_T(\boldsymbol{\rho}_d - \boldsymbol{\rho}) - \dot{\boldsymbol{\alpha}}_2 + \boldsymbol{z}_1) \\ &\quad - \boldsymbol{z}_1(\boldsymbol{C}(\boldsymbol{\nu}) + \boldsymbol{D}(\boldsymbol{\nu}) + \boldsymbol{K}_d)\boldsymbol{z}_1 - \tilde{\boldsymbol{x}}^\top \boldsymbol{K}_p \tilde{\boldsymbol{x}}. \end{aligned} \quad (40)$$

Here, we note that $\boldsymbol{\rho}_d$, which is the control input to the system (22)-(24), finally appears in the CLF derivative. A control law can then be formulated for $\boldsymbol{\rho}_d$ to ensure a negative definite $\dot{V}_3$. We define the control law:

$$\boldsymbol{\rho}_d := \boldsymbol{\rho} + \boldsymbol{K}_T^{-1}\boldsymbol{B}(\boldsymbol{\rho})^{-1}(\dot{\boldsymbol{\alpha}}_2 - \boldsymbol{z}_1 - \boldsymbol{K}_{z_2}\boldsymbol{z}_2), \quad (41)$$

where $\boldsymbol{K}_{z_2} = \boldsymbol{K}_{z_2}^\top > 0$. The state derivative then becomes

$$\dot{\boldsymbol{z}}_2 = -\boldsymbol{z}_1 - \boldsymbol{K}_{z_2}\boldsymbol{z}_2, \quad (42)$$

and the CLF derivative becomes

$$\begin{aligned} \dot{V}_3 = &- \boldsymbol{z}_2^\top \boldsymbol{K}_{z_2}\boldsymbol{z}_2 - \boldsymbol{z}_1^\top(\boldsymbol{C}(\boldsymbol{\nu}) + \boldsymbol{D}(\boldsymbol{\nu}) + \boldsymbol{K}_d)\boldsymbol{z}_1 \\ &- \tilde{\boldsymbol{x}}^\top \boldsymbol{K}_p \tilde{\boldsymbol{x}}, \end{aligned} \quad (43)$$

where $\dot{V}_3 < 0 \ \forall \ \tilde{\boldsymbol{x}}, \boldsymbol{z}_1, \boldsymbol{z}_2 \in \Re^3 \notin \{\boldsymbol{0}\}$ if $(\boldsymbol{C}(\boldsymbol{\nu}) + \boldsymbol{D}(\boldsymbol{\nu}) + \boldsymbol{K}_d) > 0 \ \forall \boldsymbol{\nu} \in \Re^3$, and hence $\tilde{\boldsymbol{x}} = \boldsymbol{0}$, $\boldsymbol{z}_1 = \boldsymbol{0}$, $\boldsymbol{z}_2 = \boldsymbol{0}$ is UGAS for the control law (41), given that the system is as modelled in (1)-(9) and that the approximation of the thruster dynamics is accurate, which is indicated in Fig. 4.

In (41), we assume that the matrix $\boldsymbol{B}(\boldsymbol{\rho})$ is non-singular and hence invertible. This is not guaranteed in itself, since $\boldsymbol{B}(\boldsymbol{\rho})$ is singular if at least one of the following is true;

(a) $F = 0$,
(b) $\alpha = \pm\pi/2$,
(c) $\gamma = \pm\pi/2$.

However (a) is covered by Assumption 1, while (b) and (c) are considered by Assumption 2.

5. SIMULATION RESULTS

In this section, we present simulation results for the proposed control law in (41). In the simulations, the vessel GNC system inputs a set of waypoints with corresponding speed references, while a LOS guidance law with constant lookahead distance calculates the heading reference (Fossen et al., 2003). The speed and heading references are passed through second and third order reference filters, respectively, to get continuous acceleration and jerk references.

Simulation results are presented for a transit along a path as shown in Fig. 5, where the reference path from the waypoints is illustrated in red, and the path taken by the vessel with the proposed 3DOF controller is blue. The simulations are run with a constant disturbance in the NED frame, with a magnitude of 100 N in the direction

Table 1. Control parameters

Parameter	Value	Unit
$\boldsymbol{K}_T$	diag(1.78,2,2)	[s,s,s]
$\boldsymbol{K}_p$	diag(3,1,5)	[1/s,1/s,1/s]
$\boldsymbol{K}_d$	diag(1,1,1)	[kg/s,kg/s,kgm/s]
$\boldsymbol{K}_{z_2}$	diag(5,10,5)	[1/kg,1/kg,1/kgm]

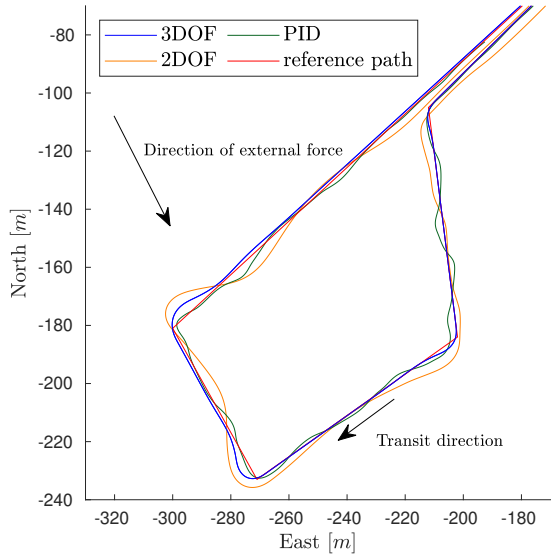

Fig. 5. Transit path from waypoints, and paths taken by the vessel. The direction of travel along the path, and direction of external forces are indicated by arrows.

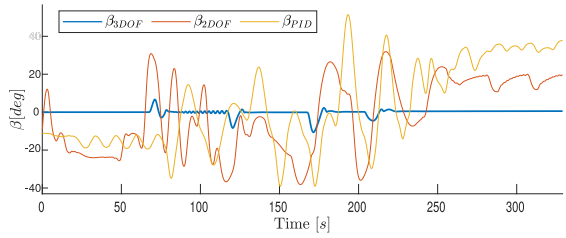

Fig. 6. Sideslip angle for the three controllers.

of the largest arrow in the figure. In addition to the results from the proposed controller, the transit path and sideslip angle from two other controllers are included for comparison:

- A 2DOF path-following controller designed through backstepping with thruster dynamics and thruster inputs F_d and α_d but not γ_d. The controller is augmented with an integrator on the course error to compensate for sideslip.
- A PID controller with velocity and acceleration feedforward, and the thrust allocation proposed by Torben et al. (2019).

The vessel path in Fig. 5 shows that the vessel tracks the reference path with satisfactory precision, where the cross-track error close to each waypoint is a consequence

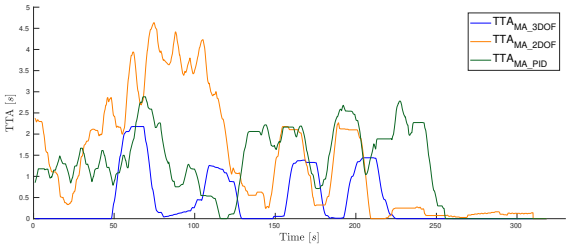

Fig. 7. Moving average over 20 s of time-to-actuation for the three controllers.

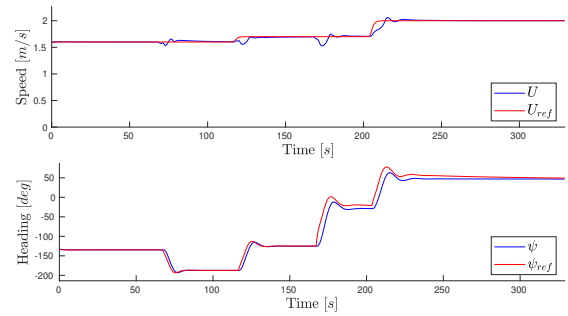

Fig. 8. Speed and heading, with references.

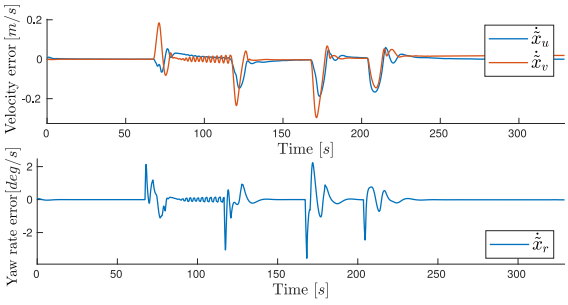

Fig. 9. Velocity error in surge and sway, and yaw rate error.

of the LOS guidance approach. From the figure, one can see that both the 2DOF controller and the PID controller track the path with comparable precision, but with more fluctuations about the reference path. This gives both high yawing and high sway velocities, as can be seen from the slip angle in Fig. 6, which, in turn, results in high derivatives in the actuator setpoints. The result of this is apparent from Fig. 7, where the TTA_{MA} is shown for the three controllers. High fluctuations in heading gives a high TTA, and hence high allocation error. This is most apparent for the 2DOF controller, where the heading is used to compensate for sway velocity, which is inefficient due to the lack of directional stability, and gives oscillations due to heading instability.

From Fig. 8, one can see that both the speed and heading reference is tracked with precision, where steady-state velocity errors resulting from external forces are compensated for by the integrator states in $\tilde{\boldsymbol{x}}$. From the graph of

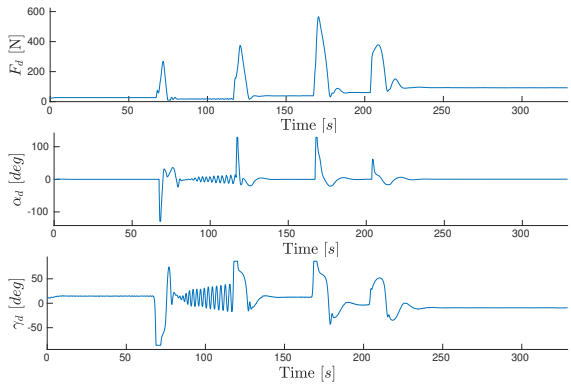

Fig. 10. Control inputs $\boldsymbol{\rho}_d$ for the 3DOF controller.

$\dot{\tilde{\boldsymbol{x}}}$ in Fig. 9, one can see that the sway velocity error is kept low, and hence the sway velocity close to its reference at 0 m/s during turning maneuvers. This keeps the sideslip angle β low, and thereby the destabilizing yaw moment low. This reduces the need for excessive actuator rate changes, which is apparent from Fig. 7, where the proposed 3DOF controller has the lowest TTA_{MA}.

On the second leg of the path, the vessel course is the most aligned with the direction of the external forces. This gives a low F_d due to the contribution of the external force to the surge velocity. In turn, this results in high α_d and γ_d control inputs to compensate for small tracking errors in yaw rate and sway velocity, respectively. These unstable tendencies are a result of Assumption 2 being challenged, and they demonstrate how the control allocation approach

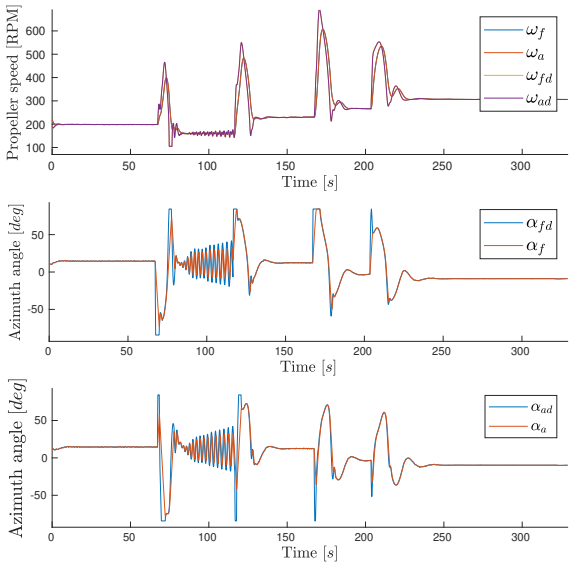

Fig. 11. Desired and actual thruster states. Due to the control allocation, ω_{fd} and ω_{ad} are superimposed.

can be restricted by the relationship between surge velocity and environmental forces.

From Fig. 11, one can see that the thruster angles α_{fd} and α_{ad} go into saturation during several of the turning maneuvers because the maneuver requires high actuation of both the sway and yaw mode simultaneously. This is another indication that Assumption 2 is being challenged, with a too small turning radius for the given surge velocity. This can be mitigated by increasing the lookahead distance, albeit at the cost of increased tracking error around the waypoints, or by a more suitable guidance method.

6. CONCLUSIONS AND FUTURE WORK

The development of a 3DOF path-following controller for a double-ended passenger ferry through a 3-step backstepping approach has been presented. The controller design is motivated by inherent issues with the physical properties of the ferry, where the lack of passive damping in sway is accounted for by active control of the sway velocity. This, in turn, reduces the effect of an inherent instability in yaw. A set of new thruster states is applied to reduce the actuator input space to be able to formulate the thrust allocation on closed form. Slow actuator dynamics are accounted for by including a simplified model of the actuator dynamics in the controller design, and thereby mitigating the erroneous assumption that the allocation error is sufficiently small to be neglected. The 3DOF controller is tested in numerical simulations, and compared to two other controllers. The proposed controller performs path following with satisfactory precision, and its performance is significantly better than the other controllers.

Future work include full-scale experiments and testing, in addition to further work on the thrust allocation to develop a hybrid system that can handle both low-speed docking and station-keeping operations as well as high-speed transit.

ACKNOWLEDGEMENTS

This work was supported by the NTNU Digital transformation project Autoferry and the Research Council of Norway through the Centres of Excellence funding scheme, project no. 223254.

REFERENCES

Eriksen, B.O.H. and Breivik, M. (2017). *Modeling, Identification and Control of High-Speed ASVs: Theory and Experiments*, 407–431. Springer International Publishing, Cham. doi:10.1007/978-3-319-55372-6_19. URL `https://doi.org/10.1007/978-3-319-55372-6_19`.

Fossen, T.I. (2011). *Handbook of Marine Craft Hydrodynamics and Motion Control*. John Wiley & Sons.

Fossen, T.I., Breivik, M., and Skjetne, R. (2003). Line-of-sight path following of underactuated marine craft. *IFAC Proceedings Volumes*, 36(21), 211 – 216. doi:https://doi.org/10.1016/S1474-6670(17)37809-6. 6th IFAC Conference on Manoeuvring and Control of Marine Craft (MCMC 2003), Girona, Spain, 17-19 September.

Johansen, T.A. and Fossen, T.I. (2013). Control allocation-A survey. *Automatica*, 49(5), 1087 – 1103. doi:https://doi.org/10.1016/j.automatica.2013.01.035.

Khalil, H.K. (2013). *Nonlinear Systems*. Pearson Education Limited.

Lefeber, E., Pettersen, K.Y., and Nijmeijer, H. (2003). Tracking control of an underactuated ship. *IEEE Transactions on Control Systems Technology*, 11(1), 52–61. doi:10.1109/TCST.2002.806465.

Pedersen, A.A. (2019). *Optimization Based System Identification for the milliAmpere Ferry*. Master's thesis, Norwegian University of Science and Technology (NTNU), Trondheim, Norway.

Pinkster, J. and Nienhuis, U. (1986). Dynamic Positioning of Large Tankers at Sea. In *Proc. 18th Annual Offshore Technology Conference*, 459–476. Houston, Texas.

Torben, T.R., Brodtkorb, A.H., and Sørensen, A.J. (2019). Control allocation for double-ended ferries with full-scale experimental results. *IFAC-PapersOnLine*, 52(21), 45–50. doi:https://doi.org/10.1016/j.ifacol.2019.12.281. 12th IFAC Conference on Control Applications in Marine Systems, Robotics, and Vehicles (CAMS 2019) , Daejeon, South Korea.

Paper D A domain-based and reactive COLAV method with a partially COLREGs-compliant domain for ASVs operating in confined waters

Published paper by E. H. Thyri and M. Breivik. "A domain-based and reactive COLAV method with a partially COLREGs-compliant domain for ASVs operating in confined waters". In: *Field Robotics* 2 (2022), pp. 632–677. DOI: https://doi.org/10.55417/fr.2022022.

Bibliography entry [26].

A domain-based and reactive COLAV method with a partially COLREGs-compliant domain for ASVs operating in confined waters

Emil Hjelseth Thyri and Morten Breivik
Centre for Autonomous Marine Operations and Systems (AMOS)
Department of Engineering Cybernetics
Norwegian University of Science and Technology (NTNU)
NO-7491 Trondheim, Norway.
emil.h.thyri@ntnu.no, morten.breivik@ieee.org

Abstract

This article presents a collision avoidance (COLAV) method for autonomous surface vessels operating in confined waters with other vessels, using a novel target ship (TS) domain. The domain is implemented as part of a reactive COLAV method pipeline through the use of control barrier functions (CBFs) to avoid domain violation. A geometric interpretation of a vessel-to-vessel encounter is used to classify the encounter type with respect to the COLREGs, and thereby which rules apply. Subsequently, a domain is assigned to the TS, where the domain parameters are rule-specific. In the domain design, the static environment is also considered, where an estimate for the available maneuverable space is calculated and applied when determining the size of each TS domain, in order to achieve a distance between vessels that is both safe and feasible for each encounter. Additionally, domains are assigned to static obstacles based on map data and lidar data. Once all domains for target ships and static obstacles are determined, CBFs are formulated based on the range to and velocity towards each domain. The set of CBFs are applied as inequality constraints in a quadratic program minimizing the vessel's thrust allocation error. The efficiency and completeness of the novel TS domain are demonstrated through an extensive simulation study. The COLAV method as a whole is demonstrated through both complex simulations with multiple maneuvering vessels, and full-scale experiments with a radar- and lidar-based target tracking system. The proposed COLAV method shows compliance with COLREGs section II.

1 Introduction

A majority of the world's large urban areas are located around waterways, where the water bore a majority of the transport for centuries until the construction of roads and railways along with the motorized land vehicles became the most efficient and cost effective means of transportation. After this shift from water to land, many of the cities left the waterways underutilized. The recent development in technology enabling autonomous maritime operations, has again made maritime transportation in urban waterways a competitive option, and several

Figure 1: The milliAmpere (blue in the middle), a prototype of an autonomous electric passenger ferry, during testing of multi-target tracking performance in a canal area in Trondheim in November 2020. Two other vessels (upper right relative to milliAmpere) are used as target ships. Courtesy of Mikael Sætereid.

cities have taken an interest in renewed utilization of their waterways. There already exist several initiatives on this with the goal of increasing efficiency and flexibility while reducing the strain on existing infrastructure both in cargo transport, (O'Dwyer, 2021), (Blenkey, 2021), and passenger transport (Cairns, 2021). By applying electric means of propulsion, benefits such as reduced cost, maintenance, air- and noise-pollution can also be achieved.

While the potential benefits are many, so are the challenges. Maneuvering in urban waterways is no trivial task for neither human nor machine, due to the long list of considerations such as traffic from commercial vessels and leisure-craft, risk of grounding, global and local rules of maneuvering and navigation, traffic regulations, weather and sea current. Not only do these aspects need to be considered in the autonomous planning, guidance, navigation and vessel control system, but the information itself needs to be acquired through situational awareness systems consisting of sensors and algorithms for interpretation and comprehension to produce reliable information that can be applied by the planners.

Due to the task complexity of autonomous maritime operations, and in particular the collision avoidance (COLAV) objective, autonomous guidance navigation and control (GNC) systems are often composed of multiple layers of planners in what is referred to as a hybrid structure. In such structures, the effectiveness of several planners can be exploited by distributing the planning responsibility to match each planner's capacity. An illustration of a three-layered structure is displayed in Fig. 2 along with several examples of situational awareness modules that one or more of the planners might apply.

The high-level COLAV module performs long-term or global path or trajectory planning with respect to e.g. map data from electronic nautical charts (ENC), weather and ocean current data, departure and arrival time, and traffic regulations such as allocated fairways or traffic separation schemes. The high-level planner can run once at the start of a transit or periodically with a long period between each iteration.

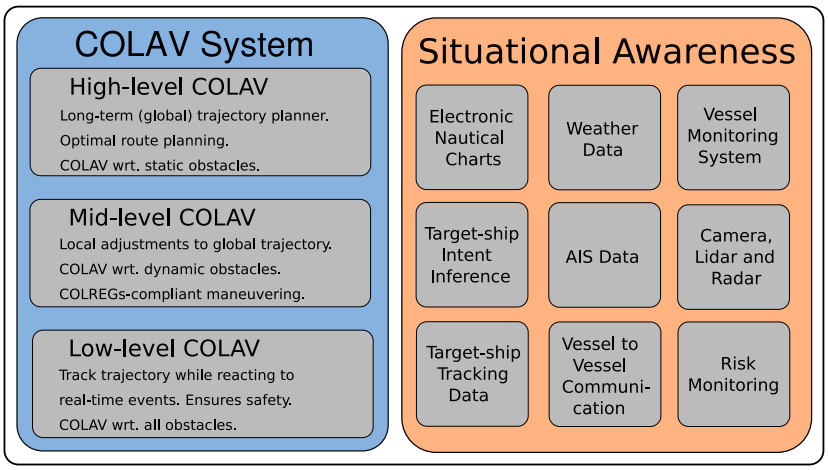

Figure 2: Example of a hybrid COLAV structure, where each of the modules in the COLAV system might apply one or more of the situational awareness modules.

The mid-level COLAV module considers COLREGs in vessel-to-vessel (V2V) encounters, and makes adjustments to the nominal path or trajectory from the high-level planner to comply with the relevant regulations. The planning can be performed based on target data from either AIS or a target tracking system based on exteroceptive sensors. The planning horizon of the mid-level COLAV can be from several seconds to several minutes, with planning period suitable for the rate of change of the relevant features in the environment.

The low-level COLAV module should have a short planning horizon relative to the dynamics of the operational environment, and for several applications, it can be purely reactive, where it reacts to current states without deliberation. The task of the low-level planner is to resolve immediate situations in a safe manner. For autonomous surface vessels (ASVs), that is mainly avoiding collision with all obstacles, both static and dynamic, while adhering to the relevant protocol.

The benefit of a hybrid approach is demonstrated in (Loe, 2008), (Svec et al., 2013) and (Eriksen et al., 2020), where the latter article is an excellent example of a three layer structure where the top-layer performs energy optimized path planning, the mid-level handles long-term COLAV regarding static and dynamic obstacles while enforcing parts of the relevant protocol, and the lowest level handles reactive COLAV and emergency situations. A noteworthy feature in the hybrid structure proposed in (Eriksen et al., 2020), is that the mid-level algorithm disregards dynamic obstacles with a distance at closest point of approach (DCPA) and time at closest point of approach (TCPA) below some threshold-value, since its run period and horizon makes it unsuited for considering those obstacles in the planner This leaves the low-level COLAV algorithm to resolve the immediate situations. This is particularly relevant in highly dynamic environments where the obstacle behaviour is changing at periods equal to or smaller than the available planning periods, and the plan from a higher level planner might be outdated before a new and updated plan is produced. This applies in particular in urban maritime environments, where the field of view can be restricted by both static and dynamic obstacles, and variety of vessels and vessel operators make the traffic unpredictable. The lack of AIS equipment on smaller vessels restricts the detection range to the field of view of the vessel's exteroceptive sensor system, often composed of radar, lidar and camera combinations, which reduces the effectiveness of the long-terms planners. A complete and safe low-level COLAV is

therefore paramount for operation in such environments. A suitable low-level COLAV module can ensure the baseline safety of the whole hybrid collision-avoidance structure by resolving close-range encounters in a satisfactory and safe manner, every time.

The contribution of this paper is a reactive COLAV system for ASVs, suitable for the lowest level in a hybrid structure like the one in Fig. 2. The method is designed for operation in confined waters where traffic is unpredictable and detection is limited by the field of view. However, it also performs well in open waters where the presence of leisure vessels makes predictions on future TS behaviour uncertain. The method handles static and dynamic obstacles, where considerations on relevant parts of the COLREGs are included, in particular compliance with Rules 13-15 and partial fulfillment of Rules 8 and 17, regarding vessels in sight of one another. The main novelty of this work is the target ship (TS) domain design, where a rule-based approach is applied to assign a domain to each of the tracked dynamic obstacles, and the COLREGs considerations are encoded in the qualities of the domain. Additionally, a metric for the available maneuverable space is included in the dimensioning of the TS domain to ensure that the DCPA is adjusted to suit each individual encounter. The domain design is simple and intuitive, and is encoded by a small set of parameters for each of the relevant rules in the COLREGs. Additionally, similar domains are assigned to relevant static obstacles. Once a domain is assigned, a safe set is defined as a function of the range to, and relative velocity towards each TS domain and static obstacle domain. Lastly, a control barrier function (CBF) is formulated for each domain. The CBFs are applied as inequality constraints in an optimization problem that minimizes the error between a virtual control from the trajectory tracking control system, and a virtual control that ensures forward invariance of the safe set. The proposed TS domain is demonstrated through an extensive set of simulations, while the method as a whole is demonstrated through both simulations and full-scale experiments in a relevant environment, with a radar and lidar-based target tracking system, and a combination of lidar and map data for COLAV with static obstacles.

The remainder of this paper is structured as follows: Section 2 provides a review of relevant previous work. Section 3 presents theory on COLREGs and CBFs. In Section 4, we present the considerations that go into the TS domain design, and define the domain. Section 5 shortly describes how the domain for static obstacles is constructed. In Section 6, we formulate the CBFs that ensure that the domains for static and dynamic obstacles are not violated. Section 7 and Section 8 present the simulation and experimental results, respectively, before Section 9 finally concludes the paper.

2 Previous work

This section reviews previous work on COLAV for ASVs. We focus the review in particular on work directed towards confined waters operations with high traffic, and work with an experimental contribution. For a more substantial review of COLAV algorithms, the reader is advised to consult the following recent survey papers on the field; (Vagale et al., 2021b) for a review of the field of path planning and COLAV for ASVs, (Vagale et al., 2021a) for a comparative study of existing COLAV algorithms, and (Huang et al., 2020) for a structured breakdown of the techniques that go into maritime COLAV, and a discussion of state-of-the-art approaches to each subproblem of maritime COLAV.

In (Benjamin et al., 2006), perhaps the first demonstration of an autonomous partial protocol compliant COLAV system tested on a marine platform is presented. The proposed method calculates a utility for a set of candidate legs for an ASV trajectory, parameterized by course, speed and duration from the current state, and realizes the highest utility maneuver. The base utility for each leg is a measure of its contribution to progress towards the mission goal position. Inclusion of COLAV is encoded by a reduction in utility based on the estimated closest point of

approach (CPA) for that leg. COLREGs considerations for rules 14-16 as well as parts of Rule 8, are included by further reduction in utility for non-readily apparent maneuvers, maneuvers that pass in front of crossing vessels and starboard to starboard in head-on encounters. The method is demonstrated through experiments with two kayak-based ASVs, with shared GPS position for target tracking. The method is only tested in V2V encounters, and does not make any considerations for static obstacles.

In (Schuster et al., 2014), a method for target tracking is presented, where data from a low-cost radar is applied. The method is intended for smaller vessels, and considers a use-case with leisure vessels maneuvering on an inland lake. In the paper, a grid-based graph-search method is applied for finding the shortest-path collision-free trajectory at constant speed. The method applies the TS domain proposed in (Goodwin, 1975), where three circle sectors of varying radial extension are assigned to the TS's starboard forward side, port forward side, and aft of the TS, with the longest radial extension on the starboard forward side, and the shortest radial extension at the aft. The domain makes the trajectory planner favour maneuvering to pass port to port in head-on encounters, and behind the TS in crossing encounters. The paper presents a full-scale experiment, where two leisure vessels of approximately 6 meters in length meet in a crossing encounter. However, since no classification of an encounter is made, and the TS domain is the same for all encounters, the method has no distinction between stand-on or give-way encounters.

In (Kuwata et al., 2014), a version of the velocity obstacle (VO) algorithm assigns a domain to the TS that includes both the extension of the ownship (OS), which is the vessel that is controlled, and the TS. The method also accounts for uncertainty in the velocity estimate of the TS when computing the velocity obstacle. The authors have encoded rules 14-15 of the COLREGs directly into the velocity space by considering at what side of the TS the OS should pass. Detected hazards with a speed below a certain threshold are treated as stationary hazards where no rules apply. The method is demonstrated through full-scale experiments in scenarios with up to three target ships, where a radar and stereo cameras are applied as perceptive sensors for target tracking.

Further protocol considerations are included in the VO algorithm in (Woerner, 2016), by designing explicit metrics for protocol compliance with each of the relevant rules, which are used in cost calculations for each velocity pair. The proposed method shows good performance and protocol compliance with the relevant COLREGs parts. The algorithm is demonstrated through extensive simulation, where a proposed automatic evaluation scheme shows clear distinction between the algorithm with and without COLREGs considerations. The work also includes an extensive experimental effort with up to 5 vessels in multi-agent scenarios. In the experiments, the GPS position of each vessel were transmitted to all vessels for target tracking.

In (Eriksen et al., 2019) and (Eriksen and Breivik, 2019) a graph-based COLAV algorithm for high-speed ASVs, named the branching-course model predictive control algorithm, which considers both static and dynamic obstacles, is presented. The algorithm simulates combinations of a finite set of course and speed change maneuvers in succession, to get a set of trajectories candidates from the current position. The proposed method handles protocol compliance by assigning cost to each trajectory candidate based on its intersection with a TS domain, where the domain is elliptical-like with increasing cost towards the center, and the TS shifted towards the port and back side of the domain to favour maneuvers that pass behind or on the port side of the TS. This motivates trajectories that comply with Rules 13-15. The algorithm is demonstrated through full-scale experiments with a high-speed ASV and one TS, where a radar-based target-tracking system is applied. An effort is also made to make the algorithm robust to noise from the target tracking system by applying a cost on transition from the current trajectory, and hence reducing the risk of alternating between several trajectories.

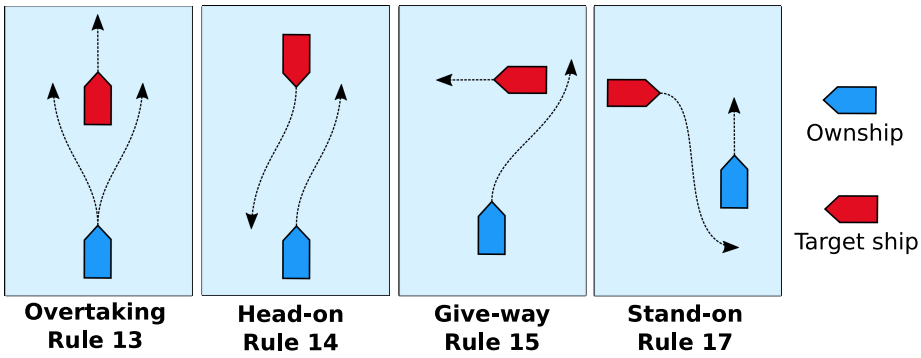

Figure 3: Illustration of COLREGs rules 13-15 and 17, as seen from the OS in blue.

In (Shah et al., 2016), explicit steps are taken towards handling the problem of high traffic, where the authors present a lattice-based risk and contingency-aware planner for congested waters with high traffic. In the approach, the common assumptions of constant TS behaviour is mitigated by predicting protocol compliant trajectories for each TS, and applying it in the search for feasible trajectories. The method is demonstrated through simulations with up to three target ships, and compared to a variation of the VO described in (Kuwata et al., 2014), where it achieves a reduced number of collisions.

The mentioned methods do all consider COLAV with respect to both static and moving obstacles with some regard to COLREGs. However, very few of the existing methods consider explicitly COLAV in confined waters, where the presence of static obstacles need to be taken into account when considering maneuvers wrt. dynamic obstacles. In particular, acceptable distance at CPA, which will vary greatly with the available maneuverable space, needs to be taken into account in the domain design when applying strict TS domains, to ensure feasibility in confined spaces, and safety in more open waters.

3 Background theory

This section introduces background theory for the reactive COLAV method that will be presented in the next sections. First an introduction to the relevant paragraphs in the COLREGs is given, and subsequently we introduce the vessel model that we consider. Lastly we provide background theory on CBFs and how they effortlessly can be applied as inequality constraints to a quadratic optimization problem.

3.1 COLREGs - The rules of the road

The COLREGs is the result of a convention developed over several decades to prevent collision between two or more vessels at sea, which in 1972 was revised and given its current name. The convention is continuously tested and revised to be unambiguous as new technology and maritime applications occur. The COLREGs apply to all vessels upon the high seas and all waters connected to the high seas and navigable by seagoing vessels.

The convention has four main parts: Part A - General, Part B - Steering and Sailing, Part C - Lights and Shapes and Part D - Sound and Light signals. In the work presented here, we focus on maneuvering of an ASV in the presence of other vessels, and hence it is the rules in Part B, regarding vessels in sight of one another that are most relevant. Here follows a short

description of the rules we consider, while Fig. 3 provides illustrations of situations where rules apply, as seen from the OS in blue in a V2V encounter with a TS in red. A more comprehensive description of the rules can be found in (Cockcroft and Lameijer, 2012).

- **Rule 8** *Any action to avoid collision shall, if circumstances of the case admit, be positive, made in ample time, and with due regard to good seamanship.*
- **Rule 13** *Any vessel overtaking another vessel shall keep out of the way of the vessel being overtaken. A vessel approaching another vessel from a direction of more than* $22.5\,\mathrm{deg}$ *abaft her beam is an overtaking vessel. Any subsequent alternation of bearing between the two vessels shall not relieve the overtaking vessel of the duty of keeping clear of the overtaken vessel until she is finally past and clear.*
- **Rule 14** *When two power-driven vessels are meeting on reciprocal or nearly reciprocal courses so as to involve risk of collision each shall alter her course to starboard so that each shall pass on the port side of the other.*
- **Rule 15** *When two power-driven vessels are crossing so as to involve risk of collision, the vessel which has the other on her own starboard side shall keep out of the way and shall, if the circumstances of the case admit, avoid crossing ahead of the other vessel.*
- **Rule 16** *Every vessel which is directed to keep out of the way of another vessel shall, so far as possible, take early and substantial action to keep well clear.*
- **Rule 17** *Where one of two vessels is to keep out of the way, the other shall keep her course and speed. The latter vessel may take action to prevent collision if it is apparent that the vessel required to keep out of the way is not taking appropriate action.*

3.2 Control barrier functions

CBFs have in recent years emerged as the safety equivalent to what control Lyapunov functions (CLFs) are for stability (Ames et al., 2019). CBFs are used for set-based control to ensure forward invariance for some set $\mathcal{C}$. The set $\mathcal{C}$ can then be designed for the operational task at hand to be a safe set.

In this paper, we consider nonlinear control affine systems on the form

$$\dot{\boldsymbol{x}} = \boldsymbol{f}(\boldsymbol{x}) + \boldsymbol{g}(\boldsymbol{x})\boldsymbol{u}, \quad \boldsymbol{x}(0) = \boldsymbol{x}_0, \tag{1}$$

where $\boldsymbol{f} : \mathbb{R}^n \to \mathbb{R}^n$ and $\boldsymbol{g} : \mathbb{R}^n \to \mathbb{R}^m$ are locally Lipschitz, $\boldsymbol{x} \in D \in \mathbb{R}^n$ contains the states of the system and $\boldsymbol{u} \in U \in \mathbb{R}^m$ is the control input. Such systems describe a variety of field robotic systems in air, on land and at sea, and have the same form as the 3DOF model in (Fossen, 2011), commonly used for ASVs. Further, we assume a set $\mathcal{C}$, that is safe regarding the system task. This set is said to be forward invariant with respect to (1) if for a given solution to (1), $\boldsymbol{x} : [0, t_1] \to \mathbb{R}^n$,

$$\boldsymbol{x}(0) \in \mathcal{C} \implies \boldsymbol{x}(t) \in \mathcal{C}, \quad \forall t \in [0, t_1]. \tag{2}$$

A CBF is a continuously differentiable function $h \colon \mathbb{R}^n \to \mathbb{R}$, where the safe set $\mathcal{C}$ is defined as a super-zero level set to $h(\boldsymbol{x})$, that is,

$$\begin{aligned} \mathcal{C} &= \{\boldsymbol{x} \in \mathbb{R}^n : h(\boldsymbol{x}) \geq 0\}, \\ \partial\mathcal{C} &= \{\boldsymbol{x} \in \mathbb{R}^n : h(\boldsymbol{x}) = 0\}, \\ \mathrm{Int}(\mathcal{C}) &= \{\boldsymbol{x} \in \mathbb{R}^n : h(\boldsymbol{x}) > 0\}, \end{aligned} \tag{3}$$

where $\text{Int}(\mathcal{C})$ is the interior of $\mathcal{C}$. Ensuring invariance of $\mathcal{C}$ implies that $h(\boldsymbol{x}) \geq 0$ along the trajectories of (1). Positivity of $h(\boldsymbol{x})$ can be shown if

$$\dot{h}(\boldsymbol{x}(t)) = \frac{\partial h}{\partial \boldsymbol{x}} \left(f(\boldsymbol{x}) + g(\boldsymbol{x})\boldsymbol{u}(\boldsymbol{x}) \right) \geq -\gamma \left(h(\boldsymbol{x}(t)) \right), \tag{4}$$

for some extended class-κ function $\gamma : \mathbb{R} \to \mathbb{R}$. If there exists a continuous function $\boldsymbol{u} : \mathbb{R}^n \to \mathbb{R}^m$ such that (4) is satisfied, then $h(\boldsymbol{x})$ is a valid CBF for the system in (1).

CBFs on the form of (4) can be applied as inequality constraints to an optimization based control allocation such as

$$\boldsymbol{u}^* = \arg\min_{\boldsymbol{u}} \quad \frac{1}{2} \|\boldsymbol{u} - \boldsymbol{k}(\boldsymbol{x})\|^2, \tag{5}$$

minimizing the allocation error between a nominal control input $\boldsymbol{k}(\boldsymbol{x})$, and a control input that adhere to the constraints. The nominal control input $\boldsymbol{k}(\boldsymbol{x})$ can be provided by an arbitrary controller that is suitable for the control objective.

4 Target ship domain design

This section presents the main contribution of this work, namely the TS domain design. The proposed TS domain is rule-based, in the way that the parameters that define the domain are chosen from a set based on a geometric classification of the encounters that determine which of the rules 13-15 or 17 apply. The section starts by introducing the method for encounter classification in Section 4.1. Subsequently, in Section 4.2, we propose a measure for the available maneuverable space for the OS when passing a TS, which is used in determining the extension of the TS domain. In Section 4.3, the criteria for passing with the TS on the port or starboard side are formulated. Lastly, in Section 4.4, the TS domain is formulated.

4.1 Encounter classification

In this paper, encounter classification means the process of determining the encounter type from the viewpoint of the OS in a V2V encounter, and thereby which of the COLREGs rules the OS should abide by. There are several methods for such classification, where most of them deem the OS to be in one of the following encounters, where the corresponding rules apply.

- Overtaking (OT): **Rule 13**.
- Head-on (HO): **Rule 14**.
- Give-way (GW): **Rule 15**.
- Stand-on (SO): **Rule 17**.
- Safe (SF): No rules apply.

The author of (Woerner, 2016) describes an algorithm for encounter classification based on the relative bearing of the OS from the TS as well as the relative bearing of the TS from the OS, where numerical values from the COLREGs are applied as entry criteria. In (Tam and Bucknall, 2010) another method for classification based on the encounter geometry is described. The method is a two-step process. In the first step, the relative bearing sector (RBS)[1] is determined based on the relative bearing of the TS from the OS,

$$\varphi = \text{atan}\,2((E_{TS} - E), (N_{TS} - N)) - \chi, \tag{6}$$

[1]The RBS are denoted R1 to R6 in (Tam and Bucknall, 2010)

and a set of sector angles that divide a circle into six sectors, where the OS is at the center of the circle. Here, χ is the course of the OS, while N and E, and N_{TS} and E_{TS} are the north and east position of the OS and TS, respectively. The RBS is chosen based on which sector φ lies within. In the second step, the course of the TS relative to the OS,

$$\chi_{rel} = \chi_{TS} - \chi, \tag{7}$$

is applied, along with the same set of sector angles, to determine the situation sector (SS)[2], and hence the encounter classification.

This method is intuitive and easy to follow, as it has a visual geometric interpretation. In (Eriksen et al., 2020), this classification method is augmented by the use of the relative velocity between the OS and the TS to deem some OT, GW and SO encounters safe when the range between the vessels is increasing. In addition, a state machine is applied to hold any classification other than SF until the encounter is once again classified as safe. This ensures that the latter part of **Rule 13** is overheld, which states that a give-way vessel needs to be past and clear to be relieved of its give-way duty. In (Thyri et al., 2020a), a further addition to the classification is introduced with distinction on whether an overtaking should be conducted with the TS on the port or starboard side, denoted OT_s and OT_p respectively. The distinction is based on χ_{rel}, choosing OT_p for $\chi_{rel} \geq 0$ and OT_s for $\chi_{rel} < 0$, and facilitates crossing behind the TS in close-quarter overtaking encounters.

However, this classification method has a flaw that results in wrongful classifications in several V2V encounter geometries. The error originates from the use of χ_{rel} in the second step of the classification, while applying the same set of sector angles as was used in the first step. The relative heading between the vessels relates somewhat, but not accurately, to the criteria for encounter classification in COLREGs, as it is the visual reading of the lights of the vessels by night, or "the corresponding aspect of the other vessel" by day that is the wording of the protocol.

In this paper, we therefore apply a classification method that is very similar to the method presented in (Tam and Bucknall, 2010), where we have improved on the shortcomings so that the classification is correct, with respect to COLREGs, for all V2V geometries. A graphical representation of the method is given in Fig. 4. In the first step, the RBS is determined based on φ and the sector angles $[-\theta_2, -\theta_1, \theta_1, \theta_2]$ in the same way as for the original method, however, with a reduced set of sector angles. This will put the TS in one of the four RBS: R1, R2, R3 or R4. Subsequently, the SS is determined by χ_{rel}, with a set of rotated sector angles $[-\theta_2^{'}, -\theta_1^{'}, \theta_1^{'}, \theta_2^{'}]$, where $\theta_1^{'} = \theta_1 - \varphi_{TS}$ and $\theta_2^{'} = \theta_2 - \varphi_{TS}$, and

$$\varphi_{TS} = \operatorname{atan2}((E - E_{TS}), (N - N_{TS})), \tag{8}$$

is the bearing of the OS from the TS. Figure 5 shows how the graphical geometric representation of the method can be used to classify an encounter. In the figure, the OS is at the center, and each TS has its own shifted situation sector circle. The classification is done visually by choosing the sector which the course vector of the TS lies in. We also include a state machine as proposed in (Eriksen et al., 2020), where a classification is held static if the range between the vessels is below some threshold.

4.2 Maneuverable space

Close quarters, risk of collision, ample time, and close proximity are all relative terms. Yet they are applied in the COLREGs formulation of how and when vessels in sight of one another are obliged to maneuver. As one can imagine, quantitative interpretation of these terms are

[2]The SS are denoted TSR1 to TSR6 in (Tam and Bucknall, 2010)

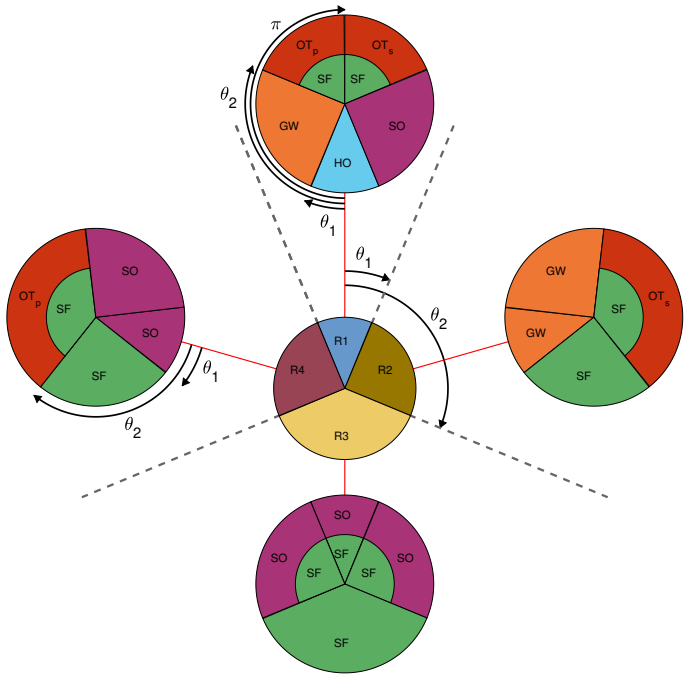

Figure 4: Graphic representation of the classification algorithm, where the position of the OS is at the center of the middle circle. In situation sectors with two encounter classifications, the outer one is chosen when the involved vessels have a closing range, while the inner one is chosen for increasing range.

very much dependent on the individual situation, and in particular the surroundings. For two vessels moving in confined waters, e.g. a harbour, canal or an area where the vessel draft is restricting maneuverability, passing at 30, 20 or even 10 meters can be considered acceptable, while doing this at open waters would be considered misconduct, and in violation with the practice of good seamanship and the COLREGs. For vessels moving in confined waters, the accepted DCPA is therefore highly dependent on the available maneuverable space, and it is paramount that this should be considered when determining the shortest allowable DCPA in an encounter.

We propose the use of an adaptive measure, r_{free}, for the available maneuverable space for an encounter, which we later will use in determining the size l of the TS domain. When calculating r_{free} for a V2V encounter, first, the pass sector, the sector around the TS where the OS should pass, is determined. Subsequently, the shortest distance from the TS to any static obstacle in the pass sector is found. The pass sector is given by the encounter classification. We denote the pass sector by two angles, $\Xi \in [-\pi, \pi]$ and $\delta_\Xi \in [-\pi, \pi]$, where the pass sector is the sector swiped by a line starting in p_{TS} and swiping the sector $[\Xi - \delta_\Xi, \Xi + \delta_\Xi]$. Fig. 6 shows the pass sector in blue for a TS located at p_{TS}. The minimum range to a static obstacle within the pass sector, r_{min} is indicated by the red dashed line. The free range is given by

$$r_{free} = r_{min} - r_{dyn} - r_{stat}, \tag{9}$$

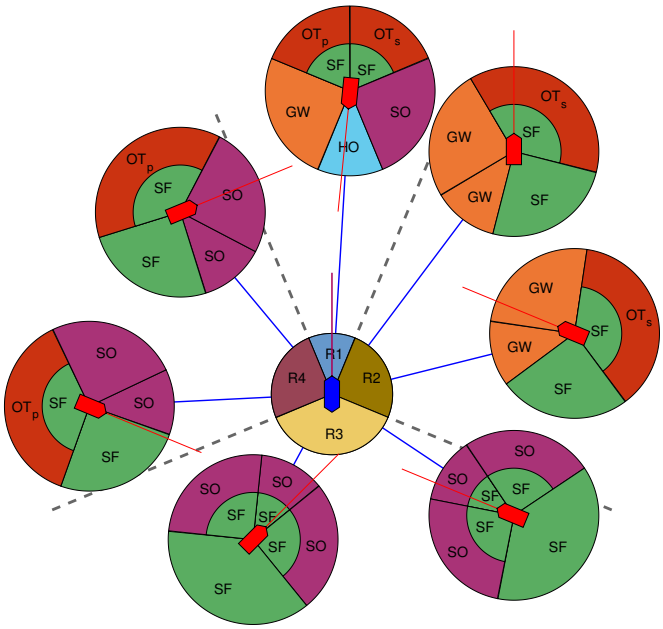

Figure 5: Classification examples for an arbitrary set of target ships (red), and the blue OS. Classification is made by selecting the encounter type of the sector that the TS course vector lies within.

where

$$r_{dyn} = \frac{1}{2}(l_{OS} + l_{TS}) + \delta_{dyn}, \tag{10}$$

is the minimum DCPA to a dynamic obstacle at which no collision will occur, and

$$r_{stat} = \frac{1}{2}l_{OS} + \delta_{stat}, \tag{11}$$

is the minimum distance to a static obstacle at which no collision will occur. Here, l_{OS} and l_{TS} are the lengths of the OS and TS, respectively. The distances δ_{dyn} and δ_{stat} are additional tolerances to dynamic and static obstacles, respectively. The tolerance should account for uncertainties in map data, target tracking and navigation. Calculating r_{free} requires a-priori knowledge of the area in the form of map data, which is a fair assumption to have for most ASV operations, in which map data would also be required for long-term path or trajectory planning. Such data is often readily available from online map services, as is the case for the map data used in the experiments in this paper[3] (Kartverket, 2020).

4.3 Passing on port or starboard

In a V2V encounter where risk of collision exist, at least one vessel is obliged by the COLREGs to take action to avoid collision. The maneuvering guidelines are in large focused on what is the preferred side of the OS the TS should be when passing. For most encounters, if the circumstances admit, it is the port side, except for overtaking encounters, where the maneuvering choice is dependent on other factors. At the same time, some close quarters encounters can

[3]Adjustments were made to the original map data to better represent floating docks and docked vessels.

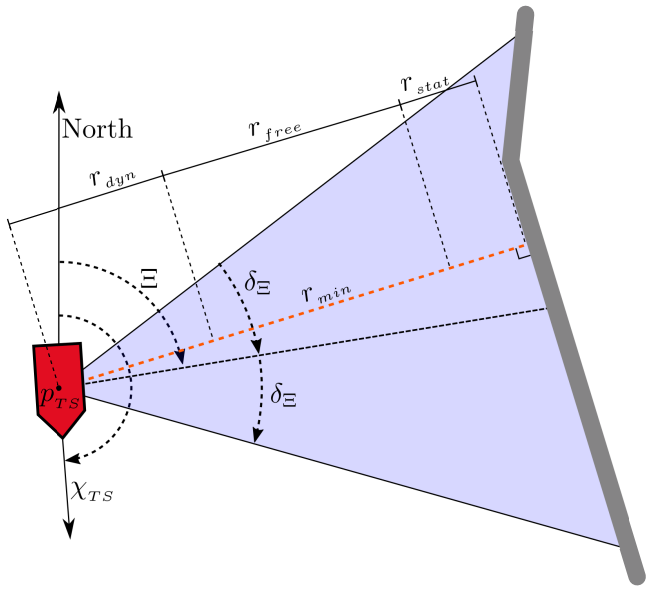

Figure 6: Illustration of a pass sector (blue) for a TS located at p_{TS} with an arbitrary static obstacle illustrated by the thick grey line. The minimum free range of the pass sector, $r_{min} \geq 0$, is indicated by the dashed red line. The distances $r_{dyn} \geq 0$ and $r_{stat} \geq 0$ are the minimum ranges that are considered not to be a collision with a dynamic obstacle or static obstacle respectively.

be resolved by passing with the TS on the starboard side with little or no maneuvering effort, where passing with the TS on the port side would require extensive maneuvering effort, either due to the encounter geometry or the velocity of the vessels. We therefore propose a method of distinction on what side to pass the TS that considers these factors through the encounter classification, the geometry of the encounter, and the relative velocity vector between the two vessels,

$$\boldsymbol{U}_{rel} = \boldsymbol{U}_{TS} - \boldsymbol{U}_{OS}, \tag{12}$$

where $\boldsymbol{U}_{OS} \in \mathbb{R}^2$ and $\boldsymbol{U}_{TS} \in \mathbb{R}^2$ are the north-east velocity vectors of the OS and TS, respectively. The distinction is made based on the bearing of the OS from the TS relative to the port-starboard split angle

$$\alpha_s = \alpha_{U\_rel} + \alpha_{\delta\_s}, \tag{13}$$

where

$$\alpha_{U\_rel} = \operatorname{atan2}(U_{E\_rel}, U_{N\_rel}), \tag{14}$$

is the angle of the relative velocity vector relative to north, with U_{N_rel} and U_{E_rel} as the north and east component of $\boldsymbol{U}_{rel}$, respectively. The bias $\alpha_{\delta\_s} \in [-\pi/2, \pi/2]$ is a classification specific offset that will facilitate protocol compliant maneuvers. Maneuvering to the port, to pass with the TS on the OS starboard side is preferred if $\varphi_{TS} > \alpha_s$ and maneuvering to the starboard to pass with the TS on the OS port side is preferred if $\varphi_{TS} \leq \alpha_s$.

Since the α_{U_rel} is undefined when the relative velocity is zero, and is prone to noise from both target tracking and navigation when the relative velocity is low, a weighted average between the α_{U_rel} and φ_{TS} is applied when $\|U_{rel}\| < U_{lim}$. That is

$$\alpha_s = \begin{cases} \alpha_{U\_rel} + \alpha_{\delta\_s}, & \text{if } \|U_{rel}\| \geq U_{lim} \\ \frac{\|U_{rel}\|}{U_{lim}} \alpha_{U\_rel} + (1 - \frac{\|U_{rel}\|}{U_{lim}}) \varphi_{TS} + \alpha_{\delta\_s}, & \text{if } \|U_{rel}\| < U_{lim}. \end{cases} \tag{15}$$

In addition to the broad considerations in this distinction, the α_s angle also reduces the chance of oscillating behaviour that can result from noise or uncertainty in the position and velocity estimates for the OS and TS when the φ_{TS} is close to α_s, since the absolute difference $|\alpha_s - \varphi_{TS}|$ will increase once a maneuver is initiated due to the resulting changes in the relative velocity vector, effectively increasing the commitment to the maneuver. The same is true for maneuvers by the TS.

4.4 Target ship domain definition

Once the encounter is classified, the available maneuverable space is estimated, and at what side of the TS the OS should pass is determined, a domain can finally be assigned to the TS. The TS domain that we propose is a straight line dividing the north-east plane into two halves. The half plane containing the TS is the TS domain. The domain is defined by the position of the TS, and two variables:

- $l \geq r_{dyn}$ is the shortest distance from the TS to the line defining the domain,
- $\alpha \in [-\pi, \pi]$ is the angle of the normal vector to the domain, pointing away from the TS.

The TS domain is considered as an unsafe set, denoted $\mathcal{C}_{u\_dyn\_i}$ for TS i, where $i \in [1, N_{TS}]$ and N_{TS} is the number of tracked target ships. We will later use $\mathcal{C}_{u\_dyn\_i}$ to define the safe set $\mathcal{C}$. In the choice of l, the available maneuverable space is considered, where we choose

$$l = \begin{cases} r_{dyn} & \text{if } r_{free} <= 0, \\ r_{dyn} + k_l r_{free} & \text{if } r_{free} < r_{free\_max}, \\ r_{dyn} + k_l r_{free\_max} & \text{if } r_{free} >= r_{free\_max}, \end{cases} \tag{16}$$

where $k_l \in [0, 1]$ is a design parameter that splits the free maneuverable space between the TS and a potential static obstacle. The angle of the normal vector is defined as

$$\alpha := \alpha_s + \alpha_D \tag{17}$$

where

$$\alpha_D = \begin{cases} \varphi_{TS} - \alpha_s + \alpha_d, & \text{if } \varphi_{TS} > \alpha_s, \\ \varphi_{TS} - \alpha_s - \alpha_d, & \text{else.} \end{cases} \tag{18}$$

Here $\alpha_d \in (-\pi/2, \pi/2)$ is the deflection angle, a classification specific parameter. This angle is used to alter the deflection of the OS on the TS domain to both avoid stagnation when the OS is approaching the TS at a near right angle, and to facilitate passing the TS with a geometry that comply with the relevant rule. The reason we go through α_D when calculating α is that saturation is applied to this variable so that $\alpha_D \in [\alpha_{D\_min}, \alpha_{D\_max}]$. The rationale behind this saturation will be discussed shortly.

Lastly, we define two points on the TS domain, namely, $\boldsymbol{p}_D$, the point on the domain closest to the TS

$$\boldsymbol{p}_D = \boldsymbol{p}_{TS} + \begin{bmatrix} \cos(\alpha) \\ \sin(\alpha) \end{bmatrix} l, \tag{19}$$

and $\boldsymbol{p}_B$, the point on the domain closest to the OS

$$\boldsymbol{p}_B := \boldsymbol{p}_D + (\boldsymbol{p} - \boldsymbol{p}_D)^\mathsf{T} \boldsymbol{n}_{p_D} \boldsymbol{n}_{p_D}, \tag{20}$$

where

$$\boldsymbol{n}_{p_D} = \begin{bmatrix} \cos\left(\alpha + \frac{\pi}{2}\right) \\ \sin\left(\alpha + \frac{\pi}{2}\right) \end{bmatrix}, \tag{21}$$

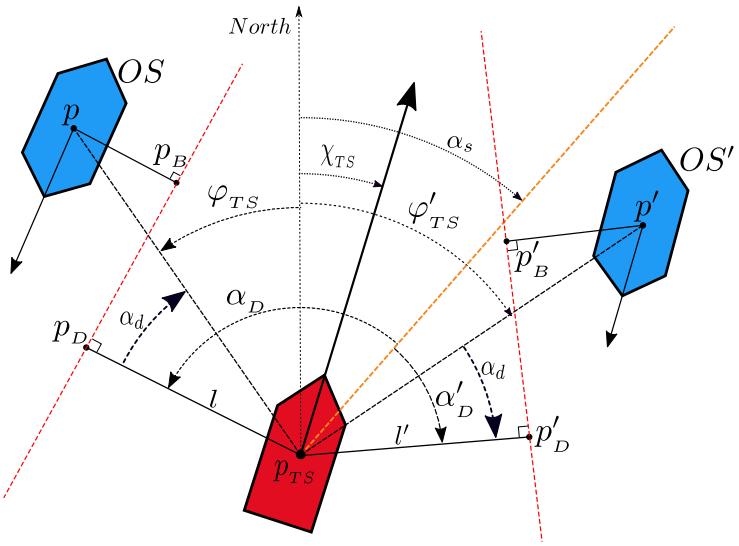

Figure 7: Parameters for the TS domain for a red TS located at $\boldsymbol{p}_{TS}$ with course χ_{TS}, and two instances of the OS, namely OS and OS', located at p and p' at either side of the orange port-starboard split line defined by α_s, with bearing from the TS φ_{TS} and φ'_{TS} respectively. The TS domain is given by the red dashed line passing through $\boldsymbol{p}_D$ and $\boldsymbol{p}'_D$ at a distance $l > r_{dyn}$ from the center of the TS. The point $\boldsymbol{p}_B$ and $\boldsymbol{p}'_B$ are the closest point on the TS domain to the OS and OS' respectively. All angles are positive in the clockwise direction.

is the tangent unit vector to the TS domain. An illustration of the TS domain is given in Fig. 7 for two instances of the ownship, denoted OS and OS', one located on each side of the port-starboard split angle α_s.

Figure 8 shows a grid with normal vectors to the TS domain for an OS located at the base of each normal vector. The port-starboard split angle α_s is indicated by an orange line. The effect of the deflection angle α_d is apparent from the vector field close to the orange line, where it will cause the OS to deflect to one or the other side.

The effect of the saturation of α_D is also apparent from the unidirectional vector-field in the top right and top left parts of the overtaking, head-on and give-way vector fields. The saturation limits on α_D are applied to ensure that the OS maintains a give-way maneuver until it is finally past and clear, in particular to prevent the OS from moving into the path of the TS at close range after an overtaking maneuver. Additionally, the use of a high deflection angle α_d, in combination with effective saturation limits on α_D, we can achieve an extended effective TS domain in desired directions. This is apparent from Fig. 8, where the TS domain extends aft of the TS in overtaking encounters, in front of the TS in head-on encounters and to the front and either side of the TS in give-way crossing encounters, without ineffective extensions of the TS domain that only contribute to restricting the maneuverable space. The TS domain that we propose is in line with choosing a TS domain in such a way that when contouring, the OS behaves in accordance with protocol.

The safe set regarding all dynamic obstacles is defined as the complement set of the sum of the unsafe sets. That is

$$\mathcal{C}_{dyn} = \mathcal{C}^c_{u\_dyn}, \tag{22}$$

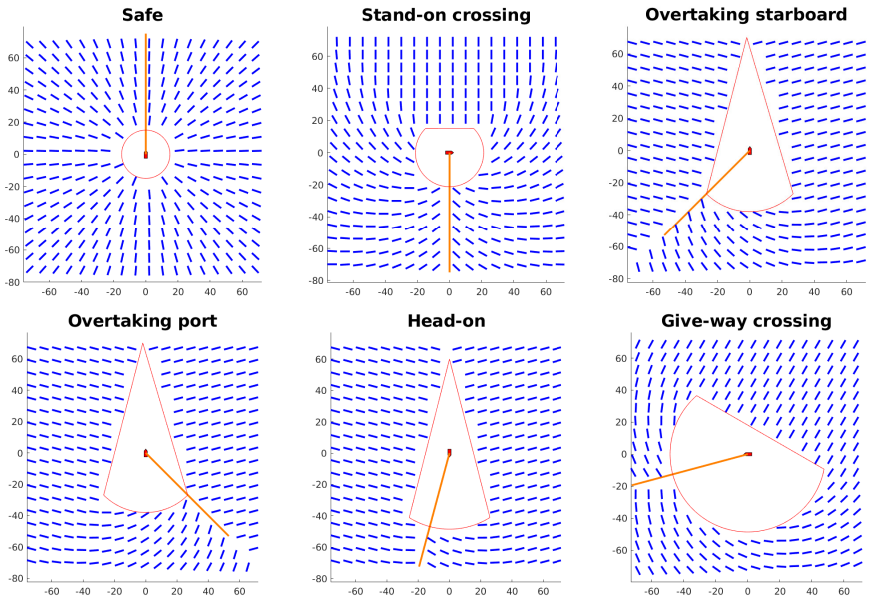

Figure 8: Illustration of TS domain. In blue, a vector-field of normal vectors to the TS domain for an OS located at the base of each vector. The OS has its heading aligned with its course at $\chi = 0$ and speed of 1 m/s. The orange line indicates the port-starboard split angle α_s and the red contour around the TS indicates the shortest allowable range to the TS at any approach angle.

with

$$\mathcal{C}_{u\_dyn} := \sum_{i=1}^{N_{TS}} \mathcal{C}_{u\_dyn\_i}. \tag{23}$$

where $\mathcal{C}_{u\_dyn\_i}$ is the domain of TS i. The set $\mathcal{C}_{dyn}$ is convex.

5 Static obstacle domain

Confined waters operations do not only require consideration of the available maneuverable space when moving in vicinity to other vessels, but also active COLAV regarding static obstacles. Unexpected maneuvers by a TS during a close quarter passing can move the TS domain closer to the OS, and hence push the OS towards static obstacles. Additionally, the position and size of the static obstacles in the map might differ from the reality due to quasi-static features such as docked or stationary vessels, or floating harbours that change position as a result of periodic water movements or other external forces.

We propose to handle static obstacles in a similar way to dynamic obstacles, where first, a set of relevant static obstacles are determined, then, a domain is assigned to each of the relevant static obstacles, and lastly, we try to avoid entering that domain. To determine the set of relevant static obstacles, we apply a simple approach that is general and applicable for most map data, and most importantly, is easily unifiable with real-time lidar data, which we will apply in the experiments to mitigate the effects of unprecise map data as well as estimation errors in the vessel's navigation system.

First, the area around the OS is split into n_{sect} equally sized sectors, with the OS as the center. Subsequently, the closest point on any of the map-entries and the closest point for a lidar measurement within each sector is found. The one of these two points that are closest to the OS is considered the relevant static obstacle in that sector. For sector i, this point is denoted $\boldsymbol{p}_{stat\_i} \in \mathbb{R}^2$. The method for finding the closest point in each sector should be chosen to match the specific map data, e.g. for map data consisting of convex polygons it can be computed at a considerably lower cost than for non-convex polygons (Atallah et al., 1991).

We then define a domain for each point $\boldsymbol{p}_{stat\_i}$. The domain has the same form as for dynamic obstacles, with a straight line that divides the north-east plane into two halves. When determining the orientation, and hence a normal vector to the domain line, the method presented in (Martinsen et al., 2020) is applied. The method calculates the tangent vector to the domain line for each point $\boldsymbol{p}_{stat\_i}$ so that it is tangent to an ellipse around the OS, where the major axis of the ellipse is aligned with the desired OS course from the guidance system. The safe set regarding static obstacles is defined as the complement set of the unsafe set, that is

$$\mathcal{C}_{stat} = \mathcal{C}_{u\_stat}^{c}, \tag{24}$$

with

$$\mathcal{C}_{u\_stat} := \sum_{i=1}^{n_{sect}} \mathcal{C}_{u\_stat\_i}, \tag{25}$$

where $\mathcal{C}_{u\_stat\_i}$ is the unsafe set to the point $\boldsymbol{p}_{stat\_i}$. The set $\mathcal{C}_{stat}$ is by design a convex set in $\mathbb{R}^2$. In Fig. 9, $\mathcal{C}_{stat}$ is illustrated for the vessel in blue, with the parameters from Table 2. The green polygon is $\mathcal{C}_{stat}$ for the OS in blue with $n_{sect} = 12$, while the orange line indicates a more refined set, with $n_{sect} = 2000$. The set approximated by $n_{sect} = 12$ gives a sufficiently good approximation, and will greatly reduce the computational cost compared to a higher n_{sect} by reducing both the number of lookups in map data and the number of inequality constraints in the optimization problem that will be defined later. From the figure, the effect of choosing domain tangent angles according to (Martinsen et al., 2020) is also apparent, where the blue graph shows the boundary of a set for $n_{sect} = 12$, but the domain tangent vector instead is made tangent to a circle around the OS. The figure shows that $\mathcal{C}_{stat}$ is stretched out along the canal, which is the desired direction of travel. This reduces the chance of $\mathcal{C}_{stat}$ being restricted so much by obstacles to either side in front of the OS as to totally obstruct further transit along the reference path, which improves the COLAV method's ability to traverse highly confined areas.

6 Safe set and CBF synthesis

The safe operating set of the OS can now be defined as

$$\mathcal{C} := \{\boldsymbol{p} \mid \boldsymbol{p} \in \mathcal{C}_{dyn} \wedge \boldsymbol{p} \in \mathcal{C}_{stat}\}, \tag{26}$$

where we consider the vessel to be safe from collision and maneuvering in compliance with the mentioned COLREGs rules as long as it stays within this set. In this section, we introduce the means of forward invariance of $\mathcal{C}$, namely the CBF. In the following subsections, we will formulate the CBFs for both dynamic and static obstacles, such that the combined set of CBFs will ensure that $\boldsymbol{p}$ stays in $\mathcal{C}$ by restricting the control inputs. In the CBF formulation we apply the 3DOF vessel model from (Fossen, 2011), with

$$\dot{\boldsymbol{p}} = \boldsymbol{R}_{\psi}\boldsymbol{\nu}, \tag{27}$$

$$\dot{\boldsymbol{\nu}} = \boldsymbol{M}^{-1}\left(\boldsymbol{C}(\boldsymbol{\nu})\boldsymbol{\nu} + \boldsymbol{D}(\boldsymbol{\nu})\boldsymbol{\nu}\right) + \boldsymbol{M}^{-1}\boldsymbol{\tau}, \tag{28}$$

where $\boldsymbol{M}$ is the inertia matrix including hydrodynamic added mass, $\boldsymbol{C}(\boldsymbol{\nu})$ is the Coriolis-centripetal matrix, $\boldsymbol{D}(\boldsymbol{\nu})$ is the damping matrix, $\boldsymbol{\tau} \in \mathbb{R}^3$ are the generalized forces produced

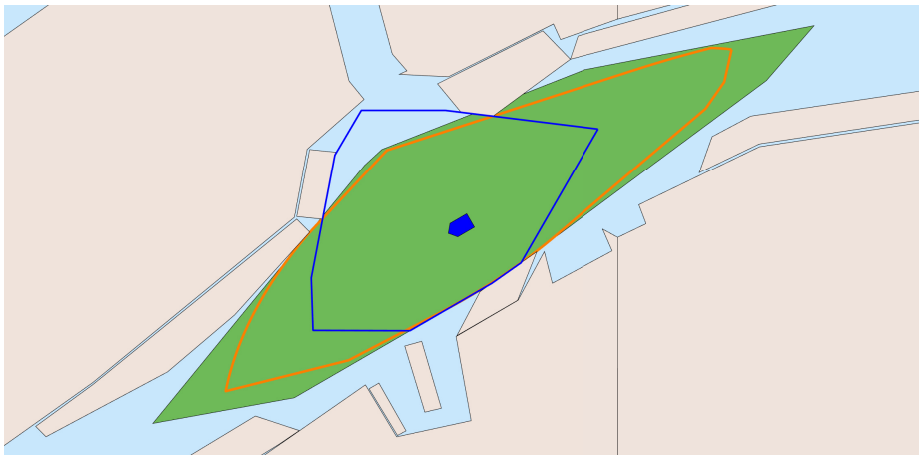

Figure 9: The green polygon gives the set $\mathcal{C}_{stat}$ for $n_{sect} = 12$. The boundary of a more refined set with $n_{sect} = 2000$ is given by the orange graph. The set with $n_{sect} = 12$ gives a sufficiently good $\mathcal{C}_{stat}$, with reduced computational cost compared to a high n_{sect}. The blue graph is the boundary of a set with $n_{sect} = 12$, where the normal vector for domain i is aligned with the vector from the $\boldsymbol{p}_{stat\_i}$ to $\boldsymbol{p}$. The benefit of the method from (Martinsen et al., 2020) is apparent, as it gives a $\mathcal{C}_{stat}$ that is more open in the desired direction of travel.

by the actuators, and

$$\boldsymbol{R}_{\psi} = \begin{bmatrix} \cos(\psi) & -\sin(\psi) & 0 \\ \sin(\psi) & \cos(\psi) & 0 \end{bmatrix}. \tag{29}$$

6.1 CBF for dynamic obstacles

The CBFs for dynamic obstacles, are formulated with respect to each TS domain at the current time. In the formulation, we do not consider the dynamics of the domain. The domain can therefore be considered as a straight line moving in $\mathbb{R}^2$ with a constant velocity and a constant rate of rotation about the point $\boldsymbol{p}_{TS}$, hence, the effect on the domain dynamics from the accelerations of the OS $\ddot{\boldsymbol{p}}$ are omitted. The reasons for this will be discussed shortly.

It is with respect to the point $\boldsymbol{p}_B$ that we define the CBF as

$$h_{dyn}(\boldsymbol{x}) := \boldsymbol{n}_{\tilde{p}}^{\mathsf{T}} \tilde{\boldsymbol{p}} + c_{dyn} \boldsymbol{n}_{\tilde{p}}^{\mathsf{T}} \dot{\tilde{\boldsymbol{p}}}, \tag{30}$$

where $\boldsymbol{x} = [\boldsymbol{p}^{\mathsf{T}}, \dot{\boldsymbol{p}}^{\mathsf{T}}, \boldsymbol{p}_{TS}^{\mathsf{T}}, \dot{\boldsymbol{p}}_{TS}^{\mathsf{T}}, \chi_{TS}]^{\mathsf{T}} : \mathbb{R}^2 \times \mathbb{R}^2 \times \mathbb{R}^2 \times \mathbb{R}^2 \times \mathbb{S}$,

$$\tilde{\boldsymbol{p}} = \boldsymbol{p} - \boldsymbol{p}_B, \tag{31}$$

and

$$\boldsymbol{n}_{\tilde{p}} = \begin{bmatrix} \cos(\alpha) \\ \sin(\alpha) \end{bmatrix}, \tag{32}$$

is the unit vector of $\tilde{\boldsymbol{p}}$. The first and second term in (30) are the Euclidean distance to and the relative velocity towards the TS domain, respectively, where the parameter $c_{dyn} > 0$ mitigates between the distance to the domain and the velocity at which the OS is allowed to approach the domain. The parameter c_{dyn} serves as a direct method of setting a threshold for how early the OS should start to manuever in an encounter. This is illustrated by the simulations presented in Fig. 10, where the parameter demonstrates its suitability for enforcing the parts

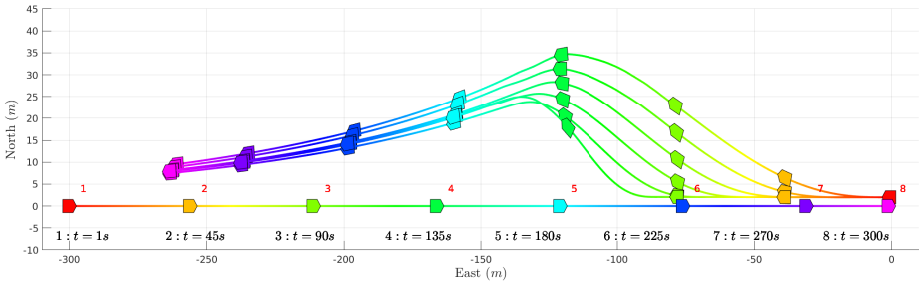

Figure 10: Simulations from a head-on encounter with varying values of c_{dyn}, The TS is traveling east and the OS is traveling west, at parallel paths with a 2 m separation. Both vessels have a speed of 1 m/s. The six OS trajectories are for $c_{dyn} = [10, 30, 50, 70, 90, 110]$, where the southmost trajectory has $c_{dyn} = 10$, and the northmost has $c_{dyn} = 110$.

of Rule 8 concerning making maneuvers "in ample time". The parameter, c_{dyn}, should also reflect the physical aspect of the vessel as discussed by the authors in previous work (Thyri et al., 2020a).

To apply the CBF as an inequality constraint in the quadratic program (QP), we need it on the affine form in (4). Hence, we need the time-derivative of $h_{dyn}(\boldsymbol{x})$,

$$\dot{h}_{dyn}(\boldsymbol{x}) = \dot{\boldsymbol{n}}_{\tilde{p}}^{\mathsf{T}}\tilde{\boldsymbol{p}} + \boldsymbol{n}_{\tilde{p}}^{\mathsf{T}}\dot{\tilde{\boldsymbol{p}}} + c_{dyn}(\dot{\boldsymbol{n}}_{\tilde{p}}^{\mathsf{T}}\dot{\tilde{\boldsymbol{p}}} + \boldsymbol{n}_{\tilde{p}}{}^{\mathsf{T}}\ddot{\tilde{\boldsymbol{p}}}), \tag{33}$$

with $\dot{\tilde{\boldsymbol{p}}} = \dot{\boldsymbol{p}} - \dot{\boldsymbol{p}}_B$, where $\dot{\boldsymbol{p}} = [\dot{N}, \dot{E}]^{\mathsf{T}}$ is the north-east velocity of the OS, and

$$\dot{\boldsymbol{n}}_{\tilde{p}} = \frac{\partial \boldsymbol{n}_{\tilde{p}}}{\partial \alpha}\dot{\alpha}. \tag{34}$$

Further,

$$\begin{aligned}\dot{\boldsymbol{p}}_B =& \dot{\boldsymbol{p}}_D + (\dot{\boldsymbol{p}} - \dot{\boldsymbol{p}}_D)^{\mathsf{T}}\boldsymbol{n}_{p_D}\boldsymbol{n}_{p_D} + (\boldsymbol{p} - \boldsymbol{p}_D)^{\mathsf{T}}\dot{\boldsymbol{n}}_{p_D}\boldsymbol{n}_{p_D} \\ &+ (\boldsymbol{p} - \boldsymbol{p}_D)^{\mathsf{T}}\boldsymbol{n}_{p_D}\dot{\boldsymbol{n}}_{p_D},\end{aligned} \tag{35}$$

where

$$\dot{\boldsymbol{n}}_{p_D} = \frac{\partial \boldsymbol{n}_{p_D}}{\partial \alpha}\dot{\alpha}, \tag{36}$$

and

$$\dot{\boldsymbol{p}}_D = \dot{\boldsymbol{p}}_{TS} + \begin{bmatrix} -\sin(\alpha) \\ \cos(\alpha) \end{bmatrix} l\dot{\alpha}, \tag{37}$$

is the derivative of (19). In the CBF formulation we assume that the TS keeps a constant course and speed, and hence

$$\dot{\alpha} = \begin{cases} \dot{\varphi}_{TS} & \text{if } \alpha_D \text{ is not in saturation,} \\ 0 & \text{if } \alpha_D \text{ is in saturation,} \end{cases} \tag{38}$$

with

$$\dot{\varphi}_{TS} = \left(\boldsymbol{R}_2(\tfrac{\pi}{2})\frac{\bar{\boldsymbol{p}}}{\bar{\boldsymbol{p}}^{\mathsf{T}}\bar{\boldsymbol{p}}}\right)^{\mathsf{T}}\dot{\tilde{\boldsymbol{p}}}, \tag{39}$$

where $\dot{\tilde{\boldsymbol{p}}} = \dot{\boldsymbol{p}} - \dot{\boldsymbol{p}}_{TS}$ denotes the relative velocity between the two vessels, and

$$\boldsymbol{R}_2(\phi) = \begin{bmatrix} \cos(\phi) & -\sin(\phi) \\ \sin(\phi) & \cos(\phi) \end{bmatrix}. \tag{40}$$

Lastly, from (33), we need the double time derivative of $\tilde{\boldsymbol{p}}$. In the calculations of $\ddot{\tilde{\boldsymbol{p}}} = \ddot{\boldsymbol{p}} - \ddot{\boldsymbol{p}}_B$, we set $\ddot{\boldsymbol{p}}_B = \boldsymbol{0}$, since the acceleration of the TS domain is omitted. This is done in order to facilitate a desired behaviour when close to the domain. By setting $\ddot{\boldsymbol{p}}_B = \boldsymbol{0}$, the resulting gradient of the CBF is rotated in the direction of the deflection angle, and hence facilitate the OS to traverse in that direction. This gives $\ddot{\tilde{\boldsymbol{p}}} = \ddot{\boldsymbol{p}}$, where

$$\begin{aligned} \ddot{\boldsymbol{p}} &= \frac{\partial \boldsymbol{R}_\psi}{\partial \psi}\dot{\psi}\boldsymbol{\nu} - \boldsymbol{R}_\psi \boldsymbol{M}^{-1}\left(\boldsymbol{C}(\boldsymbol{\nu})\boldsymbol{\nu} + \boldsymbol{D}(\boldsymbol{\nu})\boldsymbol{\nu}\right) + \boldsymbol{R}_\psi \boldsymbol{M}^{-1}\boldsymbol{\tau}, \\ &= \boldsymbol{F}_{\ddot{p}} + \boldsymbol{G}_{\ddot{p}}\boldsymbol{\tau}, \end{aligned} \tag{41}$$

with

$$\boldsymbol{F}_{\ddot{p}} = \frac{\partial \boldsymbol{R}_\psi}{\partial \psi}\dot{\psi}\boldsymbol{\nu} - \boldsymbol{R}_\psi \boldsymbol{M}^{-1}\left(\boldsymbol{C}(\boldsymbol{\nu})\boldsymbol{\nu} + \boldsymbol{D}(\boldsymbol{\nu})\boldsymbol{\nu}\right), \tag{42}$$

and

$$\boldsymbol{G}_{\ddot{p}} = \boldsymbol{R}_\psi \boldsymbol{M}^{-1}\boldsymbol{\tau}. \tag{43}$$

By inserting for (41) into (33), the CBF derivative takes the form

$$\begin{aligned} \dot{h}(\boldsymbol{x}) &= \dot{\boldsymbol{n}}_{\tilde{p}}^{\mathsf{T}}\tilde{\boldsymbol{p}} + \boldsymbol{n}_{\tilde{p}}^{\mathsf{T}}\dot{\tilde{\boldsymbol{p}}} + c_{dyn}\left(\dot{\boldsymbol{n}}_{\tilde{p}}^{\mathsf{T}}\dot{\tilde{\boldsymbol{p}}} + \boldsymbol{n}_{\tilde{p}}{}^{\mathsf{T}}\boldsymbol{F}_{\ddot{p}}\right) + c_{dyn}\dot{\boldsymbol{n}}_{\tilde{p}}^{\mathsf{T}}\boldsymbol{G}_{\ddot{p}}\boldsymbol{\tau}, \\ &= \boldsymbol{F}_{\dot{h}} + \boldsymbol{G}_{\dot{h}}\boldsymbol{\tau} \end{aligned} \tag{44}$$

with

$$\boldsymbol{F}_{\dot{h}} = \dot{\boldsymbol{n}}_{\tilde{p}}^{\mathsf{T}}\tilde{\boldsymbol{p}} + \boldsymbol{n}_{\tilde{p}}^{\mathsf{T}}\dot{\tilde{\boldsymbol{p}}} + c_{dyn}\left(\dot{\boldsymbol{n}}_{\tilde{p}}^{\mathsf{T}}\dot{\tilde{\boldsymbol{p}}} + \boldsymbol{n}_{\tilde{p}}{}^{\mathsf{T}}\boldsymbol{F}_{\ddot{p}}\right), \tag{45}$$

and

$$\boldsymbol{G}_{\dot{h}} = c_{dyn}\dot{\boldsymbol{n}}_{\tilde{p}}^{\mathsf{T}}\boldsymbol{G}_{\ddot{p}}, \tag{46}$$

which is affine in the control input $\boldsymbol{\tau}$. From (44), we can formulate an inequality constraint on the form of (4) as

$$\boldsymbol{F}_{\dot{h}} + \boldsymbol{G}_{\dot{h}}\boldsymbol{\tau} \geq -\gamma(h_{dyn}(\boldsymbol{x})), \tag{47}$$

which can be applied as an inequality constraint in an optimization problem on the form $A\boldsymbol{\tau} \leq b$, with

$$A = -\boldsymbol{G}_{\dot{h}}, \tag{48}$$

$$b = \gamma(h_{dyn}(\boldsymbol{x})) + \boldsymbol{F}_{\dot{h}}. \tag{49}$$

6.2 CBF for static obstacles

For static obstacles a similar CBF is formulated. The CBF takes the same form as for dynamic obstacles,

$$h_{stat}(x) = \boldsymbol{n}_{stat}^{\mathsf{T}}\tilde{\boldsymbol{p}}_{stat} + c_{stat}\boldsymbol{n}_{stat}^{\mathsf{T}}\dot{\tilde{\boldsymbol{p}}}_{stat}, \tag{50}$$

where $\boldsymbol{n}_{stat}$ is the normal vector to the domain assigned to $\boldsymbol{p}_{stat}$ and $\tilde{\boldsymbol{p}}_{stat} = \boldsymbol{p} - \boldsymbol{p}_{stat}$. Since $\dot{\boldsymbol{n}}_{stat} = 0$ and $\dot{\boldsymbol{p}}_{stat} = 0$, the CBF derivative takes the simple form

$$\dot{h}_{stat}(\boldsymbol{x}) = \boldsymbol{n}_{stat}^{\mathsf{T}}\dot{\boldsymbol{p}} + c_{stat}\boldsymbol{n}_{stat}^{\mathsf{T}}\ddot{\boldsymbol{p}}. \tag{51}$$

By inserting for (41) into (51), we get

$$\dot{h}_{stat}(\boldsymbol{x}) = \boldsymbol{n}_{stat}^{\mathsf{T}}\dot{\boldsymbol{p}} + c_{stat}\boldsymbol{n}_{stat}^{\mathsf{T}}\left(\boldsymbol{F}_{\ddot{p}} + \boldsymbol{G}_{\ddot{p}}\boldsymbol{\tau}\right), \tag{52}$$

which again can be put on the form of (4) as

$$\boldsymbol{F}_{\dot{h}_{stat}} + \boldsymbol{G}_{\dot{h}_{stat}}\boldsymbol{\tau} \geq -\gamma(h(\boldsymbol{x})_{stat}), \tag{53}$$

with

$$\boldsymbol{F}_{\dot{h}_{stat}} = \dot{\boldsymbol{p}}^{\mathsf{T}} \boldsymbol{n}_{stat} + c_{stat} \boldsymbol{n}_{stat}^{\mathsf{T}} \boldsymbol{F}_{\ddot{p}}, \tag{54}$$

and

$$\boldsymbol{G}_{\dot{h}_{stat}} = c_{stat} \boldsymbol{n}_{stat}^{\mathsf{T}} \boldsymbol{G}_{\ddot{p}}. \tag{55}$$

The inequality of (53) can be applied as a constraint in an optimization problem on the same form as (47).

6.3 Application to the GNC pipeline

To apply the constraints from the CBFs, a quadratic problem is formulated as

$$\begin{aligned} \min_{\boldsymbol{\tau}} \quad & \frac{1}{2}(\boldsymbol{\tau} - \boldsymbol{\tau}_d)^{\mathsf{T}} \boldsymbol{K}_\tau (\boldsymbol{\tau} - \boldsymbol{\tau}_d), \\ \text{s.t.} \quad & \dot{\mathcal{H}}_{dyn} \text{ and} \\ & \dot{\mathcal{H}}_{stat}, \end{aligned} \tag{56}$$

where $\boldsymbol{K}_\tau > 0$ is a 3 by 3 weighting matrix, $\dot{\mathcal{H}}_{dyn}$ and $\dot{\mathcal{H}}_{stat}$ are the set of inequalities from (47) and (53) for all dynamic and static obstacles respectively, and $\boldsymbol{\tau}_d \in \mathbb{R}^3$ is a desired virtual force that can be provided by an arbitrary controller that is suitable for the control objective. Additional constraints are applied to ensure that the actuator magnitude constraints are overheld. The resulting $\boldsymbol{\tau}$ should be realized without further steps in the GNC pipeline to ensure the integrity of the proposed method. If the system is prone to allocation errors from e.g. thruster dynamics such as rate-constraints or thruster deadband, the thruster dynamics should be included in the vessel model, as proposed in (Basso et al., 2020), where the QP solves the trajectory tracking, COLAV and thrust allocation.

7 Simulations

In this section, the simulation results are presented. First, an extensive set of simple V2V encounters in open waters are presented and discussed. The motivation for this is to demonstrate the effectiveness and completeness of the proposed TS domain. Thereafter, we include a set of three simulations in complex environments with up to three maneuvering vessels. In these simulations, two or more of the vessels are running the proposed COLAV method. The intent of these simulations is to demonstrate the method as a whole, and show that it is suitable for multi-agent operation. Lastly, we demonstrate the capacity of the method, and provide some remarks on runtime through a simulation with 12 vessels running the proposed COLAV method. The simulations are run in a simulator implemented in Matlab with a 3DOF vessel model of the milliAmpere experimental platform depicted in figures 1 and 19a. The model parameters used in the simulations are estimated based on a data-driven approach through the work presented in (Pedersen, 2019). In the simulator, the Matlab ODE45 solver is applied for state integration.

A model of the GNC pipeline with auxillary systems is visualized in Fig. 11. The simulator setup consists of the following modules:

- The **Path Waypoints** module is the input to the system, which is a set of waypoints with corresponding velocities.
- A **LOS Guidance** method with saturated yaw-rate dynamics is applied to calculate the desired course reference

$$\chi_d = \chi + \Delta_t r_d, \tag{57}$$

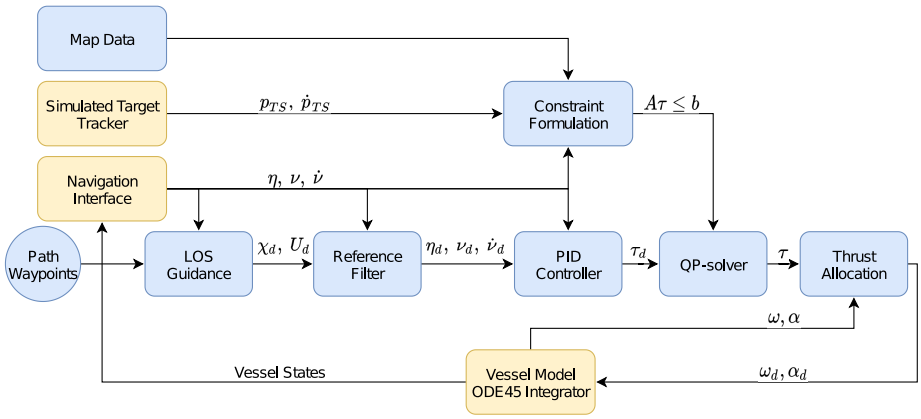

Figure 11: GNC pipeline for simulations. Blue modules are the same in simulations and experiments. Yellow boxes are simulator-specific.

where Δ_t is the run period of the guidance module, and

$$r_d = saturate(\frac{1}{\tau_\chi}(\chi_r - \chi), min_{r_d}, max_{r_d}). \tag{58}$$

is a saturated reference yaw rate, where

$$\chi_r = \theta - \text{atan}\Big(\frac{e}{\Delta}\Big), \tag{59}$$

is a course reference calculated from a constant lookahead distance $\Delta_{lookahead}$, where θ is the course from the previous waypoints to the current waypoint, and e is the cross-track error. This guidance scheme reduces the effect of conflicting objectives between the guidance and the COLAV, compared to simply applying χ_r as a course reference, which is a common approach. This would result in an increasing course error as the OS is maneuvering away from the path in an avoidance maneuver, where the χ_r in the worst case can be perpendicular to a TS domain, resulting in stagnation or a deadlock. The saturated yaw rate reference, and using χ in (57) limits the course error, and hence allows the OS to continue an avoidance maneuver until the safe set enables the OS to move back towards the reference path. The rationale behind this is that the COLAV objective has higher priority than the path following objective.

- A third order **Reference Filter:** is applied to calculate smooth position, velocity and acceleration references.
- A **PID Controller** with velocity feed-forward performs path following.
- The **Simulated Target Tracker** provides position and velocity states from the other vessels in the simulation.
- The **Navigation Interface** outputs the OS position, velocity and acceleration.
- The **Map Data** contains all static obstacles in the form of convex polygons.
- The **Constraint Formulation** formulates constraints for all relevant static and dynamic obstacles in accordance with the method presented in sections 4-6.
- The **QP solver** applies the Matlab solver *mpcqpsolver* to (56).

Table 1: Rule-based parameters for the TS domain.

Parameter	SF	SO	OT_p	OTs	HO	GW	**Unit**
α_d	0	$\pi/4$	$\pi/3$	$\pi/3$	$2\pi/5$	$2\pi/5$	rad
α_s	0	$\pi/2$	-$3\pi/4$	$3\pi/4$	$\pi/12$	-$\pi/8$	rad
α_{D_max}	π	π	$\pi/3$	$5\pi/6$	$\pi/2$	$2\pi/5$	rad
α_{D_min}	$-\pi$	-π	-$5\pi/6$	-$\pi/3$	-$2\pi/3$	-$6\pi/5$	rad
c_{dyn}	10	10	40	40	60	60	s
δ_{dyn}	1	1	4	4	1	1	m

Table 2: Non rule-based parameters.

Parameter	**Value**	**Parameter**	**Value**
γ_{dyn}	$0.100\,\mathrm{s}^{-1}$	r_{free_max}	40 m
γ_{stat}	$1.00\,\mathrm{s}^{-1}$	k_l	0.50
c_{stat}	5 s	n_{sect}	12
δ_{stat}	6 m	Δ_t	0.05 s
$\Delta_{lookahead}$	100 m	τ_χ	0.2 second
min_{r_d}	-0.5 rad/s	max_{r_d}	0.5 rad/s
$\boldsymbol{K}_\tau$	$diag(1,1,1)$	U_{lim}	0.2 m/s

- The **Thrust Allocation** realizes the virtual force $\boldsymbol{\tau}$ by calculating appropriate set-points for the two azimuth thrusters according to the method developed by the authors of (Torben et al., 2019)

7.1 TS domain validation

We now present results for evaluating the effectiveness of the TS domain. The results are produced through an extensive simulation study, with the OS and TS on straight line paths, where the TS does not maneuver, but keeps a constant speed and course. Two parameters have been applied to construct the set of simulations: the relative course χ_{rel} between the vessels, and the lateral offset, δ_{lat}, of the OS reference path from a point-of-collision at the origin of the local NED frame. The OS and TS waypoints are calculated so that both vessels will be at the origin after 200 s if $\delta_{lat} = 0$. The parameter χ_{rel} is iterated from 0 to 2π at steps of $\pi/16$, while the δ_{lat} is iterated from -300 m to 400 m at 10 m steps, resulting in a total of 2272 simulations. The OS and TS have a reference speed of 1.5 m/s and 1 m/s respectively. The OS path goes from west to east with a course of $\pi/2$ while the TS path is adjusted for each χ_{rel} so that it passes through the origin. A subset of the simulations are presented in Fig. 12, where all OS trajectories for a given TS course are combined in one plot. The full set of figures can be viewed at this OneDrive **repository** [4].

Figures 12a and 12b show results from encounters where the OS have give-way obligations. From the trajectories, one can see that for most encounters where the OS maneuvers from its nominal path, it adjusts course to starboard to pass behind the TS, in accordance with the protocol. In Fig. 12b, the OS starts a small port maneuver along some trajectories, before performing a starboard maneuver and passing behind the TS. This is a result of the OS initially being on the positive side of α_s, but ends up on the negative side as the encounter evolves.

Figures 12c and 12d show results from stand-on encounters. According to protocol, it is the TS

[4]Full url: `https://studntnu-my.sharepoint.com/:f:/r/personal/emilht_ntnu_no/Documents/shared%20data%20publications/cbf_based_colav_journal_paper/batch_simulations?csf=1&web=1&e=Tow8cg`

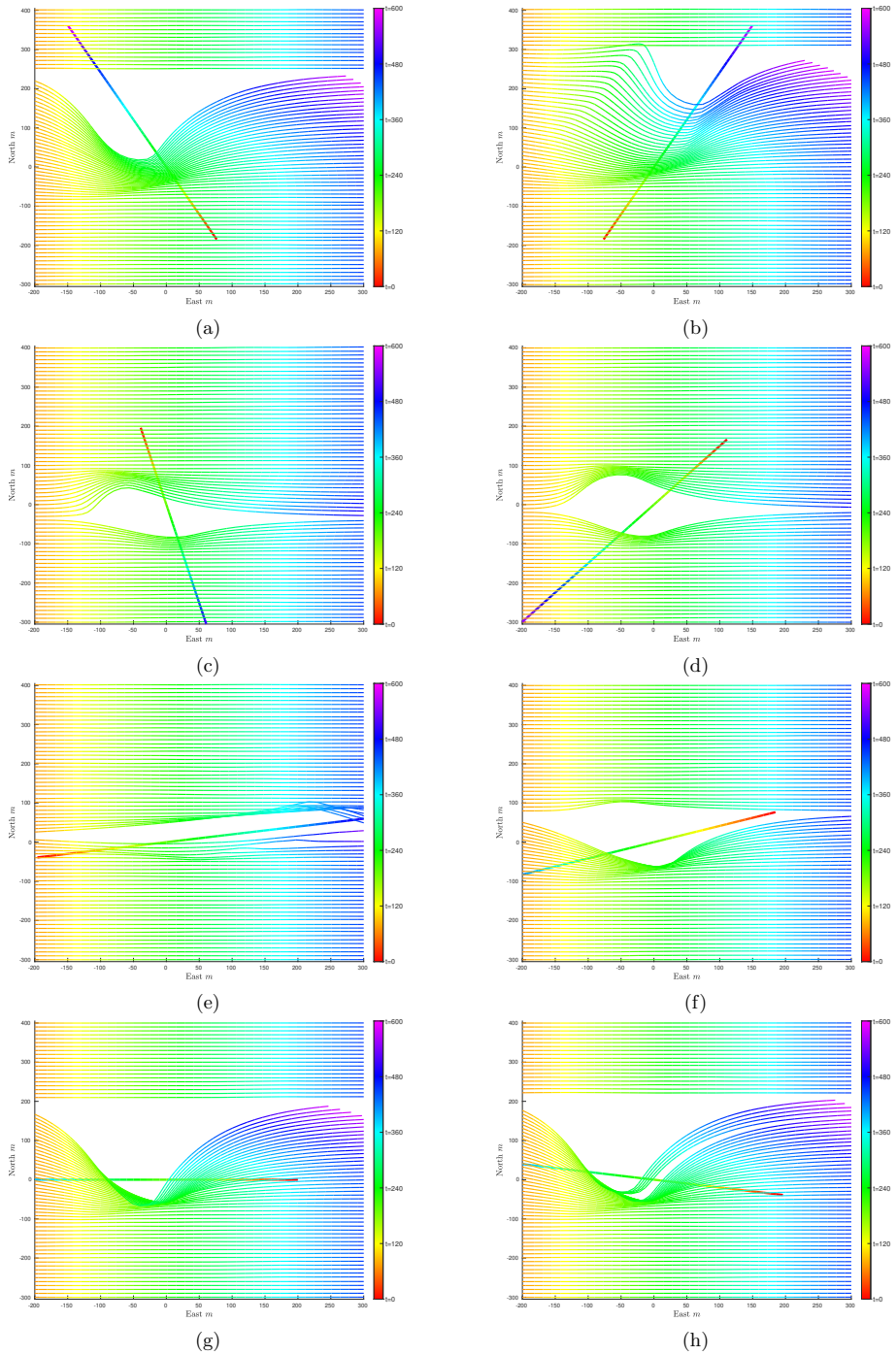

(a) (b) (c) (d) (e) (f) (g) (h)

Figure 12: Batches of V2V encounter simulations. In each subfigure, the TS travels along the same trajectory, while the OS trajectory has a varying offset.

that is obliged to give way, where the OS shall keep its course and speed, and only maneuver when it is apparent that the TS is not abiding its duty, and the situation can not be resolved by maneuvers from the TS alone. This is a difficult evaluation to make, as it requires an understanding of the maneuvering capacity of the TS. Our approach to this is to apply a small c_{dyn}, to allow the OS to hold its velocity for longer as the range to the TS domain is reduced. If an understanding of each unique TS was available, this could be used to determine a suitable value for c_{dyn} for each encounter. In the presented simulations, a comparable portion of the simulations maneuver to pass in front and aft of the TS, due to the choice α_{δ_s}. A preference of passing in front or aft of the TS can be achieved by respectively increasing or decreasing α_{δ_s}.

Figure 12e shows results from overtaking encounters. The course of the TS relative to the OS favours overtaking with the TS on the port side. The trajectories for the simulations where the OS starts in the area behind the TS, the OS is able to perform a starboard maneuver to pass behind the TS in the overtaking. The trajectories where the OS starts further north, it starts on the positive side of the port-starboard split angle, and hence adjusts course to port to travel alongside the TS until it can pass clear in front of it. The OS behaviour is compliant with Rule 13.

Figures 12f-12h show results from head-on encounters. In most cases where the OS takes action to stay in the safe set, it adjusts course to starboard to pass the TS port to port in compliance with Rule 14. In the head-on simulations where the OS maneuvers and still passes the TS starboard to starboard, it is due to the OS initially or by the TS velocity, appears on the positive side of the port-starboard split angle. In these situations, the OS is in such a position that it will require excessive maneuvering to pass port to port. This is apparent from figures 12g - 12h, where the OS, along some trajectories, maneuvers a long way to starboard in order to pass port to port in cases where keeping a constant course or performing a small port maneuver seems sufficient. Nevertheless, a starboard maneuver is the protocol compliant maneuver in head-on encounters, where Rule 14 dictates that the two vessels shall pass port to port. The port maneuver from the OS is also excessive due to lack of maneuvering from the TS, which is also obliged to maneuver, and should hence split the maneuvering effort.

7.2 Complex scenarios

We now present results from simulations in complex scenarios with several maneuvering vessels in confined waters with restricted maneuverability.

7.2.1 Head-on: Simulation 1

In Simulation 1, two vessels are meeting in a head-on encounter between two breakwaters in a narrow entry to a harbour area. Both vessels are autonomous agents, and track the same set of waypoints in the opposite order. The trajectories of the two vessels, as well as the path between the waypoints are shown in Fig. 13. Due to the geometry between the two vessels at the range of static classification, Vessel 1 classifies the encounter as give-way, while Vessel 2 classifies it as a stand-on encounter, despite the vessels in reality being in a head-on encounter. The wrongful classification is held in place by the classification state-machine holding the classification until it is reclassified as safe. Despite the faulty classification, both agents resolve the situation without risk of collision and in accordance with Rule 14 by passing port to port.

The erroneous classification results from the primitive prediction of the TS intention. In the presented work, it is assumed that the TS will keep a constant course and speed, which is a poor assumption in such confined-water scenarios, where the trajectories of the target ships are very much affected by the presence of static obstacles. By applying knowledge about the

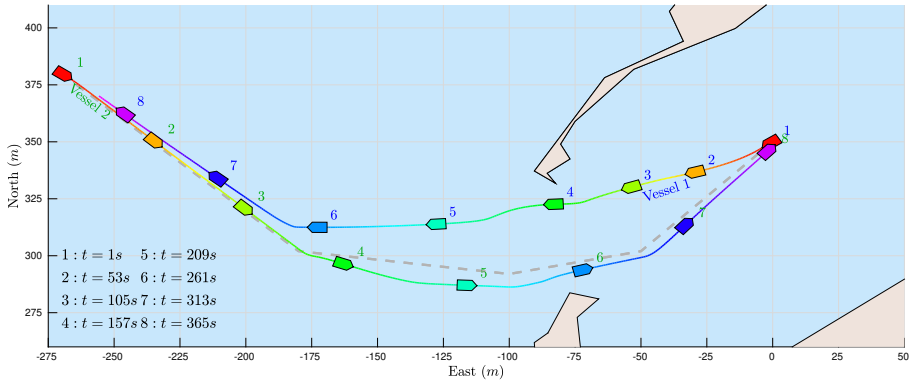

Figure 13: Simulation 1: Harbour area entry: Encounter in entrance to harbour area. Both vessels are autonomous agents, and travel along the same path in opposing directions. Vessels are scaled for visualization.

operational environment such as typical arrival and departure points and traffic patterns from historical data, a more qualified prediction of the TS trajectory can be made. However, this is outside the scope of this paper, and is left for future work.

From the vessel trajectories one can see that the vessel travelling west initially starts a starboard maneuver to abide its give-way duties. The maneuver seems premature from the context, and is a result of the large TS domain of the east-bound vessel, which initially receives the maximum addition, r_{free_max}, for maneuverable space as it approaches from open waters. The premature starboard maneuver of the west-bound vessel is reduced by CBFs of the static obstacle on its starboard side, as is apparent from the small course adjustments to port between timestep 2 and 3, and the subsequent starboard maneuver as the safe-set opens up just before timestep 4. In the same way, the small starboard maneuver of the east-bound vessel puts it at collision risk with the south breakwater, where it performs a small port maneuver between timestamp 5 and 6 to stays in the safe set.

7.2.2 Head-on and overtaking: Simulation 2

In Simulation 2, three vessels are traveling along a canal-area. Vessel 1 and Vessel 2 are autonomous agents, while Vessel 3 is performing simple path following. All vessels track the same set of waypoints, the vessels traveling west in reversed order from the vessels traveling east. The trajectories of the vessels are shown in Fig. 14. Vessel 1 is in a head-on encounter with both vessels traveling east. It performs a starboard maneuver and holds its starboard side of the canal to pass both east-bound vessels port to port. Vessel 2 is initially in a head-on encounter with Vessel 1, and subsequently in an overtaking encounter with Vessel 2. It first moves to starboard to pass port to port in the head-on encounter in accordance with Rule 14, and subsequently maneuvers to its port side of the canal to overtake Vessel 3 on its port side due to the relative course of the two vessels, and hence avoid crossing in front of it, in accordance with Rule 13.

Note how Vessel 1 and Vessel 2 splits the available space in the overtaking maneuver at timestamp 3, since they both have about the same amount of maneuverable space in their pass-sector. Also note how Vessel 2 keeps well clear during the overtaking maneuver, due to the saturation limits on α_D, visualized by the unidirectional parts of the vector field in Fig. 9.

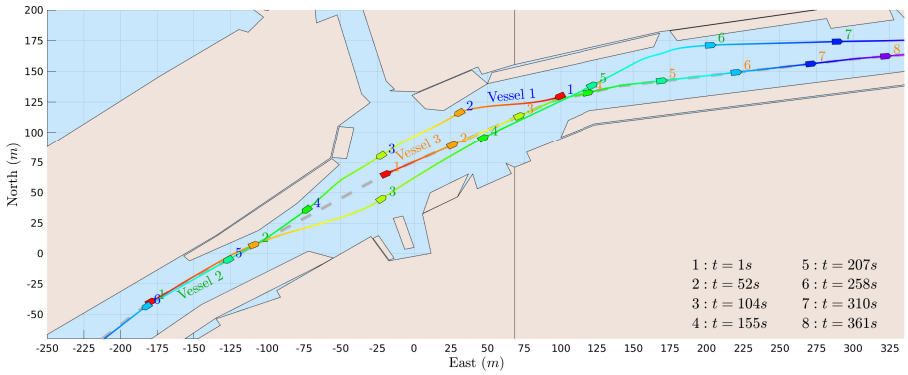

Figure 14: Simulation 2: Multiple encounters in a canal with two autonomous agent vessels and one non-autonomous vessel. All vessels track the same path, indicated by the grey dashed line. Vessels are scaled for visualization.

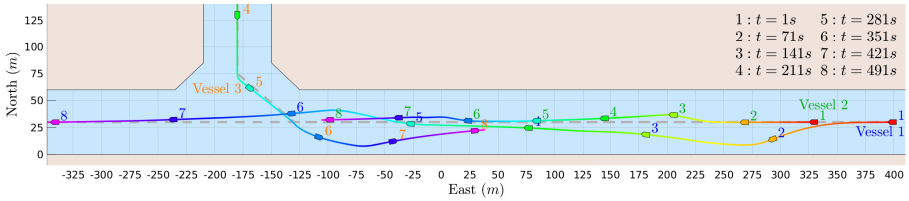

Figure 15: Simulation 3: Multiple encounters where all three vessels are autonomous agents.

7.2.3 Head-on, overtaking and crossing: Simulation 3

In Simulation 3, three vessels are traversing a canal system. Vessel 1 and Vessel 2 are travelling west. Vessel 3 enters the canal from the north before travelling east. All vessels are autonomous agents, and track the same path at the centerline of the canal, where Vessel 3 first tracks a path that merges into the centerline path. The trajectories of the vessels are shown in Fig. 15. Initially, Vessel 1 is in an overtaking encounter and performs an overtaking maneuver on the port side of Vessel 2. As the overtaking comes to an end, Vessel 1 is in a give-way crossing encounter with Vessel 3, and moves to starboard to pass behind the vessel in accordance with Rule 15. Vessel 2 is initially in a give-way encounter with Vessel 3, but the encounter is reclassified as head-on before the range of static classification is reached, due to the course changes of Vessel 3 .

The starboard maneuver of Vessel 2 in the head-on encounter is small due to the speed and heading of Vessel 3 at the time, which in turn restricts the port course-change maneuver of Vessel 3, causing its trajectory to pass close to the south canal bank. The purely reactive features of this method does not provide Vessel 2 with any comprehension of intention of Vessel 3, and hence does not make a greater maneuvering effort to leave more room.

Note that in all three complex simulations, all the participating vessels track the same nominal path close to the centerline of the waterway, and are hence on direct collision course with each other at some point along the path. Yet, all encounters are resolved in accordance with protocol. This suggests that the proposer reactive COLAV method, which is intended as a bottom layer method in a hybrid structure, is robust to unfeasible or delayed trajectories from

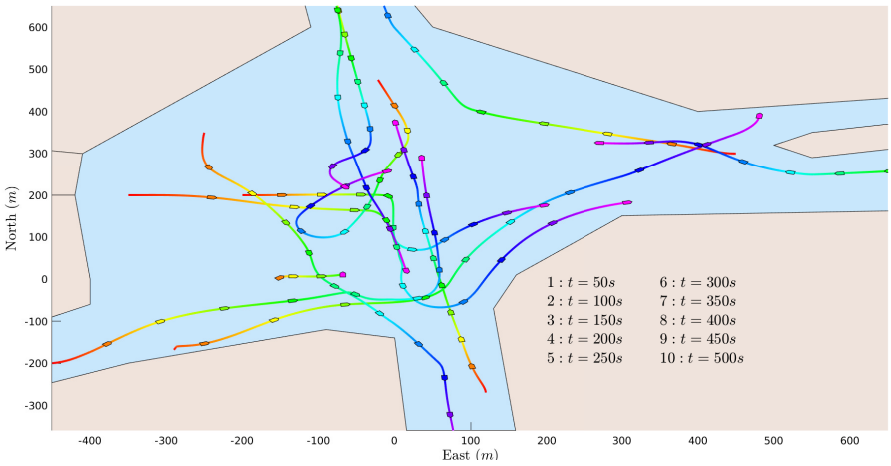

Figure 16: Simulation 4: Crowded waters where all vessels are running the proposed COLAV method. The minimum DCPA for the simulation is 25.74 m.

the mid and top-layer planners, which is of paramount importance for such a system. And, as running the proposed method results in trajectories that are in line with the COLREGs, it will merge well with higher level planners that output trajectories that are in compliance with, or at least do not contradict the COLREGs.

7.2.4 Traffic capacity and runtime: Simulation 4

The simulations presented to this point have demonstrated a set of simple yet realistic scenarios for ASV operation in confined waters. The small set of involved vessels allow us to demonstrate a subset of the qualities of the proposed COLAV method in each simulation. However, there are no aspects of the method that makes it unsuitable for handling encounters where a higher number of vessels are involved. This is demonstrated through Simulation 4, which involves 12 vessels, where all vessels run the proposed COLAV method. An overview of the simulation is displayed in Fig. 16. The high traffic density makes it challenging to comment on the behaviour of specific vessels, however, all vessels resolve the scenario without collision and in compliance with the COLREGs. The minimum DCPA in the simulation is 25.74 m. From the scenario overview it is apparent that several of the vessels would benefit from running a hybrid COLAV structure with a more long-term and deliberate planner, as they initiate maneuvers that at a later stage result in situations requiring additional, and sometimes more substantial maneuvers. In these situations a more refined initial maneuver might have resolved the scenario without further avoidance maneuvers. However, the scope of this paper concerns a reactive COLAV method, and this simulation demonstrates that the proposed COLAV method can handle high-traffic situations in a safe and COLREGs-compliant manner, and hence ensure the baseline safety of a hybrid COLAV structure.

Since the proposed COLAV method is of a reactive nature, it is important that it has a runtime that allows for real-time operation. In Fig. 17, the runtime of the method is displayed for three simulated scenarios, with 3, 8 and 12 vessels, where all vessels run the proposed method. The runtimes are visualized in a normalized histogram. The simulations are run on a single core on a Dell Precision 5540 with a 32 GB memory and an Intel Core i9-9880H processor running at 2.30 GHz. The code is written in Matlab with no particular regard to runtime optimization, and runs as a Matlab script. From the figure, one can see that the method has an average

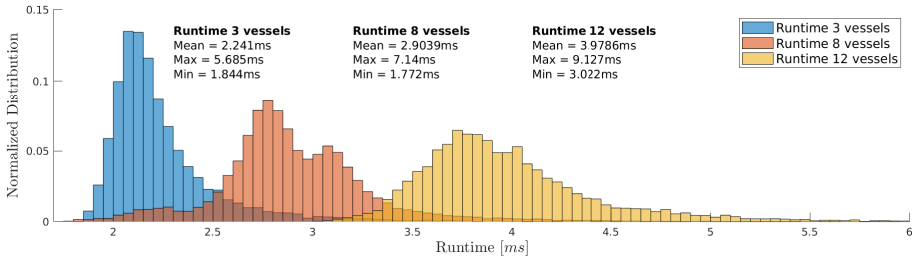

Figure 17: Normalized distribution of runtime for the proposed COLAV algorithm. Results from three simulations with 3, 8 and 12 vessels. The latter one is Simulation 4.

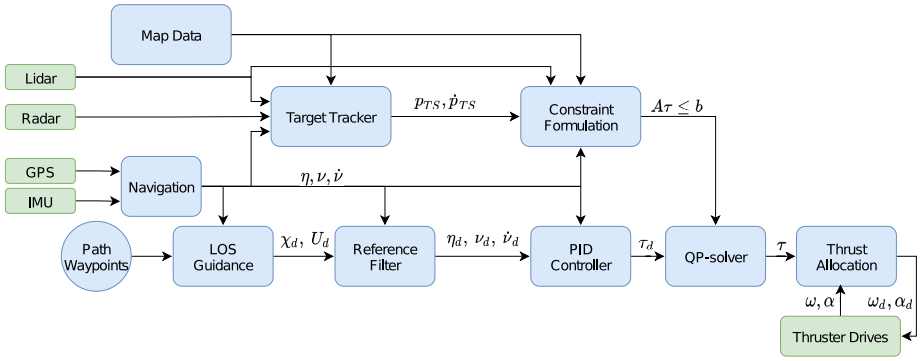

Figure 18: Guidance, navigation and control pipeline for the experiments. Modules in blue boxes run on the on-board computers. Green boxes are the vessel-mounted equipment.

runtime between 2 ms and 4 ms, with a worst case runtime of 9.127 ms. This is more than sufficient for ASV operations, where a suitable run period for a reactive COLAV system would be in the range between 0.1 s and 10 s, depending on the ASV dynamics and the operational environment. For the simulations and experiments in this paper, a run period of 0.1 s was applied.

8 Experiments

The experiments are conducted with the milliAmpere vessel depicted in Fig. 1 and Fig. 19a. The vessel is a 5 m by 2.8 m prototyping platform hosted by NTNU for developing and testing enabling technology for fully autonomous maritime operations in urban areas. The vessel is fully electric, and equipped with two 2KW azimuth thrusters for propulsion. The vessel is also equipped with several sensors for navigation and situational awareness. Relevant hardware is listed in Table 3. The GNC pipeline used in the experiments is visualized in Fig. 18, where the green modules are vessel-mounted hardware, and the blue modules run on one of the on-board computers. The code for the map data, LOS guidance, reference filter, controller, thrust allocation and QP solver is generated from Simulink to run in ROS[5].

We apply a lidar- and radar-based target tracker, where an integrated probabilistic data association (IPDA) is used for track initiation and maintenance (Wilthil et al., 2018). The tracker

[5]Robot operating system, `https://www.ros.org/about-ros/`

Table 3: milliAmpere hardware

Equipment	Make	Type	Info
Thruster	Torqeedo	Pod Cruise 2.0FP	500 N reversible thrust
Azimuth Servo	Intecno	BLDC	32 deg / sec rotation speed
On-Board computer	Axiomtek	eBOX670-883-FL	I7 processor. Ubuntu with ROS.
GPS system	Vector	VS330	RTK capacity. 10 mm position accuracy
IMU	Xsens	MTi20	Linear acceleration and rate of turn.
Radar	Simrad	Broadband 4G^{TM}	36 RPM
Lidar	Velodyne	Puck / VLP16	100 m range

is described in detail in (Wilthil et al., 2017). In (Kufoalor et al., 2019), a further discussion on the tracker and its application to decision support for COLAV is presented, where it is also demonstrated through full-scale experiments in open waters. The output of the target tracker is a list of confirmed tracks, each with a unique ID and an estimate on the target's position and velocity vector.

In initial experiments in the canal, we experienced issues where the tracker confirmed tracks on several of the docked vessels, where clustering and de-clustering of two or more vessels docked side-by-side resulted in high velocity estimates due to the resultant change in the track's center of mass. We therefore apply a mask to filter out tracks on docked vessels before passing the list of confirmed tracks on to the COLAV system, where tracks under the mask are omitted from the list. The mask was drawn up manually, based on lidar data, and can be seen in figures 21-29, as the green field on either side of the canal.

In the experiments, lidar data is used in combination with the map data for COLAV wrt. static obstacles. Two stages of filtering is applied to the lidar data. Detections on confirmed tracks is omitted, by removing detections within a range of 4 m of the estimated position of the track. Additionally, filtering of single and double detections that are not in proximity to other detections are omitted. This is done to reduce the risk of noise on the surface of the water, which have been experienced when raining, and when the wind causes a certain type of small waves.

The TS used in the experiments is called Havfruen, and is depicted in Fig. 19b. The vessel is a Jeanneau Marlin 695 with a Yamaha 150hp outboard engine. The vessel is equipped with a Garmin eTrex 10 GPS for logging the TS position. There was no information-sharing between the OS and the TS during the experiments.

The experiments are conducted in a canal in the northern part of Trondheim, depicted in Fig. 20. The canal is between 60 m and 80 m wide with floating docks on both sides, reducing the free width to 30 m in some places. The location provides a realistic and relevant testing ground for urban ASVs, and is also the transit location for an urban autonomous passenger ferry pilot project hosted by among others NTNU, Trondheim municipality and Zeabuz (Stensvold, 2020), where an autonomous ferry will transport pedestrians across the canal.

8.1 Experimental results

Experimental results from 9 experiments are presented. Experiments 1.1-1.3 are head-on encounters, experiments 2.1-2.2 are overtaking encounters and experiments 3.1-3.4 are crossing encounters, where three are give-way crossings and one is a stand-on crossing. All experiments are run in the same area, either along or across the canal. Only one TS, the Havfruen TS (HTS), was used in the experiments, yet, the canal is a populated harbour area, and several

(a) milliAmpere (b) Havfruen

Figure 19: Vessels used in the experiments.

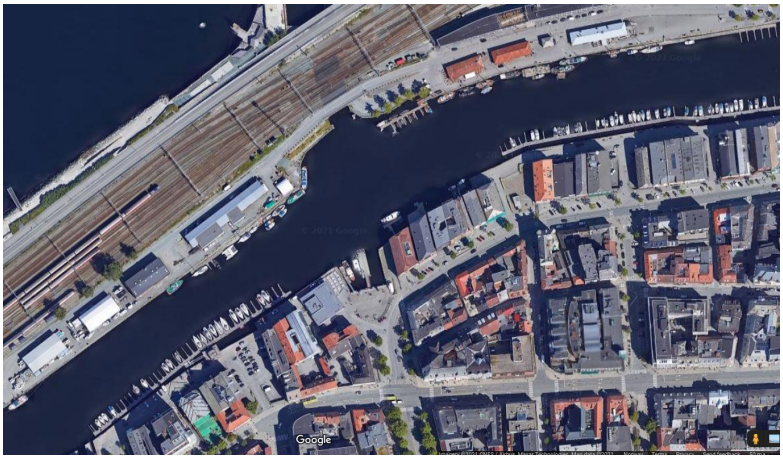

Figure 20: Testing location. Canal area in the northern part of Trondheim.

other docked vessels, as well as false tracks, were detected by the tracker which in some experiments affected the trajectory of the OS. The data from each experiment is presented through a single figure containing the following information:

- The trajectory of the OS from GPS data, and the estimated trajectory of the controlled HTS, Havfruen, are visualized as thick, colored lines, where the color change from red, through yellow, green and blue, to purple, as time evolves.
- Vessel representations of the OS and TS tracks at matching 10 s intervals, where the OS representation is a fore-aft symmetric polygon, and the TS representations are flat at the aft. Since the tracker does not provide any size-estimates of the tracks, a constant size of 5 m by 3 m is used for all tracks, which is the approximate size of the HTS.
- A scaled down vessel representation on the recorded GPS position of the HTS, at matching time intervals.
- The trajectory of tracks belonging to docked vessels in the canal that are not filtered by the mask, or false tracks, are plotted as thin colored lines, with vessel representations

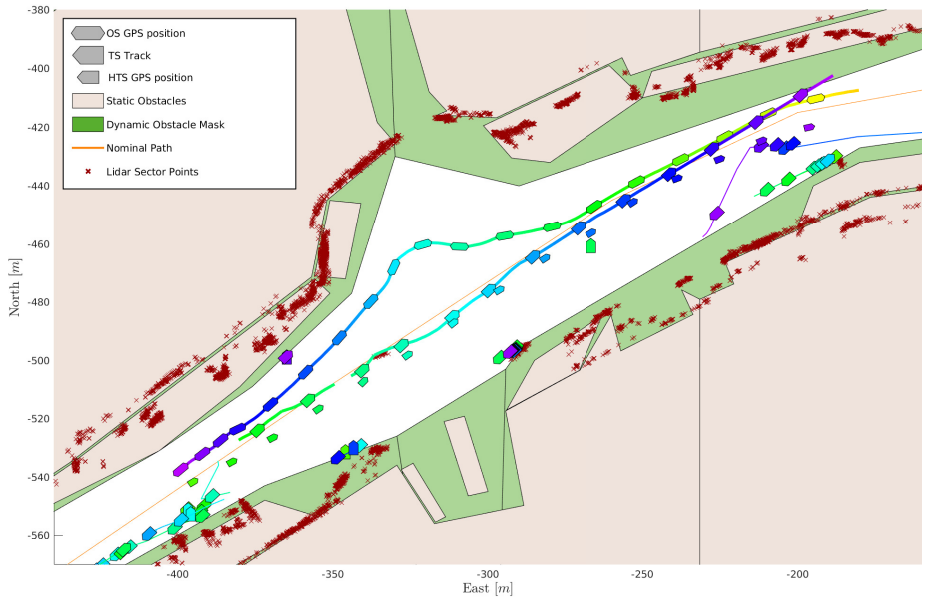

Figure 21: Experiment 1.1: The OS is travelling east to west, and performs a starboard maneuver to give way to the HTS. The HTS does not abide its give-way duty.

at matching timesteps to the OS and the HTS. However, most tracks belonging to stationary vessels have velocity estimates close to zero, and most false tracks have a very short duration.

- The closest point in each static obstacle sector from the lidar data are visualized as dark red crosses.

Videos showing the time evolvement of the experiment overviews are available at this OneDrive **link** [6], where additional features such as lidar raw-data, the convex set $\mathcal{C}_{stat}$, and lines indicating the domains of the tracks are visualized.

8.1.1 Head-on: Experiment 1.1

An overview of the experiment is shown in Fig. 21, where the OS is travelling east to west, and the HTS is traveling in the opposite direction. The tracker detects a false track for a short period of time close to the point $[N, E] = [-460, -270]$, which causes the OS to start a starboard maneuver to pass in front of the false track. As the false track disappears, the OS continues the starboard maneuver to pass port to port in the head-on encounter with the HTS. As the track on the HTS disappears for approximately 5 s, and then re-appears with an initial course pointing more towards the OS, a further increased starboard manuever is performed by the OS to stay clear of the TS domain of the HTS, before a port maneuver is performed in order to get back on the nominal path and ensure a safe margin to the static obstacles in front of the OS.

The lidar points along the trajectory of the HTS originate from detection on the HTS vessel.

[6] Full url: `https://studntnu-my.sharepoint.com/:f:/g/personal/emilht_ntnu_no/EnEoh28gB25IjzA8LnxuTWMBPmxI7TFZ-vLYSIzFR1P7dA?e=sHrwWJ`

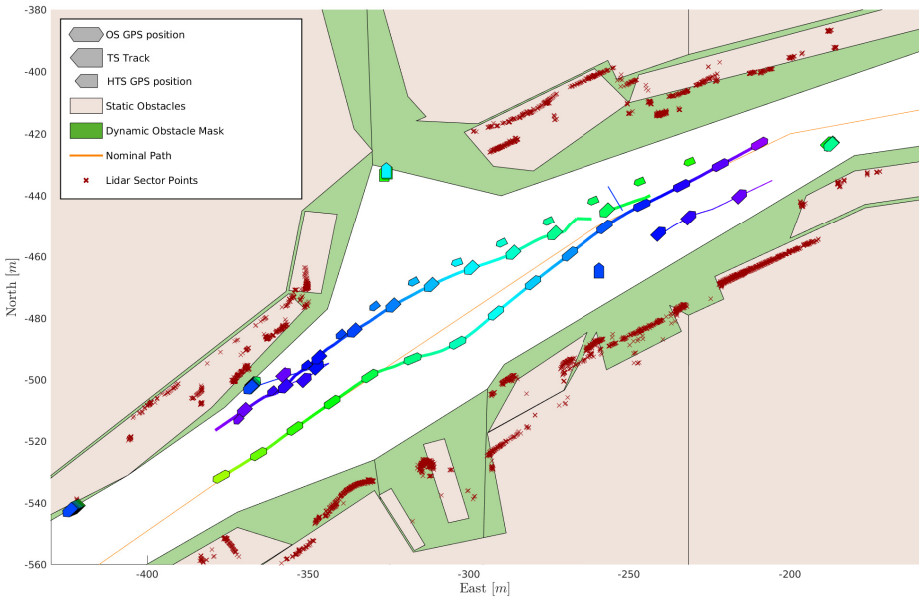

Figure 22: Experiment 1.2: The OS is travelling west to east, and performs a starboard maneuver to give way to the HTS. The starboard maneuver is small, but sufficient due to the course of the HTS.

These detections should be filtered out from the raw lidar data, as the detections are within the given range of the HTS track position (this is apparent from the video). We believe this fails to happen due to the asynchronous messages in ROS, where sufficient care is not taken to ensure that all tracks are included in the filtering of lidar data. However, this does not affect the performance of the COLAV method, since the restrictions from dynamic obstacles are stricter than for static obstacles. The raw lidar data will therefore only ensure that collision is avoided if the target tracker fails to initiate a track on a vessel, and hence provide redundancy for the target tracker.

8.1.2 Head-on: Experiment 1.2

In this encounter, the OS is travelling west to east, and the HTS is travelling in the opposite direction. An overview of the experiment is shown in Fig. 22. The detection of the HTS is somewhat late, yet at sufficient distance for the OS to perform an early and smooth starboard maneuver and pass port to port with the HTS in accordance with Rule 14. The magnitude of the starboard maneuver is small due to the course of the HTS, which is also on a small starboard manuever. The two vessels pass each other with a safe distance, both between vessels, and from vessels to static obstacles, and share the available space in the canal between them in a similar way as would be expected in an encounter by two manned vessels of equal size. This indicates that the algorithm is not only rules compliant, but produces behaviour that is suitable for maneuvering among other manned vessels. The OS trajectory is unaffected by the false track detected to its starboard side close to the end of the transit, as this track is estimated to have zero velocity.

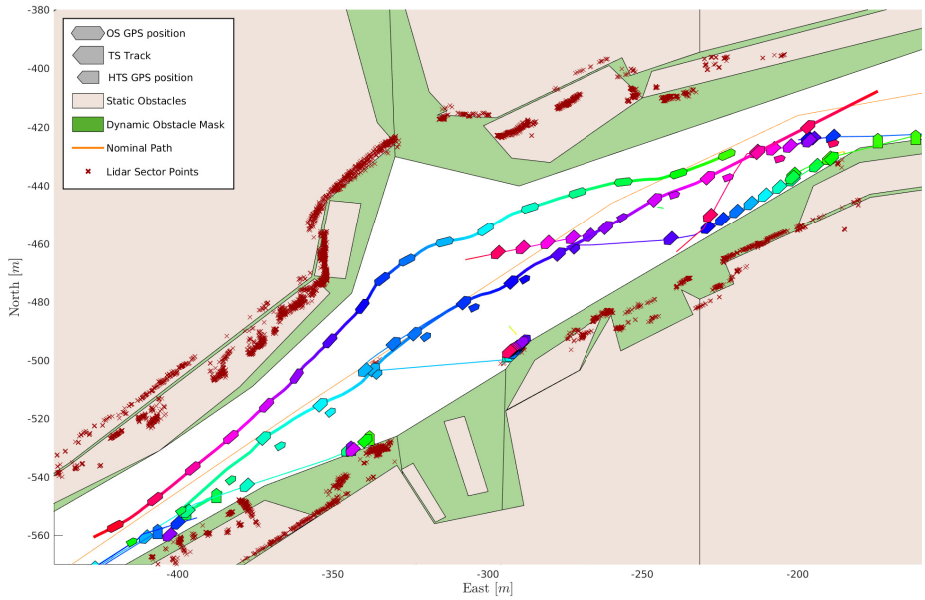

Figure 23: Experiment 1.3: The OS is travelling east to west. The starboard maneuver is initiated by a false track. The OS holds its starboard side of the canal until it is past and clear of the HTS.

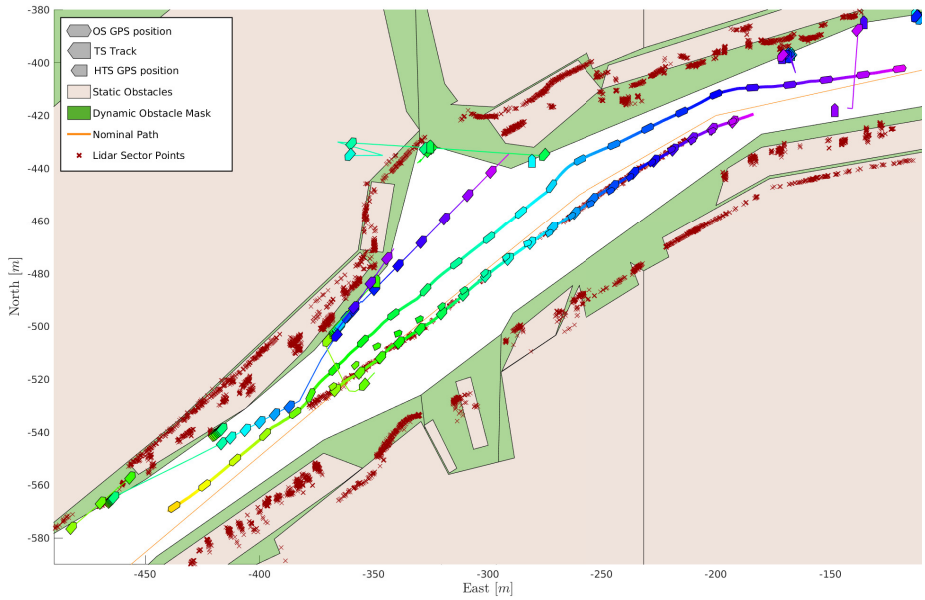

Figure 24: Experiment 2.1: The OS is traveling west to east and overtakes the HTS on its port side. The OS keeps to its port side of the canal until it is past and clear in front of the HTS.

8.1.3 Head-on: Experiment 1.3

The OS is travelling east to west, opposite to the HTS, as can be seen by the experiment overview in Fig. 23. The overview shows that several false tracks were detected, yet most of them were not in proximity to the OS. However, one track close to $[N, E] = [-450, -240]$ existing for only a few seconds, caused the OS to start a starboard maneuver, which is continued until the HTS is past and clear. Since the estimated position of the HTS as CPA is close to the center of the widest part of the canal, the size of the TS domain of the HTS is dimensioned based on the available maneuverable space to the port of the HTS at this point, making it larger than what is representative for the canal as a whole. This, in turn, results in a larger than necessary starboard maneuver, putting the OS in conflict with the static obstacles further down the canal, and causing it to maneuver back towards the path with a higher effort than desired, similar to what happened in Experiment 1.1.

8.1.4 Overtaking: Experiment 2.1

In this experiment, visualized in Fig. 24, both the OS and the HTS are travelling west to east, where the OS starts off behind the HTS. The encounter is classified as an overtaking encounter, and the OS maneuvers to the port to pass the HTS on its port side. Due to the small relative velocity between the vessels, the overtaking maneuver lasts for more than 200 meters through the canal. Yet, the OS keeps a safe distance to the HTS throughout the maneuver, and only moves back onto its path when it is finally past and clear, in accordance with Rule 13.

8.1.5 Overtaking: Experiment 2.2

In this overtaking scenario, both the OS and the HTS are travelling east to west. An overview is given in Fig. 25. The OS starts a maneuver to overtake the HTS on its port side and continues this maneuver throughout the scenario. Note how the OS moves closer to the HTS towards the end of the overtaking due to the reduced free space, yet still keeps a safe distance as a result of the considerations introduced in Section 4.2. Due to the low relative velocity between the OS and the HTS, the maneuver lasts so long that the OS travels out of the area of the mask for the dynamic obstacles. Towards the end of the transit, the OS reacts to several tracks that originate from the vessels docked along the canal. Several of the tracks also receive estimated velocities from movement of its center of mass due to clustering and de-clustering of several vessels, resulting in the OS performing a port maneuver due to an oncoming false track.

8.1.6 Crossing: Experiment 3.1

In this crossing scenario, the OS is crossing the canal from south to north, while the HTS is traveling east to west along the canal. The OS is initially on DP at the start of the nominal path, and the transit is initiated when the HTS is in a position that will result in an encounter. An overview of the scenario is given in Fig. 26. The OS starts off with a starboard maneuver to pass behind the HTS, and proceeds towards the destination waypoint once it is is clear behind the HTS.

8.1.7 Crossing: Experiment 3.2

In this scenario, the OS is crossing the canal from north to south, while the HTS is traveling west to east. An overview is given in Fig. 27. The OS has give-way obligations, and starts with a starboard maneuver to pass behind the HTS, and proceeds along the transit once it is

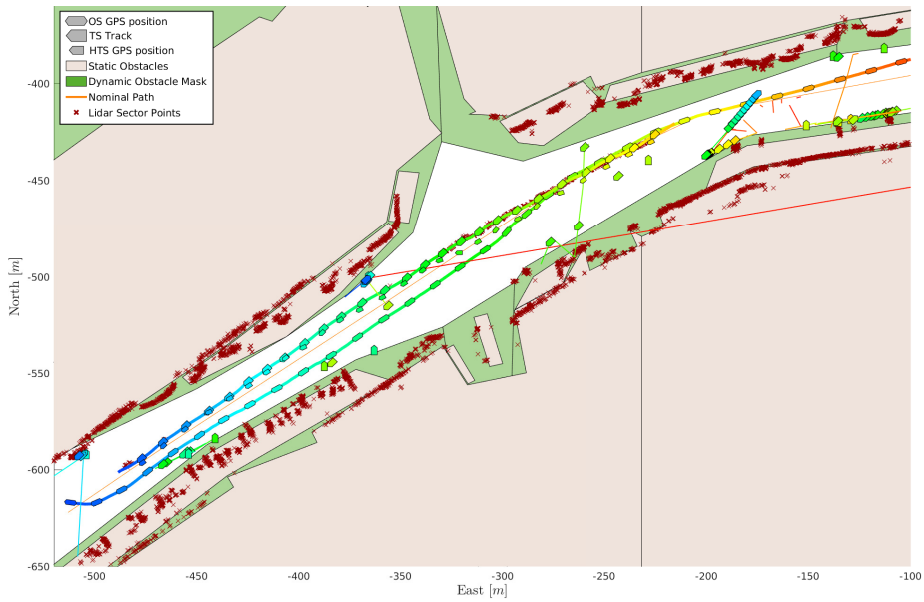

Figure 25: Experiment 2.2: The OS is travelling east to west, and overtakes the HTS in a long overtaking maneuver, where the available space is reduced towards the end. At the end of the maneuver, the OS performs a starboard maneuver due to a detected false track.

passed and clear behind the HTS. The encounter is resolved without collision, and the OS acts in accordance with Rule 16.

8.1.8 Crossing: Experiment 3.3

In this crossing scenario, the OS is crossing the canal from south to north, while the HTS is traveling east to west along the canal. A scenario overview is given in Fig. 28. The OS has give-way obligations, and starts a starboard maneuver to pass behind the HTS. The maneuver is subsequently halted by the presence of a static obstacle detected by the lidar, as is apparent from the concentration of lidar sector points to the east of the OS in the scenario overview. In this scenario, the transit is started with the HTS further from the nominal path of the OS, compared to Experiment 3.1, which means the OS has to make a larger starboard maneuver in order to stay clear of the HTS domain while maintaining the reference speed. Additionally, since the conflicting static obstacle is missing from the map data, and is not taken into account when calculating the available maneuverable space and the size of the TS domain, the HTS TS domain is larger than the actual encounter would require. The combination of these factors results in a restricted safe set, and hence the OS has to wait for the HTS to pass before proceeding the transit.

8.1.9 Crossing: Experiment 3.4

In this scenario, the OS is travelling south to north, while the HTS is travelling west to east. It is therefore the HTS that has give-way obligations, while the OS is the stand-on vessel. An overview is given in Fig. 29. Since the HTS is not abiding its give-way obligations, the OS performs a starboard maneuver to avoid collision and passes in front of the HTS. This

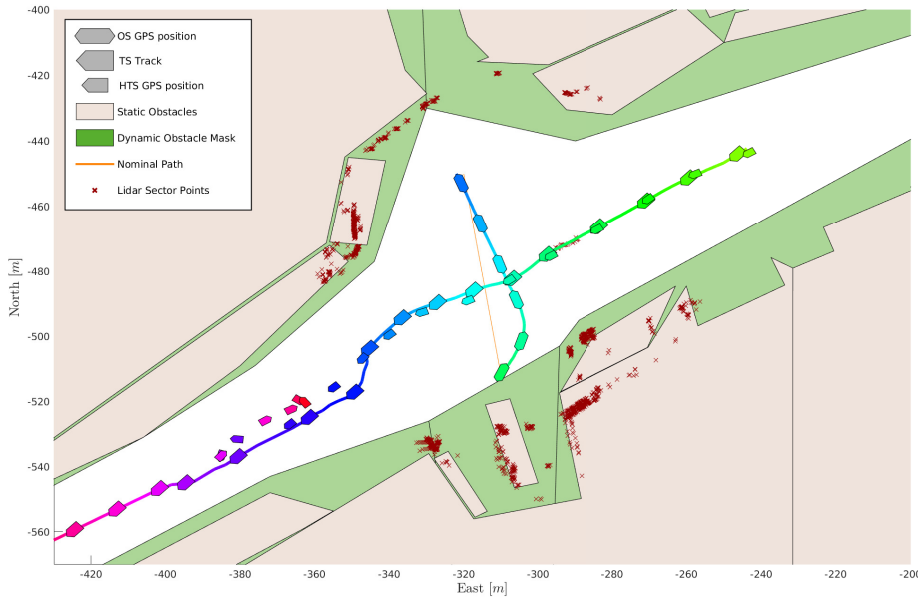

Figure 26: Experiment 3.1: The OS has give-way obligations in the crossing, and performs a starboard maneuver to pass behind the HTS.

encounter could also be resolved by a port maneuver by the OS. However, this would be in conflict with a rules-compliant starboard maneuver from the HTS, and could, depending on the encounter geometry, involve a higher risk of collision. The threshold for maneuvering in front versus behind the TS in such encounters can be set through the classification-specific α_{δ_s} parameter.

8.2 Discussion

In several of the experiments, the position of the OS is outside the safe set $\mathcal{C}$ for longer periods. This is not obvious from the scenario plots presented in this paper, but can be seen from the video animations of the experiments at this OneDrive **link** [7]. The violation may arise from one of two causes:

- a TS is detected with a position and velocity so that it immediately puts the OS in conflict with $\mathcal{C}$, or in such a way that it is inevitable that the OS will violate $\mathcal{C}$
- the OS is initially in $\mathcal{C}$, but does not apply the appropriate maneuvering effort to stay within $\mathcal{C}$ as the boundaries of the set changes.

The first cause can be mitigated by improving the situational awareness modules, and in particular the target detection and tracking, by either improving algorithms or augmenting the perception system with additional sensors such as EO and IR cameras. The second cause arises from both modelling errors and state estimation errors on the models and state included in the CBF. In particular, estimates for $\boldsymbol{p}_{TS}$ and $\dot{\boldsymbol{p}}_{TS}$, and the exclusion of $\ddot{\alpha}$ in the dynamics of the TS domain. Additionally, any potential allocation error, the error between $\boldsymbol{\tau}$ and the

[7] Full link provided in earlier footnote

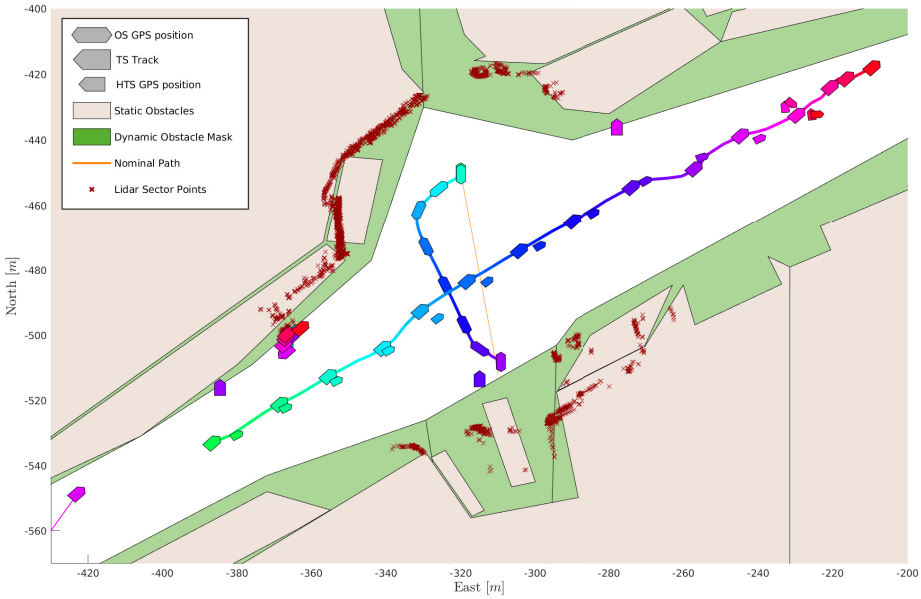

Figure 27: Experiment 3.2: The OS is travelling north to south and performs a starboard maneuver to cross behind the HTS.

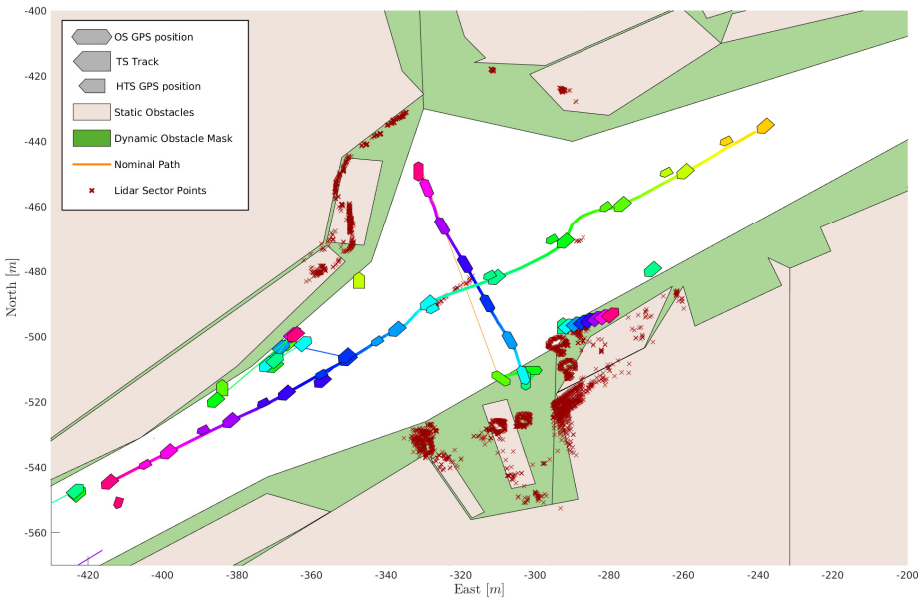

Figure 28: Experiment 3.3: The OS has give-way obligations to the HTS in the crossing encounter. An early starboard maneuver is halted by the presence of unmapped static obstacles detected by the lidar. The OS proceeds the transit when the HTS has passed.

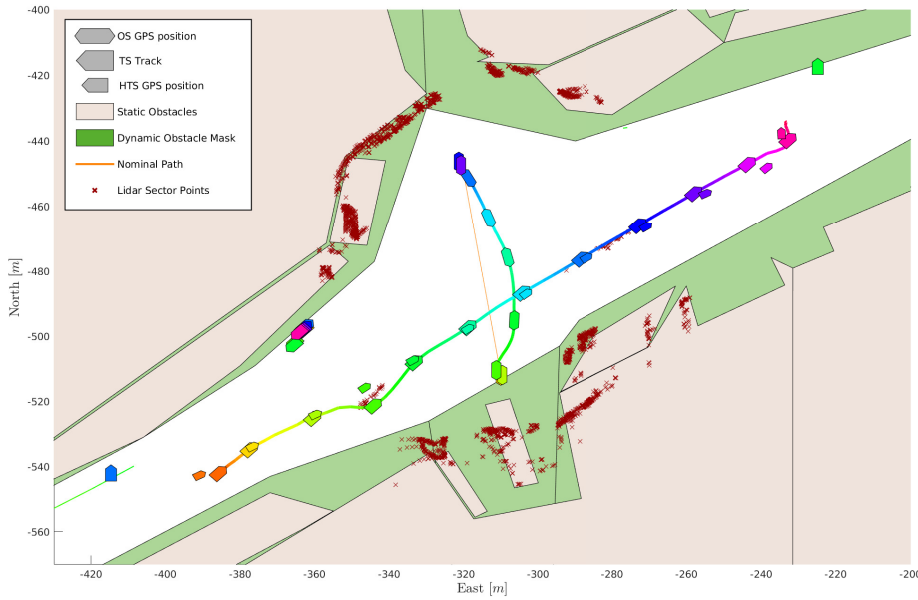

Figure 29: Experiment 3.4: The OS has stand-on obligations, but performs a starboard maneuver to stay clear of the HTS as the HTS fails to abide its give-way duty.

resultant force produced by the thrusters is unaccounted for due to the absence of thruster dynamics in the vessel model. A way to mitigate this problem is to apply a hybrid CBF, where the c_{dyn} gain can be switched based on whether the corresponding domain is in violation or not. By reducing c_{dyn} once the domain is violated, the CBF constraint would require a higher velocity vector pointing out of the domain, and hence reduce the duration that the domain is in violation. Another approach is to apply robust CBFs to mitigate the effect of the uncertainties in the estimations, as proposed in (Cheng et al., 2020).

The proposed COLAV method favours course change maneuvers over speed change maneuvers, due to the dual objective of traversing along the path at transit speed while avoiding collision. Major speed adjustments are only made when traveling with a velocity component in the direction of the nominal path is made impossible by the presence of obstacles, as is the case in Experiment 3.3, where the OS moves in the opposite direction of the path at an early point in the transit. However, the COLREGs does dictate that "if there is sufficient sea-room", alteration of course alone is the preferred action. Furthermore, it is suggested that any alteration of course (or speed) should be of such magnitude that it is readily apparent to other vessels observing visually or by radar. For vessels operating in open waters, and observing each other at distances of several thousand meters, course change maneuvers of more than 60° are advised, as this will increase the chances of observing it by radar. However, for vessels moving in more confined spaces, and at much closer range, such maneuvering efforts might not be feasible, nor necessary in order to be readily apparent, as the proximity and the presence of static obstacles to relate observations to make the maneuvers easier to comprehend. As an example, one can consider Experiment 1.2, where a small course change of about 15 degrees in the narrow canal is sufficient to demonstrate that the OS is maneuvering to its starboard side of the canal to give way for the approaching HTS. However, as can be seen from Fig. 12, when sufficient room to maneuver is present, applying the proposed method does result in course change maneuvers of much higher magnitude in encounters where the OS has give-way obligations.

In all the crossing scenarios, the OS resolves the encounter by maneuvering away from the nominal path to pass either in front of, or behind the HTS. Even though the COLREGs favours course change maneuvers over speed change maneuvers, the maneuver considerably increases the transit length, and the maneuvering effort is large compared to reducing the speed and waiting for the TS to pass before proceeding on the transit. This is a result of the reactive nature of the approach, where it reacts only to the current states, and does not have any means for global optimization. This is mostly relevant for shorter transits, where the relative increase in trajectory length from course change maneuvers is large. This issue can however be mitigated by applying the approach in a hybrid structure, with a long-term trajectory planner capable of adjusting the speed, such as the one in (Thyri et al., 2020b), which is designed specifically for short-transit operations.

From the lidar data in the overview figures, one can get an indication that there is a slowly varying bias in the position estimate of the OS. This is most apparent when comparing the lidar points on the south bank in the eastern part of the canal in Fig. 21 and Fig. 24, where the lidar sector points are in the water in the first figure, and several meters inside the polygon representing the canal bank in the second figure. This navigation error is outside the limits of the RTK GPS precision, and seems to arise from the GPS system failing to maintain a link with the RTK antenna during several of the experiments, and hence fall back on a standard GPS solution. Although the navigation bias can be compensated for by for example lidar-based SLAM algorithms, the risk of navigation errors and failure will always exists. This highlights the need for a COLAV method for static obstacles that are based on exteroceptive sensors which provide obstacle position estimates relative to the position of the OS, and hence is unaffected by navigation errors.

Lastly, note the number of static obstacles that are detected in vicinity to the OS during a transit, but is not represented in the map data, such as the obstacle halting the transit in Fig. 28, which in reality is two thick wooden poles tied together with a sign on the top, and the object to the southwest in Fig. 22 that has the shape of the hull of a boat, is actually the hull of a boat, as can be seen from the drone footage in Fig. 1 taken from the north side of the canal. These objects effectively occupy relatively large parts of the free space from the map data, which again highlights the importance of a reactive COLAV module based on exteroceptive sensors. However, for a more robust solution, the map for static obstacles should be continuously updated, based on new sensor data, to include unmapped static features such as sea markings, poles and harbours, and temporarily or quasi-static features such as docked vessels and floating harbours. By applying such an approach, superior estimates of r_{free} can be made.

9 Conclusion and future work

A domain-based reactive COLAV method has been presented, where the method is made compliant with COLREGs rules 13-15 and 17 through a novel target ship (TS) domain design. The TS domain is parameterized by a few rule-based parameters, and the domain size is adaptive, and based on the available space to maneuver around the TS at CPA. The rule-based parameters of the TS domains are determined by a COLREGs-based classification of each vessel-to-vessel encounter, where we propose improvements to an existing encounter classification method. Violation of the TS domains and domains for static obstacles is avoided by formulating control barrier functions for each domain.

The effectiveness of the TS domain is demonstrated through an extensive set of simulations of V2V encounters where the TS keeps a constant course and speed. The proposed COLAV method produces both protocol compliant and well-behaved trajectories for a vast majority of the simulations, and avoids collision in a compliant manner in all simulations. The method is

also demonstrated through simulation of complex scenarios, with multiple autonomous vessels operating in a confined area. In these simulations, the method proves to be robust, where the adaptive domain size effectively distributes the available space between the vessels to ensure safe conduct.

Lastly, the method is demonstrated through several full-scale experiments in a relevant environment with a controlled TS. In the experiments, a target tracker based on radar and lidar is applied for estimating the position and velocity of target ships. Additionally, lidar is used to compensate for uncertainty in map data for COLAV wrt. static obstacles. The proposed method shows good performance in combination with a realistic target tracking system, and handles all encounters in a COLREGs-compliant manner. By including lidar for COLAV wrt. static obstacles, risks associated with unmapped obstacles and uncertainties in map data, navigation and target tracking can be mitigated, and the baseline safety of the method can be ensured.

Future work includes:

- Applying the TS domain to a model predictive controller in a deliberate mid-level COLAV module, to improve performance w.r.t. Rule 8 regarding early action, and also to reduce the effect of the stagnation points of the TS domain, and improve the tradeoff between course change maneuvers and speed change maneuvers.
- More extensive simulation-based verification of the method in multi-vessel encounters.
- Further work on the encounter classification through improved intent inference.
- Pairing the proposed reactive COLAV method with a deliberate planner that considers a complementing subset of the COLREGs, in particular trajectory planning wrt. local traffic regulations, and adapting the velocity to ensure safe conduct when vessels are approaching in confined waters.

Acknowledgments

This work was supported by the NTNU Digital transformation project Autoferry and the Research Council of Norway through the Centres of Excellence funding scheme, project no. 223254. The authors would like to thank Erik Wilthil for his contribution to the experiments, both as crew member on the milliAmpere, and for providing the target tracker.

References

Ames, A. D., Coogan, S., Egerstedt, M., Notomista, G., Sreenath, K., and Tabuada, P. (2019). Control barrier functions: Theory and applications. In *Proceedings of the 2019 18th European Control Conference (ECC)*, pages 3420–3431, Naples, Italy.

Atallah, M. J., Ribeiro, C. C., and Lifschitz, S. (1991). Computing some distance functions between polygons. *Pattern Recognition*, 24(8):775–781.

Basso, E. A., Thyri, E. H., Pettersen, K. Y., Breivik, M., and Skjetne, R. (2020). Safety-critical control of autonomous surface vehicles in the presence of ocean currents. In *Proceedings of the 2020 4th IEEE Conference on Control Technology and Applications (CCTA)*, pages 396–403, Montreal, Canada.

Benjamin, M. R., Leonard, J. J., and Newman, P. M. (2006). A method for protocol-based collision avoidance between autonomous marine surface craft. *Journal of Field Robotics*, 25(5):333–346.

Blenkey, N. (2021). Kongsberg gets EU funding to demo two autonomous vessels. *Marine Log.*

Cairns, R. (2021). Norway pioneered electric ferries. Now it's making them self-driving. *CNN Travel.*

Cheng, R., Khojasteh, M. J., Ames, A. D., and Burdick, J. W. (2020). Safe multi-agent interaction through robust control barrier functions with learned uncertainties. In *Proceedings of the 2020 59th IEEE Conference on Decision and Control (CDC)*, pages 777–783, Jeju Island, Republic of Korea.

Cockcroft, A. N. and Lameijer, J. N. F. (2012). *Guide to the Collision Avoidance Rules.* Butterworth-Heinemann.

Eriksen, B.-O. H., Bitar, G., Breivik, M., and Lekkas, A. M. (2020). Hybrid collision avoidance for ASVs compliant with COLREGs rules 8 and 13–17. *Frontiers in Robotics and AI*, 7:11.

Eriksen, B.-O. H. and Breivik, M. (2019). Short-term ASV collision avoidance with static and moving obstacles. *Modeling, Identification and Control*, 40:177–187.

Eriksen, B.-O. H., Breivik, M., Wilthil, E., Flaten, A., and Brekke, E. (2019). The branching-course model predictive control algorithm for maritime collision avoidance. *Journal of Field Robotics*, 36:1222–1249.

Fossen, T. I. (2011). *Handbook of Marine Craft Hydrodynamics and Motion Control.* John Wiley & Sons.

Goodwin, E. M. (1975). A statistical study of ship domains. *Journal of Navigation*, 28(3):328344.

Huang, Y., Chen, L., Chen, P., Negenborn, R. R., and van Gelder, P. (2020). Ship collision avoidance methods: State-of-the-art. *Safety Science*, 121:451–473.

Kartverket (2020). Kartkatalogen. *https://kartkatalog.geonorge.no/.*

Kufoalor, D. K. M., Wilthil, E., Hagen, I. B., Brekke, E. F., and Johansen, T. A. (2019). Autonomous COLREGs-compliant decision making using maritime radar tracking and model predictive control. In *Proceedings of the 2019 18th European Control Conference (ECC)*, pages 2536–2542, Naples, Italy.

Kuwata, Y., Wolf, M. T., Zarzhitsky, D., and Huntsberger, T. L. (2014). Safe maritime autonomous navigation with COLREGs, using velocity obstacles. *IEEE Journal of Oceanic Engineering*, 39(1):110–119.

Loe, Ø. A. G. (2008). Collision avoidance for unmanned surface vehicles. Master's thesis, Norwegian University of Science and Technology, Trondheim, Norway.

Martinsen, A. B., Bitar, G., Lekkas, A. M., and Gros, S. (2020). Optimization-based automatic docking and berthing of ASVs using exteroceptive sensors: Theory and experiments. *IEEE Access*, 8:204974–204986.

O'Dwyer, R. (2021). ASKO to build two autonomous vessels for Oslo fjord operations. *Smart Maritime Network.*

Pedersen, A. A. (2019). Optimization based system identification for the milliAmpere ferry. Master's thesis, Norwegian University of Science and Technology (NTNU), Trondheim, Norway.

Schuster, M., Blaich, M., and Reuter, J. (2014). Collision avoidance for vessels using a low-cost radar sensor. *IFAC Proceedings Volumes*, 47(3):9673–9678. 19th IFAC World Congress.

Shah, B. C., vec, P., Bertaska, I. R., Sinisterra, A. J., Klinger, W., von Ellenrieder, K., Dhanak, M., and Gupta, S. K. (2016). Resolution-adaptive risk-aware trajectory planning for surface vehicles operating in congested civilian traffic. *Autonomous Robots*, 40:1139–1163.

Stensvold, T. (2020). Trondheim første by med autonom passasjertransport på vannet - Oslo kan bli neste. *Teknisk Ukeblad*.

Svec, P., Shah, B. C., Bertaska, I. R., Alvarez, J., Sinisterra, A. J., von Ellenrieder, K., Dhanak, M., and Gupta, S. K. (2013). Dynamics-aware target following for an autonomous surface vehicle operating under COLREGs in civilian traffic. In *Proceedings of the 2013 IEEE/RSJ International Conference on Intelligent Robots and Systems*, pages 3871–3878.

Tam, C. and Bucknall, R. (2010). Collision risk assessment for ships. *Journal of Marine Science and Technology*, 15:257–270.

Thyri, E. H., Basso, E. A., Breivik, M., Pettersen, K. Y., Skjetne, R., and Lekkas, A. M. (2020a). Reactive collision avoidance for ASVs based on control barrier functions. In *Proceedings of the 2020 4th IEEE Conference on Control Technology and Applications (CCTA)*, pages 380–387, Montreal, QC, Canada.

Thyri, E. H., Breivik, M., and Lekkas, A. M. (2020b). A path-velocity decomposition approach to collision avoidance for autonomous passenger ferries in confined waters. In *Proceedings of the 20th IFAC World Congress*, pages 14628–14635, Berlin, Germany.

Torben, T. R., Brodtkorb, A. H., and Sørensen, A. J. (2019). Control allocation for double-ended ferries with full-scale experimental results. *IFAC-PapersOnLine*, 52(21):45–50. 12th IFAC Conference on Control Applications in Marine Systems, Robotics, and Vehicles (CAMS), Daejeon, South Korea.

Vagale, A., Bye, R. T., Oucheikh, R., Osen, O. L., and Fossen, T. (2021a). Path planning and collision avoidance for autonomous surface vehicles II: A comparative study of algorithms. *Journal of Marine Science and Technology*, pages 1–17.

Vagale, A., Oucheikh, R., Bye, R., Osen, O., and Fossen, T. (2021b). Path planning and collision avoidance for autonomous surface vehicles I: A review. *Journal of Marine Science and Technology*, pages 1–15.

Wilthil, E. F., Brekke, E., and Asplin, O. B. (2018). Track initiation for maritime radar tracking with and without prior information. In *Proceedings of the 2018 21st International Conference on Information Fusion (FUSION)*, pages 1–8, Cambridge, UK.

Wilthil, E. F., Flåten, A. L., and Brekke, E. F. (2017). *A Target Tracking System for ASV Collision Avoidance Based on the PDAF*, pages 269–288. Springer International Publishing, Cham.

Woerner, K. (2016). *Multi-Contact Protocol-Constrained Collision Avoidance for Autonomous Marine Vehicles*. PhD thesis, Massachusetts Institute of Technology.

Paper E Partly COLREGs-compliant collision avoidance for ASVs using encounter-specific velocity obstacles

Published paper by E. H. Thyri and M. Breivik. "Partly COLREGs-compliant collision avoidance for ASVs using encounter-specific velocity obstacles". In: *Proceedings of the 14th IFAC Conference on Control Applications in Marine Systems, Robotics, and Vehicles (CAMS) 2022*. Copenhagen, Denmark, 2022.

Bibliography entry [27].

Partly COLREGs-compliant collision avoidance for ASVs using encounter-specific velocity obstacles

Emil H. Thyri * **Morten Breivik** *

* *Centre for Autonomous Marine Operations and Systems (AMOS), Department of Engineering Cybernetics, Norwegian University of Science and Technology (NTNU). NO-7491 Trondheim, Norway. (e-mail: emil.h.thyri@ntnu.no, morten.breivik@ieee.org)*

Abstract: A velocity obstacle (VO) based collision avoidance method for autonomous surface vessels operating in restricted and unstructured environments with traffic is considered. We propose a novel VO for enforcing maneuvering compliance with rules 13-15 and 17 in the International Regulations for Preventing Collisions at Sea (COLREGs), where the vessel-to-vessel encounter is first classified w.r.t. the COLREGs, then an encounter-specific domain is assigned to the opposing vessel, and finally a VO for that domain is formulated. The maneuvers of the opposing vessel throughout the encounter is considered when evaluating which side is appropriate to pass the vessel on. This increases robustness to non-compliant behaviour by the opposing vessel. The domain size is determined based on a measure for the available space to maneuver, which ensures an appropriate separation of the vessels in both confined spaces and open waters. Furthermore, collision avoidance with static obstacles from electronic charts is included, where a convex set that is free of static obstacles is constructed to simplify complex geometries, and the boundary of the set is enforced by VOs. The performance of the proposed collision avoidance method is demonstrated through numerical simulation, where it show compliance with COLREGs rules 13-15 and 17. Furthermore, the novel VO shows improved COLREGs compliance compared to another popular COLREGs-specific VO.

Keywords: Collision avoidance, autonomous surface vessel, velocity obstacle, COLREGs

1. INTRODUCTION

As the potential potential for autonomous systems becomes apparent in the automotive and aviation sectors, the maritime domain is also exploring solutions for increasing efficiency and safety in current operations through autonomy technology. Such technology can also enable new types of operations by reducing operational costs, such as small-scale urban passenger ferries (Reddy et al., 2019).

Maneuvering of autonomous surface vessels (ASVs) in high-traffic and confined area operations, such as urban areas, harbours, and canals, requires a reactive maneuvering and collision avoidance (COLAV) system capable avoiding collision with other vessels and static obstacles. In this work, we consider the task of collision-free maneuvering of ASVs in such domains by the velocity obstacle (VO) algorithm.

The VO algorithm, invented by Fiorini and Shiller (1993), is a popular approach to COLAV in dynamic environments. It was developed for land robots, but has later been applied to aviation (Jenie et al., 2015), maritime (Huang et al., 2018), and underwater applications (Zhang et al., 2017). The method consist of representing obstacles as VOs in the velocity space of the system to be controlled, where velocities within the VOs will result in a collision at some point if assuming constant relative velocity. After representing all obstacles in a velocity space, COLAV becomes reduced to selecting a velocity outside the VOs.

The performance and simplicity of the VO algorithm has made it popular in COLAV research. In (Wilkie et al., 2009), a generalized VO (GVO) is proposed, where dynamical constraints are considered in the VOs. A reciprocal VO (RVO) is proposed by van den Berg et al. (2008) to account for cooperative behaviour by opposing vessels.

As with automotive and aerial vehicles, maritime vessels are also subject to regulations. In particular, the International Regulations for Preventing Collisions at Sea (COLREGs), is a set of rules that apply to all vessels upon the high seas. The COLREGs give a common understanding of the social conduct at sea, and hence enable vessels to maneuver in proximity to each other with minimal risk of collision. In particular, part B of the regulations considers conduct when in presence of other vessels. The rules in part B describe how to distribute the responsibility and interpret the maneuvering obligation of each vessel involved in an encounter. A COLAV method for ASVs must consider these regulations.

In (Kuwata et al., 2014), the VO algorithm is applied for ASV collision avoidance. Furthermore, the authors

⋆ This work was supported by the NTNU Digital transformation project Autoferry and the Research Council of Norway through the Centres of Excellence funding scheme, project no. 223254.

propose a VO denoted $VO^{\mathcal{K}}$ for COLREGs-aware maneuvering. They evaluate the risk of collision based on distance at closest point of approach (DCPA) and time to closest point of approach (TCPA) for each vessel, and subsequently classify the vessel-to-vessel (V2V) encounter w.r.t. COLREGs to determine the maneuvering obligations of the ASV. If a risk of collision is present, and the ASV has give-way obligations, they apply the $VO^{\mathcal{K}}$, which covers all velocities that result in passing other the vessel starboard to starboard with a decreasing range.

The $VO^{\mathcal{K}}$ is later applied by several others, like (Kufoalor et al., 2018), where an assessment of the level of cooperative behaviour between encountering vessels is considered in the RVO framework, and (Zhao et al., 2016), where evidential reasoning is applied to evaluate the risk of collision, and (Cho et al., 2019), where collision risk is evaluated by DCPA and TCPA estimates, and the COLREGs VO is enforced as a soft constraint, and (Shaobo et al., 2020), where GVO is applied to consider the dynamic constraints of large vessels, and risk of collision is evaluated by a fuzzy-logic system. Furthermore, (Shaobo et al., 2020) also proposes a finite state machine (FSM) to monitor interactive actions by other vessels during a maneuver, enabling re-evaluations if the maneuver is not effective.

These methods apply a measure of collision risk to evaluate the need for the COLREGs-specific VO, where they propose distinct methods for evaluating this risk of collision for large vessels moving in unrestricted waters. In confined area-operations with high traffic, highly maneuverable vessels, and unstructured traffic, evaluating the risk of collision is challenging. Furthermore, enforcing COLREGs by restricting all velocities passing on the port side of a vessel can be over-restrictive, and does not adapt well to the immediate maneuvering of other vessels. Alternatively, in (Cho et al., 2019), $VO^{\mathcal{K}}$ is enforced as a soft constraint in the objective function. This is however not optimal since it enables non-compliant maneuvers if it gives sufficient increase in performance w.r.t. other objectives.

Furthermore, in confined areas, the available space to maneuver should be considered when determining the minimum DCPA to other vessels. This is critical to avoid over-restricting the velocity space in very confined areas while also ensuring an appropriate separation in open waters. This aspect has not been sufficiently considered in the previous work.

The contribution of this paper is a novel method for constructing a VO that ensures reactive collision-free maneuvering of ASVs in restricted areas with unstructured traffic. The proposed VO enforces partly COLREGs-compliant maneuvering without estimating the risk of collision. It is constructed by assigning an extended domain to the dynamic obstacle, and subsequently formulating the VO w.r.t. that domain. Consideration to what side of the obstacle vessel that the ASV should pass on is made, and adapting to contingency maneuvers by the opposing vessel is inherent to the method. The domain size is scaled to match the available space to maneuver, which ensures a suitable minimum DCPA in both open sea and very confined areas. Furthermore, we also propose a method for considering COLAV with static obstacles that is ignorant of the complexity of the obstacle geometry. The proposed method is demonstrated through a variety of numerical simulations, and it is compared to the performance of the $VO^{\mathcal{K}}$ from Kuwata et al. (2014).

The remainder of this paper is structured as follows: In Section 2, the velocity obstacle algorithm is introduced. In Section 3, we introduce the COLREGs and propose a novel VO that ensures compliance with a relevant subset of the regulations. In Section 4, the method is demonstrated by numerical simulations, and its performance is discussed. Finally, Section 5 concludes the paper and proposes future work.

2. VELOCITY OBSTACLES

In this section, we introduce the velocity obstacle algorithm as described in (van den Berg et al., 2008). Let A be a vessel where its domain is denoted $\mathcal{A}$, and let B be a dynamic obstacle moving in the plane where its domain is denoted $\mathcal{B}$. For the work presented here, we apply circular domains to the vessels so that $\mathcal{A}$ and $\mathcal{B}$ are circles with radius $r_A > 0$ and $r_B > 0$ respectively. Let $\boldsymbol{p}_A \in \mathbb{R}^2$ and $\boldsymbol{p}_B \in \mathbb{R}^2$ denote the current positions of A and B, respectively, and let $\boldsymbol{v}_B \in \mathbb{R}^2$ be the velocity of B.

It follows that the velocity obstacle for A induced by B, denoted $VO_{A|B}(\boldsymbol{v}_B)$, is the set of velocities $\boldsymbol{v}_A \in \mathbb{R}^2$ that will result in a collision between A and B at some time $t \in [0, \tau_{VO}]$, assuming B maintains a constant velocity $\boldsymbol{v}_B$.

Furthermore, let

$$\mathcal{A} \oplus \mathcal{B} = \{\boldsymbol{a} + \boldsymbol{b} | \boldsymbol{a} \in \mathcal{A}, \boldsymbol{b} \in \mathcal{B}\}, \tag{1}$$

be the Minkowski sum of the sets $\mathcal{A}$ and $\mathcal{B}$, and let

$$\lambda(\boldsymbol{p}, \boldsymbol{v}) = (\boldsymbol{p} + t\boldsymbol{v} \mid t < \tau_{VO}), \tag{2}$$

be a line representing the predicted trajectory up to some time τ_{VO}, for a point starting in $\boldsymbol{p}$ at $t = 0$ with constant velocity $\boldsymbol{v}$. Then, the VO from B in the velocity space of A is defined as

$$VO_{A|B}(\boldsymbol{v}_B) := \{\boldsymbol{v}_A | \lambda(\boldsymbol{p}, \boldsymbol{v}_A - \boldsymbol{v}_B) \cap \mathcal{B} \oplus -\mathcal{A} \neq \emptyset\}, \tag{3}$$

where any $\boldsymbol{v}_A \in VO_{A|B}(\boldsymbol{v}_B)$ will lead to a collision between A and B at some time $t < \tau_{VO}$, and if $\boldsymbol{v}_A \notin VO_{A|B}(\boldsymbol{v}_B)$, then A and B will not collide, assuming both vessels maintain their velocity.

3. COLREGS-COMPLIANT VELOCITY OBSTACLE

In this section, we formulate a novel VO that includes COLREGs considerations by assigning a second domain $\mathcal{C}_{A|B}$, to B if the COLREGs dictate that A is obliged to maneuver such as to not impede the free passage of B. The domain $\mathcal{C}_{A|B}$ is designed specifically for the V2V encounter between A and B, and is a function of the geometry and relative velocity of the encounter, and the COLREGs encounter type.

The VO in the velocity space of A resulting from $\mathcal{C}_{A|B}$ is defined as

$$VO^{\mathcal{C}}_{A|B}(\boldsymbol{v}_B) := \left\{\boldsymbol{v}_A | \lambda(p, \boldsymbol{v}_A - \boldsymbol{v}_B) \cap \mathcal{C}_{A|B} \neq \emptyset\right\} \tag{4}$$

The design of $\mathcal{C}_{A|B}$ is motivated by the novel target ship domain proposed in (Thyri and Breivik, 2022), where the boundary of the domain is a line, and hence the domain is a half-plane in $\mathbb{R}^2$. In Fig. 1, the proposed domain $\mathcal{C}_{A|B}$

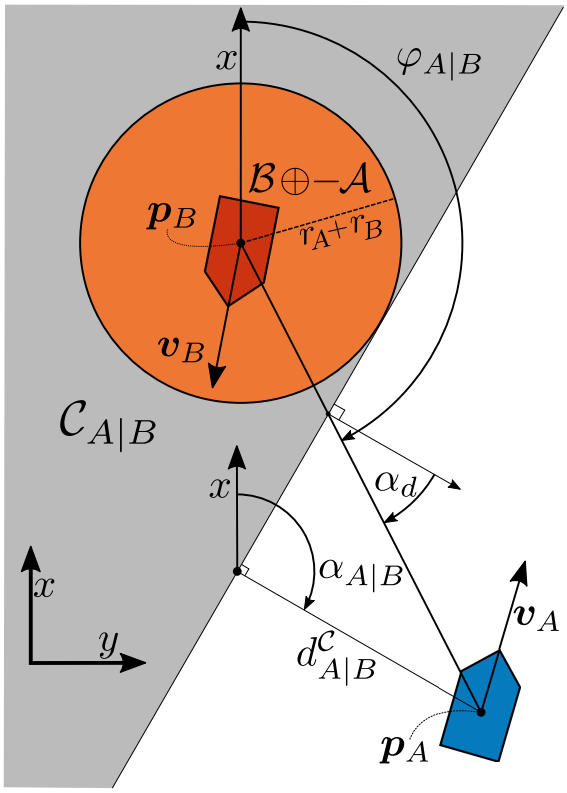

Fig. 1. The set $\mathcal{C}_{A|B}$ for an encounter between the vessels A and B. The set is defined by its orientation, given by $\alpha_{A|B}$ and the distance from $\boldsymbol{P}_A$ to the domain boundary, given by $d^{\mathcal{C}}_{A|B}$.

is illustrated for an arbitrary geometry between A and B. The domain line is defined by the orientation of the normal vector of the domain boundary, denoted $\alpha_{A|B}$, and the minimum distance from $\boldsymbol{p}_A$ to the domain boundary, denoted $d^{\mathcal{C}}_{A|B}$.

In the following, the details for determining the parameters of the encounter-specific COLREGs domain are given. The process consists of the following steps:

(1) Classify the V2V encounter w.r.t. COLREGs
(2) Determine the preferred side for A to pass B
(3) Determine orientation of and distance to $\mathcal{C}_{A|B}$

3.1 COLREGs classification

The COLREGs classification is done to determine the encounter type between two vessels, and hence which of the encounter-type specific rules that apply to the ASV. The encounter types between A and B, and the corresponding rule that applies to A are shown in Fig. 2. The criteria for the classification are given in the COLREGs, and the classification comes down to calculating the relative bearings between the vessels, and comparing them to entry-criteria for each encounter type. In this work, the classification method by Thyri and Breivik (2022) is applied, where in addition to classifying an encounter between two vessels, a

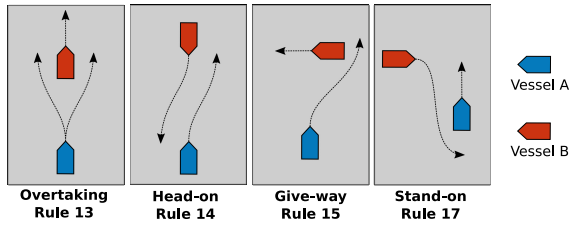

Fig. 2. COLREGs encounter types from the viewpoint of vessel A.

state machine is applied to hold the classification until the encounter is resolved. The state machine ensures that the responsibility of the involved vessels does not change as a result of the maneuvering of the vessels. The classification method determines the encounter to be one of the following categories: Head-on (HO), give-way (GW), overtaking on port side (OT_p), overtaking on starboard side (OT_s), stand-on (SO) or safe (SF).

3.2 Passing port or starboard

Determining what side of B that A should pass on is an important distinction in the COLREGs. For this, we apply the bearing of A from B

$$\varphi_{A|B} = atan2((y_A - y_B), (x_A - x_B)) \tag{5}$$

relative to the threshold value

$$\alpha_s = \begin{cases} \alpha_{v\_B|A} + \alpha_{\delta\_s}, & \text{if encounter type} \in \{GW, HO, OT_p\} \\ \alpha_{v\_B|A} - \alpha_{\delta\_s}, & \text{if encounter type} \in \{OT_s\} \end{cases} \tag{6}$$

where $\alpha_{\delta\_s} > 0$ ensures a bias towards maneuvering to the rules-compliant side, and $\alpha_{v\_B|A} \in [0, 2\pi)$ is the angle of the relative velocity vector

$$\boldsymbol{v}_{B|A} = \boldsymbol{v}_B - \boldsymbol{v}_A. \tag{7}$$

For A to pass with B on its port side is preferred if $\varphi_{A|B} \leq \alpha_s$, and for A to pass with B on its starboard side is preferred if $\varphi_{A|B} > \alpha_s$. This distinction explicitly accounts for maneuvers by B throughout the encounter by considering $\boldsymbol{v}_B$ in (7).

3.3 COLREGs VO Orientation

When the side at which to pass B is determined, the orientation of the COLREGs-specific domain $\mathcal{C}_{A|B}$ can be defined as

$$\alpha_{A|B} := \begin{cases} \varphi_{A|B} + \alpha_d, & \text{if } \varphi_{A|B} > \alpha_s, \\ \varphi_{A|B} - \alpha_d, & \text{else.} \end{cases} \tag{8}$$

where $\alpha_d \in (-\pi/2, \pi/2)$ is the deflection angle. The deflection angle rotates the domain boundary to be more obstructive for velocities passing on the non rules-compliant side of B. Finally, the distance to the domain is given by

$$d^{\mathcal{C}}_{A|B} := cos(\alpha_{A|B})||\boldsymbol{p}_A - \boldsymbol{p}_B||_2 - (r_A + r_B)\,. \tag{9}$$

The behaviour of the method is dependent on the values of r_A and r_B, as these parameters set the threshold for the minimum DCPA. For vessels maneuvering in confined areas, the acceptable DCPA is very much dependent on the available space to maneuver. Values for r_A and r_B that give an acceptable DCPA in semi-open waters could result in a blocked passage in more confined waters. Similarly, an

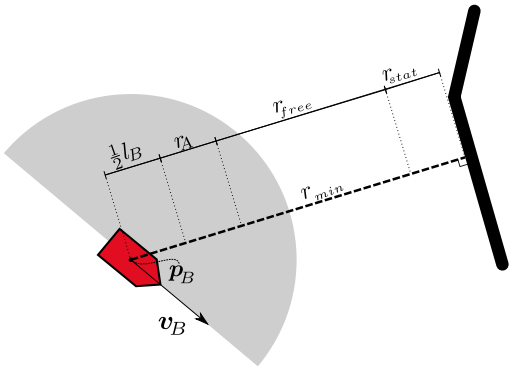

Fig. 3. Vessel B in the presence of a static obstacle given by the thick black line. The free space to maneuver r_{free} as a function of the distance r_{min} to the closest static obstacle on the side of the dynamic obstacle B that vessel A should pass, indicated by the grey sector.

acceptable DCPA in confined waters can in many cases be considered so low as to be termed misconduct in more open waters.

To mitigate this, a dynamic domain size is proposed for B, where r_B is a function of the available space to maneuver for A when passing B. The available space to maneuver is approximated by the free distance $r_{free} > 0$, which is determined by first searching the map data to find the shortest distance $r_{min} > 0$ to any static obstacle on the side of B that A should pass, and then subtracting the minimum margins for dynamic and static obstacles. The free distance is defined as

$$r_{free} := r_{min} - 0.5l_B - r_A - r_{stat}, \tag{10}$$

where $l_B > 0$ is the length of B, $r_{stat} = r_A + \delta_{stat}$ and $\delta_{stat} > 0$ is a margin to static obstacles. This is illustrated in Fig. 3. Furthermore, by saturation, we ensure that $r_{free} \in [0, r_{free\_max}]$. The size of B is then defined as

$$r_B := 0.5l_B + k_l r_{free} \tag{11}$$

where $k_l \in (0, 1)$ is a factor dividing the free space between B and the static obstacle.

3.4 Stand-on encounters

If the encounter type is one of HO, GW, OT_p or OT_s, COLREGs-specific VOs are formulated. If the encounter type is SO, A has stand-on obligations while it is B that is obliged to give-way. However, if B does not comply with its give-way obligation, A is obliged to take action to avoid collision. This is addressed by not assigning a COLREGs-specific VO to B in SO encounters, but still include the traditional VOs in (3) with $\tau_{SO} = 0.5\tau_{VO}$ instead of τ_{VO} in (2), allowing A to maneuver at a later point if B fails to give-way.

3.5 Static obstacles

In confined waters, the presence of static obstacles can limit the set of available maneuvers. Therefore, the static obstacles must also be represented in the velocity space of A. A common approach is to represent static obstacles by circular domains. However, in areas where the density of static obstacles is high, or the geometry of the obstacles is not easily approximated by circles, the number of VOs from static obstacles can become high. To mitigate this, we propose to construct a convex set $\mathcal{S}$ that is free of static obstacles, where $\boldsymbol{p}_A \in \mathcal{S}$. This allows for only considering each edge in $\mathcal{S}$ as a static obstacle, and still ensure COLAV with all static obstacles. In constructing $\mathcal{S}$, we apply the method from (Thyri and Breivik, 2022), where the area around $\boldsymbol{p}_A$ is segmented into n_{edge} equally sized sectors, and subsequently, the closest point on any static obstacle in each sector is found. Then, a line going through that point is defined, and the set of lines is combined to construct the convex set $\mathcal{S}$ which will have at most n_{edge} edges. When defining the line passing through the closest point in each sector, the normal vector to the line is calculated to be normal to an ellipse centered at $\boldsymbol{p}_A$ with its major axis aligned with the desired course for A, as proposed by Martinsen et al. (2020). This gives a set $\mathcal{S}$ that is stretched out it the desired direction of travel, which then reduces the risk of over-restricting the velocity space of A when the waters are very confined. The effect of this is demonstrated in Fig. 4 for a vessel in a narrow channel. The VOs resulting from static obstacles is then defined as

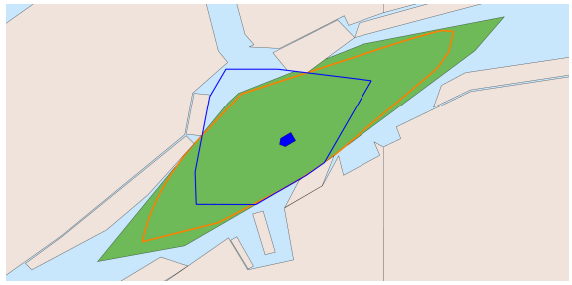

Fig. 4. Convex free set $\mathcal{S}$ for the blue vessel. The green set is for $n_{edge} = 12$, while the orange boundary is for $n_{edge} = 2000$. The figure indicates that $n_{edge} = 12$ gives a good approximation. The blue boundary also has $n_{edge} = 12$, however, the method of orienting the edges to be tangential to an ellipse is not applied, and hence the resulting convex set is more restricted in the desired direction of travel.

$$VO_{A|\mathcal{S}} := \{\boldsymbol{v}_A | \lambda(\boldsymbol{p}_A, \boldsymbol{v}_A) \cap \mathcal{S}^c \neq \emptyset\} \tag{12}$$

where $\mathcal{S}^c$ is the complement of $\mathcal{S}$. Furthermore, we apply τ_{stat} instead of τ_{VO} in (2) when defining $VO_{A|\mathcal{S}}$, to set different thresholds for the speed at which A is allowed to approach static and dynamic obstacles.

3.6 Optimal course and speed

In selecting the optimal course and speed, we apply the cost function

$$J(\chi, U) = K_U \|U - U_d\| + \|\chi - \chi_d\|, \tag{13}$$

where $\chi_d \in (-\pi, \pi]$ and $U_d \geq 0$ are the desired course and speed respectively, and $K_U > 0$ is a gain that weights deviation from the desired speed relative to the deviations from the desired course.

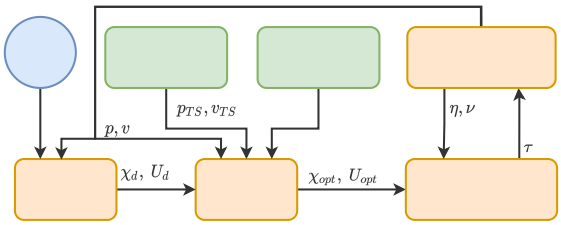

Fig. 5. Pipeline for simulations. The desired transit path is given by a set of waypoint. The guidance module calculates course and speed references, while the VO algorithm calculates the optimal collision-free course and speed.

4. SIMULATIONS

In this section, the simulator setup and numerical results are presented. The results are presented in two sets: A large set of simulations to validate the COLREGs compliance of the proposed VO in V2V encounters, and a set of more complex simulations to demonstrate the versatility of the proposed method.

4.1 Simulator

The simulator setup is shown in Fig. 5. We apply a 3DOF vessel model on the form

$$\begin{aligned} \dot{\boldsymbol{\eta}} &= \boldsymbol{R}(\psi)\boldsymbol{\nu} \\ \dot{\boldsymbol{\nu}} &= \boldsymbol{M}^{-1}\left(\boldsymbol{\tau} - (\boldsymbol{C}(\boldsymbol{\nu}) + \boldsymbol{D}(\boldsymbol{\nu}))\,\boldsymbol{\nu}\right) \end{aligned} \tag{14}$$

where $\boldsymbol{\eta} = [x, y, \psi]^\mathsf{T}$ is the vector containing the position and heading of a vessel in a NED frame, and $\boldsymbol{\nu} = [u, v, r]^\mathsf{T}$ is the vector containing the velocities and yaw rate of the vessel in the body frame (Fossen, 2011). Furthermore, $\boldsymbol{M}$ is the vessel inertia matrix including hydrodynamically-added mass, $\boldsymbol{C}(\boldsymbol{\nu})$ is the Coriolis-centripetal matrix, $\boldsymbol{D}(\boldsymbol{\nu})$ is the damping matrix, $\boldsymbol{\tau} \in \mathbb{R}^3$ represents the generalized forces produced by the actuators, and $\boldsymbol{R}(\psi)$ is the rotation matrix as a function of the vessel heading ψ. The model parameters are taken from (Pedersen, 2019).

The guidance module inputs a set of waypoints with corresponding speed references, as well as the vessel position and velocity, and outputs a desired course and speed, denoted χ_d and U_d, respectively. When calculating χ_d, a LOS guidance method method is first applied to find a reference course

$$\chi_{LOS} = \theta - \text{atan}\left(\frac{e_{cross\_track}}{\Delta_{lookahead}}\right) \tag{15}$$

which gives convergence to the reference path. Here, θ is the course of the reference path, e_{cross_track} is the cross track error of $\boldsymbol{p}$ from the path, and $\Delta_{lookahead} > 0$ is the lookahead distance. Furthermore, the desired course is calculated by

$$\chi_d = \chi + \Delta_t r_d \tag{16}$$

where χ is the current course, Δ_t is the run-period of the VO algorithm, and

$$r_d = \frac{1}{\tau_\chi}\left(\chi_{LOS} - \chi\right) \tag{17}$$

is the desired yaw rate. The desired yaw rate is saturated so that $r_d \in [r_{d\_min}, r_{d\_max}]$. This guidance method ensures that the vessel converges to the reference path if the velocity space is unrestricted, while facilitating the vessel to deviate from the path in an avoidance maneuver when the velocity space is restricted.

Table 1. Simulation parameters

Parameter	Value	Parameter	Value
τ_{VO}	50 s	r_{free_max}	50 m
τ_{stat}	20 s	k_l	0.50
α_d	$\pi/3$ rad	n_{sect}	12
α_{δ_s}	$\pi/10$ rad	Δ_t	1.0 s
$\Delta_{lookahead}$	100 m	τ_χ	0.2 s
r_{d_min}	-0.5 rad/s	r_{d_max}	0.5 rad/s
r_A	5.00 m	K_U	4.00 s/m
l_B	5.00 m	δ_{stat}	5.00 m

The input to the VO algorithm is the position and velocity of all dynamic obstacles, and a map of the static obstacles. The VO algorithm outputs the optimal course χ_{opt} and velocity reference U_{opt}. The optimal references are passed through a third-order reference filter to produce smooth reference signals for $\boldsymbol{\eta}$ and $\boldsymbol{\nu}$, which are applied in a velocity feed-forward PID controller to calculate a generalized force $\boldsymbol{\tau}$. Lastly, the Matlab ODE45 integrator is applied to integrate (14).

4.2 Batch Simulations

In this section, we present results that demonstrate the proposed VO's ability to produce maneuvers that are compliant with the maneuver-specific rules of the COLREGs from Section 3.1. The simulations are of V2V encounters between vessel A and vessel B, where A is running the proposed VO algorithm, and B keeps a constant velocity throughout the simulation. The results are presented in batches in figures 6-8, where a set of trajectories for A tracking a path in the positive y direction, with a 10 m separation in the x direction are superimposed in each figure. Vessel B has the same trajectory for all simulations in one figure.

Figure 6 shows encounters where A has give-way obligations. In Fig. 6(a), the novel VO that we propose is applied, while in Fig. 6(b), the $VO^{\mathcal{K}}$ is applied [1]. From 6(a), the results demonstrate that when A maneuvers to avoid collision with B, it does so by making a starboard maneuver to give-way and pass behind B, in compliance with Rule 15. In the case when A passes in front of B, it does so with sufficient margin, and, due to the switching orientation of $\mathcal{C}_{A|B}$ introduced by (8), it does not make a port maneuver to avoid close quarters. In comparison, for several of the trajectories in Fig. 6(b), A makes a port maneuver to pass at a sufficient distance in front of B, contrary to Rule 15. This is a result of the $VO^{\mathcal{K}}$, which only covers the velocities that pass on the non-compliant side with decreasing range, and hence allows passing in front as long as the range is maintained by a port maneuver. The $VO^{\mathcal{K}}$ does hence not stay true to the maneuvering principles of the COLREGs, and using it would require an additional VO or COLREGs considerations in the cost function to be able to match the compliance of the VO proposed in this paper. Furthermore, the trajectories in Fig. 6(a) start maneuvering at an earlier stage compared to Fig. 6(b), in particular for encounters where a large avoidance maneuver is required. This is

[1] Results from a large set of simulations with the VO that we propose and $VO^{\mathcal{K}}$ can be found at: `https://studntnu-my.sharepoint.com/:b:/g/personal/emilht_ntnu_no/EcfZpqrxzI9EvRoGfAldLuQB_Lyb5UrMu-9Eu5l5laSqxg?e=8CUWGk`

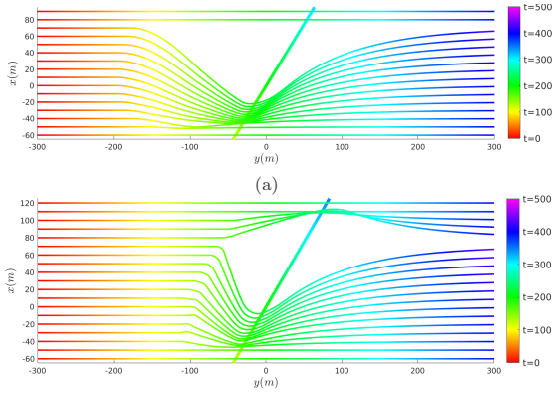

(a)

(b)

Fig. 6. Crossing give-way encounters. a) The proposed VOs for COLREGs is applied. b) The $VO^{\mathcal{K}}$ is applied.

due to the COLREGs-specific VO that we propose, which extends towards A, and comes into effect at an earlier stage when a large maneuver is required.

In Fig 7, head-on encounters are presented. Also in these situations, A makes a starboard maneuver to avoid collision, and pass B port-to-port in compliance with Rule 14.

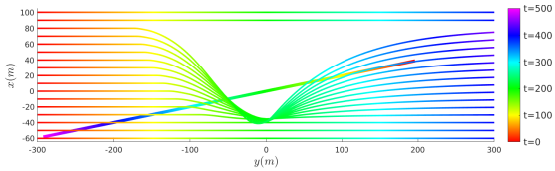

Fig. 7. Batch of head-on encounters.

In Fig. 8, results where A is overtaking B are shown. Due to the relative heading between the vessels, the encounter is classified as OT_s, where A in compliance with Rule 13 overtakes with B on its starboard side to avoid crossing in front of it after the overtaking.

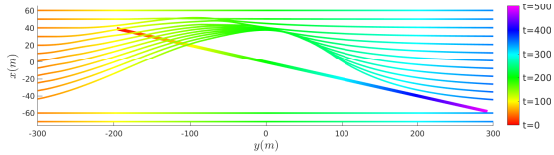

Fig. 8. Batch of overtaking encounters.

4.3 Complex scenarios

In Scenario 1, shown in Fig. 9, three ASVs are maneuvering in a canal area. All vessels run the proposed VO method. ASV 1 is running from right to left, and is in a head-on encounter with ASV 2 and ASV 3. All three vessels resolve the head-on encounters by making a starboard maneuver in compliance with Rule 14. Subsequently, ASV 3 is in an overtaking encounter with ASV 2, which, due to the relative heading of the encounter, is resolved by ASV 3 making a port maneuver to ASV 2 on its port side in accordance with Rule 13. At the same time ASV 2 maintains its speed while tracking its reference path in accordance with Rule 17.

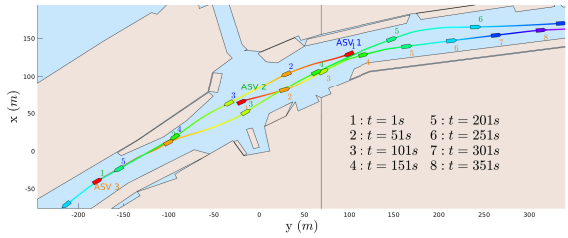

Fig. 9. Scenario 1: Three ASVs encountering each other in a canal area. All vessels run the proposed VO method.

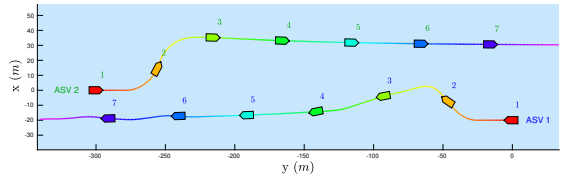

Fig. 10. Scenario 2: Non-compliant Behaviour. Two ASVs in a head-on encounter. ASV 1 runs the proposed VO method. ASV 2 performs a non-compliant port maneuver. The vessels are plotted at 50 s intervals.

In Scenario 2, shown in Fig. 10, ASV 1 and ASV 2 are meeting on a reciprocal course to pass each other starboard to starboard at a small DCPA. ASV 1 runs the proposed VO algorithm while ASV 2 tracks a predefined path. Here, ASV 1 manuevers to starboard to avoid close quarters, in compliance with Rule 14. At the same time, ASV 2 makes a non-compliant port maneuver to increase the DCPA. ASV 1 reacts by making a port maneuver to pass starboard to starboard at a safe distance. This reaction is due to the mechanism described in Section 3.2, where the preferred side at which to pass the opposing vessel is a function of the relative velocity. Hence, the distinction inherently accounts for maneuvers by the opposing vessel.

In Fig. 11, a simulation of 11 vessels running the proposed VO algorithm is presented. The vessels are initiated at the boundary of a 600 m by 600 m square, and follows a reference trajectory along an angle towards the centre of the square plus a random offset $\delta_{rand} \in [-\pi/1.3, \pi/1, 3]$, and at a random velocity uniformly distributed in $[1.25, 2.25]$m/s. All encounters are resolved without collision, and with a minimum DCPA of 35 m. The results demonstrate the proposed method's robustness, and indicate that the proposed VOs for COLREGs are applicable for resolving encounters in other domains with a high vehicle population.

5. CONCLUSIONS AND FUTURE WORK

A novel velocity obstacle (VO) for partly COLREGs-compliant maneuvering for ASVs in the presence of other vessels and static obstacles is proposed. The VO is formulated with respect to a domain assigned to the opposing vessel in a vessel-to-vessel (V2V) encounter. The domain is constructed by first classifying the V2V encounter w.r.t. the COLREGs, and subsequently formulating a domain boundary as a function of the encounter type, encounter geometry, relative velocity, and available space to maneuver. The effect of the novel VO is demonstrated through a set of numerical simulations, where it shows compliance with COLREGs rules 13-15 and 17. Handling of non-

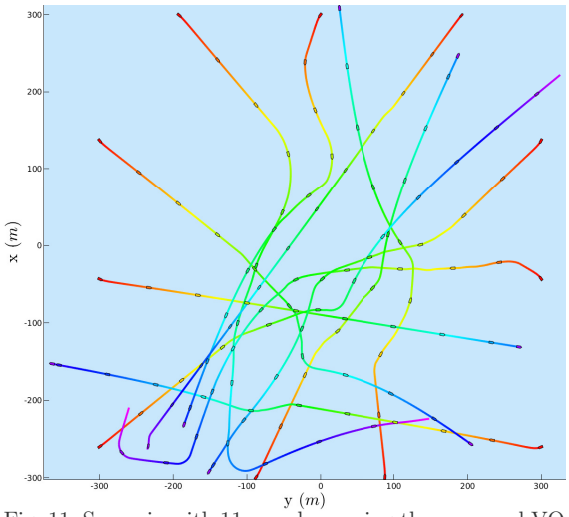

Fig. 11. Scenario with 11 vessels running the proposed VO method.

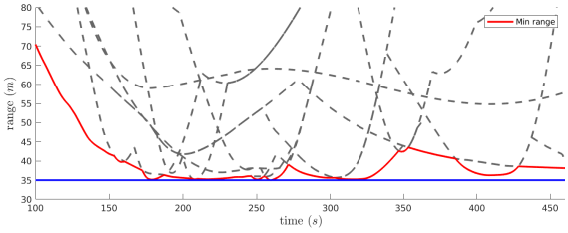

Fig. 12. Minimum range between any two vessels in an encounter with 11 vessels. The blue line indicates the minimum allowable range $r_A + r_B$.

compliant behavior by the other vessel is inherent to the domain, which is demonstrated in a head-on encounter. Furthermore, the proposed VO shows improved compliance with the COLREGs when compared to an existing COLREGs-specific VO. Future work includes further simulation-based verification of the performance of the proposed VO, as well as full-scale experiments.

REFERENCES

Cho, Y., Han, J., Kim, J., Lee, P., and Park, S.B. (2019). Experimental validation of a velocity obstacle based collision avoidance algorithm for unmanned surface vehicles. *IFAC-PapersOnLine*, 52(21), 329–334. doi:https://doi.org/10.1016/j.ifacol.2019.12.328.

Fiorini, P. and Shiller, Z. (1993). Motion planning in dynamic environments using the relative velocity paradigm. In *Proc. IEEE International Conference on Robotics and Automation*, 560–565. doi:10.1109/ROBOT.1993.292038.

Fossen, T.I. (2011). *Handbook of Marine Craft Hydrodynamics and Motion Control*. John Wiley & Sons.

Huang, Y., vanGelder P.H.A.J.M, and Wen, Y. (2018). Velocity obstacle algorithms for collision prevention at sea. *Ocean Engineering*, 151, 308–321. doi:https://doi.org/10.1016/j.oceaneng.2018.01.001.

Jenie, Y.I., Kampen, E.J.v., de Visser, C.C., Ellerbroek, J., and Hoekstra, J.M. (2015). Selective velocity obstacle method for deconflicting maneuvers applied to unmanned aerial vehicles. *Journal of Guidance, Control, and Dynamics*, 38(6), 1140–1146. doi:10.2514/1.G000737. URL `https://doi.org/10.2514/1.G000737`.

Kufoalor, D.K., Brekke, E.F., and Johansen, T.A. (2018). Proactive collision avoidance for ASVs using a dynamic reciprocal velocity obstacles method. In *Proc. IEEE/RSJ International Conference on Intelligent Robots and Systems (IROS)*, 2402–2409. doi:10.1109/IROS.2018.8594382.

Kuwata, Y., Wolf, M.T., Zarzhitsky, D., and Huntsberger, T.L. (2014). Safe maritime autonomous navigation with COLREGs, using velocity obstacles. *IEEE Journal of Oceanic Engineering*, 39(1), 110–119. doi:10.1109/JOE.2013.2254214.

Martinsen, A.B., Bitar, G., Lekkas, A.M., and Gros, S. (2020). Optimization-based automatic docking and berthing of ASVs using exteroceptive sensors: Theory and experiments. *IEEE Access*, 8, 204974–204986. doi:10.1109/ACCESS.2020.3037171.

Pedersen, A.A. (2019). *Optimization Based System Identification for the milliAmpere Ferry*. Master's thesis, Norwegian University of Science and Technology (NTNU), Trondheim, Norway. URL `https://ntnuopen.ntnu.no/ntnu-xmlui/handle/11250/2625699`.

Reddy, N.P., Zadeh, M.K., Thieme, C.A., Skjetne, R., Sørensen, A.J., Aanondsen, S.A., Breivik, M., and Eide, E. (2019). Zero-emission autonomous ferries for urban water transport: Cheaper, cleaner alternative to bridges and manned vessels. *IEEE Electrification Magazine*, 7(4), 32–45. doi:10.1109/MELE.2019.2943954.

Shaobo, W., Yingjun, Z., and Lianbo, L. (2020). A collision avoidance decision-making system for autonomous ship based on modified velocity obstacle method. *Ocean Engineering*, 215, 1–21. doi:https://doi.org/10.1016/j.oceaneng.2020.107910.

Thyri, E.H. and Breivik, M. (2022). A domain-based and reactive COLAV method with a partially COLREGs-compliant domain for ASVs operating in confined waters. *Field Robotics*, 2, 632–677. doi:https://doi.org/10.55417/fr.2022022.

van den Berg, J., Lin, M., and Manocha, D. (2008). Reciprocal velocity obstacles for real-time multi-agent navigation. In *Proc. IEEE International Conference on Robotics and Automation (ICRA)*, 1928–1935. doi:10.1109/ROBOT.2008.4543489.

Wilkie, D., van den Berg, J., and Manocha, D. (2009). Generalized velocity obstacles. In *Proc. IEEE/RSJ International Conference on Intelligent Robots and Systems (IROS)*, 5573–5578. doi:10.1109/IROS.2009.5354175.

Zhang, W., Wei, S., Teng, Y., Zhang, J., Wang, X., and Yan, Z. (2017). Dynamic obstacle avoidance for unmanned underwater vehicles based on an improved velocity obstacle method. *Sensors*, 17(12). doi:10.3390/s17122742.

Zhao, Y., Li, W., and Shi, P. (2016). A real-time collision avoidance learning system for unmanned surface vessels. *Neurocomputing*, 182, 255–266. doi:https://doi.org/10.1016/j.neucom.2015.12.028.

Paper F Collision avoidance for ASVs through trajectory planning: MPC with COLREGs-compliant nonlinear constraints

Published paper by E. H. Thyri and M. Breivik. "Collision avoidance for ASVs through trajectory planning: MPC with COLREGs-compliant nonlinear constraints". In: *Modeling, Identification and Control* 43.2 (2022), pp. 55–77. DOI: https://doi.org/10.4173/mic.2022.2.2.

Bibliography entry [28].

Collision avoidance for ASVs through trajectory planning: MPC with COLREGs-compliant nonlinear constraints

Emil H. Thyri [1] Morten Breivik [1]

[1] *Centre for Autonomous Marine Operations and Systems (AMOS), Department of Engineering Cybernetics, Norwegian University of Science and Technology (NTNU), Trondheim, Norway.*
E-mail: emil.h.thyri@ntnu.no, morten.breivik@ieee.org

Abstract

This article presents a trajectory planning method for autonomous surface vessels that is compliant with Rule 8 and rules 13-17 from the Convention on the International Regulations for Preventing Collisions at Sea (COLREGs). The method is suitable for operation in restricted waters, where it both handles collision avoidance with static obstacles, and also considers the available room to maneuver when determining the appropriate safe distance to other vessels. The trajectory planner is formulated as a finite-horizon nonlinear model predictive controller, minimizing the deviation from a reference trajectory and the acceleration. Collision avoidance with static obstacles is included through the use of convex free sets. Collision avoidance with other traffic is done by assigning so-called target ship domains to each vessel, and formulating constraints for that domain. COLREGs rules 13-15 and 17 are included by first classifying each vessel-to-vessel encounter to find which rule applies, and subsequently assigning an encounter-specific domain to the opposing vessel. The domain is designed so that if the trajectory does not violate the domain, compliance with COLREGs rules 13-15 and partial compliance with Rule 17 is ensured. Furthermore, compliance with COLREGs Rule 8 and Rule 16 is included through a novel method for calculating the objective function cost-gains. By constructing windows of reduced tracking error and acceleration cost, the start time, duration and magnitude of a maneuver can be controlled, and hence readily apparent maneuvers made in ample time can be facilitated. The method's effectiveness and its completeness in terms of COLREGs compliance is demonstrated through an extensive set of simulations of vessel-to-vessel encounters in open waters. Furthermore, the robustness of the method is demonstrated through a set of complex simulations in confined areas with several maneuvering vessels. In all simulations, the method demonstrates compliance with COLREGs Rule 8 and rules 13-17.

Keywords: Autonomous surface vessels, trajectory planning, trajectory optimization, collision avoidance, marine navigation, marine transportation, marine vehicles.

1 Introduction

Utilizing autonomy or high levels of automation to increase efficiency and reduce cost of current operations is a vision for several actors in maritime applications such as autonomous container vessels for short sea and inland shipping, see Wärtsilä (2021), DB Schenker (2022), Executive (2022). Others see autonomy as an enabler to new markets and operations like Zeabuz (2022) and RoBoat (2021), who are proposing small autonomous passenger ferries as an urban mobility changemaker. Another motivator for devel-

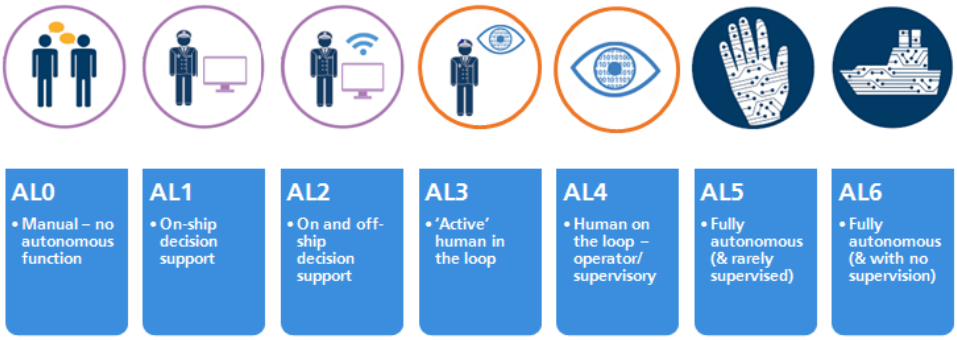

Figure 1: Levels of autonomy for maritime vessels. Courtesy of Lloyd's Register.

oping green autonomous vessels is reducing the strain on current land-based infrastructure by moving transportation to the underutilized waterways, and at the same time reduce the carbon footprint of operations by applying zero-emission vessels (Reddy et al., 2019; Čorić and Nikšić, 2022).

Introducing autonomy in maritime domains with other vessels or third parties is however not an overnight process. Like the automotive and aviation sector, maritime traffic is also subject to a set of rules and regulations, which any vessel upon the high seas, autonomous or not, must abide by. What makes this particularly challenging is that the Convention on the International Regulations for Preventing Collisions at Sea (COLREGs), which are "the rules of the road" on water, are developed over several centuries by sailors for sailors, and have several paragraphs that are left intentionally vague, and relies on the competence and experience of the navigator to evaluate the situation and make the correct choice of action. Furthermore, there are regulatory aspects that are not yet adapted to account for autonomous technology. In particular when the responsibility for comprehension and decision making is moved from human to machine, specific challenges related to this is further discussed by Ringbom (2019).

The development, deployment and operation of autonomous maritime vessels must therefore happen incrementally, and in parallel with the development of rules and regulations, so that assurance and thrust in the system can be build by all stakeholders. This can to a large extent be done through simulators, but must ultimately come through extensive operation. To aid this discussion between the technology and regulatory development, a taxonomy for maritime autonomy has been formulated by Lloid's Register (2016), where seven levels of autonomy are defined, describing the distribution of jurisdiction and responsibility between the operator and the autonomy. The autonomy-levels are illustrated in Fig. 1, where they range from fully manual operation, through decision support and increasing autonomous control, where the operator take a supervisor role, and eventually is removed from and active role in the control of the vessel.

Replicating the capacity of a skilled operator or crew in an autonomous maneuvering system has proven hard to solve by one algorithm alone. This has led to the distribution of the planning, maneuvering and collision avoidance (COLAV) objectives in what is often referred to as a hybrid COLAV system (Loe, 2008). An example of a three-layer hybrid COLAV system is shown in Fig. 2. In such as a system, the high level planner considers long term strategic planning with objectives such as transit time, energy optimization and risk mitigation. The mid-level planner considers both dynamic and static obstacles, by making local adjustments to the global path or trajectory. In the case of supervised autonomy, it would fall on the mid-level COLAV method to produce a trajectory that assures the supervisor of the soundness of the autonomous maneuvering. The trajectory from the mid-level COLAV should therefore consider all the relevant rules from the COLREGs in the planning. The low-level COLAV also considers static and dynamic obstacles. It is responsible for the baseline safety of the maneuvering, and handles immediate and unforeseen situations. The system should consider COLREGs to the extent it is possible, and bring the vessel to a minimum risk condition if needed.

The main contribution of this paper is a deliberate COLAV method for autonomous surface vessels (ASVs) that handles both static and dynamic obstacles, and is compliant with COLREGs rules 8 and 13-17, regarding maneuvering in proximity to other vessels, and actions to avoid collision. The proposed method comprises a trajectory planner that is suitable for the mid-

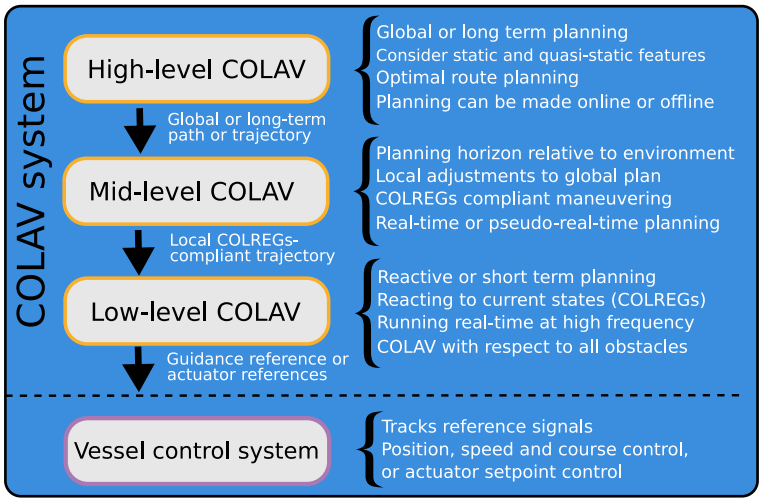

Figure 2: Three-layer hybrid COLAV structure, where the responsibility of path planning, trajectory planning, and reactive maneuvering is distributed over three separate methods. The figure is inspired by Eriksen and Breivik (2017).

level in a hybrid COLAV system like the one in Fig. 2, and has capacity suitable for autonomy-levels 3-6. The trajectory is calculated by formulating and solving an optimal control problem (OCP), where COLAV is enforced through inequality constraints. This work features two main novelties: (i) the constraints we formulate to enforce COLREGs rules 13-15 and 17, which are encounter-specific nonlinear constraints spanning both the position and velocity space, and (ii) the method for considering the more vague parts of the protocol, specifically Rule 8 and Rule 16, where we use dynamic cost-gain profiles with windows of reduced cost in the OCP objective function to control the timing and magnitude of a maneuver.

The remainder of this paper is structured as follows: Section 2 provides a review of relevant previous work. Section 3 presents theory on COLREGs, the target ship (TS) domain, and optimal control. In Section 4, we formulate the OCP, and present the features that ensure COLAV and COLREGs compliance. Section 5 presents simulation results, and Section 6 concludes the paper.

2 Previous work

In this section, a review of relevant previous work on collision avoidance for ASVs is presented. The review is not exhaustive, and for a more comprehensive overview, the reader is advised to consult Vagale et al. (2021b) and Ülkü Öztürk et al. (2022), for a general review of planning, maneuvering and collision avoidance methods for ASVs, and Vagale et al. (2021a) for a comparative study.

One way to categorize algorithms for autonomous maneuvering and collision avoidance for ASVs is as reactive or deliberate algorithms. The reactive algorithms calculate an immediate action based on the current state of events, while the deliberate algorithms comprises capacity for planning for some horizon into the future, based on predictions of future states of events.

Some reactive algorithms applied to maritime surface vessels are the Velocity Obstacle (VO) algorithm in (Kuwata et al., 2014; Thyri and Breivik, 2022b), and the control barrier function (CBF)-based methods proposed by Thyri et al. (2020a) and Thyri and Breivik (2022a). These methods show some degree of COLREGs compliance, where they consider the maneuvering-specific rules 13-15 and 17. However, the reactive nature of the methods makes it challenging to consider the more general parts of the regulations such as rules 8 and 16 regarding making early and substantial maneuvers if circumstances of the case admit. Considering these regulations requires an understanding of the future states of the environment to enable a situation with considerable risk of collision to be resolved at an early stage, and hence avoid close quarters all together.

An approach to improving compliance with these rules is to apply trajectory-planning methods with a planning horizon extending a suitable time into the fu-

ture, as this enables improved deliberation when determining the optimal maneuver. A useful categorization of trajectory planning algorithms can be made w.r.t. its continuity. Discrete algorithms explore discrete parts of the configuration-space to find a trajectory connecting the start and goal position. Depending on the discretization method, the resulting trajectory has varying degrees of smoothness, and often require post-processing to ensure dynamic feasibility. In (Thyri et al., 2020b), a discrete trajectory planning method is proposed for an ASV canal crossing operation. The domain of dynamic obstacles are represented in a path-time space, and a visibility-graph is built and traversed to find a collision free trajectory connecting the start and goal. The method is demonstrated through a 3 hour continuous autonomous dock-to-dock operation in a canal in Trondheim[1]. The method proves effective for very short transit, such as canal crossing, but, lacks the maneuvering capacity for COLREGs-compliant maneuvering in a more general operational domain due to the path-velocity decomposition approach.

Alternatively, continuous methods, such as model predictive control (MPC), work in the continuous configuration-space by means of a dynamic vessel model. Such methods are popular in a wide range of applications, as they feature effective and versatile mechanisms for both formulating objectives for, and constraining, the system states in the control horizon. This makes them ideal for trajectory planning and collision avoidance, since primary objectives such as collision avoidance can be enforced through constraints, and secondary objectives such as path following, energy consumption, comfort or protocol adherence can be incentivized through the objective function.

In (Eriksen and Breivik, 2017; Xue et al., 2021; Abdelaal et al., 2018), nonlinear model predictive control is applied for ASV trajectory planning. The planners consider collision avoidance w.r.t. both static and dynamic obstacles by modeling them as circular domains and formulating constraints for the ASV position w.r.t. the circle boundaries. Furthermore, Eriksen and Breivik (2017) propose a cost function that favours readily apparent course change maneuvers in accordance with COLREGs Rule 8. However, COLREGs Part B regarding obligations of give-way and stand-on vessels is not considered. In (Xue et al., 2021) and (Abdelaal et al., 2018), COLREGs are considered through an increased cost on port maneuvers, and thereby favouring maneuvering to starboard. A similar approach is made in Abdelaal and Hahn (2016), where a soft constraint on the rate of change of yaw moment is applied to favour starboard maneuvers. All three methods demonstrate collision avoidance in encounters with a single TS in open waters. The robustness of the methods COLREGs compliance is however uncertain, since a bias towards starboard maneuvers provides little robustness to the principles of the protocol. Furthermore, without proper care, these mechanisms can also affect the maneuvering performance of the algorithms, by enforcing different response in port and starboard turns in situations without any dynamic obstacles. Additionally, the methods of modelling static obstacles as circular domains is feasible in areas with sparse island-like static features, however, it does not scale well to confined space with more complex obstacle geometry. This is considered by Martinsen et al. (2020), where an approach to docking for ASVs in urban areas is proposed. In the work, a convex set free of static obstacles is constructed around the ASV, allowing an arbitrary complex static obstacle environment to be represented by a small set of linear constraints.

A limiting factor to the COLREGs compliance of these methods is the TS domain they apply, which is the mechanism that ensures a safe distance between the vessels. Such domains have been applied by mariners for decades, either in collision risk warning systems, or as a tool for manually determining risk of collision. A critical review of such methods is given by Szlapczynski and Szlapczynska (2017), where they also propose a new ship domain for risk assessment. The use-case of these domains in risk assessment is however not the same as for autonomous maneuvering and collision avoidance algorithms. In the first case, the domains are used to determine the risk of collision, and if sufficient risk is deemed to exist, a navigator determines the appropriate action. For the second case, the TS domain is a mechanism that influences the nature of the manuever, since the trajectory is planned to not violate the domain. Therefore, TS domains for trajectory planning algorithms, should be designed to not only cover the state-space where risk of collision is high, but also the state-space that is in violation of the COLREGs.

In (Eriksen et al., 2019), a TS domain with COLREGs considerations is proposed for trajectory planning for a high-speed ASV in open waters. The domain is constructed from quarter ellipses with increased extension to the fore and starboard of the TS. The domain is enforced as a soft constraint, where the objective function carries a term of penalty as a function of the duration of the trajectory's violation of the domain. The shape of the domain incentivizes passing port to port in head-on encounters and behind in give-way crossing encounters. A disadvantage of using soft constraints for high priority objectives such as

[1] Video from the demonstration at:
https://www.youtube.com/watch?v=7i1YkmdticO&list=PLc2vvxBHfBcoHvfcIRsFROmJzXhbJCvb5&index=4&ab_channel=NTNUCybernetics

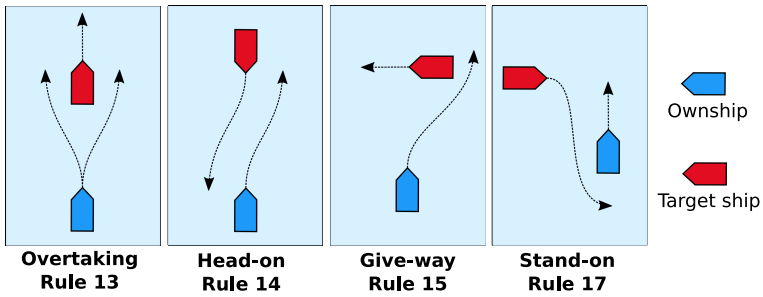

Figure 3: Illustration of COLREGs rules 13-15 and Rule 17, as seen from the OS in blue.

collision avoidance or COLREGs compliant maneuvering, is that they are often in conflict with other mission objectives such as path-following. Without a clear distinction between the mechanisms for enforcing the conflicting objectives, the trajectory planner is prone to plan a trajectory that is in conflict with the COLREGs or safety objective, but has an increased performance w.r.t. less critical objectives.

In (Thyri and Breivik, 2022a), an approach that mitigates this is presented. The authors propose a novel TS domain that is enforced through CBFs for a fully actuated ASV. The TS domain is designed explicitly for COLREGs compliance, and by formulating the CBFs w.r.t. both the distance to and velocity towards the domain, it is extended to also occupy regions in the combined position and velocity configuration-space. Through simulations, the authors demonstrate how the extended domain effectively covers COLREGs critical regions in the velocity-space without excessive extension in the position configuration-space, making it suitable for confined-space operation. Furthermore, through extensive simulations and full-scale experiments, the domain shows compliance with the encounter-type specific rules 13-15 and 17.

In this work, we apply the domain from (Thyri and Breivik, 2022a), by formulating hard constraints w.r.t. the distance to the domain boundary and the relative velocity towards the domain boundary, in order to ensure collision safety and to compliance with the encounter-type specific regulations. Furthermore, we expand the COLREGs compliance by predicting future risk of collision and considering rules 8 and 16 through maneuvering incentives in the objective function.

3 Background Theory

In this section, we introduce some background theory on the relevant rules from the COLREGs, and a method for classifying a vessel-to-vessel encounter w.r.t. COLREGs. Furthermore, the TS domain that we apply is described, and relevant theory on optimal control is provided.

3.1 COLREGs - The rules of the road

The COLREGs is the result of a convention developed over several centuries to prevent collision between two or more vessels at sea. It applies to all vessels upon the high seas and all waters connected to the high seas and navigable by seagoing vessels (Cockcroft and Lameijer, 2012).

The convention has four main parts: Part A - General, Part B - Steering and Sailing, Part C - Lights and Shapes and Part D - Sound and Light signals. In the work presented here, we consider maneuvering in the presence of other vessels in good visibility, and hence it is the rules in parts A and B, regarding vessels in sight of one another, that are most relevant. Here follows a short description of the rules we consider. Figure 3 illustrates vessel-to-vessel encounters where a subset of the rules applies to the ownship (OS).

- **Rule 8** *Any action to avoid collision shall, if circumstances of the case admit, be positive, made in ample time, and with due regard to good seamanship.*

- **Rule 13** *Any vessel overtaking another vessel shall keep out of the way of the vessel being overtaken. A vessel approaching another vessel from a direction of more than* 22.5 deg *abaft her beam is an overtaking vessel. Any subsequent alternation of bearing between the two vessels shall not relieve the overtaking vessel of the duty of keeping clear of the overtaken vessel until she is finally past and clear.*

- **Rule 14** *When two power-driven vessels are meeting on reciprocal or nearly reciprocal courses so as to involve risk of collision each shall alter her*

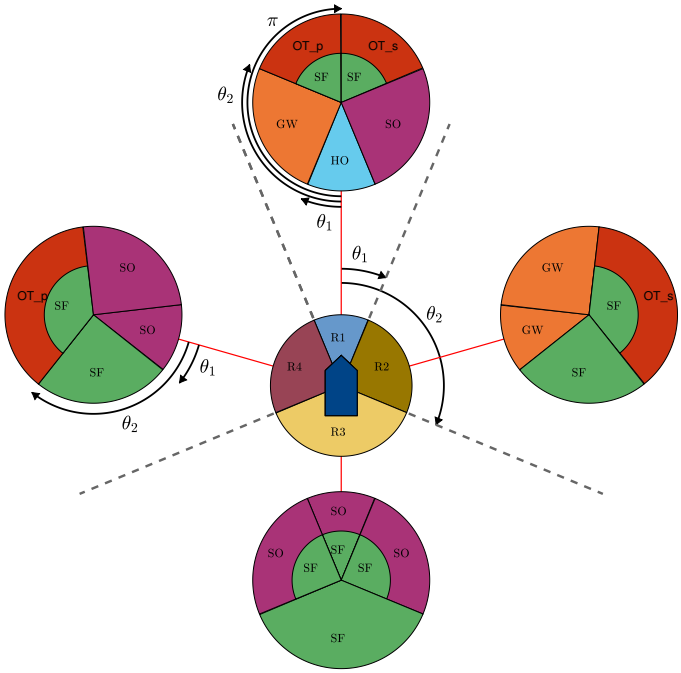

Figure 4: Graphic representation of the classification algorithm, where the position of the OS is at the center of the middle circle. In situation sectors with two encounter classifications, the outer one is chosen when the involved vessels have a closing range, while the inner one is chosen for increasing range.

course to starboard so that each shall pass on the port side of the other.

- **Rule 15** *When two power-driven vessels are crossing so as to involve risk of collision, the vessel which has the other on her own starboard side shall keep out of the way and shall, if the circumstances of the case admit, avoid crossing ahead of the other vessel.*

- **Rule 16** *Every vessel which is directed to keep out of the way of another vessel shall, so far as possible, take early and substantial action to keep well clear.*

- **Rule 17** *Where one of two vessels is to keep out of the way, the other shall keep her course and speed. The latter vessel may take action to prevent collision if it is apparent that the vessel required to keep out of the way is not taking appropriate action.*

Rules 13-15 and Rule 17 are specific to the encounter type, where only one of the rules applies to the OS. Therefore, to determine which rule applies, the encounter type must be determined. The criteria for classifying a vessel-to-vessel encounter are stated in the regulations, and classification is therefore a matter of calculating the required states and comparing them to the entry-criteria in the COLREGs. A method for this is proposed by Thyri and Breivik (2022a), where the proposed classification algorithm determines the encounter type to be one of the following, where the corresponding rule applies.

- Overtaking starboard side (OT_s): **Rule 13**
- Overtaking port side (OT_p): **Rule 13**
- Head-on (HO): **Rule 14**
- Give-way crossing (GW): **Rule 15**
- Stand-on crossing (SO): **Rule 17**
- Safe (SF): No rules apply

A graphical interpretation of the classification algorithm is shown in Fig. 4. In the figure, the OS is located at the center, with heading pointing up. The

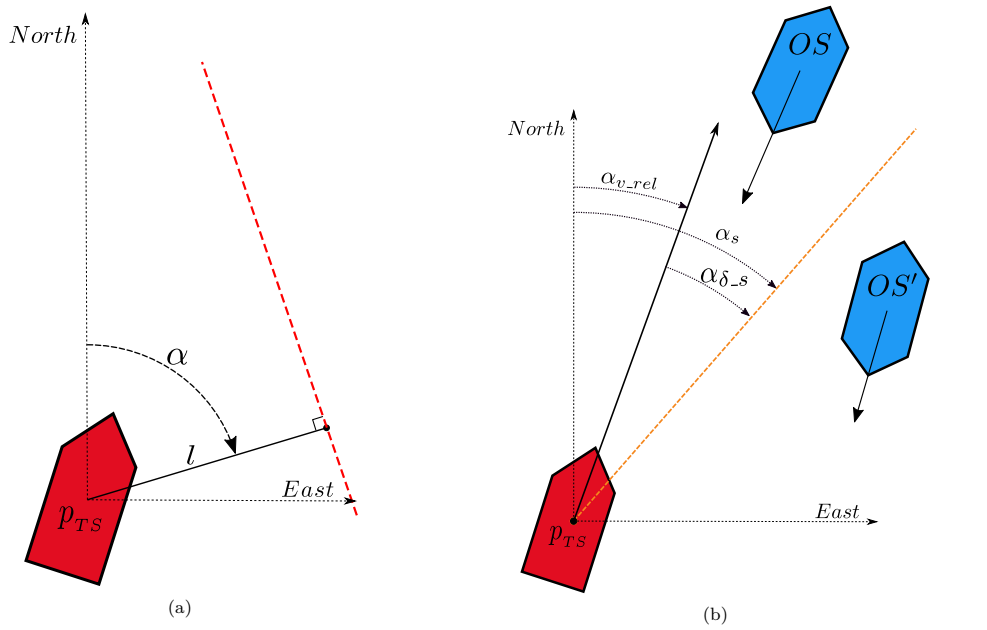

Figure 5: TS domain: a) TS domain defined by the angle α and the distance $l > 0$. b) Two instances of the OS on either side of the port-starboard split line.

area around the OS is split into four relative bearing sectors, where the relative bearing of the TS from the OS,

$$\varphi = \text{atan2}((E_{TS} - E), (N_{TS} - N)) - \chi, \quad (1)$$

along with the sector angles θ_1 and θ_2, is applied to determine the relative bearing sector to be one of R1, R2, R3 or R4. Here $[N, E]$ and $[N_{TS}, E_{TS}]$ are the north-east positions of the OS and TS in a local NED frame, and χ is the course of the OS. Subsequently, the encounter type is determined by the relative course of the TS to the OS

$$\chi_{rel} = \chi_{TS} - \chi, \quad (2)$$

where χ_{TS} is the course of the TS, along with a set of rotated sector angles $\theta_1^{'}$ and $\theta_2^{'}$, where $\theta_1^{'} = \theta_1 - \varphi_{TS}$ and $\theta_2^{'} = \theta_2 - \varphi_{TS}$, and

$$\varphi_{TS} = \text{atan2}((E - E_{TS}), (N - N_{TS})), \quad (3)$$

is the bearing of the OS from the TS. For further details on the classification method, see (Thyri and Breivik, 2022a).

3.2 Target ship domain

In this work, we apply the TS domain from (Thyri and Breivik, 2022a). The domain is designed so that if the OS maneuvers in such a way that it does not enter the TS domain, it also maneuvers in compliance with COLREGs rules 13-15 and 17. The proposed domain is specific to each TS, and is a function of the geometry and relative velocity of the encounter, the encounter type, and the available space to maneuver.

The TS domain is defined by a straight line dividing the north-east plane into two halves, where the TS is within one of the halves. An illustration of the domain is shown in Fig. 5(a) for a red TS. From the figure, one can see that in addition to the position of the TS at p_{TS}, the TS domain is defined by two variables: The shortest distance from the TS to the TS domain, denoted $l > 0$, and the angle of the normal vector to the domain boundary pointing away from the TS, denoted $\alpha \in (-\pi, \pi]$.

The orientation of the domain is a function of geometry and relative velocity of the encounter, in addition to encounter-type specific parameters. To determine the angle α, first the side of the OS that the TS should be when passing it is determined. This is determined by the bearing of the OS from the TS relative to a port-starboard split angle

$$\alpha_s = \alpha_{v\_rel} + \alpha_{\delta\_s}, \quad (4)$$

where α_{δ_s} is an encounter-type specific bias towards

maneuvering to the rules-compliant side, and α_{v_rel} is the angle of the relative velocity vector

$$\boldsymbol{v}_{rel} = \boldsymbol{v}_{TS} - \boldsymbol{v}, \tag{5}$$

with $\boldsymbol{v} = [\dot{N}, \dot{E}]^\intercal$ and $\boldsymbol{v}_{TS} = [\dot{N}_{TS}, \dot{E}_{TS}]^\intercal$ are the north-east velocities of the OS and TS, respectively. The angle α is defined as

$$\alpha := \begin{cases} \varphi_{TS} + \alpha_d, & \text{if } \varphi_{TS} > \alpha_s, \\ \varphi_{TS} - \alpha_d, & \text{else.} \end{cases} \tag{6}$$

where $\alpha_d \in (-\pi/2, \pi/2)$ is the deflection angle, which is an encounter-type specific parameter. This angle is used to facilitate passing the TS with a geometry that complies with the relevant rule.

The minimum distance from the TS to the domain line, and hence the minimum allowable distance between the OS and the TS, is

$$l = \begin{cases} r_{dyn} & \text{if } r_{free} \leq 0, \\ r_{dyn} + k_l r_{free} & \text{if } r_{free} \in (0, r_{free\_max}), \\ r_{dyn} + k_l r_{free\_max} & \text{if } r_{free} \geq r_{free\_max}. \end{cases} \tag{7}$$

where r_{free} is an estimate of the available free space to maneuver on the side of the TS that the OS should pass, while

$$r_{dyn} = \frac{1}{2}(l_{OS} + l_{TS}) + \delta_{dyn}, \tag{8}$$

is the minimum distance at which no collision will occur between the OS and TS independent of the encounter geometry. Here, l_{OS} and l_{TS} are the lengths of the OS and TS respectively, and $\delta_{dyn} > 0$ is an additional tolerance. Furthermore, r_{free} is a measure of the available space for the OS to maneuver between the TS and any static obstacles on the side of the TS that the OS will pass, and $k_l \in [0, 1]$ splits the free maneuverable space between the TS and a potential static obstacle. The parameter $r_{free\_max} > 0$ limits the contribution to l from the available space, and hence saturates the domain size in unrestricted waters. For further details on the TS domain, the reader is advised to see (Thyri and Breivik, 2022a).

3.3 Optimal control problem

In this work, we consider a system on the form

$$\dot{\boldsymbol{x}} = \boldsymbol{f}(\boldsymbol{x}(t), \boldsymbol{u}(t)), \ \boldsymbol{x}(0) = \boldsymbol{x}_0 \tag{9}$$

where $\boldsymbol{f} : \mathbb{R}^n \times \mathbb{R}^m \to \mathbb{R}^n$, is locally Lipschitz, $\boldsymbol{x} \in D \in \mathbb{R}^n$ contains the states of the system and $\boldsymbol{u} \in \boldsymbol{U} \in \mathbb{R}^m$ is the control input. This model applies to a variety of field robotics systems in air, on land and at sea.

A general OCP for such a system can be formulated as

$$\begin{aligned} \text{minimize} \quad & \theta(\boldsymbol{x}(t), \boldsymbol{u}(\boldsymbol{t})) \\ \text{subject to} \quad & \dot{\boldsymbol{x}}(t) = \boldsymbol{f}(\boldsymbol{x}(t), \boldsymbol{u}(t)) \\ & \boldsymbol{h}(\boldsymbol{x}(t), \boldsymbol{u}(t)) \geq \boldsymbol{0} \\ & \boldsymbol{x}(t_0) = \bar{\boldsymbol{x}}_{t_0} \end{aligned} \tag{10}$$

where $\theta : \mathbb{R}^n \times \mathbb{R}^m \to \mathbb{R}$ is the objective function, $\boldsymbol{h} : \mathbb{R}^n \times \mathbb{R}^m \to \mathbb{R}^{n_h}$ forms a set of n_h inequality constraints, and $\bar{\boldsymbol{x}}_{t_0} \in \mathbb{R}^n$ is the system state at $t = t_0$.

While such continuous OCPs in some cases can be solved analytically, this is generally not feasible. Instead, the problem is discretized and solved by nonlinear programming (NLP). In this paper, we apply a direct multiple shooting approach, where the system state and control input at each discretization step are explicitly defined as decision variables. The OCP with N_p discretized steps in the control horizon then becomes

$$\begin{aligned} \text{minimize} \quad & \theta(\boldsymbol{\omega}) \\ \text{subject to} \quad & \boldsymbol{g}(\boldsymbol{\omega}) = \boldsymbol{0} \\ & \boldsymbol{h}(\boldsymbol{\omega}) \geq \boldsymbol{0} \end{aligned} \tag{11}$$

where $\boldsymbol{\omega} = [\boldsymbol{x}_0^\intercal, \boldsymbol{u}_0^\intercal, ..., \boldsymbol{x}_{N_p-1}^\intercal, \boldsymbol{u}_{N_p-1}^\intercal, \boldsymbol{x}_{N_p}^\intercal]^\intercal \in \mathbb{R}^{(n+m)N_p+n}$ is a vector of decision variables, $\theta(\boldsymbol{\omega})$ is the objective function, $\boldsymbol{g}(\omega)$ is a set of equality constraints and $\boldsymbol{h}(\boldsymbol{\omega})$ is a set of inequality constraints.

When using multiple shooting, the vessel model (9) is enforced by formulating shooting constraints that are included in $\boldsymbol{g}(\omega)$. For this, an integrating function is applied to integrate the system states at timestep k subject to the control input at timestep k for the duration of the discretization step $h > 0$ to get the system states at timestep $k + 1$,

$$\boldsymbol{x}_{k+1} = \boldsymbol{F}(\boldsymbol{x}_k, \boldsymbol{u}_k). \tag{12}$$

One candidate for such an integrating function is the 4th order Runge Kutta method

$$\begin{aligned} k_1 &= \boldsymbol{f}(\boldsymbol{x}_k, \boldsymbol{u}_k) \\ k_2 &= \boldsymbol{f}(\boldsymbol{x}_k + \frac{h}{2}k_1, \boldsymbol{u_k}) \\ k_3 &= \boldsymbol{f}(\boldsymbol{x}_k + \frac{h}{2}k_2, \boldsymbol{u_k}) \\ k_4 &= \boldsymbol{f}(\boldsymbol{x}_k + hk_3, \boldsymbol{u_k}) \\ \boldsymbol{F}(\boldsymbol{x}_k, \boldsymbol{u}_k) &= \boldsymbol{x}_k + \frac{h}{6}\left(k_1 + 2k_2 + 2k_3 + k_4\right). \end{aligned} \tag{13}$$

The shooting constraints are defined as

$$\boldsymbol{g}(\boldsymbol{w}) = \begin{bmatrix} \bar{\boldsymbol{x}}_{t_0} - \boldsymbol{x}_0 \\ \boldsymbol{F}(\boldsymbol{x}_0, \boldsymbol{u}_0) - \boldsymbol{x}_1 \\ \boldsymbol{F}(\boldsymbol{x}_1, \boldsymbol{u}_1) - \boldsymbol{x}_2 \\ \vdots \\ \boldsymbol{F}(\boldsymbol{x}_{N_p-1}, \boldsymbol{u}_{N_p-1}) - \boldsymbol{x}_{N_p} \end{bmatrix}, \tag{14}$$

resulting in $n_g = n(N_p + 1)$ constraints.

4 OCP-based trajectory planner

In this section, the approach to COLREGs-compliant and collision-free maneuvering by trajectory planning is presented. The trajectory planning problem is formulated as an OCP, where collision avoidance is enforced through inequality constraints. Furthermore, COLREGs rules 13-15 and 17 are encoded in the constraints for the dynamic obstacles, and rules 8 and 16 are included through dynamic cost gains in the OCP objective function.

4.1 System model

The system model that we apply is a simple model on the form

$$\dot{\boldsymbol{x}} = \begin{bmatrix} \boldsymbol{v} \\ \boldsymbol{a} \end{bmatrix} \tag{15}$$

where $\boldsymbol{x} = [\boldsymbol{p}^\mathsf{T}, \boldsymbol{v}^\mathsf{T}]^\mathsf{T}$ is the system state vector and $\boldsymbol{a}$ is the control input. Here,

$$\boldsymbol{p} = \begin{bmatrix} N \\ E \end{bmatrix}, \tag{16}$$

is the north-east position of the system

$$\boldsymbol{v} = \begin{bmatrix} \dot{N} \\ \dot{E} \end{bmatrix}, \tag{17}$$

is the north-east velocity of the system, and

$$\boldsymbol{a} = \begin{bmatrix} \ddot{N} \\ \ddot{E} \end{bmatrix}, \tag{18}$$

is the north-east acceleration of the system. In choice of system model, the objectives of the OCP should be considered. High-fidelity vessel models allow for optimal control w.r.t. features such as energy efficiency, and by including actuator dynamics, non-holonomic properties of underactuated vessels can be considered. However, increased model complexity and nonlinearity comes at the cost of increased runtime, which can be decisive for the feasibility of applying OCPs in real-time applications. Therefore, care should be taken so that the fidelity of the model is sufficient for its purpose, without introducing unnecessary complexity. The trajectory planner we propose is intended as a mid-level COLAV method in a hybrid structure like the one shown in Fig. 2, where lower levels of the hybrid architecture considers higher fidelity vessel dynamics. Since the control objectives of the OCP that we propose are a function of the vessel position, velocity and acceleration, it is sufficient to apply a second-order linear system as in (15). Furthermore, by formulating constraints on the velocity states and the control input, feasibility of the optimal trajectory with respect to the actual vessel dynamics can still be ensured.

4.2 Problem definition and notation

The problem at hand is to plan a trajectory for the system in (15) that extends for some finite time horizon of duration

$$T_{horizon} = N_p h \tag{19}$$

from the current time, where $N_p > 0$ is the number of steps in the horizon, and $h > 0$ is the discretization interval. The inputs to the problem are:

1. A discretized reference trajectory $\boldsymbol{x}_{ref}$, which is used to calculate a desired trajectory for the OS extending throughout the planning horizon, on the form

   $$\boldsymbol{x}_d = [\boldsymbol{p}_{d,1}^\mathsf{T}, \boldsymbol{v}_{d,1}^\mathsf{T}, \boldsymbol{p}_{d,2}^\mathsf{T}, \boldsymbol{v}_{d,2}^\mathsf{T}, ..., \boldsymbol{p}_{d,N_p}^\mathsf{T}, \boldsymbol{v}_{d,N_p}^\mathsf{T}]^\mathsf{T} \tag{20}$$

   where

   $$\boldsymbol{p}_{d,k} = \begin{bmatrix} N_{d,k} \\ E_{d,k} \end{bmatrix}, \tag{21}$$

   is the desired position at timestep k and

   $$\boldsymbol{v}_{d,k} = \begin{bmatrix} \dot{N}_{d,k} \\ \dot{E}_{d,k} \end{bmatrix}, \tag{22}$$

   is the desired velocity at timestep k. In Section 4.6, we discuss how we calculate $\boldsymbol{x}_d$ from $\boldsymbol{x}_{ref}$.

2. A discretized trajectory prediction for every TS in line of sight from the OS, and the TS size. The predicted trajectory for TS i is on the form

   $$\boldsymbol{x}_{TS\_i} = [\boldsymbol{p}_0^{TS\_i}, \boldsymbol{v}_0^{TS\_i}, \boldsymbol{p}_1^{TS\_i}, \boldsymbol{v}_1^{TS\_i}, ..., \boldsymbol{p}_{N_p}^{TS\_i}, \boldsymbol{v}_{N_p}^{TS\_i}], \tag{23}$$

   where $\boldsymbol{p}_k^{TS\_i}$ and $\boldsymbol{v}_k^{TS\_i}$ are the predicted position and velocity of the TS at timestep k.

3. A map of static obstacles.

The objective is to calculate a trajectory that tracks the desired trajectory $\boldsymbol{x}_d$ with minimal tracking error,

while at the same time minimizes the control input. To achieve this, we proposed to use the objective function

$$\phi(\boldsymbol{p}, \boldsymbol{a}) = \sum_{k=0}^{N_p-1} \tilde{\boldsymbol{p}}_{k+1}^{\mathsf{T}} K_{k+1}^{p} \tilde{\boldsymbol{p}}_{k+1} + \boldsymbol{a}_k^{\mathsf{T}} K_k^{a} \boldsymbol{a}_k \tag{24}$$

where

$$\tilde{\boldsymbol{p}}_k = \boldsymbol{p}_k - \boldsymbol{p}_{d,k}, \tag{25}$$

is the relative error to the desired position at timestep k, and $K_k^p > 0$ and $K_k^a > 0$ are the cost-gains at timestep k for the position error and acceleration, respectively.

The output of the problem is a discretized trajectory on the form

$$\boldsymbol{x}^{opt} = [\boldsymbol{a}_0^{opt}, \boldsymbol{p}_1^{opt}, \boldsymbol{v}_1^{opt}, \tag{26}$$

$$\boldsymbol{a}_1^{opt}, \boldsymbol{p}_2^{opt}, \boldsymbol{v}_2^{opt}, ... \tag{27}$$

$$\boldsymbol{a}_{N_p-1}^{opt}, \boldsymbol{p}_{N_p}^{opt}, \boldsymbol{v}_{N_p}^{opt}] \tag{28}$$

that is optimal w.r.t. the cost function (24) while adhering to the constraints of $\boldsymbol{g}$ and $\boldsymbol{h}$, which will be defined shortly. The first term of $\phi(\boldsymbol{p}, \boldsymbol{a})$ in (24) motivates the optimal trajectory to track the desired trajectory by minimizing the tracking error at each timestep, while the second motivates a smooth trajectory by penalizing acceleration. For a dynamic trajectory, these two objectives are conflicting. The same is true for situations where another vessel is in conflict with the desired trajectory and an avoidance maneuver resulting in both tracking error and acceleration usage is required. However, by appropriately assigning the cost-gain profiles for the control horizon, a satisfactory compromise can be reached. The design of the cost-gain profiles is discussed in Section 4.8

4.3 Constraints for trajectory feasibility

To ensure feasibility of the trajectory, inequality constraints for the velocity state $\boldsymbol{v}_k \forall k \in [1, N_p]$ and control input $\boldsymbol{a}_k \forall k \in [0, N_p - 1]$ are formulated. The velocity constraints are formulated as

$$\boldsymbol{h}_v = \begin{bmatrix} U_{max}^2 - \boldsymbol{v}_1^{\mathsf{T}} \boldsymbol{v}_1 \\ U_{max}^2 - \boldsymbol{v}_2^{\mathsf{T}} \boldsymbol{v}_2 \\ \vdots \\ U_{max}^2 - \boldsymbol{v}_{N_p}^{\mathsf{T}} \boldsymbol{v}_{N_p} \end{bmatrix} \tag{29}$$

where $U_{max} > 0$ is the upper velocity limit for the trajectory. In the same way, the constraints on acceleration are formulated as

$$\boldsymbol{h}_a = \begin{bmatrix} a_{max}^2 - \boldsymbol{a}_0^{\mathsf{T}} \boldsymbol{a}_0 \\ a_{max}^2 - \boldsymbol{a}_1^{\mathsf{T}} \boldsymbol{a}_1 \\ \vdots \\ a_{max}^2 - \boldsymbol{a}_{N_p-1}^{\mathsf{T}} \boldsymbol{a}_{N_p-1} \end{bmatrix} \tag{30}$$

where $a_{max} > 0$ is the upper acceleration limit for the trajectory. To ensure dynamic feasibility of the trajectory, U_{max} and a_{max} should reflect the maneuvering capacity of the vessel.

4.4 Constraints for dynamic obstacles

The constraints for the dynamic obstacles are formulated with respect to the TS domain introduced in Section 3. The TS domain is designed with broad consideration to the COLREGs, so that as long as it is not violated, the trajectory will be collision-free with dynamic obstacles, and comply with COLREGs rules 13-15 and Rule 17.

The constraint is formulated with respect to the point

$$\boldsymbol{p}_B = \boldsymbol{p}_D + (\boldsymbol{p} - \boldsymbol{p}_D)^{\mathsf{T}} \boldsymbol{n}_{p_D} \boldsymbol{n}_{p_D}, \tag{31}$$

which is the point on the TS domain closest to the OS, where

$$\boldsymbol{p}_D = \boldsymbol{p}_{TS} + \boldsymbol{n}_D l \tag{32}$$

is the point on the TS domain closest to the TS,

$$\boldsymbol{n}_D = \begin{bmatrix} \cos(\alpha) \\ \sin(\alpha) \end{bmatrix} \tag{33}$$

is the normal vector to the domain boundary pointing out of the domain, and

$$\boldsymbol{n}_{p_D} = \begin{bmatrix} -\sin(\alpha) \\ \cos(\alpha) \end{bmatrix} \tag{34}$$

is the tangent vector to the domain boundary.

The constraint is then defined as the distance from the position of the OS at $\boldsymbol{p}$ to the domain

$$h_{TS}(\boldsymbol{p}, \boldsymbol{p}_{TS}) = \boldsymbol{n}_D^{\mathsf{T}} (\boldsymbol{p} - \boldsymbol{p}_B). \tag{35}$$

In addition to the constraint in (35), we propose to use an augmented constraint that not only considers the distance to the domain, but also the velocity at which the OS is approaching the domain. The augmented constraint is defined as

$$h_{TS}(\boldsymbol{p}, \boldsymbol{v}, \boldsymbol{p}_{TS}, \boldsymbol{v}_{TS}) = \boldsymbol{n}_D^{\mathsf{T}} (\boldsymbol{p} - \boldsymbol{p}_B) + c_{dyn} \boldsymbol{n}_D^{\mathsf{T}} (\boldsymbol{v} - \boldsymbol{v}_B) \tag{36}$$

where $\boldsymbol{v}_B$ is the velocity of the point $\boldsymbol{p}_B$, given by

$$\begin{aligned} \dot{\boldsymbol{p}}_B =& \dot{\boldsymbol{p}}_D + (\dot{\boldsymbol{p}} - \dot{\boldsymbol{p}}_D)^{\mathsf{T}} \boldsymbol{n}_{p_D} \boldsymbol{n}_{p_D} + (\boldsymbol{p} - \boldsymbol{p}_D)^{\mathsf{T}} \dot{\boldsymbol{n}}_{p_D} \boldsymbol{n}_{p_D} \\ &+ (\boldsymbol{p} - \boldsymbol{p}_D)^{\mathsf{T}} \boldsymbol{n}_{p_D} \dot{\boldsymbol{n}}_{p_D}. \end{aligned} \tag{37}$$

Here,

$$\dot{\boldsymbol{n}}_{p_D} = \frac{\partial \boldsymbol{n}_{p_D}}{\partial \alpha} \dot{\alpha}, \tag{38}$$

and

$$\dot{\boldsymbol{p}}_D = \dot{\boldsymbol{p}}_{TS} + \boldsymbol{n}_{p_D} l \dot{\alpha}, \tag{39}$$

is the velocity of the point $\boldsymbol{p}_D$. When formulating the constraints, we assume that the TS keeps a constant course and speed, and hence $\dot{\alpha} = \dot{\varphi}_{TS}$, with

$$\dot{\varphi}_{TS} = \left(\boldsymbol{R}_2(\tfrac{\pi}{2}) \frac{\bar{\boldsymbol{p}}}{\bar{\boldsymbol{p}}^\mathsf{T} \bar{\boldsymbol{p}}} \right)^\mathsf{T} \dot{\bar{\boldsymbol{p}}}, \tag{40}$$

where $\bar{\boldsymbol{p}} = \boldsymbol{p} - \boldsymbol{p}_{TS}$ and $\dot{\bar{\boldsymbol{p}}} = \boldsymbol{v} - \boldsymbol{v}_{TS}$ denote the relative position and velocity between the two vessels, respectively, and

$$\boldsymbol{R}_2(\phi) = \begin{bmatrix} \cos(\phi) & -\sin(\phi) \\ \sin(\phi) & \cos(\phi) \end{bmatrix}. \tag{41}$$

The parameter $c_{dyn} > 0$ in (36) mitigates between the distance to the domain, and the velocity at which the OS is allowed to approach the domain, and hence serves as an effective way of setting a lower threshold for when a maneuver to avoid collision should be initiated. This is in-line with Rule 8, regarding taking early action to avoid collision.

The constraints for TS_i for the control horizon is

$$\boldsymbol{h}_{TS\_i} = \begin{bmatrix} h_{TS}(\boldsymbol{p}_1, \boldsymbol{p}_1^{TS\_i}) \\ h_{TS}(\boldsymbol{p}_2, \boldsymbol{p}_2^{TS\_i}) \\ \vdots \\ h_{TS}(\boldsymbol{p}_{N_p}, \boldsymbol{p}_{N_p}^{TS\_i}) \end{bmatrix}, \tag{42}$$

and

$$\boldsymbol{h}_{\dot{T}S\_i} = \begin{bmatrix} h_{\dot{T}S}(\boldsymbol{p}_1, \boldsymbol{v}_1, \boldsymbol{p}_1^{TS\_i}, \boldsymbol{v}_1^{TS\_i}) \\ h_{\dot{T}S}(\boldsymbol{p}_2, \boldsymbol{v}_2, \boldsymbol{p}_2^{TS\_i}, \boldsymbol{v}_2^{TS\_i}) \\ \vdots \\ h_{\dot{T}S}(\boldsymbol{p}_{N_p}, \boldsymbol{v}_{N_p}, \boldsymbol{p}_{N_p}^{TS\_i}, \boldsymbol{v}_{N_p}^{TS\_i}) \end{bmatrix}, \tag{43}$$

resulting in $2N_p$ constraints for each TS, and the set of constraints for dynamic obstacles

$$\boldsymbol{h}_{TS} = \bigcup_{i}^{\mathcal{N}_{pri}} \left(\boldsymbol{h}_{TS\_i} \cup \boldsymbol{h}_{\dot{T}S\_i} \right), \tag{44}$$

where $\mathcal{N}_{pri}$ is the set of vessels to be considered. The construction of $\mathcal{N}_{pri}$ is discussed in Section 4.7.

4.5 Constraints for static obstacles

The approach propose for COLAV with static obstacles is to formulate a convex free set at the reference position of timesteps $k \in \mathcal{C}_{stat}$ where the set $\mathcal{C}_{stat} \subseteq \{1, 2, ..., N_p\}$. When designing the subset $\mathcal{C}_{stat}$, the dynamics of the vessel and discretization interval of the OCP should be considered to ensure safety, while at the same time avoiding excessive constraints and overhead related to lookups in map-data.

The convex free set for timestep k is constructed in the following way:

1. a set of N_{sect} non-overlapping equally sized sectors covering the complete circle around the reference position at $\boldsymbol{p}_{d,k}$ is defined
2. the closest point on any static obstacle within each sector is found by a search in the map data, where the points are denoted $\boldsymbol{p}_{stat\_i}, i \in [1, 2, ..., N_{sect}]$
3. a domain is assigned to each point $\boldsymbol{p}_{stat\_i}$ by constructing a normal vector $\boldsymbol{n}_{\boldsymbol{p}_{stat\_i}}$ for the point, and considering the domain boundary as the line passing through the point perpendicular to the normal vector. The normal vector for each point is found by the method in (Martinsen et al., 2020), where it is constructed to be normal to the boundary of, and pointing into, an ellipse centered in $\boldsymbol{p}_{d,k}$, with its major axis aligned with the desired course at timestep k, defined as

$$\chi_{d_k} := atan2(\dot{E}_{d,k}, \dot{N}_{d,k}), \tag{45}$$

and the relationship between the major and minor axis given by

$$\sigma = \begin{cases} \sigma_{min} \;\; if \;\; d_{min} > d_{\sigma\_min} \\ \sigma_{max} - \rho(d_{min}) \;\; if \;\; d_{min} \in [d_{\sigma\_max}, d_{\sigma\_min}] \\ \sigma_{max} \;\; if \;\; d_{min} < d_{\sigma\_max} \end{cases}, \tag{46}$$

where

$$\rho(d_{min}) = (d_{min} - d_{\sigma\_max}) \frac{\sigma_{max} - \sigma_{min}}{d_{\sigma\_min} - d_{\sigma\_max}}, \tag{47}$$

and

$$d_{min} = \min_{i}^{N_{sect}} ||\boldsymbol{p}_{d,k} - \boldsymbol{p}_{stat\_i}||, \tag{48}$$

is the minimum distance from the reference position to any static obstacle, and $\sigma \in [\sigma_{min}, \sigma_{max}]$, and d_{σ_max} and d_{σ_min} are the distances at which σ has its minimum and maximum value respectively, where $d_{\sigma\_max} < d_{\sigma\_min}$.

Here, step 3 reduces the chances of restricting the optimal trajectory from traversing along the reference trajectory in very confined spaces by increasing the relationship between the major and minor axis in the ellipse, and hence stretching out the convex free set in the direction travel. However, when the distance to static obstacles is large, the relationship σ is decreased, and the convex free set takes a more circular form. This opens up the areas to the starboard and port of the reference trajectory for maneuvers. This is demonstrated by Fig. 6, where a convex free set is constructed at 70 s intervals along a reference trajectory. In the figure, the convex free set is more circular when the reference position has a larger margin to static obstacles, like the darker of the two green sets and the red set, while the

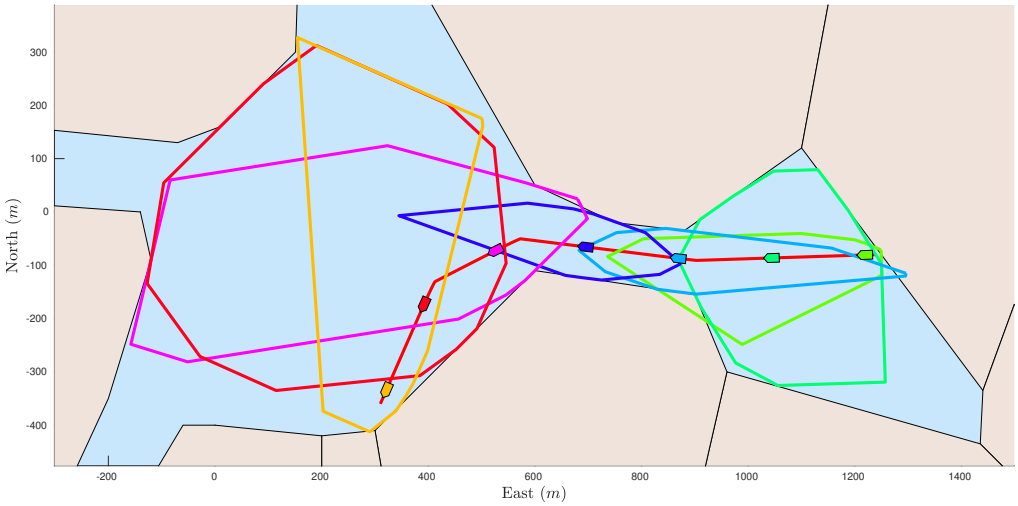

Figure 6: Convex free sets w.r.t. static obstacles with $N_{sect} = 12$. The figure shows sets for OS at intervals of 70 s along a reference trajectory in red. Color of set boundary correspond to color of vessel.

convex free set is more ellipse-shaped for the two blue sets, where the reference position is in a narrow area.

To constrain the trajectory to the convex free set, linear constraints are formulated as a function of the distance to the domain of each point $\boldsymbol{p}_{stat\_i}$

$$\boldsymbol{h}_{stat\_k} = \begin{bmatrix} \boldsymbol{n}^{\mathsf{T}}_{\boldsymbol{p}_{stat\_1}}(\boldsymbol{p}_k - \boldsymbol{p}_{stat\_1}) - \delta_{stat} \\ \boldsymbol{n}^{\mathsf{T}}_{\boldsymbol{p}_{stat\_2}}(\boldsymbol{p}_k - \boldsymbol{p}_{stat\_2}) - \delta_{stat} \\ \vdots \\ \boldsymbol{n}^{\mathsf{T}}_{\boldsymbol{p}_{stat\_N_{sect}}}(\boldsymbol{p}_k - \boldsymbol{p}_{stat\_N_{sect}}) - \delta_{stat} \end{bmatrix}, \tag{49}$$

where $\delta_{stat} > 0$ ensures a minimum distance to the obstacle. The complete set of constraints for static obstacles then becomes

$$\boldsymbol{h}_{stat} = \bigcup_{k}^{C_{stat}} \boldsymbol{h}_{stat\_k}. \tag{50}$$

4.6 Reference trajectory

Since any dynamic obstacle can be passed on both sides, the proposed OCP is non-convex whenever a TS is considered. There is therefore a local minima to the OCP corresponding to a trajectory passing on either side of a TS, and the number of local minima increases exponentially with the number of TSs. Additionally, since avoidance maneuvers by definition will make the solution deviate from the reference trajectory, and hence increase the cost, the solver is prone to produce solutions that are oscillating between two or more local minima at successive iterations of the solver with minor changes in the problem input. Since, by design, each of the local minima are collision-free and partially COLREGs-compliant trajectories, it is not paramount to find the global minimum. However, fluctuations between several local minima at successive iterations can result in non-predictable OS behaviour, which is unfortunate and in conflict with the protocol requirements.

We propose to mitigate this by two means: First, a trajectory for an initial guess of the OCP, $\boldsymbol{x}_{initial\_guess}$, is calculated based on the time-shifted optimal solution from the previous iteration $\boldsymbol{x}_{opt\_prev}$. Padding at the end of the trajectory to extend it to match the control horizon is added by simulating a Nomoto model with LOS guidance with initial states that correspond to the end of the previous optimal trajectory. Assuming that any TS is maneuvering close to its predicted trajectory in the previous iteration, then $\boldsymbol{x}_{opt}$ will be close to $\boldsymbol{x}_{initial\_guess}$.

Secondly, the desired trajectory $\boldsymbol{x}_d$ for the OCP is calculated as a weighted average between the reference trajectory $\boldsymbol{x}_{ref}$ and the initial guess, as

$$\boldsymbol{x}_d = \kappa \boldsymbol{x}_{ref} + (1 - \kappa)\boldsymbol{x}_{initial\_guess}, \tag{51}$$

where $\kappa \in [0, 1)$ and $\boldsymbol{x}_{ref}$ is a discretized reference trajectory on the form of (20), where $\boldsymbol{x}_{ref}$ can be provided by an arbitrary higher level planner. Details on how we calculate $\boldsymbol{x}_{ref}$ is provided in Section 5. By appropriate choice of κ, the fluctuations between local minima at successive solutions of the OCP can be reduced by moving the current global optima closer to the previous optimal solution, and hence closer to the initial guess.

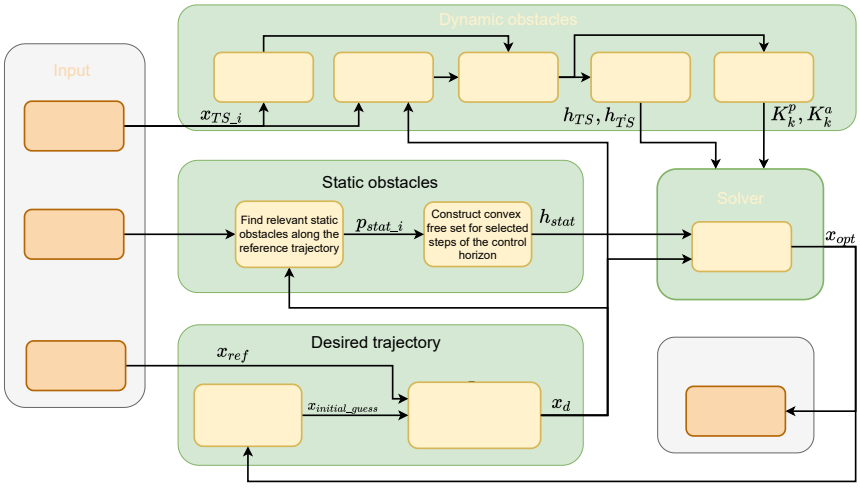

Figure 7: Overview of the pipeline for the proposed trajectory planning method.

The rationale behind this is that the COLAV objective has higher priority than the trajectory tracking objective, and that when $\boldsymbol{x}_{opt}$ deviates from $\boldsymbol{x}_{ref}$, it is a beneficial deviation w.r.t. safety and COLREGs compliance, and should be facilitated. If there are no constraints from dynamic or static obstacles in conflict with the input trajectory $\boldsymbol{x}_{ref}$, then both $\boldsymbol{x}_d$ and $\boldsymbol{x}_{initial\_guess}$ will converge to $\boldsymbol{x}_{ref}$, and hence the optimal solution $\boldsymbol{x}_{opt}$ will converge towards $\boldsymbol{x}_{ref}$, restricted only by the acceleration cost in (24).

4.7 Target ship priority

An operational domain can include several vessels, where the vessels might not interfere with the OS trajectory at all, and hence do not need to be assigned constraints in the OCP. Additionally, the OS might be in a stand-on encounter with vessels, and is therefore obliged, conditionally, to keeps its course and speed while the give-way vessel maneuvers, or until it is clear that the give-way vessel is not abiding its duty, and the encounter can not be resolved by maneuvering from the TS alone. Constraints should therefore not be assigned to vessels which the OS is in a stand-on encounter with, until the absence of a maneuver from the TS is apparent. To resolve this, we propose a list of prioritized vessels denoted $\mathcal{N}_{pri}$, where constraints are formulated only for vessels in $\mathcal{N}_{pri}$. The entry criteria are based on a critical distance at closest point of approach (DCPA), $d_{crit} > 0$, as well as the time until the OS enters and exits a circular region around the TS with radius d_{crit} , denoted t_{crit}^{enter} and t_{crit}^{exit}, respectively. For a TS with DCPA larger than d_{crit}, t_{crit}^{enter} and t_{crit}^{exit} are not defined, however by appropriate choice of d_{crit}, such a TS need not be included in $\mathcal{N}_{pri}$.

Target ships in encounters that are classified as either give-way, overtaking or head-on are included in the priority list if either

$$t_{crit}^{exit} < T_{horizon} - T_{after\_pass\_padding}, \tag{52}$$

or

$$t_{crit}^{enter} < T_{critical}. \tag{53}$$

The first criteria admits vessels to the list once the control horizon extends for a time $T_{after\_pass\_padding} > 0$ beyond the point where the previous optimal trajectory exits critical distance. This increasing the chances of $\boldsymbol{x}_{opt}$ to actually resolve the encounter with the relevant TS, and not for example reduce speed to avoid encountering the TS within the horizon. The second criteria ensures that the vessel is included in $\mathcal{N}_{pri}$ if t_{crit}^{enter} drops below a critical threshold $T_{critical} > 0$, even though t_{crit}^{exit} is not sufficiently in the control horizon. This is relevant for encounters where the relative velocity between the vessels is low e.g. in overtaking encounters. A TS in an encounter classified as stand-on is entered into the list if

$$t_{crit}^{enter} < T_{crit\_stand-on}. \tag{54}$$

Here, $T_{crit\_stand-on}$ serves as a threshold for when it is assumed that the TS is not abiding its give-way obligations, and the OS needs to take action to avoid collision.

4.8 Positive maneuvers in ample time

The features of the OCP described so far will ensure that $\boldsymbol{x}_{opt}$ is collision-free with static and dynamic obstacles while avoiding dynamic obstacles in a manner that is compliant with COLREGs rules 13-15 and 17. However Rule 8 and Rule 16 are yet to be addressed. Some regard was given to this by the introduction of the second constraint type for dynamic obstacles, where the relative velocity in the encounter is restricted by the range between the vessels. This does however only set a lower limit for the range to start a maneuver for a given relative velocity, but does not consider the magnitude of the maneuver, or whether it is initiated in ample time.

To improve compliance with rules 8 and 16, and facilitate readily apparent maneuvers made in ample time, we propose to design a cost profile for the gains of the cost function, namely K_k^p and K_k^a for $k \in [1, N_p]$. In particular, we design separate cost reduction windows (CRW) for the position and acceleration cost, where windows of reduced cost in the OCP horizon will facilitate a required maneuver to be made within that window. In particular, an acceleration cost reduction window (ACRW) will facilitate any maneuver to avoid or give-way to an oncoming vessel to happen within that window. Then it is only a matter of placing the ACRW so that it both starts and ends "in ample time" before t_{crit}^{enter} for that vessel to ensure that, if possible, the maneuver is completed within an appropriate time. Further, by assigning an appropriately short duration to this ACRW, the magnitude of the maneuver can also be manipulated. To allow the optimal trajectory to deviate from $\boldsymbol{x}_d$ from the start of the ACRW until the encounter is resolved, a position cost reduction window (PCRW) is assigned.

The design of the CRWs is made based on the estimated t_{crit}^{enter} and t_{crit}^{exit} for the vessels in $\mathcal{N}_{pri}$. The start time for the ACRW is

$$t_{ACRW}^{start} = \min_{\mathcal{N}_{pri}}(t_{crit}^{enter}) - T_{ample\_time}, \tag{55}$$

where $T_{ample\_time} > 0$ is an estimate for what is considered ample time for that specific encounter. The end time for the acceleration window is given by

$$t_{ACRW}^{end} = t_{ACRW}^{start} + T_{maneuver}, \tag{56}$$

where $T_{maneuver} > 0$ is the desired duration of the maneuver. From this, the acceleration cost-gain is defined as

$$K_k^a := \begin{cases} k^a k_{maneuver}^a & \text{if } kh \in [t_{ACRW}^{start}, t_{ACRW}^{end}] \\ k^a & \text{otherwise} \end{cases} \tag{57}$$

where $k_{maneuver}^a \in (0, 1]$ is the cost reduction for acceleration usage within the ACRW. For the work presented here, we apply fixed values for T_{ample_time} and $T_{maneuver}$, however, a more qualified estimate of these parameters should be made for each vessel-to-vessel encounter based on factors such as the size, type, velocity and maneuvering capacity of the involved vessels. This is outside the scope of this paper, and is left for future work.

The start time for the PCRW is the same as for the ACRW

$$t_{PCRW}^{start} = t_{ACRW}^{start}, \tag{58}$$

and the end time is

$$t_{PCRW}^{end} = \max_{\mathcal{N}_{pri}}(t_{crit}^{exit}). \tag{59}$$

The PCRW extend from the time where the initial maneuver should start, until the trajectory is clear of the last vessel in $\mathcal{N}_{pri}$. The cost-gain for the tracking error is defined as

$$K_k^p := \begin{cases} k^p k_{maneuver}^p & \text{if } kh \in [t_{PCRW}^{start}, t_{PCRW}^{end}] \\ k^p & \text{otherwise,} \end{cases} \tag{60}$$

where $k_{maneuver}^p \in (0, 1]$ is the cost reduction for the position error within the PCRW. The PCRW reduces the cost of the tracking error from $\boldsymbol{x}_d$ when maneuvering, and hence also the motivation to converge back to $\boldsymbol{x}_d$ between TSs in the case of several TSs in $\mathcal{N}_{pri}$.

For each new iteration of the trajectory planner, the cost reduction profiles are time-shifted by the time since last iteration to match the new control horizon. Every time a new TS is included in $\mathcal{N}_{pri}$, it is assumed that a maneuver by the OS is needed, and new CRWs are calculated.

4.9 OCP formulation

Finally, the OCP can be defined on the form in (11), with the objective function given by (24), with gains according to (57) and (60). The equality constraints are on the form of (14), with the integrating function (13), where the $f(\boldsymbol{x}, \boldsymbol{v})$ is the system in (15), $\boldsymbol{x}$ is the system state and $\boldsymbol{a}$ is the control input. The set of inequality constraints is defined as

$$\boldsymbol{h} := \boldsymbol{h}_v \cup \boldsymbol{h}_a \cup \boldsymbol{h}_{TS} \cup \boldsymbol{h}_{stat} \tag{61}$$

where $\boldsymbol{h}_v$, $\boldsymbol{h}_a$, $\boldsymbol{h}_{TS}$ and $\boldsymbol{h}_{stat}$ are given by (29), (30), (44) and (50), respectively.

5 Simulations

In this section, simulation results are presented. First, an extensive set of vessel-to-vessel encounters in open waters are presented and discussed. These simulations cover a distributed subset of possible vessel-to-vessel

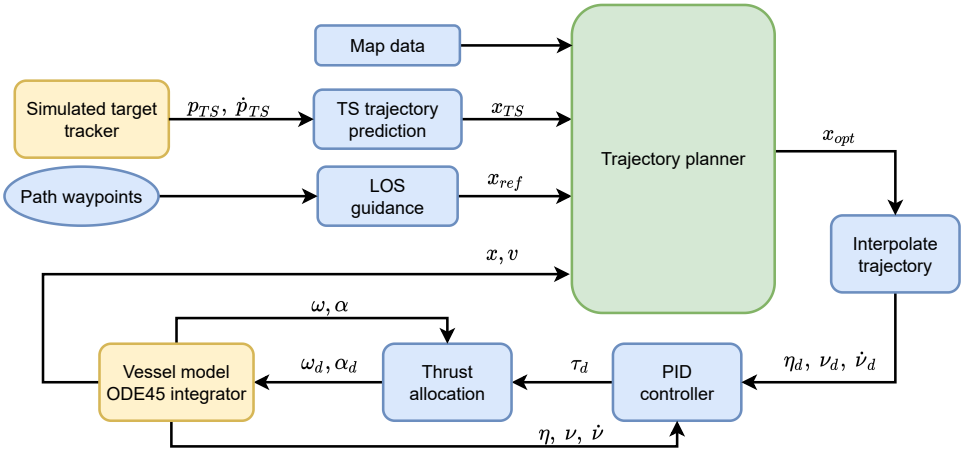

Figure 8: Guidance, navigation and control pipeline for the simulations. The internals of the green box are illustrated in Fig. 7.

encounters, and serve to demonstrate the completeness of the method in terms of COLREGs compliance with the rules from Section 3. Thereafter, we include a set of simulations from more complex urban environments where the presence of static obstacles and several maneuvering vessels demonstrate the capacity of the proposed method to handle an unstructured and highly relevant environment.

An overview of the simulator setup is shown in Fig. 8. The simulator is implemented in Matlab where the OS model is a 3DOF model of the milliAmpere experimental platform. The model parameters used in the simulations can be found in (Pedersen, 2019). In the simulations, the Matlab ODE45 solver is applied for state integration. The parameter values used in the simulations are given in tables 1 and 2.

The simulator consists of the following modules:

- The **Map data** module contains all static obstacles on the form of convex polygons.
- The **Simulated target tracker** module provides position and velocity states for all vessels that have a line of sight from the OS that is unobstructed by static obstacles.
- The **TS trajectory prediction** module makes a discretized trajectory prediction for the duration of the control horizon for each TS. The prediction is made based on a constant velocity model.
- The **Path waypoints** module is a set of waypoints that describes the desired transit route. Each waypoint has an associated reference speed.
- The **LOS guidance** module calculates $\boldsymbol{x}_{ref}$. This is done by simulating a kinematic vessel model starting at the initial conditions of the OCP, where the vessel tracks the path waypoints by means of a constant lookahead-distance LOS guidance method. The LOS guidance method inputs the path-waypoints and administers waypoint switching. The kinematic vessel model is simulated for the duration of the control horizon, where $\boldsymbol{x}_{ref}$ is constructed by discretizing the simulated trajectory with a timestep of h, and for N_p steps, resulting in a trajectory on the form of (20).
- The mid-level **Trajectory planner** module is the COLAV method described in Section 4. An overview of this module is shown in Fig. 7.
- The **Trajectory interpolation** module interpolates the discretized optimal trajectory $\boldsymbol{x}_{opt}$ to get reference signals for the PID controller.
- The **PID controller** module performs trajectory following by a velocity and acceleration feed forward PID controller.
- The **Thrust allocation** module realizes the generalized reference force $\boldsymbol{\tau}_d$ by calculating appropriate setpoints for the two azimuth thrusters.

5.1 Batch simulations

In this section, we present results for evaluating the completeness of the method in terms COLREGs compliance in vessel-to-vessel encounters without static ob-

Table 1: Rule-based parameters for the TS domain.

Parameter	SF	SO	OT_p	OTs	HO	GW	**Unit**
α_d	0	$\pi/4$	$\pi/3$	$\pi/3$	$2\pi/5$	$2\pi/5$	rad
α_{δ_s}	0	$\pi/2$	-$3\pi/4$	$3\pi/4$	$\pi/12$	-$\pi/8$	rad
c_{dyn}	10	10	40	40	60	60	s

Table 2: Non rule-based parameters.

Parameter	**Value**
N_p	150
h	4 s
k^p	$2.5 \times 10^{-5}\,\mathrm{m}^{-2}$
k^a	$50\,\mathrm{m}^2\mathrm{s}^{-4}$
$k^p_{maneuver}$	0.0005
$k^a_{maneuver}$	0.007
κ	0.7
δ_{dyn}	1 m
σ_{max}	4
σ_{min}	1
$T_{after\_pass\_padding}$	40 s
$T_{critical}$	140 s
$T_{crit\_stand-on}$	20 s
T_{ample_time}	120 s
$t_{maneuver}$	40 s
d_{σ_max}	20 m
d_{σ_min}	100 m
r_{free_max}	40 m
d_{crit}	50 m
k_l	0.50
N_{sect}	12
δ_{stat}	8 m

stacles. The results are produced through an extensive simulation study, with the OS and TS on straight line paths, where the TS keeps a constant course and speed in each simulation. The set of simulations is constructed by varying two parameters: the relative course χ_{rel} between the vessels, and the lateral offset, δ_{lat}, of the OS reference path from a point-of-collision at the origin of the local NED frame. The OS and TS waypoints are calculated so that both vessels will be at the origin after 200 s if $\delta_{lat} = 0$. The parameter χ_{rel} is iterated from 0 to 2π at steps of $\pi/16$, while the δ_{lat} is iterated from -200 m to 200 m at 10 m steps, resulting in a total of 1312 simulations. The OS and TS have a reference speed of 1.5 m/s and 1 m/s respectively. The OS path goes from west to east with $\chi = \pi/2$ while the TS path is adjusted for each χ_{rel}. A subset of the simulations are presented in figures 9 - 13 where all OS trajectories for a given TS course are combined in one figure.

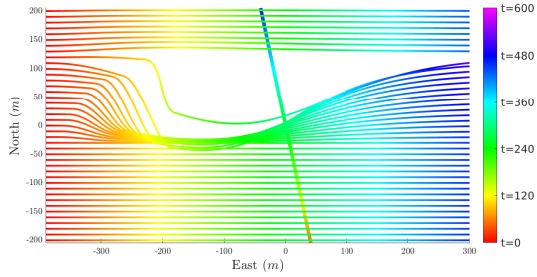

Figure 9: Batch 1: Give-way crossing.

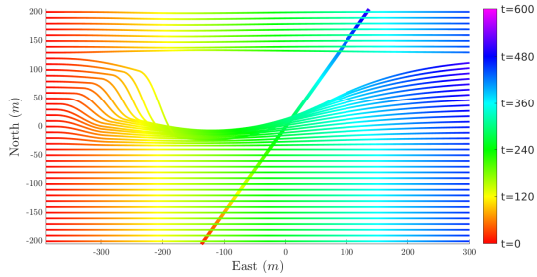

Figure 10: Batch 2: Give-way crossing.

Figures 9 and 10 show results from encounters where the OS has give-way obligations and is on a crossing course with the TS. One can see from the OS trajectories that the encounters are resolved by performing a starboard maneuver to pass behind the TS for a majority of the simulations where the OS has to maneuver from its reference trajectory to avoid TS domain violation. In one or two encounters in each of the figures, the OS instead performs a small port maneuver to pass in front of the TS. However, all encounters are resolved without domain violation, and in the situations where the OS maneuvers and still passes in front of the TS, it does so with such a margin that it does not impede the TS. The effects of the CRWs are also apparent from the OS trajectories between 50 s and 200 s into the transit, where the course change maneuver is visible and readily apparent, in compliance with Rule 8, in addition

to being made in ample time due to the ACRW and PCRW offset from the minimum t_{crit}^{enter}.

In Fig. 11, results from stand-on crossing encounters are presented. In these encounters, the TS is the give-way vessel and the OS has stand-on obligations, and shall keep its course and speed until it is apparent that the TS is not abiding its give-way duty, and the encounter can not be resolved by a maneuver from the TS alone. By only including stand-on vessels with a $tcpa^{+}_{critical}$ below a threshold value, this behaviour can be achieved, as demonstrated in Fig. 11. However, determining the threshold value $tcpa^{+}_{critical}$ is not trivial, where it should include considerations on several aspects of the TS, such as its maneuvering capabilities and vessel type. Such information can be acquired either through AIS or comprehended by the vessels situational awareness system based on exteroceptive sensors.

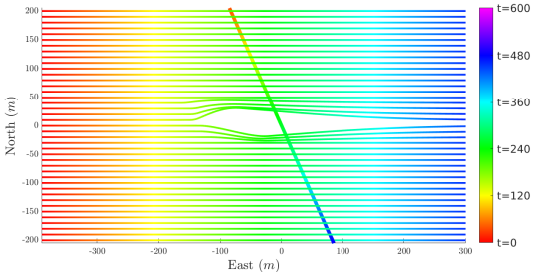

Figure 11: Batch 3: Stand-on crossing.

In Fig. 12, results from overtaking encounters are presented. From the figure, one can see that the OS gives way to the TS in all encounters. The effect of the CRWs is not as apparent in the overtaking encounters since the relative velocity between the vessels is small, and the duration of the manuever, and hence the reduced position cost window, extends throughout a majority of the control horizon. Additionally, the close to parallel courses of the OS and TS limits the need for course-change maneuvers from the OS to pass clear of the TS domain, and therefore the initial course change maneuver is less apparent than in the give-way crossing encounters. However, the maneuver is visible and made in ample time.

Finally, Fig. 13 shows results from head-on encounters. Also in these simulations, all encounters are resolved without violation of the TS domain. Similar to the give-way crossing encounters, the OS performs a readily apparent starboard maneuver in ample time, and passes the TS port to port in compliance with rules 8, 14 and 16.

Two substantial improvements are achieved by applying a deliberate trajectory planning approach, as opposed to the reactive method presented in (Thyri and Breivik, 2022a) which uses the same TS domain. Both improvements are clearly demonstrated in Fig. 14, where a batch of simulations for the deliberate and reactive method under similar conditions are presented. First, the reactive method has a stagnation problem that occurs when the OS is approaching the TS domain at a near right angle with no clear direction of deflection, as is apparent in the red frame in Fig. 14(b), where the OS trajectory slows down before deflecting to starboard. The trajectory planner that we propose in this paper avoids this problem as long as the control horizon extends beyond the duration of the encounter from the point at which the maneuver starts. The local optimal trajectory does not maneuver into these areas, as it results in both high acceleration and tracking error, and hence high cost. Furthermore, applying a deliberate planning approach, as opposed to the reactive one in Fig. 14(b), enables improvements w.r.t. the requirements of Rule 8, where "Any action taken to avoid collision shall, if the circumstances of the case admit, be positive, made in ample time and with due regard to the observance of good seamanship", which is achieved through the CRWs.

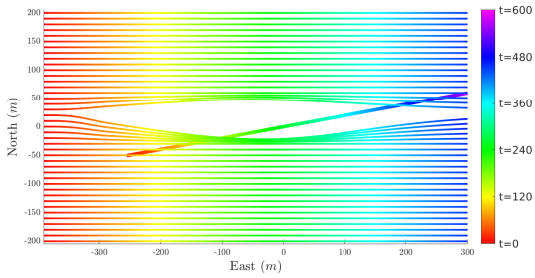

Figure 12: Batch 4: Overtaking.

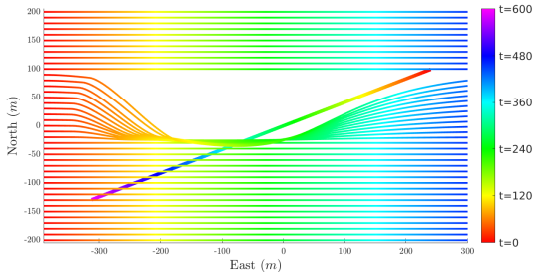

Figure 13: Batch 5: Head-on.

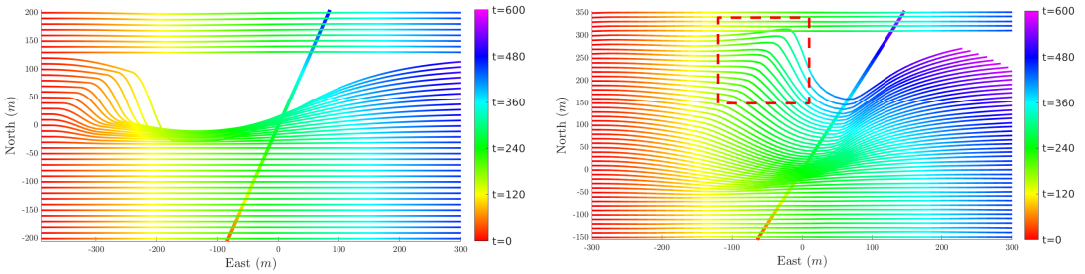

(a) Give-way crossing encounters with the trajectory planning method proposed in this paper.

(b) Give-way crossing encounters with the reactive COLAV method proposed in Thyri and Breivik (2022a).

Figure 14: Comparison of give-way encounters.

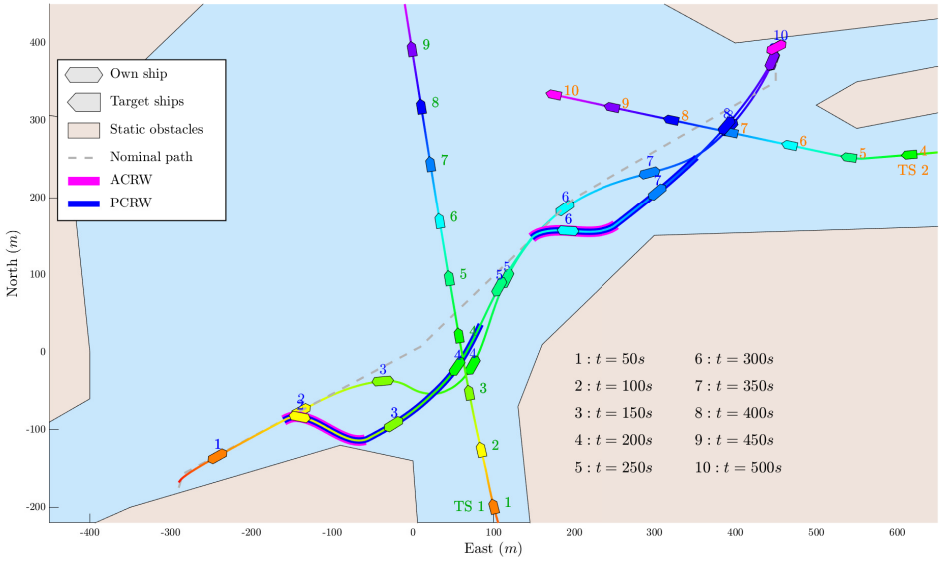

Figure 15: Simulation 1: Transit between two docking locations where the OS encounters two TSs in give-way encounters. The figure includes the OS trajectory for a run with and without CRWs. The TSs have identical behaviour in both runs.

5.2 Complex scenarios

In this section, we present a set of more complex simulations where the OS is maneuvering in a confined space with several other maneuvering vessels. These simulations demonstrates the proposed COLAV method's robustness in terms of COLREGs, where it handles a variety of encounters while adhering to the maneuvering principles of the rules presented in Section 3.1. An overview of each scenario is presented in a single figure with representations of the OS and each TS at matching 50 s intervals. The figures also show the OS nominal path and trajectory along with the trajectory of each TS. Furthermore, pink and blue lines are superimposed on the OS trajectory at the areas where the ACRWs and PCRWs are active and hence reduce the acceleration cost-gain and tracking error cost-gain respectively.

5.2.1 Simulation 1: Double give-way with and without CRWs

In this simulation, the OS performs a transit between two docking locations in an urban environment where

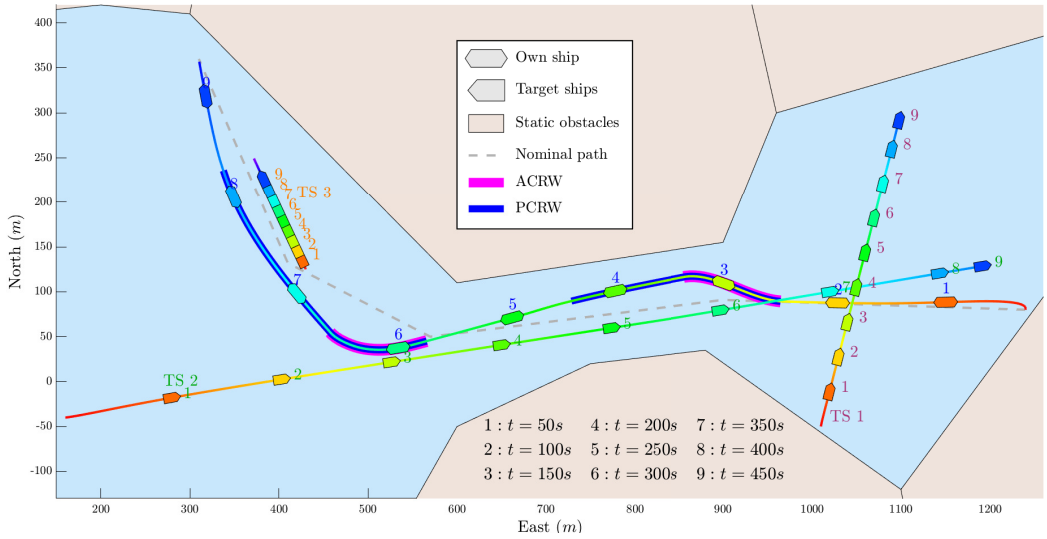

Figure 16: Simulation 2: Transit between two docking locations, with a stand-on, head-on and overtaking encounter.

it encounters two TSs in give-way crossing encounters. An overview of the simulation is given in Fig. 15, where the trajectory of the OS is included for a run both with and without the use of CRWs to calculate the tracking error and acceleration cost-gains.

From the overview in Fig. 15, one can see that the OS resolves both encounters in accordance with Rule 17 by performing a starboard maneuver and pass behind each TS in both runs. However, the effect of the CRWs are apparent, where for the run with CRWs, the avoidance maneuvers are of another magnitude, and come earlier compared to the run without CRWs.

This is further demonstrated in Fig. 17 where the OS course profile from the two simulations is shown. One can see that the CRWs motivate a maneuver that starts T_{ample_time} before the TCPA of each TS, where the course change maneuver is concentrated in a window of duration $T_{maneuver}$ to produce a positive and readily apparent course change maneuver. In the simulation with CRWs, the course change maneuvers have a magnitude of approximately 60°, where without CRWs, the first encounters is resolved by an initial gradual course change, followed by a sudden course change at close range, and the second encounter is resolved by a long-lasting continuous course change maneuver. This simulation clearly demonstrate the benefit of the proposed CRWs, where the maneuvering behaviour of the ownship can be made to comply with rules 8 and rule 16 by a small set of parameters.

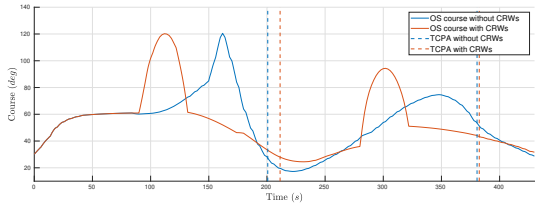

Figure 17: Simulation 1: Course profile for OS trajectory with and without CRWs.

5.2.2 Simulation 2: Stand-on, head-on and overtaking

In this simulation, the OS is transiting between two docking locations in an urban environment with three TSs. The first TS is met in a crossing encounter where the OS has stand-on obligations, the second TS is encountered head-on, and the final TS is met in an overtaking encounter where the TS is moving at a very low speed. An overview of the simulation is shown in Fig. 16. Due to the encounter type and the DCPA in the encounter with TS 1, the vessel is not included in $\mathcal{N}_{pri}$. This is apparent from Fig. 16 since no CRWs are assigned prior to the encounter. Hence, the OS keeps its stand-on obligations to TS 1 in accordance with Rule 17. As the encounter with TS 2 moves within the control horizon, TS 2 is included in $\mathcal{N}_{pri}$, and appropri-

Figure 18: Simulation 3: Transit between two docking locations, with a give-way crossing, stand-on crossing and a head-on/give-way encounter.

ate CRWs are assigned. As a result, the OS performs a course-change maneuver, and moves to its starboard side of the narrow area, to pass the oncoming vessel port to port. Note that at the CPA, the OS splits the available space between TS 2 and land close to equally between them, as $r_{free} < r_{free\_max}$. In the same way, when TS 3 is included in $\mathcal{N}_{pri}$, the CRWs are recalculated, resulting in a trajectory that continues straight when the nominal trajectory is turning, and performs the starboard maneuver at a later point. This prevents the OS from maneuvering onto a collision course with TS 3, and hence clearly demonstrate the OS's intention to give-way in the encounter in accordance with Rule 13. The OS completes the transit without collision while maneuvering in accordance with the COLREGs.

In this simulation, the OS transits between two docking locations in a harbour environment with traffic, where the TSs track reference trajectories that are maneuvering. An overview of the simulation is shown in Fig. 18. The OS is moving from east to west, while three other TSs are maneuvering within the area. The TSs are only visible to the planner when there is an unobstructed line of sight between the OS and the TS, and the predictions for the future TS trajectories assume constant velocity.

As the OS departs, it does not observe any other vessels. But, as it moves beyond the pier on its starboard side, it detects TS 1 exiting the northeast harbour and classifies the encounter as give-way crossing. Initially, the trajectory of the OS does not have a critical DCPA to the predicted trajectory of TS 1, but as TS 1 maneuvers, the estimated DCPA is reduced and TS 1 is included in $\mathcal{N}_{pri}$. This triggers the set of CRWs to be calculated. The CRWs are apparent from the pink and blue regions along the early parts of the OS trajectory. The resulting trajectory maneuvers to starboard to pass behind TS 1, in accordance with the Rule 15.

Later, the OS detects TS 2 exiting the harbour on its forward port side. This encounter is classified as a stand-on crossing. Despite TS 2 having a course that is on close to collision course with the OS, it does not have a t_{crit}^{enter} below the $T_{crit\_stand-on}$ threshold, and is therefore not included in $\mathcal{N}_{pri}$. As TS 2 subsequently maneuvers to starboard, the margins are increased, and it is therefore never included in $\mathcal{N}_{pri}$.

Lastly, the OS approaches TS 3 arriving from east.

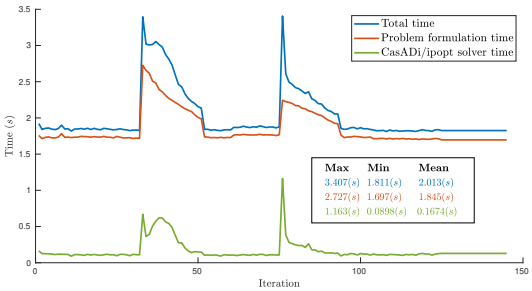

Figure 19: Runtime for the proposed algorithm for Simulation 3. The total time is split into the time for formulating the OCP, and the time the solver uses to find an optimal solution. The spikes clearly clearly indicate when TS 1 and TS 3 is included in $\mathcal{N}_{pri}$.

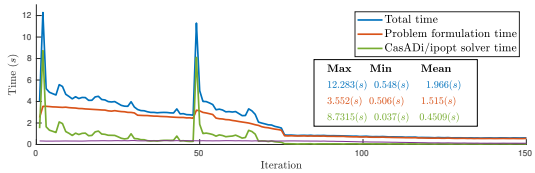

Figure 20: Runtime for the proposed algorithm for a very confined space simulation with 4 TSs that require avoidance maneuvers.

This TS is detected early, but due to its initial course, its predicted trajectory did not interfere sufficiently with the OS trajectory to be considered until it performed the starboard maneuver towards the harbour. It is then included in $\mathcal{N}_{pri}$, and a new set of CRWs are calculated. The OS performs a small starboard maneuver to pass TS 3 port to port, and eventually behind it. This OS maneuvers in accordance with both Rule 14 and Rule 15.

5.3 Runtime

For such a trajectory planning algorithm to be applied on a vessel, its runtime must support real-time operation. By this we mean that the period from a new input to an optimal trajectory is calculated should be of magnitude seconds or less to ensure that the optimal trajectory is still valid and relevant. When detecting a new TS that requires an avoidance maneuver, an updated trajectory should be calculated fast enough so that maneuvering in ample time is feasible. Additionally, a short runtime reduces jumps in tracking error when the initial part of the new trajectory deviates from the previous optimal trajectory, and hence dynamic feasibility and smooth transient behaviour is maintained. In Fig. 19, the runtime for the algorithm that we propose is displayed for Simulation 3, while Fig. 20 shows the runtime of a more complex scenario[2] with 4 TSs, where several of the vessels must be considered simultaneously.

Our code is written in Matlab with no particular regard to runtime, and runs on a Dell Precision 5540 with a 32 GB memory and an Intel Core i9-9880H processor running at 2.30 GHz. The results from Fig. 19 show that the algorithm uses on average 2 s, and a maximum of 3.407 s, on formulating and solving the OCP in Simulation 3. Furthermore, we see that the majority of the runtime comes from formulating, not solving, the OCP. This indicates some potential for further reduction in runtime by improving code efficiency. However, the runtime is within acceptable limits for real-time application. From Fig. 20, we see spikes in the runtime of about 12 s. The spikes come when TSs that require avoidance maneuvers are added to $\mathcal{N}_{pri}$, resulting in a large discrepancy between $\boldsymbol{x}_{initial\_guess}$ and $\boldsymbol{x}_{opt}$ combined with a large number of nonlinear constraints from the total set of vessels in $\mathcal{N}_{pri}$. The runtime analysis is not conclusive, however it indicates that the proposed algorithm is suitable for realtime operation in reasonably complex scenarios, while increasing traffic complexity can result in a runtime that extend beyond acceptable limits.

[2]The scenario is not included in the results of this paper, but an illustration of it can be viewed at: https://rb.gy/xxeruc

6 Conclusion and Future Work

An MPC-based approach to COLAV for ASVs that is compliant with COLREGs rules 8 and 13-17 has been presented. We propose to formulate and solve an optimal control problem for a simplified ASV model where the objective is to find a dynamically feasible trajectory that minimizes both the tracking error to some reference trajectory, and the induced acceleration. Collision avoidance with both static and dynamic obstacles is handled by assigning domains to each obstacle, and then formulating constraints for each domain.

Compliance with the encounter-type specific maneuvering requirements of rules 13-15 and 17 is handled by first classifying each vessel-to-vessel encounter, and then formulating constraints w.r.t. an encounter-type specific domain for each target ship (TS). The constraints are formulated so that if the trajectory does not violate them, the trajectory is in compliance with the relevant rule for that encounter.

Furthermore, compliance with rules 8 and 16 is facilitated through assignment of windows of reduced

cost on acceleration and tracking error, where the windows incentivize any avoidance maneuvers to fall within them. The position of the windows relative to an estimated time to a critical distance between the OS and TS is parameterized by a small set of intuitive parameters, and enables placement of the windows, and hence the maneuver, in ample time before close quarters.

The COLREGs compliance of the method is demonstrated through an extensive and systematic set of simulations of vessel-to-vessel encounters in open waters. The proposed method produces smooth maneuvers and resolves all encounters without collision, in accordance with the COLREGs rules 8 and 13-17.

Finally, we demonstrate the method in a relevant application through simulations of dock-to-dock transit in urban environments with several maneuvering vessels. The proposed method completes the transit in each case, and avoids collision or close quarters with the other vessels by performing COLREGs-compliant maneuvers. Lastly, the runtime of the method is demonstrated to be within feasible limits for real-time operation.

Future work includes:

- Improving compliance w.r.t. Rule 8 and Rule 16 by making an individual estimate of "ample time" for each vessel-to-vessel encounter.
- Further work on the encounter classification through improved intent inference.
- Full-scale experiments and closed-loop testing in combination with a target-tracking system based on exteroceptive sensors.
- Runtime improvements.

Acknowledgments

This work was supported by the NTNU Digital transformation project Autoferry and the Research Council of Norway through the Centers of Excellence funding scheme, project no. 223254.

References

Abdelaal, M., Fränzle, M., and Hahn, A. Nonlinear model predictive control for trajectory tracking and collision avoidance of underactuated vessels with disturbances. *Ocean Engineering*, 2018. 160:168–180. doi:https://doi.org/10.1016/j.oceaneng.2018.04.026.

Abdelaal, M. and Hahn, A. NMPC-based trajectory tracking and collision avoidance of unmanned surface vessels with rule-based colregs confinement. In *Proc. IEEE Conference on Systems, Process and Control (ICSPC)*. pages 23–28, 2016. doi:10.1109/SPC.2016.7920697.

Cockcroft, A. N. and Lameijer, J. N. F. *Guide to the Collision Avoidance Rules*. Butterworth-Heinemann, 2012. doi:https://doi.org/10.1016/C2010-0-68322-2.

Čorić, M. and Nikšić, M. Possibilities of Using Autonomous Green Vessels for Passenger Transport in Urban Environments. In M. Petrović, L. Novačko, D. Božić, and T. Rožić, editors, *The Science and Development of Transport—ZIRP 2021*, pages 91–109. Springer International Publishing, 2022. doi:10.1007/978-3-030-97528-9_7.

DB Schenker. DB Schenker plans to operate a zero-emission autonomous coastal container feeder for Ekornes ASA in Norway. *DB Schenker Press Center. Accessed May. 06, 2022.*, 2022. URL https://www.dbschenker.com/global/about/press/autonomous-vessel-norway-788212.

Eriksen, B.-O. and Breivik, M. MPC-based mid-level collision avoidance for ASVs using nonlinear programming. In *Proc. 1st IEEE Conference on Control Technology and Applications (CCTA)*. Hawaii, USA, pages 766–772, 2017. doi:10.1109/CCTA.2017.8062554.

Eriksen, B.-O. H., Breivik, M., Wilthil, E., Flaten, A., and Brekke, E. The branching-course model predictive control algorithm for maritime collision avoidance. *Journal of Field Robotics*, 2019. 36:1222–1249. doi:10.1002/rob.21900.

Executive, T. M. China launches its first autonomous container ship service. *The Maritime Executive. Accessed May. 06, 2022.*, 2022. URL https://www.maritime-executive.com/article/china-reports-first-autonomous-containership-entered-service.

Kuwata, Y., Wolf, M. T., Zarzhitsky, D., and Huntsberger, T. L. Safe maritime autonomous navigation with COLREGs, using velocity obstacles. *IEEE Journal of Oceanic Engineering*, 2014. 39(1):110–119. doi:10.1109/JOE.2013.2254214.

Lloid's Register. ShipRight procedure - autonomous ships. *Cyber-enabled ships.*, 2016.

Loe, Ø. A. G. *Collision Avoidance for Unmanned Surface Vehicles*. Master's thesis, Norwegian University of Science and Technology, Trondheim, Norway, 2008. URL http://hdl.handle.net/11250/259696.

Martinsen, A. B., Bitar, G., Lekkas, A. M., and Gros, S. Optimization-based automatic docking and berthing of ASVs using exteroceptive sensors: Theory and experiments. *IEEE Access*, 2020. 8:204974–204986. doi:10.1109/ACCESS.2020.3037171.

Pedersen, A. A. *Optimization Based System Identification for the milliAmpere Ferry*. Master's thesis, Norwegian University of Science and Technology (NTNU), Trondheim, Norway, 2019. URL http://hdl.handle.net/11250/2625699.

Reddy, N. P., Zadeh, M. K., Thieme, C. A., Skjetne, R., Sorensen, A. J., Aanondsen, S. A., Breivik, M., and Eide, E. Zero-emission autonomous ferries for urban water transport: Cheaper, cleaner alternative to bridges and manned vessels. *IEEE Electrification Magazine*, 2019. 7(4):32–45. doi:10.1109/MELE.2019.2943954.

Ringbom, H. Regulating autonomous ships—concepts, challenges and precedents. *Ocean Development & International Law*, 2019. 50(2-3):141–169. doi:10.1080/00908320.2019.1582593.

RoBoat. Self-driving technology to transform urban waterways. *Accessed Dec. 14, 2021*, 2021. URL https://roboat.org/.

Szlapczynski, R. and Szlapczynska, J. Review of ship safety domains: Models and applications. *Ocean Engineering*, 2017. 145:277–289. doi:https://doi.org/10.1016/j.oceaneng.2017.09.020.

Thyri, E. H., Basso, E. A., Breivik, M., Pettersen, K. Y., Skjetne, R., and Lekkas, A. M. Reactive collision avoidance for ASVs based on control barrier functions. In *Proc. 4th IEEE Conference on Control Technology and Applications (CCTA)*. Montreal, QC, Canada, pages 380–387, 2020a. doi:10.1109/CCTA41146.2020.9206340.

Thyri, E. H. and Breivik, M. A domain-based and reactive COLAV method with a partially COLREGs-compliant domain for ASVs operating in confined waters. *Field Robotics*, 2022a. 2:632–677. doi:https://doi.org/10.55417/fr.2022022.

Thyri, E. H. and Breivik, M. Partly COLREGs-compliant collision avoidance for ASVs using encounter-specific velocity obstacles. In *Proc. 14th IFAC Conference on Control Applications in Marine Systems, Robotics, and Vehicles (CAMS)*. Copenhagen, Denmark, pages 1–7, 2022b.

Thyri, E. H., Breivik, M., and Lekkas, A. M. A path-velocity decomposition approach to collision avoidance for autonomous passenger ferries in confined waters. *IFAC-PapersOnLine*, 2020b. 53(2):14628–14635. doi:https://doi.org/10.1016/j.ifacol.2020.12.1472. 21st IFAC World Congress.

Vagale, A., Bye, R. T., Oucheikh, R., Osen, O. L., and Fossen, T. Path planning and collision avoidance for autonomous surface vehicles II: A comparative study of algorithms. *Journal of Marine Science and Technology*, 2021a. 26:1307–1323. doi:10.1007/s00773-020-00790-x.

Vagale, A., Oucheikh, R., Bye, R., Osen, O., and Fossen, T. Path planning and collision avoidance for autonomous surface vehicles I: A review. *Journal of Marine Science and Technology*, 2021b. 26:1292–1306. doi:https://doi.org/10.1007/s00773-020-00787-6.

Wärtsilä. Wätsilä to develop autonomous, zero emission barge for port of Rotterdam. *Wartsilia. Accesed Nov. 04, 2021*, 2021. URL https://www.wartsila.com/media/news/27-05-2021-wartsila-to-develop-autonomous-zero-emission-barge-for-port-of-rotterdam-2921606.

Xue, Y., Wang, X., Liu, Y., and Xue, G. Real-time nonlinear model predictive control of unmanned surface vehicles for trajectory tracking and collision avoidance. In *Proc. 7th International Conference on Mechatronics and Robotics Engineering (ICMRE)*. Budapest, Hungary, pages 150–155, 2021. doi:10.1109/ICMRE51691.2021.9384818.

Zeabuz. Zero emission autonomous urban mobility. *Zeabuz, Feb. 02, 2021. www.zeabuz.com. Accessed Jan. 25, 2022.*, 2022. URL https://zeabuz.com.

Ülkü Öztürk, Akdağ, M., and Ayabakan, T. A review of path planning algorithms in maritime autonomous surface ships: Navigation safety perspective. *Ocean Engineering*, 2022. 251:1–19. URL https://www.sciencedirect.com/science/article/pii/S0029801822004334, doi:https://doi.org/10.1016/j.oceaneng.2022.111010.

Bibliography

[1] G. West. "We're going commercial." In: *Cruise Press Release* (2022). URL: https://www.getcruise.com/news/were-going-commercial (visited on 06/18/2022).

[2] T. Kubota. "Stanford's robotics legacy". In: *Stanford News* (2019). URL: https://news.stanford.edu/2019/01/16/stanfords-robotics-legacy/ (visited on 07/19/2022).

[3] Kongsberg Maritime. *Autonomous underwater vehicle, Hugin*. 2022. URL: https://www.kongsberg.com/maritime/products/marine-robotics/autonomous-underwater-vehicles/AUV-hugin (visited on 06/30/2022).

[4] J. Larson, M. Bruch, and J. Ebken. "Autonomous navigation and obstacle avoidance for unmanned surface vehicles". In: *Unmanned Systems Technology VIII*. (Apr. 17, 2006). Ed. by G. R. Gerhart, C. M. Shoemaker, and D. W. Gage. Orlando, Florida, USA: SPIE, 2006. DOI: 10.1117/12.663798.

[5] P. E. Hagen, N. Størkersen, K. Vestgård, and P. Kartvedt. "The HUGIN 1000 autonomous underwater vehicle for military applications". In: *Proceedings of Oceans 2003. Celebrating the Past ... Teaming Toward the Future (IEEE Cat. No.03CH37492)*. Vol. 2. San Diego, CA, USA, 2003, 1141–1145 Vol.2. DOI: 10.1109/OCEANS.2003.178504.

[6] "DARPA's self-driving submarine hunter steers like a human". In: *IEEE Spectrum. https://spectrum.ieee.org/darpa-actuv-self-driving-submarine-hunter-steers-like-a-human. Accessed June. 19, 2022.* (2016). URL: https://spectrum.ieee.org/darpa-actuv-self-driving-submarine-hunter-steers-like-a-human.

[7] "ACTUV "Sea Hunter" prototype transitions to office of naval research for further development". In: *Defense Advanced Research Projects Agency* (2018). URL: https://www.darpa.mil/news-events/2018-01-30a (visited on 07/10/2022).

[8] "Falco makes world's first autonomous ferry crossing". In: *The Engineer* (2018). URL: https://www.theengineer.co.uk/content/news/falco-makes-world-s-first-autonomous-ferry-crossing (visited on 07/03/2022).

[9] European Maritime Safety Agency. "Annual overview of marine casualties and incidents 2019". In: *European Maritime Safety Agency, Technical report.* (2019).

[10] "First autonomous navigation and berthing test on a containership". In: *The Maritime Executive. https://www.maritime-executive.com/article/first-autonomous-navigation-and-berthing-test-on-a-containership. Accessed June. 18, 2022.* (2022). URL: https://www.maritime-executive.com/article/first-autonomous-navigation-and-berthing-test-on-a-containership.

[11] "China launches its first autonomous container ship service". In: *The Maritime Executive. https://www.maritime-executive.com/article/china-reports-first-autonomous-containership-entered-service. Accessed May. 06, 2022.* (2022). URL: https://www.maritime-executive.com/article/china-reports-first-autonomous-containership-entered-service.

[12] R. O'Dwyer. "ASKO to build two autonomous vessels for Oslo fjord operations". In: *Smart Maritime Network, Sep. 15, 2020. https://smartmaritimenetwork.com/2020/09/01/asko-to-build-two-autonomous-vessels-for-oslo-fjord-operations/. Accessed June 10, 2022.* (2020). Ed. by S. M. Network. URL: https://smartmaritimenetwork.com/2020/09/01/asko-to-build-two-autonomous-vessels-for-oslo-fjord-operations/ (visited on 02/09/2021).

[13] United Nations. "68% of the world population projected to live in urban areas by 2050". In: *United Nations Department of Economic and Social Affairs* (2018). URL: https://www.un.org/development/desa/en/news/population/2018-revision-of-world-urbanization-prospects.html (visited on 06/20/2022).

[14] N. P. Reddy, M. K. Zadeh, C. A. Thieme, R. Skjetne, A. J. Sørensen, S. A. Aanondsen, M. Breivik, and E. Eide. "Zero-emission autonomous ferries for urban water transport: Cheaper, cleaner alternative to bridges and manned vessels". In: *IEEE Electrification Magazine* 7.4 (2019), pp. 32–45. DOI: 10.1109/MELE.2019.2943954.

[15] M. Čorić and M. Nikšić. "Possibilities of using autonomous green vessels for passenger transport in urban environments". In: *The Science and Development of Transport—ZIRP 2021.* Ed. by M. Petrović, L. Novačko, D. Božić, and T. Rožić. Springer International Publishing,

2022, pp. 91–109. ISBN: 978-3-030-97528-9. DOI: 10.1007/978-3-030-97528-9_7. URL: https://doi.org/10.1007/978-3-030-97528-9_7.

[16] U. Skoglund. "Førerløse ferger kan erstatte gangbruer". In: *Gemini* (2018). URL: https://gemini.no/2018/06/forerlose-ferger-kan-erstatte-gangbruer/ (visited on 07/19/2022).

[17] "Zero emission autonomous urban mobility". In: *Zeabuz, www.zeabuz.com. Accessed June 14, 2022.* (2022). Ed. by zeabuz.com. URL: https://zeabuz.com.

[18] "Roboat. self-driving technology to transform urban waterways." In: *RoBoat, www.roaboat.org, Accessed June 12, 2022* (2021). Ed. by Roboat. URL: https://roboat.org/.

[19] Autoferry. "Autonomous all-electric passenger ferries for urban water transport (Autoferry)". In: *Home page of Norwegian University of Science and Technology (NTNU)* (2022). URL: https://www.ntnu.edu/autoferry/ (visited on 06/22/2022).

[20] "MF Ampere The world's first all-electric car ferry". In: *Corvus Energy* (2014). URL: https://corvusenergy.com/projects/mf-ampere/ (visited on 06/22/2022).

[21] E. F. Brekke, E. Eide, B.-O. H. Eriksen, E. F. Wilthil, M. Breivik, E. Skjellaug, Ø. K. Helgesen, A. Lekkas, A. B. Martinsen, E. H. Thyri, T. Torben, E. Veitch, O. A. Alsos, and T. A. Johansen. "milliAmpere: An autonomous ferry prototype". In: *Journal of Physics: Conference Series* 2311.1 (2022), p. 012029. DOI: https://doi.org/10.1088/1742-6596/2311/1/012029.

[22] O. A. Alsos, E. Veitch, L. Pantelatos, K. Vasstein, E. Eide, F.-M. Petermann, and M. Breivik. "NTNU shore control lab: Designing shore control centres in the age of autonomous ships". In: *Proceedings of the 4th International Conference on Maritime Autonomous Surface Ships (ICMASS)* (2022).

[23] E. H. Thyri, M. Breivik, and A. M. Lekkas. "A path-velocity decomposition approach to collision avoidance for autonomous passenger ferries in confined waters". In: *Proceedings of the 20th IFAC World Congress*. Berlin, Germany, 2020, pp. 14628–14635. DOI: https://doi.org/10.1016/j.ifacol.2020.12.1472.

[24] E. H. Thyri, E. A. Basso, M. Breivik, K. Y. Pettersen, R. Skjetne, and A. M. Lekkas. "Reactive collision avoidance for ASVs based on control barrier functions". In: *Proceedings of the 2020 4th IEEE Conference on Control Technology and Applications (CCTA)*. Montreal, QC,

Canada, 2020, pp. 380–387. ISBN: 978-1-7281-7140-1. DOI: https://doi.org/10.1109/CCTA41146.2020.9206340.

[25] E. H. Thyri, G. Bitar, and M. Breivik. "A 3DOF path-following controller for a non-directionally stable vessel with slow thruster dynamics". In: *IFAC-PapersOnLine* 54.16 (2021). 13th IFAC Conference on Control Applications in Marine Systems, Robotics, and Vehicles (CAMS) 2021, pp. 288–294. ISSN: 2405-8963. DOI: https://doi.org/10.1016/j.ifacol.2021.10.106.

[26] E. H. Thyri and M. Breivik. "A domain-based and reactive COLAV method with a partially COLREGs-compliant domain for ASVs operating in confined waters". In: *Field Robotics* 2 (2022), pp. 632–677. DOI: https://doi.org/10.55417/fr.2022022.

[27] E. H. Thyri and M. Breivik. "Partly COLREGs-compliant collision avoidance for ASVs using encounter-specific velocity obstacles". In: *Proceedings of the 14th IFAC Conference on Control Applications in Marine Systems, Robotics, and Vehicles (CAMS) 2022*. Copenhagen, Denmark, 2022.

[28] E. H. Thyri and M. Breivik. "Collision avoidance for ASVs through trajectory planning: MPC with COLREGs-compliant nonlinear constraints". In: *Modeling, Identification and Control* 43.2 (2022), pp. 55–77. DOI: https://doi.org/10.4173/mic.2022.2.2.

[29] E. A. Basso, E. H. Thyri, K. Y. Pettersen, M. Breivik, and R. Skjetne. "Safety-critical control of autonomous surface vehicles in the presence of ocean currents". In: *Proceedings of the 2020 4th IEEE Conference on Control Technology and Applications (CCTA)*. Montreal, Canada, 2020, pp. 396–403. DOI: https://doi.org/10.1109/CCTA41146.2020.9206276.

[30] J. Matouš, E. A. Basso, E. H. Thyri, and K. Y. Pettersen. "Unifying reactive collision avoidance and control allocation for multi-vehicle systems". In: *Proceedings of the 2021 5th IEEE Conference on Control Technology and Applications (CCTA)*. 2021, pp. 76–81. DOI: 10.1109/CCTA48906.2021.9658918.

[31] A. Yttisrud. "Hybrid collision avoidance for autonomous passenger ferries". MA thesis. Norwegian University of Science and Technology (NTNU), Trondheim, Norway, 2020. URL: https://hdl.handle.net/11250/2656722.

[32] H. Berget. "An area-time trajectory planning approach to collision avoidance for confined-water vessels". MA thesis. Norwegian University of Science and Technology (NTNU), Trondheim, Norway, 2021. URL: https://hdl.handle.net/11250/2781076.

[33] O. J. O. Kirkerud. "COLREGs-aware collision avoidance for autonomous surface vehicles using encounter-specific artificial potential fields". MA thesis. Norwegian University of Science and Technology (NTNU), Trondheim, Norway, 2022. URL: https://ntnuopen.ntnu.no/ntnu-xmlui/.

[34] E. Hestvik. "COLREGs-aware and MPC-based trajectory planning and collision avoidance for autonomous surface vessels". MA thesis. Norwegian University of Science and Technology (NTNU), Trondheim, Norway, 2022. URL: https://ntnuopen.ntnu.no/ntnu-xmlui/.

[35] E. Løvoll. "Evaluating collision avoidance algorithms in urban and semi-restricted waters using fuzzy logic". MA thesis. Norwegian University of Science and Technology (NTNU), Trondheim, Norway, 2022. URL: https://ntnuopen.ntnu.no/ntnu-xmlui/.

[36] J. F. Kemp. "Two hundred years of the collision regulations". In: *Journal of Navigation* 29.4 (1976), pp. 341–349. DOI: 10.1017/S0373463300039308.

[37] A. N. Cockroft and J. N. F. Lameijer. *A guide to the collision avoidance rules*. 7th ed. Butterworth-Heinemann, 2011. 200 pp. ISBN: 9780080971704.

[38] H. Ringbom. "Regulating autonomous ships—concepts, challenges and precedents". In: *Ocean Development & International Law* 50.2-3 (2019), pp. 141–169. DOI: 10.1080/00908320.2019.1582593. eprint: https://doi.org/10.1080/00908320.2019.1582593. URL: https://doi.org/10.1080/00908320.2019.1582593.

[39] O. Mitrofanov. "An anti-collision indicator". In: *Journal of Navigation* 21.2 (1968), pp. 163–170. DOI: 10.1017/S0373463300030319.

[40] I. Höivold. "Norwegian Research and Development in the Field of Ship Automation". In: *Modeling, Identification and Control* 5.3 (1984), pp. 171–178. DOI: 10.4173/mic.1984.3.4.

[41] C. E. Moore and J. D. Elpi. "Optimum collision avoidance for merchant ships". In: *IEEE Transactions on Industry Applications* IA-9.6 (1973), pp. 640–647. DOI: 10.1109/TIA.1973.349987.

[42] J. D. Luse. "Collision avoidance systems and the rules of the nautical road". In: *NAVIGATION* 19.1 (1972), pp. 80–88. DOI: https://doi.org/10.1002/j.2161-4296.1972.tb00129.x. eprint: https://onlinelibrary.wiley.com/doi/pdf/10.1002/j.2161-4296.1972.tb00129.x. URL: https://onlinelibrary.wiley.com/doi/abs/10.1002/j.2161-4296.1972.tb00129.x.

[43] R. F. Riggs. “A modern collision avoidance display technique”. In: *Journal of Navigation* 28.2 (1975), pp. 143–155. DOI: 10.1017/S0373463300037681.

[44] M. J. Dove, R. S. Burns, and C. T. Stockel. “An automatic collision avoidance and guidance system for marine vehicles in confined waters”. In: *Journal of Navigation* 39.2 (1986), pp. 180–190. DOI: 10.1017/S0373463300000059.

[45] C. Tam, R. Bucknall, and A. Greig. “Review of collision avoidance and path planning methods for ships in close range encounters”. In: *Journal of Navigation* 62.03 (2009), pp. 455–476. DOI: 10.1017/s0373463308005134.

[46] J. Larson, M. Bruch, R. Halterman, J. Rogers, and R. Webster. *Advances in autonomous obstacle avoidance for unmanned surface vehicles*. Tech. rep. Space and Naval Warfare Systems Center, 2007. URL: http://oai.dtic.mil/oai/oai?verb=getRecord&metadataPrefix=html&identifier=ADA475547.

[47] Ø. A. G. Loe. “Collision avoidance for unmanned surface vehicles”. MA thesis. Norwegian University of Science and Technology (NTNU), Trondheim, Norway, 2008. URL: http://hdl.handle.net/11250/259696.

[48] G. Casalino, A. Turetta, and E. Simetti. “A three-layered architecture for real time path planning and obstacle avoidance for surveillance USVs operating in harbour fields”. In: *Proceedings of the IEEE OCEANS Conference*. Bremen, Germany, 2009. DOI: 10.1109/OCEANSE.2009.5278104.

[49] P. Švec, B. C. Shah, I. R. Bertaska, J. Alvarez, A. J. Sinisterra, K. von Ellenrieder, M. Dhanak, and S. K. Gupta. “Dynamics-aware target following for an autonomous surface vehicle operating under COLREGs in civilian traffic”. In: *2013 IEEE/RSJ International Conference on Intelligent Robots and Systems*. Tokyo, Japan, 2013, pp. 3871–3878. DOI: 10.1109/iros.2013.6696910.

[50] E. Serigstad, B.-O. Eriksen, and M. Breivik. “Hybrid collision avoidance for autonomous surface vehicles”. In: *Proceedings of the 11th IFAC Conference on Control Applications in Marine Systems, Robotics and Vehicles (CAMS) 2018*. Opatija, Croatia, 2018.

[51] G. Bitar, B.-O. H. Eriksen, A. M. Lekkas, and M. Breivik. “Energy-optimized hybrid collision avoidance for ASVs”. In: *Proceedings of the 18th European Control Conference (ECC)*. Naples, Italy, 2019, pp. 2522–2529. DOI: 10.23919/ECC.2019.8795645.

[52] B.-O. H. Eriksen, G. Bitar, M. Breivik, and A. M. Lekkas. "Hybrid collision avoidance for ASVs compliant with COLREGs rules 8 and 13–17". In: *Frontiers in Robotics and AI* 7 (2020). DOI: 10.3389/frobt.2020.00011. arXiv: 1907.00198 [eess.SY].

[53] A. Vagale, R. Oucheikh, R. T. Bye, O. L. Osen, and T. I. Fossen. "Path planning and collision avoidance for autonomous surface vehicles I: A review". In: *Journal of Marine Science and Technology* 26 (2021), pp. 1292–1306. DOI: https://doi.org/10.1007/s00773-020-00787-6.

[54] A. Vagale, R. T. Bye, R. Oucheikh, O. L. Osen, and T. I. Fossen. "Path planning and collision avoidance for autonomous surface vehicles II: A comparative study of algorithms". In: *Journal of Marine Science and Technology* 26 (2021), pp. 1307–1323. DOI: 10.1007/s00773-020-00790-x.

[55] G. Bitar. "Optimization-based trajectory planning and automatic docking for autonomous ferries". PhD thesis. Norwegian University of Science and Technology (NTNU), Trondheim, Norway, 2021.

[56] P. Fiorini and Z. Shiller. "Motion planning in dynamic environments using the relative velocity paradigm". In: *Proceedings of the IEEE International Conference on Robotics and Automation (ICRA) 1993*. 1993, 560–565 vol.1. DOI: 10.1109/ROBOT.1993.292038.

[57] P. Fiorini and Z. Shiller. "Motion planning in dynamic environments using velocity obstacles". In: *The International Journal of Robotics Research* 17.7 (1998), pp. 760–772. DOI: 10.1177/027836499801700706.

[58] J. Ren, J. Zhang, and Y. Cui. "Autonomous obstacle avoidance algorithm for unmanned surface vehicles based on an improved velocity obstacle method". In: *ISPRS International Journal of Geo-Information* 10.9 (2021). ISSN: 2220-9964. DOI: 10.3390/ijgi10090618. URL: https://www.mdpi.com/2220-9964/10/9/618.

[59] D. F. Campos, A. Matos, and A. M. Pinto. "An adaptive velocity obstacle avoidance algorithm for autonomous surface vehicles". In: *2019 IEEE/RSJ International Conference on Intelligent Robots and Systems (IROS)*. 2019, pp. 8089–8096. DOI: 10.1109/IROS40897.2019.8968156.

[60] A. Haraldsen, M. S. Wiig, and K. Y. Pettersen. "Reactive collision avoidance for underactuated surface vehicles using the collision cone concept". In: *Proceedings of the 2021 4th IEEE Conference on Control Technology and Applications (CCTA)*. 2021, pp. 619–626. DOI: 10.1109/CCTA48906.2021.9659043.

[61] Y. Kuwata, M. T. Wolf, D. Zarzhitsky, and T. L. Huntsberger. "Safe maritime autonomous navigation with COLREGS, using velocity obstacles". In: *IEEE Journal of Oceanic Engineering* 39.1 (2014), pp. 110–119. ISSN: 0364-9059. DOI: 10.1109/JOE.2013.2254214.

[62] D. K. M. Kufoalor, E. F. Brekke, and T. A. Johansen. "Proactive collision avoidance for ASVs using a dynamic reciprocal velocity obstacles method". In: *2018 IEEE/RSJ International Conference on Intelligent Robots and Systems (IROS)*. 2018. DOI: 10.1109/iros.2018.8594382.

[63] Y. Zhao, W. Li, and P. Shi. "A real-time collision avoidance learning system for unmanned surface vessels". In: *Neurocomputing* 182 (2016), pp. 255–266. ISSN: 0925-2312. DOI: https://doi.org/10.1016/j.neucom.2015.12.028. URL: https://www.sciencedirect.com/science/article/pii/S0925231215019657.

[64] Y. Huang, L. Chen, and vanGelder P.H.A.J.M. "Generalized velocity obstacle algorithm for preventing ship collisions at sea". In: *Ocean Engineering* 173 (2019), pp. 142–156. ISSN: 0029-8018. DOI: https://doi.org/10.1016/j.oceaneng.2018.12.053. URL: https://www.sciencedirect.com/science/article/pii/S0029801818314215.

[65] W. Shaobo, Z. Yingjun, and L. Lianbo. "A collision avoidance decision-making system for autonomous ship based on modified velocity obstacle method". In: *Ocean Engineering* 215 (2020), p. 107910. ISSN: 0029-8018. DOI: https://doi.org/10.1016/j.oceaneng.2020.107910. URL: https://www.sciencedirect.com/science/article/pii/S0029801820308714.

[66] Y. Cho, J. Han, J. Kim, P. Lee, and S.-B. Park. "Experimental validation of a velocity obstacle based collision avoidance algorithm for unmanned surface vehicles". In: *IFAC-PapersOnLine* 52.21 (2019). 12th IFAC Conference on Control Applications in Marine Systems, Robotics, and Vehicles CAMS 2019, pp. 329–334. ISSN: 2405-8963. DOI: https://doi.org/10.1016/j.ifacol.2019.12.328. URL: https://www.sciencedirect.com/science/article/pii/S240589631932213X.

[67] D. Fox, W. Burgard, and S. Thrun. "The dynamic window approach to collision avoidance". In: *IEEE Robotics & Automation Magazine* 4.1 (1997), pp. 23–33. DOI: 10.1109/100.580977.

[68] B.-O. H. Eriksen, E. F. Wilthil, A. L. Flåten, E. F. Brekke, and M. Breivik. "Radar-based maritime collision avoidance using dynamic window". In: *Proceedings of the IEEE Aerospace Conference*. Big Sky, MT, USA, 2018. DOI: 10.1109/aero.2018.8396666.

[69] H.-G. Kim, S.-J. Yun, Y.-H. Choi, J.-K. Ryu, and J.-H. Suh. "Collision avoidance algorithm based on COLREGs for unmanned surface vehicle". In: *Journal of Marine Science and Engineering* 9.8 (2021). ISSN: 2077-1312. DOI: 10.3390/jmse9080863. URL: https://www.mdpi.com/2077-1312/9/8/863.

[70] S.-M. Lee, K.-Y. Kwon, and J. Joh. "A fuzzy logic for autonomous navigation of marine vehicle satisfying COLREG guidelines". In: *International Journal of Control, Automation, and Systems* 2 (2004), pp. 171–181.

[71] M.-C. Lee, C.-Y. Nieh, and J.-C. Kuo Hsin-Chuan and- Huang. "A collision avoidance method for multi-ship encounter situations". In: *Journal of Marine Science and Technology* 25 (3 2020), pp. 925–942. DOI: 10.1007/978-3-322-89521-9_13. URL: https://doi.org/10.1007/s00773-019-00691-8.

[72] B.-O. H. Eriksen and M. Breivik. "MPC-based mid-level collision avoidance for ASVs using nonlinear programming". In: *Proceedings of the 2017 1st IEEE Conference on Control Technology and Applications (CCTA)*. Mauna Lani, HI, USA, 2017, pp. 766–772. DOI: 10.1109/ccta.2017.8062554.

[73] Y. Xue, X. Wang, Y. Liu, and G. Xue. "Real-time nonlinear model predictive control of unmanned surface vehicles for trajectory tracking and collision avoidance". In: *Proc. 7th International Conference on Mechatronics and Robotics Engineering (ICMRE)*. Budapest, Hungary, 2021, pp. 150–155. DOI: 10.1109/ICMRE51691.2021.9384818.

[74] M. Abdelaal and A. Hahn. "NMPC-based trajectory tracking and collision avoidance of unmanned surface vessels with rule-based colregs confinement". In: *2016 IEEE Conference on Systems, Process and Control (ICSPC)*. 2016, pp. 23–28. DOI: 10.1109/SPC.2016.7920697.

[75] B. Brito, B. Floor, L. Ferranti, and J. Alonso-Mora. "Model predictive contouring control for collision avoidance in unstructured dynamic environments". In: *IEEE Robotics and Automation Letters* (2019), pp. 1–8. DOI: 10.1109/LRA.2019.2929976.

[76] A. B. Martinsen, G. Bitar, A. M. Lekkas, and S. Gros. "Optimization-based automatic docking and berthing of ASVs using exteroceptive sensors: Theory and experiments". In: *IEEE Access* 8 (2020), pp. 204974–204986. DOI: 10.1109/ACCESS.2020.3037171.

[77] IPOPT. *Ipopt Documentation*. URL: https://coin-or.github.io/Ipopt/.

[78] P. E. Gill, W. Murray, and M. A. Saunders. "SNOPT: An SQP algorithm for large-scale constrained optimization". In: *SIAM Review* 47 (2005), pp. 99–131.

[79] A. Tan, W. C. Wee, and T. J. Tan. "Criteria and rule based obstacle avoidance for USVs". In: *2010 International WaterSide Security Conference*. 2010, pp. 1–6. DOI: 10.1109/WSSC.2010.5730288.

[80] B.-O. H. Eriksen, M. Breivik, E. F. Wilthil, A. L. Flåten, and E. F. Brekke. "The branching-course model predictive control algorithm for maritime collision avoidance". In: *Journal of Field Robotics* 36.7 (2019), pp. 1222–1249. DOI: 10.1002/rob.21900.

[81] T. A. Johansen, T. Perez, and A. Cristofaro. "Ship collision avoidance and COLREGS compliance using simulation-based control behavior selection with predictive hazard assessment". In: *IEEE Transactions on Intelligent Transportation Systems* 17.12 (2016), pp. 3407–3422. DOI: 10.1109/tits.2016.2551780.

[82] I. B. Hagen, D. K. M. Kufoalor, E. F. Brekke, and T. A. Johansen. "MPC-based collision avoidance strategy for existing marine vessel guidance systems". In: *2018 IEEE International Conference on Robotics and Automation (ICRA)*. Brisbane, QLD, Australia, 2018, pp. 7618–7623. DOI: 10.1109/icra.2018.8463182.

[83] D. K. M. Kufoalor, T. A. Johansen, E. F. Brekke, A. Hepsø, and K. Trnka. "Autonomous maritime collision avoidance: Field verification of autonomous surface vehicle behavior in challenging scenarios". In: *Journal of Field Robotics* 37.3 (2020), pp. 387–403. DOI: 10.1002/rob.21919.

[84] T. Tengesdal, T. A. Johansen, and E. F. Brekke. "Risk-based autonomous maritime collision avoidance considering obstacle intentions". In: *2020 IEEE 23rd International Conference on Information Fusion (FUSION)*. 2020, pp. 1–8. DOI: 10.23919/FUSION45008.2020.9190212.

[85] T. Tengesdal, T. A. Johansen, and E. F. Brekke. "Ship collision avoidance utilizing the cross-entropy method for collision risk assessment". In: *IEEE Transactions on Intelligent Transportation Systems* (2021), pp. 1–14. DOI: 10.1109/TITS.2021.3101007.

[86] T. Tengesdal, E. F. Brekke, and T. A. Johansen. "On collision risk assessment for autonomous ships using scenario-based-MPC". In: *IFAC Papers Online* 52 (2 2020), pp. 14509–14516. DOI: http://dx.doi.org/10.1016/j.ifacol.2020.12.1454.

[87] B. C. Shah, P. Švec, I. R. Bertaska, A. J. Sinisterra, W. Klinger, K. von Ellenrieder, M. Dhanak, and S. K. Gupta. "Resolution-adaptive risk-aware trajectory planning for surface vehicles operating in congested civilian traffic". In: *Autonomous Robots* 40 (2016), pp. 1139–1163. DOI: https://doi.org/10.1007/s10514-015-9529-x.

[88] P. Svec, B. C. Shah, I. R. Bertaska, J. Alvarez, A. J. Sinisterra, K. von Ellenrieder, M. Dhanak, and S. K. Gupta. "Dynamics-aware target following for an autonomous surface vehicle operating under COLREGs in civilian traffic". In: *2013 IEEE/RSJ International Conference on Intelligent Robots and Systems*. 2013, pp. 3871–3878. DOI: 10.1109/IROS.2013.6696910.

[89] Y. Fujii and K. Tanaka. "Traffic capacity". In: *Journal of Navigation* 24.4 (1971), pp. 543–552. DOI: 10.1017/S0373463300022384.

[90] E. M. Goodwin. "A statistical study of ship domains". In: *Journal of Navigation* 28.3 (1975), pp. 328–344. DOI: 10.1017/S0373463300041230.

[91] H.-T. L. Chiang and L. Tapia. "COLREG-RRT: A RRT-based COLREGS-compliant motion planner for surface vehicle navigation". In: *IEEE Robotics and Automation Letters* PP (2018), pp. 1–1. DOI: 10.1109/LRA.2018.2801881.

[92] T. I. Fossen. *Handbook of marine craft hydrodynamics and motion control*. Wiley-Blackwell, 2011. ISBN: 978-1-119-99149-6. DOI: 10.1002/9781119994138.

[93] G. Bitar, A. B. Martinsen, A. M. Lekkas, and M. Breivik. "Two-stage optimized trajectory planning for ASVs under polygonal obstacle constraints: theory and experiments". In: *IEEE Access* 8 (2020), pp. 199953–199969. DOI: 10.1109/ACCESS.2020.3035256.

[94] K. Kant and S. W. Zucker. "Toward efficient trajectory planning: The path-velocity decomposition". In: *The International Journal of Robotics Research* 5 (1986), pp. 72–89.

[95] J. Magnusson. "Norwegian Zeabuz on creating the world's first and, so far, only autonomous urban ferry". In: *Scandinavian MIND* (2022). URL: https://smartmaritimenetwork.com/2020/09/01/asko-to-build-two-autonomous-vessels-for-oslo-fjord-operations/ (visited on 02/09/2021).

[96] C. Tam and R. Bucknall. "Collision risk assessment for ships". In: *Journal of Marine Science and Technology* 15.3 (2010), pp. 257–270. DOI: 10.1007/s00773-010-0089-7.

[97] K. Woerner. “Multi-contact protocol-constrained collision avoidance for autonomous marine vehicles”. PhD thesis. Massachusetts Institute of Technology, USA, 2016.